Vol II

ELECTRODEPOSITION OF METALS IN A

ROTATING CYLINDER ELECTRODE REACTOR

by

Francis Charles Walsh

B.Sc.(CNAA), M.Sc.(Loughborough),

M.I.Corr.T., M.I.M.F., C.Chem.,

M.R.S.C..

A Doctoral thesis submitted in fulfilment

of the requirements for the award of

Doctor of Philosophy of the Loughborough

University of Technology, 1981.

Supervisor: Dr. D. R. Gabe

Department of Materials

Engineering and Design

VOLUME TWO

EXPERIMENTAL WORK AT LABORATORY AND PILOT

PLANT SCALE

(Chapters 8-12)

LIST OF FIGURES (Cont'd)

8. LABORATORY EXPERIMENTAL WORK

The experimental studies described in this chapter were
generally performed at Loughborough University of Technology,
in the Department of Materials Engineering and Design.
The apparatus used was designed and built by the author to
act as a versatile rotating cylinder electrode reactor for
the study of controlled potential deposition of metals and
powder formation under mass transport control.

8.1 DESIGN CONSIDERATIONS AND APPARATUS

8.1.1 Design Considerations

There were two conflicting requirements for the design of the laboratory reactor, in that it had to be capable of:

i) performing academic mass transport studies under controlled, reproducible conditions, which were comparable with previous work, and

ii) acting as a scaled-down version of an Eco-Cell, with the capacity to treat industrial process solutions.

The general requirements may be stated as follows:

1. The non-electrode reactor components had to be fabricated from chemically resistant materials.

2. The reactor had to be capable of being readily dismantled and assembled, to facilitate cleaning and to facilitate changing electrolyte or electrodes.

3. The reactor had to be capable of being divided by an ion exchange membrane, as in Eco-Cells.

4. Insoluble anodes had to be incorporated when using the reactor in a divided mode, whereas soluble (copper) anodes had to be used for undivided operation.

5. The reactor was required to operate in batch, single pass and batch recycle modes; a flow-through design was necessary.

6. The reactor had to be operated under controlled temperature conditions.

7. The reactor had to be capable of being sealed and vented, to prevent undue vortexing, aeration or hazardous gas evolution.

8. It was desirable to minimise the use of immersed metallic components to the electrodes, to negate the possibility of stray current electrolysis.

9. The reactor geometry had to give rise to a uniform cathode
   potential and current density, and the rotating cylinder
   cathode had to be capable of potentiostatic control.

More specific requirements will be seen in further sections.
The resultant versatile working reactor and associated instru-
mentation and fluid flow assemblies is shown in Figs. 8.1 - 8.8
and will now be described in some detail.

8.1.2 Apparatus

Fig. 8.1 (a) and 8.1 (b) show an actual photograph and a schematic
sketch of the completed rotating cylinder electrode reactor assembly.
This apparatus was constructed around four "Tufnol" platforms,
which may be described as base, lower, intermediate and upper
platforms. Tufnol was employed due to its chemical resistance,
insulating properties and mechanical stability. Four 2.5 cm.
diameter nickel-plated steel rods were bolted to the base, and
these rods were screwed above a certain height and provided with
hexagonal nuts to accept three further Tufnol platforms.
The upper Tufnol platform had the drive motor mounted centrally
on its upper surface. The motor was a 1/8 h.p. Servomex Controls
Ltd. model M.C.43, equipped with a tachometer generator feedback
winding to facilitate measurement and control of its rotational
velocity, by an electronic power supply. This system enabled
rotational speeds of 180 - 1500 r.p.m. to be employed, set speeds
being controlled to within 1%. The lower limit here was governed
by the tendency of the ungeared motor to "commutate" and produce
unsteady rotation, while the upper limit was governed by the
mechanical inertia of the drive assembly and friction due to
brush loading.

The drive motor was coupled by an insulating nylon sleeve to the stainless steel drive shaft. This shaft was vertically mounted between two roller bearings held in an aluminium alloy housing. This housing was mounted between the lower and intermediate platforms, and provided with strategic grease nipples for the periodic lubrication of the bearings. The drive shaft accommodated the power slip ring as it emerged from the upper surface of the intermediate platform. The slip ring, which was silver plated for good electrical contact, was fitted on a locking taper to the shaft and secured by an additional hexagonal nut. This arrangement enabled the slip ring to be readily removed, but facilitated good electrical conductivity to the shaft. The power brush assembly was mounted on the upper side of the intermediate platform, and consisted of a twin, tinplated steel, sprung-caliper unit incorporating two silver filled graphite brushes, each of approximate surface area 8 cm.^{2} The contacting faces of the brushes were machined before use to mate with the slip ring, and the assembly was run in for several days.

A small tachometer generator was also mounted on the upper surface of the intermediate platform, and was driven from the shaft by pulleys and a rubber belt. This provided an output of 1 V at 1000 r.p.m., which was proportional at different speeds. Coupled to a voltmeter, the electro-mechanical tachometer provided a check on the rotational speed.

The lower platform carried a small 12 V. DC motor on its upper surface, and this was used to drive the anolyte bath stirrer via a thyristor speed control unit.

The rotating cylinder electrode (catholyte) compartment, which will be described below, was flanged on to a 2.5 cm. thick perspex plate. This plate was suspended from the under side of the lower platform by four screwed stainless steel rods.

A small silver plated copper slip ring was fitted on to the rotating

shaft where the latter emerged from the lower platform. This was

contacted by a small silver filled graphite brush of approximate

contact area 0.3 cm^2, which served to measure the potential of the

R.C.E. without including the potential drops across the slip ring/

brush assembly and the drive shaft.

The top plate of the reactor (Fig. 8.2 c)was provided with several

sealable apertures to mount the central drive shaft, the fluid

outlet/gas vent, a mercury thermometer, and the reference electrode

probe. The last two were sealed via PTFE screwed collars com-

pressing silicone 'O' rings. The thermometer aperture also served

as a sampling point in certain experiments, small discrete samples

of electrolyte being withdrawn with a hypodermic syringe or a

micro-pipette. The reference electrode probe consisted of a

vertical glass tube terminated in a low leakage ceramic frit located

approximately 1.5 mm. from the active cathode surface, and at half

the height of the cylinder. While a smaller distance and a luggin

capillary along the lines of current flow are clearly desirable from

the point of view of measuring an accurate electrode potential,

these considerations were relaxed to allow metal powder buildup to

occur in some cases. The liquid junction glass tube probe was

conveyed via a flexible transparent PVC tube to a polypropylene

reservoir mounted on the side of the upper platform. This reservoir

was filled with salt bridge solution, typically 1.0 M sodium sulphate

and fitted with a mercury/mercurous sulphate reference electrode and

a tap to facilitate filling, sealing and bleeding air from the system.

This design of probe and reservoir resulted in a rigid,robust,

versatile assembly, which could be readily changed for an alternative

reference electrode system, removed to aid electrode or reactor

cleaning or preparation, or used externally. Whilst the small

hydrostatic head of the salt bridge, sealed reservoir and ceramic
frit combined to give a good reproducible liquid junction with low
leakage, a sulphate reference electrode was preferred to a chloride
variety such as calomel, because sulphate ions were directly com-
patible with the sulphuric acid indifferent electrolyte used in many
experiments.   Moreover, chloride ions, even in small concentrations,
are known to exert a marked effect on the electrochemical behaviour
and deposit characteristics of copper deposition.

The catholyte compartment was an approximately cubic perspex vessel
open at the top and flanged via a 3 mm. rubber gasket to the perspex
top plate.   It was secured to the latter by 8 quick-release stainless
steel thumbscrews.   For flow through operation, or emptying the
reactor, the bottom was provided with a screwed-in polypropylene
inlet tube.   This, and the similar outlet tube on the top plate of
the catholyte compartment, (Fig. 8.2 c)) could be sealed off for batch
operation.

Fig. 8.2 provides a series of photographs to illustrate the construc-
tion of the catholyte compartment.   The four sides of the compartment
were machined from 6 mm. thick transparent "Perspex" sheet, and were
each provided with a central square 8 cm. x 8 cm. aperture.   The
sides were joined by a solvent cement (I.C.I's Tensol 6) and clamped
together with 6 BA stainless steel allen cap screws.(Fig. 8.2 a)).
The latter were counterbored and covered with an insulating layer of
solvent cement.   The top flange of the compartment consisted of a
square frame of 6 mm. perspex sheet, with a central 12 x 12 cm.
aperture.   It was bonded to the compartment sides as above (Fig 8.2 a)).
The framework of the catholyte compartment was completed by the
addition of a square 6 mm. thick perspex plate containing a central
screwed aperture to accommodate the inlet.

Each side of the compartment was fitted with a sheet of cation

exchange membrane (Ionac MC 3470, Ionac Chemical Sybron Corporation,

New Jersey, U.S.A.). This was sandwiched between 3 mm. thick rubber

gaskets, and the assembly was secured by a 6 mm. thick perspex

backing plate and M6 polypropylene fastenings.   This resulted in

an 8 x 8 cm. window of membrane in each side (Figs. 8.2 b)).   The

resilient rubber gaskets were moistened with silicone grease to aid

sealing and dismantling, and the membranes could be sealed with

little more than finger pressure on the polypropylene fastenings.

Fig. 8.2 c) shows the cell complete with its top plate.   For simple,

rapid trials it was sufficient to merely clamp the cell loosely to

the top plate, whereas for continuous flow through experiments the

fixings were used, finger pressure being sufficient to seal the

chamber.

The catholyte chamber was immersed in a square sectioned tank (Fig. 8.1 c)

This tank, fabricated from glued and screwed 10 mm. transparent perspex

sheet, held the anolyte (1.5 M sulphuric acid) and also served to

provide a constant temperature bath.   The anolyte chamber (Fig. 8.3)

had a recessed internal ledge which accepted a 10 mm. perspex cover,

and facilitated mounting of two diagonally opposed 240 V, 500 W.

silica sheathed immersion heaters.   The latter were controlled by a

capillary, mercury in copper thermostat probe which was glass sheathed.

The perspex cover also accommodated a thermometer and a flexible tube

conveying inlet liquor to the catholyte chamber.   The cover of the

anolyte chamber incorporated a stirrer gland through which a polypro-

pylene impeller shaft passed.   The end of this shaft was provided

with a polypropylene stirrer to encourage uniformity of temperature

and composition in the anolyte, and to promote escape of gas from the

anodes.   The anodes comprised four 6 mm. plates of lead/6% antimony

disposed to each side of the anolyte chamber, and connected externally.

The effective immersed anode area was approximately 100 cm^2 for each anode, i.e. 400 cm^2 total and was considerably in excess of the cathode area to prevent anode polarisation affecting studies at the R.C.E. The anodes were anodised to a stable lead oxide surface before use, and occasionally anodically protected using a "dummy" cathode during periods of disuse, to preserve the surface oxide coating. No effort was made to minimise the effective interelectrode gap, as the voltage capability of the potentiostat power supply was relatively large (20 V), and the relatively large interelectrode distance (approximately 10 cm) assisted in providing a more uniform potential and current density distribution. The anolyte chamber lid was a relatively close fit to discourage electrolyte loss via oxygen gassing, and to provide better thermal insulation. The anolyte chamber was provided with a drain plug, and mounted on a manually elevated jack to raise (Fig. 8.1 c)) and lower (Figs. 8.1 a) and d) it. When the anolyte bath was lowered, the catholyte chamber could be left in place (Fig. 8.1 a)) or allowed to fall (Fig. 8.1 d)) as appropriate. The design of the reactor assembly around platforms produced a rigid apparatus, and the platforms were individually adjustable, to allow the drive components to line up correctly.

In soluble anode experiments, a copper foil anode was employed mounted inside the catholyte chamber, which then acted as an undivided reactor rather than an individual compartment.

Catholyte solutions were conveniently prepared and stored in a thermo-statically heated and stirred 20 litre cylindrical glass reservoir (Fig. 8.4). This was provided with an inlet and outlet, and could be used as part of a pumped flow batch recirculation system, together with the rotammeters in the inlet line to the cell, and a large bore peristaltic pump. The flow rate could be controlled by both the variable speed peristaltic pump or by throttling valves in a bypass line. The outlet liquor from the reactor was then filtered by a small paper cartridge (Whatman 10 μ grade) before returning to the

reservoir. The flow apparatus (Fig. 8.4) was largely mounted in a polypropylene tray for security and cleanliness. In the majority of experiments, the reservoir merely served as a supply of fresh electrolyte, the preparation of a large volume of solution helping to prevent minor variations in composition.

The instrumentation employed for the laboratory studies is collectively shown in Fig. 8.5, although it should be noted that not all of the instruments were employed in each experiment. Fig. 8.6 shows a typical electrical circuit. The instruments will be referred to in the following sections.

The design of the R.C.E. and the rotating shaft/catholyte chamber seal both received considerable thought. The seal design, which was required to yield a low friction surface, is indicated in Fig. 8.7. The stainless shaft was machined, lapped and polished to a mirror finish in the vicinity of a stainless steel case, stainless-steel-spring-reinforced, nitrile lip seal, which was centrally installed in the perspex top plate of the catholyte chamber. The seal was removable from above or below the perspex plate; the rotor could be removed to facilitate seal replacement without disturbing the top plate. The lip seal was mounted between a fixed, lower, and an upper, adjustable PTFE collar (which also acted as steady sleeve bearings). The upper PTFE collar extended for a short distance to allow a small (5 - 10 ml) pool of water to lie above the seal and around the exposed shaft. This served two purposes: firstly, the water acted as a 'tell-tale' for electrolyte leakage, as its colour or pH would change, or it would overflow; secondly, the water served to lubricate and prolong the life of the seal from above, while electrolyte lubricated the seal from below. The shaft was only exposed to electrolyte for several millimetres in the immediate vicinity of the seal to minimise electrodeposition. In practice this did not prove to be a problem, although the small amount of plate was periodically removed. The section of the shaft extending to the R.C.E. was protected from plating by a sliding fit PTFE sleeve.

Fig 8.8 shows two designs of rotor used in this work; both types were removable from the shaft via a male thread on the upper side of the cylinder, for convenience in cleaning, electrode preparation, and deposit examination and measurement. The first design (Fig. 8.8 a)) comprised a stainless steel cylinder of diameter 6 cm. and length 6 cm., provided with insulating PTFE end caps 6 mm. thick, on its lower and upper faces. The diameter of the end caps was identical to that of the cylinder, to promote uniform hydrodynamics around the top and bottom extremities of the cylinder, and minimise edge effects. This design also facilitated cleaning or remachining of the cylinder, and the end caps could be readily sealed to the rotor, by light compression; the top cap was compressed between the shaft and cylinder while the bottom one was screwed on to the underside of the cylinder. Duplicate cylinders were knurled.

While the above design was preferred from a hydrodynamic and mass transfer point of view, it was desirable in certain experiments to be able to remove the deposit, e.g. for microscopic examination, to examine the effect of surface pretreatments, or to facilitate cleaning. This was accomplished by wrapping a thin metal foil around a stainless steel former and employing shaped end caps to secure the cylindrical foil. If a seamless foil was employed, however, the wrapped over section of the foil would have tended to promote non-uniform deposit growth due to hydrodynamic or electrocrystallisation effects, and care would have been necessary to ensure that electrolyte did not seep into the space between the foil and the rotor, resulting in unwanted deposition on the latter; eccentricity was also a problem. The foil electrode also facilitated the use of varying electrode materials, and this is especially important in the case of precious metals such as platinum, where the inventory of electroactive substance may be minimised. An alternative is always provided by electrodeposition, but this is rather inconvenient. It was desirable to use foils for

certain experiments in the present study, but to eliminate the seam.
The use of adhesives or solder proved to be tedious and unsuitable,
as foreign material was introduced on to the electrode surface.
The problem was solved by electron beam welding of copper foil around
a suitable former.   This technique was employed to produce foil
cylinders having a diameter just (say 1 mm) greater than the rotating
cylinder.   The seamless foil was readily fitted and proved to be
reasonably concentric and quite suitable for surface microscopic
studies.   Foils prepared in this way could be re-used, sectioned
for examination, or cut and straightened for storage.   Fig. 8.8 b) shows
a rotating cylinder according to this design.

The rotating cylinder and its drive assembly were machined and assembled
such as to maintain a concentric, vibration-free system;   typical run
out figures after 6 months (measured by a dial gauge) are shown in
Table 8.1.

8.2 Procedure

8.2.1 General

Laboratory solutions were prepared volumetrically by dissolution of
the required chemicals (normally A.R. grade) in the background
electrolyte.   For example, in the case of acid copper solutions,
cupric sulphate pentahydrate was dissolved in 1.5 M sulphuric acid,
which was itself prepared by dilution of concentrated sulphuric acid
(A.R. grade).   Freshly prepared solutions were normally analysed
(Section 8.2.8) by atomic absorption spectrophotometry or thiosulphate
titration to check the metal concentration, and alkaline titration
with caustic soda (phenolphalein as indicator) to check the acid
concentration.   The majority of copper solutions were 0.014 M in
copper sulphate, and hence 0.014 in copper (equivalent to 890 parts
per million metal).

During lengthy trials, the composition of the copper solutions was frequently checked and corrected. Dilution was performed by addition of 1.5 M sulphuric acid and concentration by addition of a small volume of concentrated cupric sulphate in 1.5 M sulphuric acid solution.

The majority of cupric solutions for mass transfer involved experiments with 0.014 M Cu solutions in 1.5 M sulphuric acid, to provide comparison with previous work, and to facilitate use of transport properties already documented, such as dynamic viscosity, density and diffusion coefficient.

Industrial process solutions were used in the "as received" condition, unless otherwise stated.

In the case of stainless steel electrodes, the surface was polished by wet 600 grade emery paper, then degreased by swabbing with 1,1,1-trichloroethane . Deposits were stripped by HNO_3, 50%. For copper foil electrodes, a similar procedure was adopted . Generally, prior to an experimental trial, the surface of the clean electrode was preplated potentiostatically at a low overpotential (well below that conducive to mass transport control) for 60 seconds, to yield an active, compact and adherent surface which was found to foster reproducibility. More complicated methods of electrode preparation were not undertaken, as early studies showed that no significant differences were observed, within experimental error, between chemically polished or electropolished copper foils, and those prepared according to the above method. While chemical and electrochemical methods of polishing undoubtedly have a pronounced effect on the initial stages of electrocrystallisation, this effect is rapidly swamped in the case of powder formation. In the case of foil electrodes, the surface area was reproducibly defined by wrapping stretched 0.05 mm. thick PTFE tape around the rotating cylindrical surface. A freshly prepared R.C.E. was employed for each trial and, following charging of the cell, the rotor was allowed

to turn at the appropriate stabilised and monitored speed to remove air and aid thermostatic operation of the catholyte. The catholyte temperature was controlled in the range 20 – 60° C by the surrounding anolyte bath, and was held to within $\pm$ 0.5° C at any temperature. The R.C.E. was normally controlled potentiostatically using a Chemical Electronics 20 V/50A model potentiostat according to the circuit shown in Fig. 8.6. Current was normally continuously monitored on a Bryans model 28000, y–t chart recorder, as the potential difference across a standard 1% tolerance shunt. According to the current being measured, the shunt and recorder sensitivity were selected to give a reasonable low noise signal. Generally, a 50 A/50 mV (i.e. 1 mV/A) or a 5A/50 mV (i.e. 10 mV/A) shunt was employed, with the recorder input switched within the range 0.1 mV to 100 mV. The time axis of the recorder chart was calibrated either in minutes or in terms of mV potential for polarisation work.

The cell voltage of the reactor was continuously monitored by an analogue moving coil 0 – 3 V meter, to provide a check on overall cell operation and power use. A high impedance Co ing – EIL model 12, pH meter/millivoltmeter was switched in order to measure electrode potential, cell voltage, auxiliary potentials or pH, as appropriate, to within $\pm$ 0.1 mV. In certain later experiments, the electrical charge passed to the reactor was monitored by a digital Coulombmeter (Kemitron Electronics, Chester).

8.2.2 Potentiostatic Polarisation Curves

Potentiostatic polarisation curves were obtained automatically on the 't' axis of the recorder by linearly increasing the potential applied to the working electrode (as measured by the potential pick-up brush), with time, using a Chemical Electronics Ltd. linear sweep unit. Sweep rates of 15 – 1000 mV (min)$^{-1}$ were employed, but the majority of trials utilised 60 mV (min)$^{-1}$. Current was displayed on the 'y' axis of the recorder. The electrode was prepared as described in 8.2.1, allowed to reach a steady recorded rest potential (essentially

the reversible potential of copper) and the cathodic polarisation scan
was initiated, from the open circuit potential. At a sweep rate of
60 mV $(min)^{-1}$ and an overpotential range of 0 - 700 mV, a complete
polarisation curve was displayed in less than 12 minutes. As explained
later, the scan rate was necessarily chosen as a compromise to achieve
significant, steady state, reproducible results.

Polarisation curves were obtained under a variety of conditions for both
smooth, knurled and powder-deposited rough cylinders using the above
procedure.

For a limited number of trials, a comparison was made between limiting
currents observed from polarisation curves, and the steady current
obtained by immediately raising the potential of the cylinder to a
value corresponding to a central portion of the limiting current
plateau.

For precise work, a sample of the catholyte taken under limiting
current conditions was analysed for copper concentration.

8.2.3 Potentiostatic Growth of Deposits

The smooth - rough transition for deposition of copper was followed
as a function of time while subjecting the R.C.E. to potentiostatic
control and monitoring the cell current. This was accomplished at
various cylinder speeds, and the concentration of copper in the catholyte
was held constant by a combination of a flow-through electrolyte and
soluble anodes. Soluble anodes in a sealed undivided cell did not
prove to be a suitable system, especially for lengthy studies, as
copper dissolution occurred by corrosion as well as by faradaic dissolution.

8.2.4 Concentration Decay Trials

Several trials on copper solutions were performed using a potentiostati-
cally controlled R.C.E. in a divided cell, with an insoluble anode.
The subsequent decay of concentration was followed by sampling the
solution (and analysing for copper), while the current was also monitored.
The effect of potential, electrode area, rotational speed and deposit
roughness were studied.

8.2.5 Controlled Potential Separation of Metals

Similar trials to the above were performed on mixed metal solutions including:

$0.014M$ Ag: $0.014M$ Cu in $0.15M$ HNO_3

$0.014M$ Cu; $0.014M$ Zn in $1.5M$ H_2SO_4

$0.014M$ Cu; $0.014M$ Ni in $1.5M$ H_2SO_4

and mixed Au/Ag/Cu/other metals cyanidic solutions from a precious metal plating dragout . The technique used was to obtain the polarisation curve, select a potential corresponding to mass transport control, i.e. limiting current conditions, and hold the R.C.E. at that potential for the duration of the experiment. The concentration of each metal was monitored with time. The deposit was also analysed for the less noble metal, in certain cases, by acid dissolution, dilution and atomic absorption spectrophotometry.

8.2.6 Solution Analysis for Metals

Several analytical techniques were employed during the experimental work, as appropriate. These included titrimetry, atomic absorption spectrophotometry and ion selective electrode potentiometry. Standard titrimetric techniques were employed such as a direct thiosulphate titration for copper. Atomic absorption analysis was performed using an Instrumentation Laboratory Model IL 151 machine, and an air/ acetylene or nitrous oxide/acetylene flame. Where possible, the samples were simply diluted to the linear working range, normally 1 - 10 ppm depending on the metal, and directly aspirated. The concentration was obtained by a direct digital readout following a previous calibration by volumetrically prepared spectroscopic standards. The absence of interfering species, e.g. anions or a second metal was checked by the direct standard addition technique. Atomic absorption proved tedious due to the large number of discrete samples necessary and the subsequent dilutions, and this encouraged the development of a novel ion selective electrode (I.S.E.) detector 396 cell which will be described elsewhere. Discrete samples were also analysed by direct I.S.E. potentiometry.

8.2.7 Scanning Electron Microscopy (SEM)

The development of rough deposits under potentiostatic control was studied by means of SEM. Separate copper foil R.C.E's were electro-deposited with copper for various times at a fixed potential and rpm. The deposit was washed with distilled water, then with a hot stearic acid solution to prevent oxidation and stored in a desiccator. The foils were sectioned into 8 mm x 8 mm squares, mounted on to standard aluminium alloy stubs with a conducting silver-loaded epoxy resin, and examined by a Cambridge "Stereoscan" instrument (Model 54) with a perpendicular incident beam, and an accelerating voltage of 20 KV. The above procedure was repeated for specimens undergoing deposition for fixed time and rpm, but varying overpotentials, or fixed time and over-potential but varying rpm. All experiments were performed with 0.014M $CuSO_4$ in 1.5M H_2SO_4 at 22° C.

8.2.8 Surface Profilometry

The development of deposit roughness was also studied in a direct manner by surface profilometry, in which a stylus was allowed to traverse the surface of the sample. The procedure was similar to that described in section 8.2.3, but following deposition, the rotating cylinder electrode was detached, rinsed, dried and carefully mounted on a 'V' block table. The surface profile and average surface roughness (R_A value) for the surface was then measured using a Rank Taylor Hobson Talysurf Model 10, equipped with a 5μm diamond stylus. Great care was taken to preserve the integrity of the deposit and align the sample prior to measurement.

8.2.9 Miscellaneous

In one experimental trial, an attempt was made to monitor the torque required to required to rotate the cylindrical cathode in the reactor, as electrode roughness developed. This was accomplished, in an approximate manner, by monitoring the potential difference across the armature windings of the D.C. drive motor. According to the motor manufacturer, the resultant p.d. reading was proportional to the torque.

When necessary, dynamic viscosity was measured by 'Ubbelohde' pattern, 'U-tube' glass viscrometers, immersed in a thermostatted water bath. For each determination, four separate trials were undertaken, and the mean quoted. Fluid densities were measured by means of a standard density bottle.

8.2.10 <u>Ultrasonics</u>

Preliminary studies on the effect of ultrasound on mass transport controlled deposition of copper to a R.C.E. were carried out in co-operation with Mr. C. Gould. The equipment used was designed and constructed by this worker.

The polished stainless steel R.C.E. of active dimensions d = 1.03, l = 1·76 cm was rotated at speeds of 500-3000 r.p.m. Its position was approximately central in a one litre pyrex cultᵤre vessel (QF FVIL). The rotating cylinder circumference was at a distance of approximately 2 cm from the soluble copper foil anode, and 6 cm from the radiating face of the ultrasonic probes. The three probes, mutually placed at 120° were immersed in a thermostatted 50 litre water bath, and arranged so that their radiating faces pointed towards the axis of the R.C.E.

The transducers, with a lead zirconate/titanate active element were encased in stainless steel to give a radiating face ca. 2 in. diameter. The high frequency generator (DAWE INSTRUMENTS LTD., LONDON, SONICLEAN AUTO TYPE 300/150W/1190A) operated at a power of approximately 150W average, 300W peak at maximum output level, with a frequency of 25 KHz, pulsed at 100 Hz.

9. PILOT PLANT EXPERIMENTAL WORK

This chapter describes experimental work performed on

pilot plant - scale reactors at Ecological Engineering

Ltd., Macclesfield.

Two separate reactors were evaluated:

a 500 A single cathode compartment "Eco-Cell" * and

a 200 A six cathode compartment "Eco-Cascade-Cell" *

---

* "Eco-Cell" and "Eco-Cascade-Cell" are registered trade marks

describing single and multiple cathode compartment rotating

cylinder electrode reactors manufactured by Ecological

Engineering Ltd., Macclesfield.

9.1   500 A Pilot Plant "Eco-Cell"

9.1.1 Introduction

The experimental work undertaken was aimed at evaluating the

performance of an improved design, commercial scale "Eco-Cell"

reactor.   The reactions studied were:

1. deposition of copper from 0.5M sulphuric acid at a

   temperature of ca. 40° C., and

2. deposition of cadmium from a solution containing 128 ppm

   Cd and 127 g dm^{-3} Zn at 60° C.

The first reaction had previously been extensively studied on

a range of "Eco-Cell" assemblies, providing a means for comparison,

while the second reaction was of importance to an organisation

involved in exploitation of the "Eco-Cell" in zinc hydrometallurgy.

The following aspects received attention:

1. cathodic polarisation characteristics

2. reactor conversion and performance

3. product recovery.

9.1.2 "Eco-Cell" Reactor

The 500A "Eco-Cell" reactor is shown schematically in Fig. 9.1.

The design essentially incorporated a concentric rotating cylinder

- diaphragm - anode assembly.   Complete concentricity was disturbed,

however, by the need to provide fluid manifolds and a scraping

mechanism along the length of the cylinder.   For convenience, the

outlet manifold was located in the same cavity as the scraper shaft.

The main reactor body was fabricated from machined sections of high

density polypropylene sections, joined together by welding.   Flanges

were provided at the top and bottom of the reactor body to facilitate

mounting and dismantling.   The reactor body was secured via its

top flange to a horizontal, polypropylene-covered, steel platform.

This platform also served to support a mechanical packed gland,

shaft seal assembly which was lubricated by a water feed.

The 3 inch diameter stainless-steel drive shaft was supported by two vertical roller bearing races ca. 30 cm. apart, driven by a 4 KW D.C. electrical motor and coupled to a 1:1 pulley and belt system. The motor was speed controlled, allowing rotational speeds in the range 100 - 1000 rpm. Electrical power was fed to the shaft by an assembly of eight graphite brushes, spring loaded on metal fingers; a small, auxiliary graphite brush located nearer the cylinder served as a potential pick-up.

The rotating cylinder consisted of a hollowed out, mild steel fabrication, copper plated on its working surface and incorporating polypropylene top and bottom and discs to yield electro-active dimensions of diameter 22.9 cm, length 22.7 cm and surface area 1633 cm^2. The cylinder was fitted to the drive shaft by heat shrinking. The section of drive shaft in the reactor was shrouded by a polypropylene collar which was shaped to minimise reactor volume above the cylinder. The bottom cover of the reactor had a central raised portion which performed a similar function, as did a polypropylene insert in the scraper cavity. The bottom cover carried inlet and outlet manifold tubes.

The manifolds were $\frac{1}{2}$ inch i.d. polypropylene tubes (running parallel to the rotating cylinder)which were drilled at intervals to provide good fluid dispersion. The outlet tube had 10 x 10 mm. diameter holes at a 25 mm. pitch, while the inlet tube had 16 x 5 mm. holes at a 14.5 mm. pitch. The large diameter holes in the outlet helped to prevent blocking by metal powder, while the plurality of holes prevented pressurising of the catholyte compartment.

The scraper device comprised a stellite-tipped blade, located on a vertical shaft. This shaft passed through supporting and sealing glands in the top and bottom of the reactor, and was driven pneumatically in the vertical plane. The pneumatic system automatically moved the scraper blade up the length of the cylinder at a controlled speed (typically 1 cm. s^{-1}), then quickly moved the blade off the cylinder and returned it to the starting position, ready to commence another cycle.

The anolyte and catholyte compartments were separated by a perfluorocarbon, cation exchange membrane, Nafion type. The two membrane sections were supported by perforated polypropylene backing plates and sealed around their edges by a 2 mm. rubber window gasket clamped via polypropylene bolts. The two anolyte compartments were each fitted with a precious metal oxide/titanium anode.

9.1.3 Flow System and Product Recovery

Fig. 9.2 shows a schematic diagram of the flow system which provided essential services to the reactor, including anolyte and catholyte flow circuits, and metal powder separation.

The catholyte was prepared and stored in a mixed and temperature-controlled polypropylene tank which was provided with a gas vent and a funnel for make-up additions. The catholyte solution was pumped from this holding tank through a magnetic flux flowmeter to the reactor, the flow rate being controlled by a bypass loop back to the tank. Depending on the experiment, the catholyte comprised either of the following solutions:

1. copper sulphate in 0.5 M sulphuric acid at ca 40° C, or

2. zinc sulphate, 127 gdm^{-3} with cadmium sulphate additions at 60° C.

The concentration of the metal deposited (copper in the first case and cadmium in the latter case) was maintained by controlled additions of a concentrated solution to the catholyte holding tank by means of a peristaltic pump. The total inventory of catholyte solution in the system was 400 dm^3. The catholyte passed out of the reactor to a vented, conical gas separator where any hydrogen gas could be safely removed from it. From the gas separator, the dilute depleted metal/metal powder slurry passed to a hydrocyclone solid - liquid separator. Here, a concentrated copper powder/catholyte slurry passed from the hydrocyclone underflow to a filter tray. Metal powder collected on to a filter cloth in this tray, while catholyte filtrate returned from the filter tank to the main holding tank by overflowing a weir. Powder-free liquor overflowed the cyclone to return either to the gas separator, or to the holding tank via a water cooled heat exchanger. The catholyte flow system was balanced such that a constant fluid level was maintained in the gas separator

The anolyte, 0.5 M sulphuric acid, was recycled to the anolyte compart-
ments of the reactor via a pump and a small PVC holding tank. The
anolyte inventory was 30 dm^3, and a flow rate of 5 dm^3(min)$^{-1}$ was used.
A water cooled glass coil in the anolyte tank served to maintain the
temperature at ca. 40° C.

Both the catholyte and anolyte holding tanks were provided with drain
valves and sight glasses for convenience, and the catholyte temperature
and flow rate were continuously and automatically monitored.

The catholyte pipework near both the inlet and outlet points to the
reactor was provided with 'T' junctions to facilitate sampling, either
discretely or as a continuous bleed. The sample solutions were analysed
by either discrete atomic absorption spectrophotometry, or continuous ion
selective electrode potentiometry.[396]

9.1.4 Electrical Supplies

Fig. 9.3 shows a schematic diagram of the electrical connections to the
reactor. Faradaic d.c. power was supplied to the "Eco-Cell", via aluminium
busbars and
copper cored flexible leads, from a Westinghouse transformer/rectifier
set (rated 500 A at 12 V).

The electrode potential of the cylinder was monitored relative to a
mercury/mercurous sulphate/0.5 M H$_2$SO$_4$ reference electrode system.
A polypropylene probe with a ceramic frit was positioned 4 mm. away from
the face of the cylinder, and connected to an external reference electrode
reservoir by means of a 0.5 M H$_2$SO$_4$ salt bridge. The cylinder was
potentiostatically controlled, the cell current being adjusted by a
servo-controlled "Variac" regulator in the primary circuit of the
transformer/rectifier.

The cell current was monitored by sensing the potential drop across a
50 mV/500 A shunt in the anode line, by means of a digital voltmeter (DVM).
A second high impedance DVM was used to measure electrode potential,
while an analogue panel meter monitored cell voltage.

Rotational power was supplied to the d.c. cylinder drive motor via a thyristor-controlled speed regulator (Thorn "Stardrive"), the actual shaft speed being measured periodically by a hand held tachometer. The motor armature current was also monitored, as a measure of the power applied to the rotating cylinder.

9.1.5 Experimental Procedure

Both catholyte and anolyte circuits were allowed to flow at their required rates, and the system was allowed to reach its working temperature. The cylinder was then rotated at the required speed, and its surface was preplated with a compact deposit of the metal in question (either copper or cadmium) by deposition at a current density well below that conducive to powder formation.

Electrodeposition of metal powder was carried out by raising the cylinder potential to that corresponding to limiting current operation. Steady state trials were performed by dosing the catholyte tank with the required metal salt concentrate (copper sulphate or cadmium sulphate) and scraping the cylinder continuously to maintain an effectively constant electroactive surface area and roughness.

In one trial, the concentration of metal (copper) was allowed to decay, (no external metal salt additions being made), and the concentration-time and current-time histories were followed.

Polarisation curves were obtained by manually increasing the cathode potential from the rest potential by, typically, 25 mV increments, while recording the corresponding steady currents.

In the case of all trials, the following parameters were normally measured or controlled:

1. catholyte and anolyte temperature

2. catholyte and anolyte flow rate

3. catholyte and anolyte compositions

4 cylinder rotational speed.

9.2   200 A "Cascade Eco-Cell"

9.2.1 Introduction

Following the successful operation of a 10 compartment laboratory cascade

reactor, and a 12 compartment commercial one (see Chapter 6), a "second

generation" design was evaluated.   This new design incorporated several

important features including:

1. the facility for scraping of the rotating cylinder

2. a vertical rotating cylinder

3. removable anolyte/membrane compartments

4. removable baffles to subdivide the catholyte compartment

5. a rigid rubber lined steel reactor body

6. flushed seals at both the top and bottom of the reactor.

The performance of the new design reactor was evaluated both electro-

chemically and from a product recovery point of view.   The reaction

chosen was the well-established deposition of copper powder from 0.5 M

sulphuric acid.

9.2.2 "Cascade Eco-Cell" Reactor

Fig. 9.4 shows a photograph of the six compartment cascade reactor, while

fig. 9.5 shows a schematic diagram.   The reactor body was fabricated

from welded mild steel sections, the internal surfaces being rubber coated.

The central cathode compartment was subdivided into six compartments by

regularly spaced polypropylene baffle plates, whibh were a close fit on

the internal reactor walls.   The baffle to rotating cylinder spacing

was approximately 3 mm.

The rotating cylinder cathode was mounted centrally in the reactor.

The cathode was fabricated from stainless steel and was provided with

polypropylene end caps on its top and bottom surfaces.   The cylinder

was supported by top and bottom bearings, with a seal arrangement at

each end, and was driven at 730 rpm by an oversized 13 KW a.c. motor,

via a pulley and belt arrangement.

The seal arrangement, both top and bottom, consisted of twin lip seals, with a lubricating water flush between. In addition, a positive sulphuric acid flush was provided through the seals into the reactor, to prevent metal powder settlement, and subsequent seal destruction in these areas.

The two anolyte compartments were inserted into the reactor sides, being fabricated from rubber coated steel. The curved compartment side facing the cylinder carried a cation exchange membrane (Nafion), supported between two perforated titanium plates. A soft rubber seal was used as a gasket between the anolyte compartments and the reactor body.

The anode compartments were each equipped with 3 separate anodes, manufactured by perforating 3 mm. nickel plate, followed by rolling the material to conform to the curvature of the rotating cylinder.

The top of the reactor body was flanged on to the main assembly to allow the cylinder and baffles to be removed.

Each of the six catholyte compartments was equipped with a sample point and a reference electrode probe. The effective cylinder dimensions were:

diameter 30.6 cm

compartment length 14.4 cm, and

compartment area 1387 cm^2.

9.2.3 Flow System and Product Recovery

Fig. 9.6 shows a schematic diagram of the flow system serving the reactor, which may be divided into three separate circuits: anolyte, catholyte and water.

The anolyte solution comprised 2.5 M NaOH, stored in a 200 dm^3 polypropylene tank. From this holding tank, the solution was pumped to the bottom of each of the anolyte compartments, overflowing these compartments near the top to return to the tank. Air space was provided in the tank to bleed off oxygen, which was then safely vented. The anolyte temperature was typically 30° C, while the flow rate was 25 dm^3 (min)$^{-1}$.

The 0.5 M sulphuric acid catholyte, containing copper sulphate in the range 0 - 1000 mg dm^{-3}, was maintained at constant temperature in an agitated rubber lined steel tank of approximate capacity 3000 dm^3. For normal flow, the catholyte was pumped via a rotammeter to the bottom of the reactor. After exiting at the top of the reactor, the solution passed via a gas separator and the solid-liquid separators back to the holding tank. The vast majority of copper powder adhered to the cathode. The copper concentration maintained by controlled dosing of the holding tank with a 100 gdm^{-3} H$_2$SO$_4$ solution. Following the deposition trials, copper powder was removed from the cylinder by activating the reciprocating scraper and reversing the catholyte flow to backwash the reactor. The resulting depleted copper/copper powder dilute slurry was pumped via the gas separator into a hydrocyclone. The clarified overflow from the cyclone returned to the holding tank, while the concentrated underflow passed into a thickening cone, where copper powder sedimented. Product could then be withdrawn from the valved bottom of the thickener. The labyrinth areas of the rotating shaft were fed with clarified catholyte to prevent powder settling near the seals. The seals themselves were flushed with clean mains water for lubrication, at a flow rate of 2 dm^3(min)$^{-1}$. To check the operation of the seals, the flow rate into and out of each seal was monitored, as was the labyrinth flush.

9.2.4 <u>Electrical Supplies</u>

Fig. 9.7 shows a schematic diagram of the electrical connections to the reactor, which may be divided into Faradaic supply, rotational supply and electrode potential measurement.

D.C. power was supplied to the reactor by manual adjustment of a 2000 A/16V transformer/rectifier set. The reactor was coupled by means of flexible copper cored leads and aluminium busbars. Actual currents of 0 - 300 A were passed to the reactor, monitored by a digital voltmeter across a standard 75 mV/2000A shunt. Electrical power was supplied to the bottom shaft of the rotating cylinder by two carbon-filled graphite brushes working against a copper slip ring. The anode connections were arranged

so as to engage any number of the three pairs of anodes, each pair lying in the same horizontal plane.

The electrode potential was monitored in each of the six compartments, relative to a saturated calomel electrode. Separate potential pick-up brushes were located on the top and bottom shafts of the rotating cylinder, and either of these served as a reference point, as desired. Each catholyte compartment was equipped with a polypropylene tube/ceramic frit probe, the tip of this being located approximately 4 mm. from the surface of the cylinder. Each probe was connected by a clear PVC liquid junction tube, filled with saturated KCl, to a KCl reservoir containing the saturated calomel electrode. The liquid junction tubes were of approximately the same length, and the reference electrodes had potentials which agreed to within 2 mV. Hence all the electrode potentials measured included a substantially constant liquid junction potential. A six position switch was used to connect the high impedance potential measuring DVM to the required reference electrode.

Rotational power to the a.c. drive motor was supplied by a three phase 440 V supply, and an analogue kilowatt hour meter gave an indication of the total power supplied to this motor.

9.2.5 Experimental Procedure

Two types of experiment were carried out: polarisation trials and steady state deposition trials. Cathodic polarisation data was generated by increasing the total cell current in increments, and monitoring each of the steady compartmental electrode poetntials each time. This procedure was adopted both in the absence and presence of copper in the catholyte. Steady state trials were carried out at various temperatures, flow rates, and total cell currents.

In all cases, the parameters measured or controlled included cell current, cell voltage, electrode potentials, compartment copper concentration, catholyte and anolyte flow rates and temperatures. Frequent checks on the acidity and alkalinity of the catholyte and anolyte were made.

An attempt was made to ensure that each compartment operated at or near mass transport controlled conditions, both to produce powder and to ensure high conversions.

At the end of approximately 6 hours of steady state deposition, the metal powder product was removed from the reactor as described in the previous section, and the speed and efficiency of this process was visually monitored.

10. LABORATORY RESULTS

The results of the author's laboratory studies are reported, which

concern mass transport to smooth and rough cylinders, controlled

potential, selective deposition of metals, and the growth of rough

metal deposits.   The data is presented largely without further

elaboration pending a full discussion in Chapter 12.

10.1 Polarisation Curves

It is important to establish steady state, reproducible polarisation curves in any electrochemical mass transport study. Two obvious variables which merit attention are the surface preparation of the rotating cylinder, and the potential scan rate of the linear sweep unit. Fig. 10.1 shows the limits of reproducibility of the current voltage curve for a standard condition, 0.014M $CuSO_4$, 1.5M H_2SO_4 at 22° C and a cylinder of active dimensions: d = 6.3 cm, l = 4.3 cm, (A = 85.1 cm^2) rotating at 500 r.p.m. (equivalent to 165 cm s^{-1}). The results shown in Fig. 10.1 were obtained by 10 separate trials using copper foil electrodes freshly prepared by polishing with 600 grade emery paper, and degreased with 1, 1, 1- trichloroethane; a fresh electrolyte was used for each trial. This method of preparation led to satisfactory, reproducible (Table 10.1) limiting currents in the approximate potential range - 900 to - 1150 mV (V.M.M.S.) The scan rate employed in the above constant metal concentration trials was 150 mV $(min)^{-1}$.

The effect of electrode surface preparation was also investigated by comparing the effects of chemically and electrochemically polished copper rotating cylinder electrodes against surfaces polished as described above. As shown in Table 10.1 and Fig. 10.1 there were no significant differences in the limiting current and further work was undertaken using wet, 600 grade emery polished surfaces.

The effect of the potential scan rate was investigated (Fig. 10.2), employing various values, 15, 30, 60, 150, 300, 600 and 1500 mV $(min)^{-1}$ under otherwise fixed conditions, i.e. 0.014M $CuSO_4$, 1.5M H_2SO_4, 22° C, and a copper foil rotating cylinder electrode of diameter 6.3 cm, length 4.3 cm and area 85.1 cm^2, rotating at 500 r.p.m. (165 cm s^{-1}).

Following these trials, a scan rate of 150 mV $(min)^{-1}$ was selected
as being a reasonable compromise between the requirements of steady
state and a reasonable experimental rate of progress.

The above refers to a constant electrolyte concentration, which was
maintained by a combination of soluble anodes and electrolyte adjust-
ment.   In the case of certain solutions, e.g. 'as-received' industrial
solutions, the provision of soluble anodes is not always possible.
In such cases, insoluble anodes may be used, possibly in a divided
cell.   The effect of scan rate was also studied under such conditions,
using the above conditions, and a divided cell with a PbO_2/1.5 M
sulphuric acid, anode/anolyte system.   The choice of scan rate becomes
more critical here, as a further restraint is imposed on the use of
low scan rates, where a significant lowering of concentration may
·take place before the limiting current is reached, leading to a
falsely low determination of the latter.   As shown in Table 10.2, a
scan rate of 150 mV $(min)^{-1}$ proves to be a suitable compromise once
again under such conditions.   Wherever possible, the concentration
of metal ions was held constant during polarisation measurements,
and the actual concentration was frequently analysed in the vicinity
of the limiting current, as a safeguard.

It may be noted that flow rates through the catholyte compartment
had no significant effect on the limiting current in the range
0 - 10 $1(min)^{-1}$ (corresponding to a minimum nominal residence time
in the 1 litre reactor of 6 s).

I0.2   Mass Transport to a Smooth Rotating Cylinder Electrode

As the non-concentric geometry of the experimental reactor was somewhat different from that of previous workers, it was most desirable to obtain data on mass transfer to a smooth R.C.E. over a reasonably wide range of conditions. Comparison was then sought with previous work. The approach adopted was to determine the limiting current from polarisation curves (as explained in the previous section), under a range of conditions including variable temperature, cylinder rotational speeds and metal concentration. The results of this study are shown in Table I0.3 and plotted in Figs. I0.3 and I0.4 as $(St)(Sc)^{0.644}$ vs. (Re). The transport properties of the acid cupric sulphate electrolytes used were obtained as described in Section I0.I2 .

The experimental data is seen to correspond to mass transport values greater than those predicted by the Eisenberg, Tobias and Wilke correlation (Fig.I0.3)

$$j_D' = (St)(Sc)^{0.644} = 0.079 \ (Re)^{-0.30} \qquad , \qquad \text{Equation I0.I}$$

but smaller than that predicted by the correlation due to Robinson and Gabe (Fig.I0.4)

$$j_D' = (St)(Sc)^{0.59} = 0.079I \ (Re)^{-0.3I} \qquad \text{Equation I0.2}$$

It was considered that insufficient data was available to perform a three dimensional, least squares regression analysis. The computer programme described in Appendix I was, however, used to treat Robinson's data[68]. The correlation obtained was

$$(St) = 0.0896 \ (Re)^{-0.3I}(Sc)^{-0.60} \qquad \text{Equation I0.3}$$

While the (Re) and (Sc) exponents are apparently similar to those reported by Robinson, the constant 0.0896 is appreciably (I3%) higher. Statistical information is given in Table I0.4 .

It is interesting to compare the shape of polarisation curves for
copper deposition more closely, and in particular to examine the
effects of concentration and rotational velocity under otherwise
constant conditions.

Fig. 10.5 indicates the effect of varying concentration of copper
(in the range 1 to 890 ppm) in a 1.5M H_2SO_4 electrolyte at 22° C,
using a rotating cylinder electrode of effective diameter 6.3 cm
and length 4.3 cm (area = 85.1 cm^2) rotating at 500 r.p.m. (165 cm s^{-1}).
Solutions for this study were prepared by serial dilution of a 0.014M
$CuSO_4$ + 1.5M H_2SO_4 solution by 1.5M H_2SO_4. It may be seen that with
decreasing metal concentration, the limiting current plateau becomes
less well defined. Considering Fig. 10.5, the effect of concentration
may be more clearly seen in Fig. 10.6, where the current is plotted
on a logarithmic axis. Fig. 10.6 further indicates that varying
concentrations of copper have little effect in the low potential
regions where the reaction is not under mass transport control. In
addition, it is interesting to note that the rest potential of the
copper R.C.E. becomes more negative with increasing dilution, in a
near-Nernstian fashion (Fig. 10.7) i.e. the electrode behaves as a
reversible Cu/Cu^{2+} couple.

Fig. 10.8 indicates the effect of varying rotational velocity in an
electrolyte containing 0.014M $CuSO_4$ and 1.5M H_2SO_4 at 22° C, using
a rotating cylinder as described above but rotating in the range
100 - 1000 r.p.m. (33 to 330 cm s^{-1}). It may be seen that the
limiting current plateau becomes less well defined as the rotational
velocity is increased.

Fig. 10.9 is a plot of current against rotational speed for a cylinder held at various potentials, rotating in 0.014M $CuSO_4$ + 1.5M H_2SO_4, and having dimensions identical to those described above. This figure indicates that the effect of rotational speed on the observed current becomes more marked (i.e. mass transport control becomes more important) as the overpotential is raised. At potentials in the region of -1000 mV ($VMMS/1MNa_2SO_4$), a straight line is obtained on the log I vs log (RPM) plot, with a slope 0.7, in accordance with:

$$I_L = \text{constant } U^{0.7} \qquad \text{EQN 10.4}$$

The data presented in Fig. 10.9 were obtained by impressing a fixed potential on the R.C.E., and reading a steady state current, at a given RPM. Ideally, the current - potential data points should correspond with the steady state polarisation curve values.

Considering Fig. 10.5 in more detail, as the mass transport coefficient remains constant, the limiting current observed should be proportional to the metal ion concentration:

$$I_L = \text{constant } C \qquad \text{EQN 10.5}$$

This is true to a good approximation, as shown as Fig. 10.10. The mass transport coefficient for the 500 r.p.m. trials is reasonably constant, as is expected, at 3.3×10^{-3} cm s^{-1} (Table 10.5).

Equations 10.5 and 10.4 are, of course, specific cases of the more generalised correlation shown in equation 10.2. For a fixed electrolyte at a constant temperature, and a given R.C.E., equations 10.5 and 10.4 may be combined to give:

$$I_L = \text{constant } C \ U^{0.7} \qquad \text{EQN 10.6}$$

The effect of changing the electroactive surface area, under otherwise constant conditions, is shown in Fig. 10.11. As expected, the area is approximately proportional to the limiting current (Fig. 10.12) i.e. the current density is constant. The area change in these experiments was effected by masking differing areas of a given diameter (6.3 cm) cylinder to give different effective lengths of 5.05 cm, 4.3 cm, 2.15 cm and 1.1 cm (equivalent to areas of 100 cm^2, 85 cm^2, 42.5 cm^2 and 21.5 cm^2).

Fig. 10.13 shows the effect on the polarisation curve of varying the electrolyte temperature in the range 22 - 60° C for conditions otherwise comparable with the above, and a fixed rotational velocity of 500 r.p.m. The progressive increase in the limiting current may be clearly seen. Fig. 10.14 offers a graph of limiting current against temperature.

10.3 Concentration Decay Under Potentiostatic Control

In these trials, the catholyte chamber was charged with a fresh, 1 litre batch of 0.014 M $CuSO_4$ + 1.5 M H_2SO_4, and the cylindrical cathode was preplated for 30 s at a potential of -600 mV (V.M.M.S./ 1M Na_2SO_4). The copper concentration of the solution was then corrected to 0.014M, the potential was raised to its working value, and the experiment began. The current was monitored continuously by a chart recorder, and the solution was frequently analysed by withdrawing negligibly small, discrete samples by hypodermic syringe or micropipette, followed by dilution and direct atomic absorption spectrophotometry.

Preplating the 600 grade emery paper, wet polished surface was found to be necessary to ensure reproducible behaviour in these trials. Once again, however, chemical polishing or electropolishing offered no significant advantage and it will be seen that electrode surfaces

prepared by these specialised techniques did not behave in significantly different manner to electrodes prepared by preplating.

Fig. 10.15 indicates the concentration decay obtained at 340 r.p.m. and a control potential of - 1000 mV (V.M.M.S./1M Na_2SO_4). Ideally, an exponential decay would be expected, but a 'knee' is evident in the curve after a period ≈ 60 minutes. The effect may be more clearly seen by presenting concentration on a logarithmic axis, when a straight line should result. Fig. 10.16 illustrates this together with the limits of reproducibility for 5 successive trials with the preplated electrode. The results of separate trials with chemically and electrochemically polished surfaces are shown in Fig. 10.17, and lie within the limits of reproducibility.

Fig. 10.18 shows the current-time behaviour corresponding to Fig. 10.16. It can be seen that the current decays, goes through a minimum and increases again, passing through a maximum before its eventual decay. This rather complicated behaviour may be attributed to the competitive effects of decreasing current due to a diminishing concentration, and increasing current due to development of a rough deposit.

Fig. 10.19 offers a plot of current against concentration (according to Figs. 10.17 and 10.18) while Fig. 10.20 follows the development of mass transport with time for this case.

Fig. 21 follows the change in concentration with current density, showing the apparent deterioration in the current efficiency for copper at low concentrations.

The effect of varying the potential at which deposition takes place
is illustrated in Fig. 10.22. The current histories corresponding
to these trials are shown in Fig. 10.23.

The resultant deposit from the trial described in Fig. 10.16 was used
in a further experiment. The copper concentration was corrected to
its original value of 0.014 M (890 ppm), and the experiment repeated
(Fig. 10.24). It can be seen that the rough deposit results in an
immediately high rate of decay, comparable with the fast decay of
Fig. 10.16.

The effect of rotational cylinder velocity, under otherwise comparable
conditions, is shown in Fig. 10.25. In all the cases studied, the
first order rate of decay increased after a certain time. This
critical time decreased with increased velocity. Fig. 10.25^a offers
an allometric plot of rotational velocity against rate constant for
the initial and final slopes seen in Fig. 10.25, indicating that the
initial rate constant is dependent upon the rotational velocity raised
to the power 0.73, whereas the final rate constant is directly
dependent upon the rotational velocity.

10.4 Potentiostatic, Controlled Separation of Metals

Fig. 10.26 shows the concentration decay of copper during its deposi-
tion from a 0.014M $CuSO_4$ and 0.014M $ZnSO_4$ + 1.5 M H_2SO_4 solution at a
controlled potential of - 1000 mV (M.M.S.) and 22° C. The behaviour
is similar to that already seen for copper deposition from acid
sulphate solutions. The initial and final rates of decay are com-
parable with Fig. 10.16, and the steady state polarisation curve,
Fig. 10.27 shows a clearly defined limiting current due to copper
deposition in the potential range - 900 to - 1150 mV.

Figs. 10.28 and 10.29 show analagous curves for the deposition of copper from a 0.014M $CuSO_4$, 0 014M $NiSO_4$ + 1.5M H_2SO_4 solution. Again, the behaviour was comparable to Fig. 10.16.

At the end of each decay trial, the deposits were dissolved in A.R. grade sulphuric acid, and following dilution, the solution was analysed for Zn or Ni, by atomic absorption epectrophotometry. The results indicated that the copper purity was high, being contaminated by only 0.4% W/W Zn or 0.25% W/W Ni. In the case of both Fig. 10.26 and 10.28 there was no detectable change in the zinc or nickel concentration in solution, in accordance with the above results.

The deposition of silver and copper from 0.014M $AgNO_3$ and 0.014M $Cu(NO_3)_2$ in 0.15M HNO_3 at 22° C is described by the polarisation curve of Fig. 10.30. A limiting current attributable to silver deposition is evident at potentials + 160 — + 300 (V.S.C.E.), while a limiting current copper plateau appears at - 350 to - 600 mV.

Selective deposition of silver was attempted at a controlled potential of + 222 mV S.C.E. on to a stainless steel cylinder, Fig. 10.31. The final deposit was analysed as 0.25% Cu W/W.

Following the above studies with synthetic solutions, further trials were undertaken to treat cyanidic,mixed metal solutions. Two solutions received attention, (Table 10.6), both being supplied by a large international organisation involved in precious metal electroplating.

The first solution, an electroplating dragout, contained gold as the major component and was acidic, pH 4.8. Potentiodynamic polarisation studies using a stainless steel rotating cylinder in an undivided cell with a stainless steel anode, produced the curve shown in Fig. 10.32.

In the absence of any clearly defined limiting current behaviour, controlled potential, concentration decay experiments were under- taken at 3 separate, increasing control potentials, - 1000, - 1370 and - 1750 mV $(V.M.M.S./1M\ Na_2SO_4)$. The resulting decay of the gold concentration is shown in Fig. 10.33. At all potentials, the decay followed apparent, overall first order kinetics but, surprisingly the   rate increased in the order - 1370, - 1000 and - 1750 mV. In all cases, the deposit was golden in colour, and compact, i.e. there had been no roughness development. The current-time behaviour corresponding to the above decays is shown in Fig. 10.34.

The second cyanidic solution studied was a dilute multimetal liquor obtained by backwashed caustic regeneration of a nitric acid cation exchange metal regeneration unit (Table 10.6), and had a pH of 11.7. It was revealed in preliminary studies that selective deposition was unlikely at such a high pH in a complexed, cyanide solution, and hence the liquor was gradually acidified, to progressively lower the pH. At a pH of approximately 4.0, a white precipitate began to form, and the silver content of the solution fell dramatically (Table 10.7), indicating AgCl precipitation. At lower pH values, ~ 3.5, hydrogen cyanide was evolved. Potendiodynamic polarisation curves (Fig. 10.35) were obtained at various pH values at scan rate of 300 mV $(min)^{-1}$, 20° C and a cylinder of diameter 6 cm, length 4·5 cm and active electrode area 85.1 cm^2, rotating at 500 r.p.m. It can be seen that the lowering of pH generally causes the curves to shift in the more noble direction. At pH 4.0, two apparent current plateau regions were visible, and potentials corresponding to these regions were selected for controlled potential concentration decay experiments. pH 4 was selected as a standard condition for these trials, as it appeared to represent the lowest pH obtainable without significant loss of copper and silver from solution, by precipitation.

From the polarisation curve (Fig. 10.35), it was considered that the apparent plateau in the range potential - 400 to - 650 mV might be due to mass transport controlled discharge of a silver cyanide complex, and a potential of - 550 mV was first chosen for a controlled concentration decay of duration 140 mins (Fig. 10.36), in a divided cell of catholyte volume 1 litre. The gold concentration remained constant during the electrolysis, whereas the silver concentration decreased to a sub ppm value. Some copper deposition also occurred, however, during the first 70 minutes, the Cu level decreased from 2.3 ppm to 10 ppm, remaining at the last value for the duration of the experiment.

The experiment was repeated (Fig. 10.37) using an undivided cell with a stainless steel anode. Once again, gold was not removed from solution, and copper only slightly, but the silver level fell to 2.6 ppm where it remained for the duration of the experiment.

In a final experiment (Fig. 10.38) a control potential of - 900 mV was employed with an undivided cell and the electrolyte from the previous trial. The gold level remained reasonably constant while both the copper and silver levels fell, the former at a greater rate.

10.5 Potentiostatic Growth of Copper Deposits: Current-time History

The transition from a smooth deposit to a rough one was followed by studying the increase in current with time for a fixed electrolyte, (0.014M $CuSO_4$ + 1.5M H_2SO_4, 22° C), and a given cylinder (d = 6.3 cm, l = 4.3 cm, A = 85.1 cm^2) rotating at various rotational velocities in the range 100 - 1000 r.p.m. The electrode was potentiostatically controlled at - 1000 mV (M.M.S./1M Na_2SO_4) for the duration of each trial, giving the results shown in Fig. 10.39. It can be seen that

the curves may be divided into three distinct zones, an initial, final and transition region. Initially, the current corresponds closely with the limiting current obtained on a smooth R.C.E., but after a critical time (which decreases with increasing rotational velocity), the current progressively rises, asymptotically approaching a reasonably steady value after a second critical time (which also decreases with increasing rotational velocity).

Fig. 10.40 indicates the limits of reproducibility for these trials. Despite careful surface preparation and experimental work, some scatter was always apparent, particularly at the higher rotational velocities.

Fig. 10.41 presents a log - log plot of the mass transfer coefficient against velocity (as obtained from the results of Fig. 10.39) for both initial, smooth cylinder and for rough, final mass transfer. The smooth cylinder results conform to the general equation:

$$I_L \propto u^{0.74}$$

whereas the roughened cylinder data are not well correlated. An approximate relationship would be:

$$I_L \propto u^{0.90}$$

Fig. 10.42 shows the effect of varying the control potential in the range - 600 to -1150 mV. (V.M.M.S./1M Na$_2$SO$_4$) for deposits grown at a fixed rotational velocity of 340 r.p.m.

10.6 Potentiostatic Growth of Copper Deposits: Surface Profilometry

The development of surface roughness was monitored directly using a Rank Taylor Hobson, Talysurf 10 profilometer with a 2 mN force stylus (A112/1266, or A112/1269 for low magnification) used in the skidless mode. Trials were undertaken at a fixed concentration 0.014M Cu + 1.5M H$_2$SO$_4$ at 22° C, fixed potential (- 1000 mV·VVMS/1M Na$_2$SO$_4$) and two rotational velocities, 180 and 340 r.p.m. Higher rotational velocities resulted in deposits whose roughness exceeded the capability

of the measurement instrument, even using the minimum possible magnification. Deposits were withdrawn from the cell after a given time, and subject to measurement of the Ra (average roughness) value defined as the arithmetical average of the profile departures above and below the reference centre line. Further information on the instrument and the technique are given in Appendix 2.

Fig. 10.43 shows the increase in Ra with time at both 340 and 180 r.p.m. Reproducibility was poorer at higher times, as with the current - time experiments. It should be noted that a stylus change was necessary for measurements above 5 μm.

In the case of deposits from the 340 r.p.m. trials, detailed measurements were made, and typical surface profiles were recorded at various times, as shown in Fig. 10.44.

10.7 Potentiostatic Growth of Copper Deposits: Scanning Electron Microscopy

The effects of control potential and rotational velocity were studied on the development of roughness as revealed by a scanning electron microscopy of the deposits at various times. Each deposit was extensively examined at increasing magnifications, and Figs. 10.45 to 10.47 are typical photomicrographs selected from these studies.

The series of photographs in Fig. 10.45 shows the progressive development of roughness at a potential of - 1000 mV (M.M.S./1M Na_2SO_4) in 0.014M $CuSO_4$ + 1.5 M H_2SO_4 at 22° C, using a cylinder of d = 6.3 cm, l = 4.3 cm, A = 85.1 cm^2, rotating at 340 r.p.m.

Fig. 10.46 illustrates the effect of electrode potential in the range

- 800 to - 1150 mV for deposits plated for a nominal 60 mins time at

340

340 r.p.m. in 0.014M $CuSO_4$ + 1.5M H_2SO_4 at 22° C.

Fig. 10.47 shows the effect of r.p.m. on deposits plated under conditions

comparable otherwise with the above experiments.

Several special features are shown in Figs. 10.48 - 10.50.

10.8 Mass Transfer to Rough - deposit Rotating Cylinders

Several trials were undertaken to examine the mass transport for

copper deposition on to (already) rough deposits.   These deposits had

been previously grown under controlled conditions of concentration,

potential, rotating cylinder geometry and rotational speed, and time,

as described in previous sections.

Fig. 10.52 shows the polarisation behaviour for both smooth electrodes

and for cylinders which had been electrodeposited with copper at - 1000

mV for set times.   In all cases, the curves refer to 0.014M + 1.5M H_2SO_4

at 22° C and a cylinder of diameter 6.3 cm and active length 4.3 cm,

rotating at 340 r.p.m.   It can be seen that the limiting current

progressively rises with increasing time, due to the development of

roughened deposits.   The limiting currents observed compare closely

with the values recorded in Fig. 10.39.

Fig. 10.53 indicates the relationship between the limiting current

(measured as the steady state current at - 1000 mV) and the rotational

velocity of the above cylinder for deposits previously grown for set

times.   It can be seen that for low times, $\sim$5 mins, the curve

exhibits a slope of 0.74 indicative of a substantially (hydrodynamically)

smooth electrode.   At greater times, however, the slope approximates

to 1, indicative of a hydrodynamically rough R.C.E. At times in excess
of, say, 100 min, there was relatively little difference in limiting
current values at a given r.p.m.

The effect of abruptly removing a rough deposit is illustrated in Fig.
10.54. In this experiment, a smooth preplated stainless steel rotor of
diameter 6.0 cm and length 6.3 cm rotating at 360 r.p.m. was plated at
- 1000 mV in 0.014M $CuSO_4$ + 1.5M H_2SO_4. As in Fig. 10.39, the (limiting)
current progressively increases, reaching a more stable value after, say,
120 mins. After 180 mins, the cylinder was scraped by bringing in a
full-length 2 mm thick tufnol blade perpendicular to the rotating
cylinder axis. The cylinder was rapidly wiped substantially clean
of the rough deposit, and the current dropped dramatically to a value
somewhat in excess of the original.

10.9 Mass Transport to Knurled, Rough Rotating Cylinders

Mass transport to rough electrodeposits represents a difficult system
for study, as the roughness is difficult to characterise, and is rather
random, having a varying degree and spacing of protuberances. The
production of surfaces having a deliberate, machined roughness, such
as knurling should facilitate characterisation of the roughness, and
has been utilised by other workers.

Fig. 10.55 shows limiting current as a function of rotational speed
for 1.5 cm diameter dylinders of knurled peak to valley roughness
0.0018, 0.003 and 0.025 cm, compared to a smooth electrode.

Fig. 10.56 shows a comparable plot for 6.0 cm diameter cylinders of
roughness 0.016, 0.040 and 0.060 cm, compared to a smooth electrode.

Figs. 10.55 and 10.56 indicate that the relationship for smooth R.C.E.'s
is of the form:

$$I_L \propto (w)^n$$

where n is $\approx$ 0.70.

In the case of the rough, knurled electrodes, n $\approx$ 1.0, and the mass
transport increases, for a given rotational speed, with increasing
roughness.

Fig. 10.57 offers a composite plot of $j_D' = (St)(Sc)^{0.644}$ against Re)
for the results of figs. 10.55 and 10.56.

10.10 Effect of Thiourea on Mass Transport of Copper to a Rotating
Cylinder Cathode

The effect of thiourea was studied with respect to rest potential,
polarisation behaviour, current and concentration decay under controlled
potential conditions, and current time behaviour at constant copper
concentration.

Table 10.8 shows the effect of thiourea (10^{-5} - 10^{-1} M) on the open circuit
potential of a smooth copper R.C.E. (340 r.p.m.) in 0.014M $CuSO_4$ + 1.5M
H_2SO_4 solution at 22° C. The rest potential becomes more negative (less
noble) with increasing thiourea concentration. For small thiourea
additions (10^{-4} M) there is little variation, but a much greater influence
was seen at higher levels (10^{-3} M). At high concentrations (10^{-1} M)
the rest potential became unstable, and the electrode became coated with
a dark film.

Fig. 10.58 indicates the marked effect of thiourea on the cathodic polarisa-
tion curves. The behaviour is somewhat irregular and complex, but a
general increase polarisation was seen. The effect is perhaps better
shown by Fig. 10.59 which offers a plot of overpotential against current.

At low concentrations $(10^{-3}, 10^{-4}$ M) the curve shifts to decreased currents at a given potential, while at high concentrations, the reverse trend is seen. The behaviour is irregular with respect to thiourea concentration, however.

Figs. 10.60 and 10.61 show copper concentration and current decays in a batch R.C.E.R., in the absence and presence of thiourea. At a thiourea concentration of 10^{-3} M, the concentration decay appeared similar to that of a predicted smooth R.C.E., while at lower additive concentrations $(10^{-4}$ M), an increased rate was apparent after some 100 min. At low $(10^{-5}$ M) levels, the behaviour was entirely similar to pure solutions. At high levels of thiourea, $(10^{-2}, 10^{-1}$ M) a much reduced rate of decay was observed: indeed at the 10^{-1} M level, the copper deposition reaction was almost 'poisoned' and the R.C.E. was coated by a dark film.

The growth of current with time at constant copper concentration is shown in Fig. 10.62. At low thiourea concentrations, $(10^{-5}$ M) growth is largely uninhibited. At intermediate concentrations, behaviour is roughly equivalent to a smooth electrode, while the situation is complicated at high levels $(10^{-1}, 10^{-2}$ M).

10.11 <u>Mass Transport to a Rotating Cylinder Cathode in an Ultrasonic Field</u>

Figs. 10.63 and 10.64 represent the effect of ultrasonic stimulation of a R.C.E. on copper deposition. Fig. 10.63 shows a two-fold effect. Firstly, the polarisation curves appeared to be bodily shifted to lower overpotentials by the ultrasound. Secondly, a noticeable increase in the limiting current is seen for each of the rotational speeds.

Fig. 10.64 offers a plot of mass transport coefficient against Reynolds Number for the data of Fig. 10.63. In the absence of ultrasound, the results are in reasonable agreement with the relationship:

$$K_L \propto (Re)^{0.77}$$

in common with other studies involving a smooth R.C.E.

In the presence of ultrasound, however, a marked increase in K_L is observed.

The data are not readily correlated by a simple equation.

10.12 Cell Voltage and Brush Losses

Although care was taken to avoid eccentricity, and provide a correctly fitted, smooth running, conductive power brush and slip ring assembly, some voltage loss is inevitable. In addition, the rotating shaft will also have a finite potential drop. Fig. 10.65 indicates the voltage drop at various cell currents by measuring cell voltage at the power brush electrical connection in comparison to the voltage measured at the lower potential pick up brush. Several conclusions may be drawn from this figure:

1. there was a significantly high voltage drop over the power brush/slip ring/shaft assembly, reaching some 0.61 V at 10A. This justifies the use of the separate pick up brush for monitoring and controlling potential.

2. The slope of the cell voltage versus current curve is approximately constant at currents greater than 1A, the value of this slope is equivalent to the overall effective cell resistance, 0.2 ohm.

3. The brush/shaft assembly resistance is also reasonably constant at $\approx$ 0.06 ohm.

10.13 Effect of Gas Sparging on Mass Transport to a Rotating
   ### Cylinder Cathode

Gas sparging is known to be important in enhancing mass transport to near stationary cathodes, as in certain electroplating baths for example. It was therefore interesting to study the effect of nitrogen bubbling on mass transport to a rotating cylinder. In order to achieve a good distribution of gas into the cell, the bottom of the cell contained a circular groove which carried a circular tube manifold, ca. 5 mm i.d. perforated at 6 mm intervals with 1.5 mm holes. Nitrogen was sparged through the cell at volumetric flow rates up to 1 litre per minute, but the measured

effect on the cathodic polarisation curve for copper deposition (Fig. 10.66) was very small, and insignificant, the maximum apparent increase in the limiting current being $\approx$ 6%.

10.14 Transport Properties

During the course of the studies reported in this thesis, it became necessary to collate and extend data on the density, dynamic viscosity, and diffusion coefficients of cupric ions, in sulphuric acid media in order to calculate mass transport relationships. This largely amounted to extending Robinson's data to 60° C, followed by a comparison with literature values. The results are collected in Fig. 10.67 - 10.69 for reference and completeness.

11.   PILOT PLANT RESULTS

The pilot plant results presented in this chapter largely concern mass transport controlled deposition of copper powder (or cadmium - section 11.1.2) in Eco-Cell reactors.

The data reported in sections 11.1 and 11.2 were largely obtained by the author, in co-operation with the staff of Ecological Engineering Ltd., Macclesfield.

The compendia of data in sections 11.3 and 11.4 were compiled and derived from original laboratory books and reports, and are presented by coutesy of Ecological Engineering Ltd.

11. PILOT PLANT RESULTS

11.1 500A Pilot Plant 'Eco-Cell'

11.1.1 Copper Powder Electrodeposition

The general experimental conditions are summarised in Table 11.1

Polarisation

Fig. 11.1 shows typical cathodic polarisation curves obtained for potentials
in the range - 340 to ± 1150 mV (MMS). The curves refer to a background
electrolyte of 0.5M H_2SO_4 at 20° C, and a powdery copper deposit on the
R.C.E. The two curves were obtained at analysed reactor copper concen-
trations of 138 and 7.1 mg dm^{-3}. The curve at the latter concentration
may largely be attributed to hydrogen evolution, which is evidenced by
the relatively large increase in current at potentials $>$ - 950 mV (V.M.M.S.)
The rest potential for the freshly copper plated electrode was typically
- 345 mV (V.M.M.S.)

The copper deposition curve exhibits a tendency to a plateau at potentials
in the range - 750 to - 950 mV, corresponding to mass transport controlled
deposition. The absence of a clearly defined plateau is partially due to
a varying copper concentration in the reactor, the concentration decreasing
as the current is raised (as the conversion over the reactor increased with
a substantially constant inlet concentration). The rapid increase in
current at potentials above - 950 mV reflects the incidence of hydrogen
evolution as a secondary reaction.

In order to obtain better defined limiting currents, polarisation curves
were obtained in the region of mass transport control only i.e. at potentials
in the range - 950 to - 700 mV. The copper concentration was checked
during the scanning of each curve.

It can be seen in Fig. 11.2 that the plateau region is much more clearly
defined, enabling limiting currents to be discerned. This is possibly
due to the largely undisturbed conversion over the reactor leading to a
substantially constant reactor copper concentration.

Fig. 11.2 indicates an increase in the limiting current with a higher

copper concentration.   Taking limiting current values corresponding to

a potential of - 850 mV, Table 11.2 compares mass transport coefficients,

K_L obtained from the data in Figs. 11.1 and 11.2.   Values lie within

the range 0.238 - 0.272 cm s^{-1}, showing that the calculated mass transport

is reasonably constant over the experimental range of concentrations,

40 - 484 mg dm^{-3}.

The results of Table 11.2 are plotted in Fig. 11.3 as I_L against C.   A

straight line through the origin is obtained, the parameters being related

by K_L.   An average K_L may be derived from the slope of Fig. 11.3 as

0.262 cm s^{-1}.

Steady State Electrolysis

Following the polarisation studies, a series of trials were performed

under steady state conditions;   the results are collected in Table 11.3.

For each set of data, the mass transport coefficient, K_L has been calculated

(assuming that only hydrogen evolution had occurred as a secondary reaction)

by means of equation 6.15 for a single pass   R.C.E.R:

$$\frac{C_{OUT}}{C_{IN}} = \frac{1}{1 + K_L A/N} \qquad \qquad \text{EQUATION 6.15}$$

The effective limiting current has then been obtained from K_L, knowing the

reactor concentration $\equiv C_{OUT}$.

Several observations may be made regarding the results of Table 11.3 :

1. K_L values varied in the range 0.368 - 0.425 cm s^{-1}.

2. An increase in the reciprocating scraper speed from 0.91 to 9.1 cm s^{-1}

      had no apparent effect on K_L.

3. The conversion factor C_{IN}/C_{OUT} varied within the range 1.90 - 2.04 .

4. These conversion factors are appreciably higher than the theoretical

      value of 1.73.

Fig. 11.4 offers a plot of I_L against C_{OUT} for the results of Table 11.3

(c.f. Fig. 11.3).

Decay Trials

Fig. 11.5 illustrates the decay of C_{IN}, C_{OUT} and I with time, corresponding to the data in Table 11.4. The concentration decay lines appear linear on the semilog coordinates, indicating an apparent first order decay. Results F, G and H are abruptly separated from C, D and E, due to a change in flow rate after result E. The slope of line F G H is, however, similar to that of line C D E, indicating a consistent mass transport.

The gradient of the limiting current decay curve (Fig. 11.6) is comparable with that of the concentration decay curve.

Miscellaneous

Fig. 11.7 shows a plot of total cell voltage against total cell current for the above results. A straight line relationship is evident, the slope giving the averaged effective cell resistance, as 0.0138 ohm. The curve originates from a voltage of 1.8 V at open circuit.

The faradaic power supplied to the cell is also displayed in Fig. 11.7, as a function of current. As expected by the relationship :

$P = I^2R$, the faradaic power increased steeply as cell current was raised.

11.1.2 Cadmium Powder Electrodeposition from Zinc Calcine Liquors

The general experimental conditions were as shown in Table 11.5.

Polarisation

Fig. 11.8 illustrates a typical cathodic polarisation curve, for potentials
in the range - 630 to - 1370 mV (V.M.M.S.) The inflection in the poten-
tial range - 1150 to - 1300 mV may be attributed to cadmium deposition
under mass transport control. At potentials more cathodic than - 1300 mV,
the current rises steeply due to the incidence of zinc deposition and
hydrogen evolution as additional side reactions.

Steady State Electrolysis

At the rather low limiting currents involved in the deposition of Cd from
low concentration solutions, the potentiostat controller did not function
very well, and a decision was made to operate at constant cell current.
Table 11.6 presents the results of a series of trials performed under
controlled conditions.

11.2 200 Amp Eco-Cascade Cell

11.2.1 General Conditions/Polarisation

The general operating conditions are shown in Table 11.7.

Preliminary work on this cascade reactor included polarisation curves

for each compartment with respect to hydrogen evolution.   Typical

curves are shown in Fig. 11.9 (which refers to 1.0M H_2SO_4 at 60° C) as

plots of compartment electrode potential (S.C.E.) against cell current.

For a given cell current, the measured potential generally increases

with higher compartment numbers.   A particularly rapid increase in

current, for a given apparent potential, is evidenced for potentials

more negative than, say, -450 mV (S.C.E.)

The total cell voltage as a function of current was measured during the above

polarisation work.   Fig. 11.10 displays cell voltage versus current,

approximating a linear behaviour;   the gradient gives the averaged overall

reactor resistance as 0.015 ohm.

Copper sulphate additions were made to the electrolyte, and a number of

·trials were conducted to examine the polarisation characteristics for

copper deposition,/hydrogen evolution.   Typical results are shown in

fig. 11.11.   Behaviour is rather complex, but a tendency to an inflection

suggesting mass transport control is seen at potentials in the approximate

range -350 to -450 mV

11.2.2 Steady State Electrolysis

A large number of steady state trials were undertaken, monitoring in each

case the catholyte flow rate, temperature, current, potential profile and

copper concentration profile over the cascade.   Typical results are

compiled in Tables 11.8 to 11.19.

11.2.3 Concentration Decay

In one trial, the reservoir copper dosing system was switched off, and the concentration was allowed to be depleted in the system. Fig. 11.12 shows the inlet and individual compartment concentrations recorded initially then after 30, 37 and 47 mins.

The results of section 11.2.2 generally showed a reasonable conversion in the early compartments of the reactor (1, 2, 3 and possibly 4). In higher compartments, however, the conversion was extremely low or even negative. This effect was traced to an internal channelling of electrolyte from compartment 1 to the higher compartments. The bypassing of a small flow rate of relatively high concentration from compartment 1 to 4, 5 or 6 effectively destroyed cascade action in the higher compartments.

11.2.4 General Comments

A number of observations could be made regarding general operation of the reactor. 1.The cylinder was readily scraped during the backwash/product removal cycle, the freshly scraped cylinder revolving more freely with less vibration and requiring less rotational power.

2. The glut of copper powder product obtained after 8-10 hours electrolysis rapidly blocked the hydrocyclone separation system; a simple sludge cone or large filter tray would probably have provied a more efficient device.

3. The overall power consumption of the reactor was approximately 11.5 KWhr/KgCu, which comprised contributions from Faradaic power (ca. 4.9 KWhr/Kg) and rotational power (6.6 KWhr/Kg).

4. The flushing water circuit was shown to be very important in protecting the shaft seals. In the absence of a flush on the lower seal, destruction of the component occurred rapidly, due to the sharp, abrasive copper powder.

11.3 Compendium of Eco-Cell Mass Transport Data

The results presented in this section have been compiled with the co-operation of the staff of Ecological Engineering Ltd. The data generally refer to copper deposition from acid sulphate solutions 1.0M H_2SO_4) at 60° C.

Four separate membrane reactors have been utilised in obtaining the data:

1. Lab. Rig 1 (50A)

2. Mini Cell (100A)

3. 500 Amp Pilot Plant

4. 2KA Pilot Plant

The essential characteristics of each reactor are outlined in Table 11.20.

The data for each reactor is listed in Tables 11.21 - 11.24, and presented in Figs. 11.13 - 11.16 as plots of $j_D' = St (Sc)^{0.644}$ against (Re). Comparison is made with the equation due to Holland: $j_D^1 = 0.0791 (Re)^{-0.08}$

Fig. 11.17 is a composite plot of data from Figs. 11.13 - 11.16.

It should be noted that 'limiting currents' have not been obtained by conventional polarisation curves for the above data. Rather, the 'effective' of 'useful' current for copper removal has been calculated knowing the conversion in the reactor concerned, utilising the equation:

$$I = \frac{N (C_{IN} - C_{OUT})}{329.2}$$

where N is the flow rate in $cm^3 s^{-1}$.

11.4 Compendium of Eco-Cascade-Cell Mass Transport Data

Data obtained from an improved 200A Cascade reactor has already been reported in section 11.2.   This section concerns data from previous designs:

1. 100A Laboratory Cascade Reactor

2. 1KA Commercial Cascade Reactor

Details of these reactors are listed in Table 11.25 and 11.26.

The 100A laboratory cascade was used both to study multicompartment R.C.E.R's and to obtain scale-up data to design the 1KA commercial reactor.

Tables 11.27 - 11.30 show results for the 100A reactor, including potential and copper concentration profiles for a given current, flow rate and temperature.   These results are presented in graphical form in Fig. 11.18 as a plot of LN C against compartment number.

Typical data for the commercial, 1KA reactor is shown in Table 11.31 and 11.32 and .plotted in Fig. 11.19.

12. DISCUSSION

12.1 POLARISATION BEHAVIOUR AT SMOOTH ELECTRODES.

Prior to the use of the copper deposition reaction for the study of roughness development, it was considered necessary to examine briefly the reproducibility of limiting current determinations. The conditions chosen involved a soluble copper foil anode, a smooth copper foil cathode of accurately defined surface dimensions (d = 6.3, l = 4.3 cm.) and a standard electrolyte : 0.014M Cu SO$_4$ + 1.5M H$_2$SO$_4$ at a temperature of 22°C. , a rotational speed of 500 r.p.m. and a potential scan rate of 150 mV(min.)$^{-1}$. Preliminary work (Table 10.1 ; Fig. 10.1) showed that for electrodes wet polished by 600 grade emery paper, satisfactory reproducible polarisation curves could be obtained, displaying reasonably well defined limiting currents in the potential range -900 to -1150mV (.M.M.S.).

The surface microroughness of the rotating cylinder cathode might be expected to be important, but early trials with chemically polished and electropolished foils (Table 10.1 ; Fig. 10.1) gave results comparable to electrodes prepared by the above method. Evidently, the hydrodynamic roughness present at fine emery polished surfaces was insufficient to affect mass transport (although early stages of nucleation must have been quite different).For experimental convenience, further trials were conducted with emery polished surfaces.

Steady-state polarisation data is also desirable, indicating the need for a relatively slow potential scan rate. As the present study did not involve kinetic interpretation, however, and the copper deposition reaction is known to display very fast kinetics, a moderately high scan rate could be utilised. Moreover, a slow scan rate was deliberately avoided in order to discourage the formation of roughness (and

subsequently increased limiting currents) under mass transport controlled conditions. A scan rate of 150 mV (min.)$^{-1}$ was chosen as a reasonable compromise between the requirement of steady state on one hand, and smooth deposit, short experimental trials on the other. Practical curves (e.g. Fig.10.2) showed this choice to be reasonable over a wide range of conditions.

The above considerations apply to a constant copper concentration, maintained by a combination of soluble anodes and electrolyte flow or replacement. In certain cases, such a technique could not be employed. For example, with 'as received' industrial solutions, the existence of several metals mitigates against a soluble anode. Here, an insoluble anode or a divided cell may be used. The former, while having the advantage of simplicity, may result in a deleterious decrease in pH or an increase in mass transport due to oxygen evolution. The use of a cell divided by a cation exchange membrane, while requiring a higher cell voltage, may overcome these objections, and was routinely used in the present studies(as described in Chapter 8). The choice of scan rate in this case becomes more critical, as too low a value may result in copper depletion before the limiting current is achieved. Under these circumstances, a scan rate of 150 mV (min.)$^{-1}$ was again found to be an acceptable compromise (Table 10.2).

The use of a simple cell and soluble anodes proved satisfactory for rapid determinations, with replacement of electrolyte between successive trials. For lengthy trials, however, or during open circuit conditions, marked corrosion of copper occurred in the 1.5M H_2SO_4, resulting in a gradual increase in copper concentration. In such cases, the electrolyte was adjusted either by volumetric dilution (using 1.5M H_2SO_4) or a large

buffer volume of $CuSO_4$ was employed and slowly recirculated through the

cell. As a precaution against changes in concentration, electrolyte

samples were withdrawn at intervals in the vicinity of the limiting

current and analysed for copper. A volumetric flow rate of

$\leqslant 10$ $dm^3(min.)^{-1}$ through the cell was found to have no significant effect

on the determined limiting current. This was to be expected, as the mass

transport to a <u>turbulent</u> rotating cylinder is known to be rather

insensitive to axial flow (Chapter 2).

In order to record true values of the electrode potential during

polarisation trials and obtain accurate potentiostatic control, a

separate potential pick up brush was utilised. The importance of this

(as discussed in Chapter 6.5 and indicated in Fig.6.5) has perhaps been

overlooked in previous studies, although certain workers[190] have

certainly utilised the technique.

As noted in Chapter 3, copper deposition from acid sulphate solutions is

a well known and well characterised mass transport controlled reaction

(see Table 3.5). At least two groups of research workers[77,83] have studied

this reaction at rotating cylinders with soluble copper anodes,

providing a good basis for comparison.

10.2 MASS TRANSPORT TO A SMOOTH ROTATING CYLINDER ELECTRODE.

10.2.1 General

As the non-concentric experimental reactor geometry (Chapter 8) was

somewhat different to that of previous workers, a small amount of mass

transport data was obtained to check the system. Selected results for

smooth electrodes (presented in Table 10.3) were obtained over the

range $1.0 \times 10^3 < (Re) < 1.8 \times 10^5$; $1.8 \times 10^{-5} < (St) < 1.2 \times 10^{-4}$;$452 < (Sc) < 2212$.

This relatively small range of dimensionless parameters was restricted by various factors. Only one copper concentration was utilised, as the later studies on roughness development largely referred to this condition, providing a direct basis for comparison. The rotational speed of the cylinder was restricted to the range 100- 1250 r.p.m. Low speeds resulted in non-uniform motion due to 'commutation' of the direct drive electric motor, while higher speeds demanded excessive power and tended to induce vortexing. The use of viscosity increasing additives such as glycerol was deliberately avoided, for reasons of convenience and in order to retain simple, well characterised solutions.

As noted in Section 10.2, the experimental data lie between the correlations due to Robinson and Gabe[83] ,and Eisenberg, Tobias and Wilke[57]. It may be concluded that, despite the unique nature of the experimental geometry, the data is not significantly different to that of previous workers. A review of the literature reveals a rather wide range of correlations, as noted in Chapter 4, for the case of a turbulent inner rotating cylinder in a concentric geometry. As pointed out by Robinson and Gabe[83] , the (Re) exponent has been reported as -0.30[57,58,82], -0.31[83], -0.333[89] and -0.40[77], while the (Sc) exponent values reported include -0.59[83], -0.644[57,58,82,313] and -0.666[77].
There are several possible reasons for these discrepancies, due to variations in :

(i) the reaction(s) studied

(ii) the range of operating variables and hence the range of (St), (Re) and (Sc);

(iii) the method of data correlation, and

(iv) the geometry, including the radius ratio of inner to outer cylinders

$\frac{r_I}{r_O}$, the annular gap $r_o - r_I$, the aspect ratio of length to inner cylinder radius$\frac{h}{r_I}$, the overall shape of the cell and of the electrode. These factors may be examined in more detail.

The reaction utilised to generate mass transport data has already been discussed in Chapter 3. It has been seen that the favoured reactions, ferrocyanide/ferricyanide redox and copper deposition each have merits and drawbacks. There were several reasons for preferring the latter reaction in the present study:

(i) direct comparison was possible with the work of Robinson[68,83],

(ii) the copper deposition reaction is of practical and commercial importance,

(iii) comparison was possible with data from large, pilot plant 'Eco-cell'reactors,

(iv) the majority of studies to be described involved roughness generation or characterisation. The copper deposition reaction is ideal here , as it may act both as a means of generating surface roughness, and as an indicator method of measuring mass transport (Chapter 3), and

(v) the reaction is not light sensitive.

The range of experimental variables has often been restricted by conditions including electrolyte temperature, additives and rotating cylinder geometry and speed, as previously noted. The study due to Eisenberg, Tobias and Wilke[57,58] has become almost classical for several possible reasons:

(i) it was the first to systematically obtain a mass transport correlation from the measured parameters i_L, d, υ, C, D and U,

(ii) consideration was rightly given to the reversibility of the redox reaction used,

(iii) a wide range of experimental conditions were employed,

(iv) a correlation was obtained for no less than five reaction systems involving both chemical dissolution and electrochemical redox processes, and

(v) justification of the proposed correlation was possible by known theory.

While the wide range of reaction types and conditions undoubtedly resulted in a most useful and powerful correlation, care should be taken when making comparisons with more specific or restrictive studies. For example, Makrides and Hackerman[191] have pointed out that critical study of the Eisenberg et al.[57,58] data reveals a noticeable dependence of the (Re) exponent on the actual (Re) value. For the ferro/ferricyanide redox reaction, the (Re) exponent (given by the slope of the j_D' vs. (Re) curve) was -0.32 for the interval $10^3 < (Re) < 10^4$, but only -0.23 for $3 \times 10^4 < (Re) < 10^5$ (Table II of ref. 58). The generalised correlation results in a best value of -0.30 over the full range $10^3 < (Re) < 10^5$. To be exact, comparisons should therefore be made over the same range of (Re). In addition, the (Re) exponent varied with the reaction process, being -0.28 for reduction and -0.23 for oxidation.

The importance of the method of data correlation has been discussed in Chapter 3. While both Eisenberg et al. and Robinson and Gabe[68,83] utilised a three dimensional least squares analysis, other authors have assumed a correlation of fixed format. The resulting correlations may appear markedly different.

The importance of reactor geometry has received only scant attention in in the literature, and there is a decided need for a definitive study. The R.C.E. may be contrasted with the R.D.E. in this respect. For the latter, the importance of electrode size and shape, and the containing

vessel/counter electrode geometry are well characterised (see for example refs. 251 +252). It has been previously noted (in Chapter 6) that attention should be given to both the hydrodynamics and the current/potential distribution at a R.C.E. to ensure uniform, reproducible flow regimes and an equipotential or constant current density electrode surface. The geometry of a R.C.E.R. has important implications in scale-up and will be considered in more detail.

It is evident from Table 6.7 that a wide range of R.C.E. conditions have been utilised in laboratory studies. Thus, for example, Eisenberg et al.[57] and Arvia et al.[77] utilised a very regular, concentric geometry, with complete end baffling, while Robinson and Gabe[68,83] used a concentric geometry with incomplete end baffling. The present laboratory studies involve neither a concentric geometry nor complete end baffling, and this trend is largely the result of an attempt to construct a versatile, robust and convenient reactor (as explained in Chapter 8) rather than a cell for academic studies. The R.C.E. itself must also be considered, and (as discussed in Chapter 6) design regarding hydrodynamic flow may be compromised by the need for electrode accessibility or ease of surface examination. It may be noted that, in the present studies, electrodes using overlapping end caps to hold a foil (Fig. 8.8b) gave comparable results to those involving flush mounted end caps (Fig. 8.8a).

The length to inner diameter ratio, l/d was considered by Eisenberg et al.[57], who found no significant effect on mass transport for an almost fourfold change viz. $3.0 < l/d < 11.6$. The friction factor results of Theodorsen and Regier[9] also support this finding, for $3 < l/d < 20$. As seen in Chapter 2, the functional dependence of $f/2$ upon (Re) was similar for both rotating cylinders and discs, indicating that even radical differences in the ratio l/d do not affect the dependence of mass transport

on the (Re) exponent[9].

The importance of annular gap has been the subject of some debate.
Eisenberg et al.[57,58] apparently demonstrated the importance of inner
radius r_I, rather than gap r_I-r_0, by plotting j_D' against $(Re)=\dfrac{U(r_0-r_I)}{\nu}$.
The resultant lines were parallel and of slope -0.30, indicating that the
results could be entirely correlated by using $(Re) = \dfrac{Ur_I}{\nu}$. Newman[10,51]
however, considered that the ratio r_I/r_0 should be incorporated
into the mass transport correlation, by means of a modified (Re) :

$$j_D' = (St)(Sc)^{0.644} = 0.079\left[(Re)(r_I/r_0)\right]^{-0.30} \qquad \text{Equation 12.1}$$

As noted by Gabe[25], $r_I/r_0 \simeq 1$ in practice, and $(r_I/r_0)^{-0.30} \longrightarrow 0$. By
assuming a correlation where (Re) is defined in terms of r_I, any
significance of r_0-r_I is shown by an apparent increase in the constant
0.079. The importance of $(r_I/r_0)^{-0.30}$ should not be overlooked. Table 12.1
shows that, while a small effect is expected for large cylinders with a
small annular gap (which is an important practical case), large
discrepancies are apparent for a small diameter cylinder within a large
concentric electrode- the case of a 'pole in a bucket'. In practice, the
changing hydrodynamics for large gaps would probably modify these
considerations appreciably.

In a discussion of mass transport in agitated vessels, Marangozis and
Johnson[410] have concluded that the success of Eisenberg et al.[57,58] in
correlating their data with a Chilton-Colburn form of equation was
fortuitous. This situation was suggested to have arisen as the Eisenberg
et al. data obeyed $\dfrac{r_0-r_I}{2r_0} = \text{constant}\left[\dfrac{2r_I}{r_0-r_I}\right]^{-0.30}$ Equation 12.1a

This equation is a necessary condition for the data to be expressed, with
equal success, by the Eisenberg et al. correlation

$$j_D' = \text{constant}\left[\dfrac{Ud}{\nu}\right]^{-0.30} \qquad \text{Equation 12.2}$$

or a more general Gilland-Sherwood type correlation.

$$j_D' = constant \left[\frac{r_0-r_I}{2r_0}\right] \left[\frac{U(r_0-r_I)}{\nu}\right]^{-0.30}$$

Equation 12.3

Marangozis and Johnson went on to show that such an expression could also be used to reconcile data from both rotating inner and rotating outer cylinders, by appropriate definition of (Re).

Having noted above that the Eisenberg, Tobias and Wilke[57] correlation

$$\frac{I_L}{AzFCU} = 0.079 \left[\frac{Ud}{\nu}\right]^{-0.30} \left[\frac{\nu}{D}\right]^{-0.644}$$

Equation 12.4

is a generalised one, obtained over a wide range of conditions, it is now of interest to examine mass transport over deliberately restricted conditions.

12.2.2 Effect of Copper Concentration

For a given cylinder (fixed d and A), rotating at a fixed speed (constant U), in a specific electrolyte at an invariant temperature (constant ν and D), Equation 12.4 simplifies to

$$I_L \propto C$$

Equation 12.5

Fig.IO.IO shows a plot of I_L vs. C for such conditions. The linearity shown at high concentrations becomes less well defined as concentration decreases, and this apparent increase in I_L/C may be attributed to the increasing contribution of background current, or non-mass transport controlled deposition. Such residual currents may be attributed to non-faradaic charging phenomena at the electrode and the oxygen reduction reaction. The latter is expected to be predominant, especially as the electrolyte was not deoxygenated. The influence of such residual currents is only experienced at very low metal concentrations, and is well known to polarographers. The oxygen reduction reaction in acid solution may be written: $O_2 + 2H^+ + 2e^- = H_2O_2$

Equation 12.6

followed at more cathodic potentials by:

$$H_2O_2 + 2H^+ + 2e^- = 2H_2O \qquad\qquad\qquad\qquad\qquad \text{Equation 12.7}$$

The dissolved oxygen concentration in saturated aqueous solutions at room temperature is approximately 2.5×10^{-4}M or 8p.p.m., and is therefore comparable in magnitude with the lower regions of copper concentration in the present studies.

Polarisation curves for copper deposition at various concentrations (Figs.10.5 and 10.6) show the limiting current plateau becomes ill defined at lower concentrations, reflecting the predominance of hydrogen evolution at high cathodic potentials and background currents at lower potentials. It may be noted that experimental difficulties were encountered in preparing and maintaining low concentration copper solutions. Regarding preparation, serial dilution of a concentrated solution by 1.5M H_2SO_4 necessitated the use of very pure (at least AR) H_2SO_4. The maintenance of a low Cu level ($\sim$p.p.m.) before the polarisation curve was made difficult by the use of a copper cylinder , which could readily corrode (with oxygen reduction as a complementary electrode reaction). This situation was alleviated by polarising the electrode cathodically, directly upon immersion. To safeguard against unknown increases in corrosion due to copper dissolution, the electrolyte was normally analysed before, during or after the experimental trial. The corrosion problem was aggravated by the use of a relatively large electrode area/electrolyte volume ratio. Also, use of a rotating electrode led to a well mixed solution- ironically the very conditions desirable for a high metal deposition performance (as discussed in Chapter 6).

The range of copper concentrations studied in this thesis (1 - 890 p.p.m.) was chosen to correspond to those encountered in effluent control and hydrometallurgy.

It is interesting to note, in passing, that the open circuit potential of a freshly copper plated rotating cylinder may be utilised as a crude indicator of copper concentration via the Nernst equation. Fig.IO.7 indicates an approximately linear relationship between the open circuit potential and the logarithm of copper concentration. In the presence of a constant concentration of high ionic strength electrolyte $(1.5M\ H_2SO_4)$, the activity of copper is reasonably constant over the experimental range (1-890 p.p.m.). The technique should be used as a crude guide only, as redox reactions or extensive corrosion may result in spurious open circuit potentials. In addition, the recorded values were influenced by the nature of the electrode, being more negative (by up to 10mV) for freshly plated cylinders or rotating cylinders compared to static copper foil electrodes. The presence of complexants such as Cl^- may also radically affect response, especially at low concentrations of copper.

I2.2.3 Effect of Rotational Velocity

For the case of a given cylinder (constant d and A') rotating in an electrolyte of constant concentration at fixed temperature (constant C, $\mathcal{v}$ and D), the general expression

$$(St) = a\ (Re)^b (Sc)^c$$

simplifies to

$$I_L \propto u^{I-b} \qquad \qquad \text{Equation 12.8}$$

The exact value of (I-b) is expected to depend upon the reaction type, the (Re) range and electrode shape, as discussed in section I2.2.1 . For the present results, Fig.10.9 indicates a slope of 0.73, in general agreement with previous workers (see section I2.2.1).

The family of polarisation curves in Fig.10.8, show that the limiting plateaux became poorly defined as rotational speed (and hence mass transport) increased; the plateau is seen to tilt and shorten. This effect may be

attributed to a tendency towards non-mass transport controlled reaction
limitations.

Fig.10.8 results were obtained by a rapid technique- the R.C.E. being held
at a fixed potential in the vicinity of the limiting current plateau, for
mass transport controlled results. The resulting steady current values were
then recorded for various rotational speeds and potentials. The data show an
incresing contribution to mass transport controlled deposition as the
potential is made more negative. At potentials corresponding to the limiting
current (-950 to -1150 mV M.M.S.), the data points converge to a line of
slope 0.73. This 'indicator' technique has been utilised for microelectrode
work as detailed in Chapter 3. While providing a rapid, convenient
technique which obviates the need for a full polarisation curve to be
attained each time, the method lacks the precision of a limiting current
plateau determination.

Current values in Fig.10.8 do not exactly correspond to steady state values
(Fig.10.7), but are nevertheless in reasonable agreement. The indicator
technique becomes more difficult for conditions where the plateau is ill
defined, such as low copper concentration and high rotational speeds. In
such cases, the choice of potential is critical, and care must be taken not
to apply the method indiscriminately.

For the case of a given area (A) and diameter (d) cylinder, rotating in a
constant temperature dilute copper electrolyte (where as an approximation
ν and D are constant), the expressions 12.5 and 12.8 may be coupled to
yield: $I_L \propto cU^{1-b}$ Equation 12.9

12.2.4 Effect of Electrode Size

For a given diameter cylinder (d), rotating at constant speed (U) in a
fixed electrolyte (constant C, ν and D) the limiting current density
should be constant i.e.

$$I_L \propto A \propto 1 \qquad\qquad \text{Equation 12.10}$$

where $1 =$ length of cylinder.

Fig.10.12 indicates that this is true, at least for the present results, where a straight line plot through the origin is obtained for I_L as a function of A (the area being altered by shortening the active height of the R.C.E.). The choice of area is governed largely by experimental convenience, and the need to obtain limiting current values which are sufficiently large to avoid complications due to interfering noise etc., and sufficiently small to lie within power supply capabilities. Many authors have utilised a $d/1$ ratio ≈ 1. In order to minimise edge effects due to either flow development/separation or non-uniform current density distribution, long cylinders should be used i.e. $d \ll 1$. Such electrodes may result, however, in a lengthy apparatus which is difficult to assemble. Examination of the literature shows wide variation in $d/1$ (see for example Table 6.8), and some authors have not appreciated the disadvantages of radically squat cylinders of $d \gg 1$.

12.2.5 Effect of Temperature

In contrast to the above considerations for concentration, rotational speed and area, the effect of temperature is more complex, as both ϑ and D are affected to different degrees. Fig.10.14 and Table 12.2 show the improvement in mass transport over the range 22-60°C for otherwise constant conditions of d, A, U and C. Relative to the mass transport at 22°C, raising the temperature to 60°C more than doubles the limiting current.

The Eisenberg, Tobias and Wilke correlation[57] may be written for this case:

$$I_L = A z F C U.\ 0.079 \left[\frac{U^{-0.30} d^{-0.30}}{\vartheta^{-0.30}} \right] \left[\frac{\vartheta^{-0.644}}{D^{-0.644}} \right] \qquad \text{Equation 12.11}$$

i.e. $\quad I_L \propto \upsilon^{0.344} D^{+0.644}$ Equation 12.12

As indicated by Figs.10.68 and 10.69, both D and υ vary as the reciprocal of absolute temperature:

$$T \propto \frac{1}{D\upsilon}$$ Equation 12.13

(The empirical Einstein-Stokes type relationship,

$$\frac{D\upsilon}{T} \simeq 2.23$$ Equation 12.14

has been attained by Arvia et al.[77]).

Combining Equations 12.12 and 12.13 :

$$I_L \propto \upsilon^{0.656} D^{1.644} T$$ Equation 12.15

Table 12.2 shows that the relative improvement in mass transport (referenced to $22^{\circ}C$) for the experimental results is comparable with that expected from Equation 12.15.

12.3 CONCENTRATION DECAY AND ROUGHNESS DEVELOPMENT

It has already been identified in Chapter 6 that, for the case of a simple batch R.C.E.R.,

$$C_t = C_o e^{-kt}$$ Equation 12.16

Such a regular exponential decay is often experienced for copper deposition to a smooth electrode. In the case of deposition at potentials corresponding to limiting current conditions, however, the development of surface roughness may increase the rate of decay i.e. the value of k. Fig. 10.15 shows a typical copper concentration decay for a R.C.E. held at a potential of -1000mV M.M.S. For the first 60 mins., the decay follows the predicted line, given by:

$$C_t = C_o e^{-K_L A/V \cdot t}$$ Equation 12.17

where K_L may be determined from an auxiliary polarisation curve for a smooth electrode as :

$$K_L = \frac{I_L}{A_z FC}$$

Equation I2.I8

After some 60 mins., the copper concentration departs from the predicted

line (Fig.I0.I5), indicating an increased reactor performance due to.

roughness development. The effect is more clearly seen by considering

Equation I2.I7 in LOG. form::

$$LOG_{10}C_t = LOG_{10}C_o - \frac{K_L A}{V. 2.303}.t$$

Equation I2.I9

Thus a plot of $LOG_{10}C_t$ against t might be expected to result in a straight

line, of intercept $LOG_{10}C_o$ on the t=0 axis, and slope $\frac{-K_L A}{V. 2.303}$.

Fig.I0.I6 shows such a plot for the results of Fig.I0.I5. Again, for the

first 60 mins., the data approximate to the predicted straight line. After

this time, the behaviour approximates to another line of significantly

increased slope. Fig.I0.I6 further demonstrates that the transition time

and the value of the second slope both showed a certain degree of

irreproducibility, despite care in the experimental technique. This

suggests a certain degree of randomness in the nature of roughness

development. To minimise this, and preserve reasonable reproducibility, it

was found necessary to preplate the surface of the copper R.C.E. with

freshly deposited copper. This preplating operation also served to stabilise

the open circuit potential and allow equipment to be checked.

It was considered that special preparation of the R.C.E. might result in

better reproducibility or a longer transition time for a change in slope.

This prompted chemical polishing or electropolishing of the copper foil

R.C.E. Fig.I0.I7 shows, however, that such surface preparation techniques

gave results which were entirely comparable with an electrode prepared by

wet polishing with fine (600 grade) emery paper. The last technique was

therefore employed as standard in the present studies. In a study of

roughness development during copper deposition from $1N$ $CuSO_4$ $+$ $1N$ H_2SO_4, Ibl, Javet and Stahel[380] also found that electropolishing could not prevent roughness development during (galvanostatic) deposition, at or near limiting current conditions. The explanation must be that electropolishing or chemical polishing does not remove small scale heterogeneities on the surface. Such residual micro features may include crystallographic defects such as grain boundaries, dislocations etc. Mass transport controlled deposition serves to amplify the development of small scale protuberances in such regions. Electropolishing or chemical polishing may be a pre-requisite technique for electrocrystallisation studies, however, as nucleation and early growth may be greatly influenced by scratch marks (see later).

Information on roughness development during a batch decay is also provided by the current history. Fig.10.18 shows that the current initially decays, following predicted behaviour and mimicking the concentration behaviour:

$$I_t = I_o e^{-kt}$$ Equation 12.20

$$I_t = I_o e^{-K_L A/V \cdot t}$$ Equation 12.21

or

$$LOG_{10}I_t = LOG_{10}I_o - \frac{K_L A}{V \cdot 2.303} \cdot t$$ Equation 12.22

The current-time behaviour for potentiostatic, limiting current operation is somewhat complex. The initial value, I_o is close to that recorded on a polarisation curve, as expected. After 30 mins., the current increases, passing through a broad maximum at ca. 60 mins., then decaying. This behaviour is the result of competing effects: a declining concentration encourages a smaller current in accordance with Equation 12.18, but an increasing roughness promotes a larger effective mass transport coefficient. It might be anticipated that the current at longer times would decline in a similar fashion to the corresponding concentration, indicating a constant

mass transport coefficient. Fig.IO.I9 shows that the behaviour is considerably more involved. This log-log plot of I vs. C indicates that at high I and C (corresponding to short times), the I-C behaviour may be predicted by polarisation curve values of I_L at various values of C. The current rises above the predicted value for a smooth electrode at $C \approx 650$ p.p.m., then after a further time decays with declining C. A derived plot of apparent mass transport coefficient vs. time (Fig.IO.20), shows that the calculated K_L (given by Fig.IO.I9, assuming the current to correspond to I_L), continues to increase from its original, predicted, smooth electrode value with time. There are several possible explanations for this:

(i)   the current efficiency for copper deposition declined with decreasing concentration,

(ii) a small part of the roughened deposit left the rotating cylinder due to gravity/centrifugal forces and redissolved,

(iii) background reactions such as oxygen reduction became increasingly important at lower copper concentration,(as previously discussed in Section I2.2).

The actual mass transport coefficient for longer times (and hence rough deposits) may be calculated from the concentration decay curve (by means of Equation I2.I9) as 6.7×10^{-3} cm.s^{-I}. This value is considerably greater (by a factor of 3.2) than the initial value for short times of 2.2×10^{-3} cm.s^{-I}. This last value compares favourably (within experimental error) with the corresponding value for a smooth cylinder (obtained from a subsidiary polarisation curve) of 2.32×10^{-3} cm.s^{-I}.

The increased reactor performance due to roughness development is further seen in Fig.IO.2I, where the concentration change $\Delta C = C_o - C_t$ is plotted

as a function of current. The increased performance at low concentrations

(longer times and hence roughened deposits) is manifested as a considerable

deviation from the calculated straight line for a smooth electrode.

The effect of potential during a potentiostatically controlled batch

depletion of copper is shown in Fig.I0.22. At relatively low values

$\sim$ -850 mV M.M.S., the decay approximates to a single straight line over

the experimental time interval (220 mins.), in accordance with simple

theory. Thus roughness formation does not appear to be significant under

such conditions. At higher potentials, however, a significant increase in

performance is experienced, as shown by an increase in the apparent rate

constant for the decay. The transition time for deviation from the

predicted smooth electrode slope decreases with increasing cathodic·

potential, indicating the earlier development of significant roughness.

The rate constant also increases at higher cathodic potentials.At

potentials more negative than say -I050 mV, significant hydrogen evolution

occurs, and a further marked increase in performance results. This may be

attributed   to both encouraged development of surface roughness and to

mass transport enhancement by gas stirring (Chapter 3). Evolution of gas

directly from an electrode might be expected to produce such enhancement,

as the small size hydrogen bubbles are evolved through the convective

diffusion layer, causing considerable disturbance to it.

It is often assumed that mass transport controlled reactions are

independent of the electrode potential, in contrast to activation

controlled processes. While this may generally be true for smooth electrodes,

the development of surface roughness is remarkably potential sensitive. As

indicated by Fig.I0.22, the control potential may affect both the transition

time for growth of roughness, and the extent of roughness/surface area

amplification. It is significant, in reactor performance terms, that, at

potentials corresponding to mass transport control, a relatively small
increase in potential may result in a greatly increased performance due to
a combination of roughness and surface area increases. Indeed, a certain
amount of current inefficiency may be tolerated if the hydrogen gas
evolved as a secondary reaction provides effective stirring.

It should be noted that particularly low residual concentrations were
possible in the batch decays; below I p.p.m. in certain cases (with
obvious attractions for effluent control purposes). Some difficulty was
experienced with reproducibility, however, as occasionally the concentration
would increase rapidly by several p.p.m., then continue to decay. This was
particularly experienced under gas evolution conditions, and could be
traced to the dissolution of free copper powder. Powder leaving the
cylinder via gravity or centrifugal force was free to dissolve either by
open circuit corrosion, or the induction of bipolar dissolution in the
interelectrode gap of the divided cell. (In the case of an undivided cell,
direct contact with the anode provides a third possibility- simple anodic
dissolution).

At very low concentrations, the concentration decay tended to decrease in
rate, the residual concentration being relatively stable (in the absence
of rapid redissolution as described above). The existence of such a minimum
practical concentration for a given metal/electrolyte combination has been
experienced by several workers, including Kuhn and Houghton (Sb $\lessgtr$ 5p.p.m.)[408]
and Newman (Pb $\lessgtr$ 0.5 p.p.m.)[406]. An equilibrium concentration is apparently
reached when the rates of deposition and redissolution are identical. A
thermodynamic approach by Trainham and Newman[407] (who considered packed
bed electrodes) has enabled an estimation to be made of such a concentration.
In some cases, the use of a more negative potential may result in a
further decrease in concentration. Alternatively, further metal removal

may be encouraged by a decrease in the corrosive properties of the solvent. However, the use of a more negative potential may result in higher power costs and the incidence of side reactions. Choice of electolyte is seldom possible in industrial practice, and the use of a less acidic solvent may lead to codeposition of hydroxide. It should also be remembered that the application of constant potential may effectively result in a declining applied overpotential due to the Nernstian shift. In the case of severe decadic changes in concentration, the potential may fall below that necessary for limiting current operation.

The effect of potential on the current time behaviour for a batch decay is illustrated in Fig. 10.23. The initial currents (t = 0 min.) are generally comparable with values from corresponding steady state polarisation curves. At low potentials, e.g. -850 mV M.M.S., the decay approximates to a straight line, mimicking the concentration behaviour. As the potential becomes more negative, however, deviation occurs, the current decaying to a minimum, then increasing through a maximum before a final decay. This apparently complex behaviour is the result of competition between current increase due to enhanced mass transport (via a combination of increased hydrodynamic shear and electroactive surface area) and current decline due to decreasing concentration. Initially, the latter effect dominates for the smooth electrode, giving way to the influence of roughness at intermediate times (resulting in the maxima), and regaining control towards the later stages (for a roughened electrode). At high potentials corresponding to hydrogen evolution, a final decay was not experienced, and the current levelled at a relatively high value, governed by gas evolution at the roughened surface.

In one trial, an already roughened deposit from a previous batch decay was used as the starter electrode for a repeat experiment (Fig.10.24). The

decay immediately followed a rate comparable to the final stages of the previous run. The increased metal deposition did not markedly enhance performance as the trial continued.

The effect of rotational speed is shown in Fig. IO.25. Am increase in speed is seen to increase both the early and later decay slopes, and to decrease the transition time. The latter effect is presumably mainly due to the earlier development of significant roughness as a result of increased rate of deposition. As previosly seen, the early concentration history may be approximated by a line predicted from smooth electrode limiting current considerations. At very low concentrations, $<$ I p.p.m., there is evidence again of tailing, and in the case of I'OOO r.p.m., a constant concentration of 0.5 p.p.m. was attained after some I60 mins. Reproducibility worsened as the rotational speed increased, necessitating . many determinations to obtain significant results.

In Table I2.3, am attempt is made to compare initial and final slopes for Fig.IO.25, approximating decay behaviour to two distinct lines of different gradient. The relative improvement factor due to roughness development compared to the early smoother electro. e surface varies between 3.3 for I80 r.p.m. and 4.9 for IOOO r.p.m. These results plotted in log-log form in Fig.IO.26 as apparent rate constant against rotational speed, to determine the velocity exponent. The early results display a slope of 0.73 in accordance with polarisation data .for smooth electrodes under similar hydrodynamic conditions. The later results, however, show a significantly higher slope $\approx$ 0.88, in addition to giving appreciably higher mass transport values. Insufficient points are available to precisely define this last value, unfortunately.

It is interesting to note that the development of roughness during cementation reaction has also been seen to result in an increase in the

apparent rate constant for decay. Strickland and Lawson[402] have reported a rotating disc study of the cementation of Cu on Zn, Cd on Zn, Pb on Zn and Ag on Cu, Cd or Zn from aqueous acid solution. When the deposited material exceeded 0.2-0.4 mg cm^{-2}, the rate was enhanced, the effect being more marked with increased rotational speed.

The batch decay type of experiment is a most convenient technique, as a relatively large amount of information may be provided using a relatively small volume of electrolyte. The monitoring of both current and concentration history allows performance to be steadily evaluated over a wide range of conditions. The multiple sampling of a batch solution is tedious, however, and may decrease the effective volume. The use of continuous monitoring devices such as ion selective electrodes[396] is to be encouraged in this respect.

In the present studies, the use of a relatively high mass transport electrode (the R.C.E.) and a moderately high area to volume ratio has enabled concentration decay over some three decades in a reasonable time scale (up to 3 hours). Faster experimental trials would be possible using either a smaller, concentric interelectrode gap to decrease the effective cell volume or a more rapid rotational speed. For example, the use of end baffling and a fully concentric cell with a Icm gap would reduce the present I000 cm^3 volume to approximately I00 cm^3.

The development of roughness at the electrode as a direct consequence of metal removal creates a somewhat complicated condition, as the growth of roughness occurs over a range of concentration. The extent and type of roughness is expected to be a function of concentration; constant conditions may lead to quite different growth to the averaged batch decay coditions.

In the case of the R.C.E.R., the stirring provided by a turbulent rotating cylinder serves to provide an easily modelled, simple vessel, batch C.S.T.R. system. In the case of other reactors, however, an external flow circuit and reservoir are often necessary to enable the electrode to function, as in the case of porous, packed and fluidised bed electrodes. The resultant batch recirculation mode (Section 5.2.3) has been examined in the case of metal recovery in several works[120,164,199,207,208,403].

12.4 CONTROLLED- POTENTIAL SEPARATION OF METALS

Many of the existing techniques for metal removal from solution are non-selective. For example, ion exchange may be applied to remove cationic species, while chemical precipitation as hydroxide may remove all metals having sufficiently insoluble hydroxides under chosen conditions. Electro-deposition, however, is a potentially elegant technique, as metal may be removed directly onto the cathode as massive material. In addition, one reactor may be utilised to produce a variety of individual metals by variation in the operating conditions, notably the potential.

There are several instances where a noble metal is required from a multi-metal mixture, for commercial and/or ecological considerations. For example, in the stripping of reject silver plating on a base metal, acid dissolution will result in a mixed metal solution; silver may be selectively recovered for reuse or resale. In hydrometallurgy, the leaching of ore frequently results in mixed metal solutions; cadmium, for example, is normally found with zinc. By judicious choice of electrolyte and conditions, the selective extract of cadmium may be practised by electro-deposition. Both cementation and solvent extraction are routinely employed in hydrometallurgical processing, but it may be noted that the first introduces a base metal into solution, while solvent extraction fluids are expensive and sometimes difficult to handle. Following solvent

extraction, conventional electrodeposition is often utilised to recover
metal in any case.

The absence of controlled potential deposition on an industrial scale may
be attributed to two factors. Firstly, there have been few electrochemical
reactors capable of controlled potential deposition. The R.C.E.R. is
particularly suitable here due to its substantially uniform electrode
potential under potentiostatic conditions. Secondly, large scale potentiostats
are not readily available. On an industrial scale, sophisticated circuitry
is not necessary, however, as response time is not a critical factor.

The theory behind controlled potential separations has been discussed in
Chapter 5, where it was noted that the technique is ideally akin to
polarography with a large, solid electrode. It has already been noted that
the principles involved are similar to the converse case of alloy deposition
322,346,357, and that the electroanalytical literature[210,211,226,227]
contains many routine examples of selective recovery.

The ease and success of separation depends upon:

(i) the separation of standard potentials,

(ii) the relative activity of metal ions, and

(iii) the degree of polarisation of each cathodic reaction.

The situation may be complicated in practice, as pH, temperature, relative
metal concentration and complexant composition may each change the metal
complex present, and its decomposition potential. In the case of electro-
active complexants, the cell design may radically affect the result. For
example, in the case of an undivided cell, cyanide may be oxidised at an
insoluble anode.

It was noted in Chapter 5 that the literature is sparse concerning large
scale controlled potential separation of metals. The contributions of the

Swiss-Roll cell[126] and the Akzo Fluidised Bed Electrode Reactor[167] for copper

deposition should be mentioned, however.(See Chapter 5 for further details).

One application of the technique is the purification of electroplating baths

contaminated by secondary (noble) metals. Such contamination occurs routinely,

as a consequence of corrosion of the substrate or transference of liquor

from a previous stage. The secondary metal may be present at very low levels

$\sim$ 1 - 500 p.p.m., and a high mass transport reactor is necessary to remove

the metal at a reasonable rate. Vaaler[409] has reviewed some early work and

reported further studies involving silver, copper and zinc removal from

nickel plating baths. It is interesting to note that 'INCO' workers[180-182]

have deliberately added controlled quantities of a noble metal (Ag or Cu)

to nickel baths and utilised the deposition rate of the secondary metal as

a mass transport indicator (see Chapter 3).

In the present laboratory studies[323], the possibility of selective removal

was investigated under well stirred batch conditions, as discussed in

Section 12.3 . Before a batch decay was attempted, a polarisation curve was

traced, establishing the limiting current in order to provide a norm for

smooth electrode performance (Equation 12.19). This curve also aided

judicious selection of control potential, corresponding to mass transport

controlled operation.

In the case of copper deposition from either zinc sulphate/sulphuric acid

solutions (Fig.10.27), or nickel sulphate/sulphuric acid solutions (Fig.10.29),

the polarisation curves for copper deposition are similar to the case of

copper from acid copper sulphate, indicating that copper is the nobler

metal under mass transport control. The limiting current values are also

comparable to those in 1.5M H_2SO_4 alone. This is to be expected, as the

addition of small concentrations of $ZnSO_4$ (0.014M) or $NiSO_4$ (0.014M) would

not radically affect the viscosity of the electrolyte, the diffusion
coefficient of cupric ions or the active species (Cu^{2+}). The importance of
control potential is shown by the corresponding Figs.IO.26 and IO.28 . At
potentials below the limiting current (-850 mV M.M.S.), the semi-logarithmic
decay of concentration approximates to a straight line which may be
estimated from limiting current considerations. At higher potentials,
however, (-IOOO mV M.M.S.), the decay increases in rate after some 45 mins.,
due to the development of rough deposits, as discussed in Section I2.3 .
Deposition was reasonably selective, there being no detectable change in
solution concentration (of Zn or Ni) by atomic absorption analysis ($\pm$ 3%)..
A more discerning test of selective deposition was provided by the deposit
analysis for the -IOOO mV M.M.S. results, values of 0.4 % w/w Zn or 0.25 %
w/w Ni being recorded. This corresponded to deposited metal ratios of
Cu/Zn = 250 and Cu/Ni = 400.

In the case of a mixed $AgNO_3/Cu(NO_3)_2/HNO_3$ solution, selective deposition of
silver was possible under limiting current conditions, an increase in decay
rate via roughness formation being once again apparent. The selective
deposition yielded a substantially pure (99.75% w/w) Ag powder. The
individual polarisation behaviour for Ag and Cu (Fig.IO.30), indicated a
wide separation in deposition and mass transport control potentials,
facilitating a straightforward separation.

The above examples utilising synthetic, well characterised solutions have
some relevance to industrial practice. The $CuSO_4/ZnSO_4$ solution is typical
of a sulphuric acid pickle for brass. Selective copper removal would provide
substantial metal savings for a large processor and extend the lifetime of
the pickling liquor. Similar considerations apply to $CuSO_4/NiSO_4$, although
it is realised that cupro-nickel alloys are somewhat rare. Silver recovery

from a $Ag/Cu/HNO_3$ solution may be practised following nitric acid stripping

of silver plated copper substrates. Such material is regularly found in

decorative plating, the production of heavy electrical conductors or

processing of low silver, copper alloys. Selective recovery of silver provides

a cost effective process, while the copper recovery may be uneconomic.

The above studies regarding synthetic, uncomplexed acid solutions represent

conditions which are favourable to selective deposition. In practice,

however, many liquors are heavily complexed. Considering electroplating, the

addition of relatively large concentrations of cyanide to baths is often

necessary to enable codeposition of metals, or to achieve smooth, adherent

deposits. Also, cyanide based solutions are frequently encountered in hydro-

metallurgy and the metal processing industries for ore, leaching or metal

dissolution purposes.

Two industrial cyanidic solutions were studied. The first was a dragout in

which carry over of a gold plating solution had allowed a concentration of

830 p.p.m. Au to develop, with few other contaminants. The second was a

multi-metal rinse water arising from the alkaline regeneration of a cation

exchange column. A polarisation scan for the dragout solution at a stainless

steel R.C.E. in an undivided cell (Fig.10.32) showed no obvious limiting

current inflections in the potential range studied (-0.5 to -1.75 V.M.M.S.).

Three arbitrary potentials were therefore chosen at -1.0, -1.3, and -1.75 V.

M.M.S. for batch decay trials (Fig.10.33). Smooth, golden deposits were

obtained in all cases, suggesting sub-limiting current operation. The

deposition was partly under mass transport control, however, as indicated

by a faster decay for higher rotational speeds. The decay results are

somewhat anomalous in that the rate at -1.000 V is greater than at -1.370 V.

Use of an appreciably higher potential (-1.750 V) resulted in a much faster

decay. The corresponding current histories are complex. At -1.000 V and

-I.370 V, an approximation to a semilogarithmic decay is experienced, with a greater slope for the latter. At -I.750 V, however, the current behaviour is somewhat unpredictable, falling slightly and passing through a poorly defined minimum before increasing beyond its original value. In all cases, the initial currents (t = 0) were in reasonable agreement with the polarisation curve values. This complex behaviour may be due to the continuous variation in cathode current efficiency as the gold depletes from solution. In contrast to the case of silver and copper removal above, overall current efficiencies were appreciably lower than I00%, due to hydrogen evolution in the acid (pH 4.8) solutions. For example, the -I.75 V decay removed 0.778 g in I.53 A hr. ; this is equivalent to a faradaic current efficiency of ca. 7.0% based on a one electron change. Current efficiencies were somewhat higher for the lower control potentials, being 38% at -I.3 V. M.M.S. and 28% at -I.0 V. M.M.S.

The second cyanidic solution provided a considerable challenge to electrodeposition as a metal removal technique. Not only was the solution contaminated by cyanide, but several metals were present in very low concentrations: Au, Ag, Cu, Ni, Sn and Fe in a solution of relatively high pH. Selective deposition was considered highly unlikely under such conditions, and attempts were made to acidify the solution (Table I0.7). At pH 4.0, the silver concentration started to fall dramatically, due to AgCl precipitation, while at lower pH values, toxic HCN was evolved. While the chemical removal of Ag as AgCl was certainly a possible preliminary technique for treatment, it was considered desirable to maintain the Ag concentration in solution prior to electrodeposition. A pH value of 4.0 was therefore chosen as a reasonable compromise. Potentiodynamic polarisation curves at various pH values generally indicate a depolarisation at lower pH, which may be interpreted as a reduction in the degree of complexing, with a

corresponding increase in the free metal ion concentration. The irregular

trend in the curves may be attributed to the change in stability and

electroactive nature of the metal complexes with change in pH. At pH 4.0,

two apparent limiting current plateaux were discernable and potentials

corresponding to these regions were selected for batch decay trials. At

- 0.550 V. M.M.S. in a divided cell, silver decayed in a semilogarithmic

fashion from 20 to 0.6 p.p.m. in I20 mins., levelling at this value for the

duration of the trial. While some copper was codeposited, in early stages

(O- 60 mins.) the concentration stabilised at ca. 9 p.p.m. There was no

detectable change in Au concentration throughout the experiment. Thus gold

appeared appreciably less noble than either silver or even copper, in

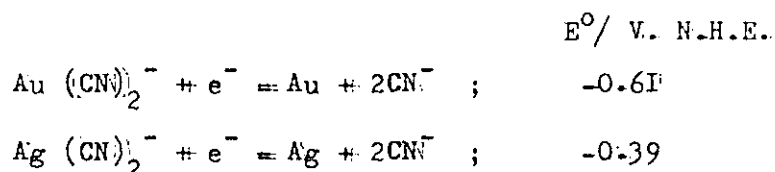contrast to uncomplexed acid solutions, (c.c.f. standard reduction potentials:

$Au(I) = +I.70$; $Ag(I) = + 0.80$; $Cu(II) = + 0.34$ V. N.H.E. or

$Au(I) = +I.05$; $Ag(I) = + 0.I5$; $Cu(II) = - 0.3I$ V. M.M.S.   ).

Comparable trials in an udivided cell with an insoluble stainless steel

anode once more resulted in an unaltered Au concentration, and a substantially

constant Cu concentration. Silver was again removed in a semilogarithmic

fashion down to 2.6 p.p.m., where it remained for the rest of the experiment.

Thus this trial was more selective with respect to copper removal, but

resulted in higher residual silver concentrations. This level of silver may

be reduced by more severe conditions such as a higher potential, although

an electrical power penalty is incurred. Fig.IO.38 indicates that a potential

of -900 mV M.M.S. in a still undivided cell resulted in a marked fall in Cu,

while Ag. decayed very slowly indicating formation of a stable complex. Even

at this higher negative potential, there was no marked gold removal.

In cyanidic solutions, the relative nobility (and hence stability) of metals

and the rate of mass transport (and hence rate of deposition) are largely

governed by the type of complex present. Decomposition of $Au(CN)_2^-$ is

considered to be the mass transport limited step, however[404]. In cyanidic

solutions, it is accepted that Au is appreciably less noble than Ag, the

standard potentials being as follows:[405]

$$E^{o}/ \text{ V. N.H.E.}$$

$$\text{Au } (CN)_{2}^{-} + e^{-} = \text{Au} + 2CN^{-} \quad ; \qquad -0.61$$

$$\text{Ag } (CN)_{2}^{-} + e^{-} = \text{Ag} + 2CN^{-} \quad ; \qquad -0.39$$

The considerable difference between the standard potential of Au^{+} and

$Au (CN)_{2}^{-}$ of some 2.3 V is a measure of the thermodynamic stability of the

cyano-complex. In the case of cyano-silver complexes, the deposition

potential depends greatly on the relative metal/cyanide ratio. At low

values, $Ag (CN)^{2-}$ predominates, whereas $Ag (CN)_{2}^{-}$ discharge is determining

at higher potentials. At high values, $Ag (CN)_{2}^{-}$ exists and discharge of

$Ag CN$ is decisive. In contrast to other metals, the influence of (CN^{-}) is

relatively weak for Au, due to the stability of $Au (CN)_{2}^{-}$.

I2.5   CURRENT HISTORY DURING POTENTIOSTATIC GROWTH.

In the previous sections, I2.3 and I2.4, the concentration in the reactor

was allowed to deplete, using a divided cell. Important information may also

be gained by studying roughness development at a constant copper concentration,

maintained by a soluble anode. This represents the start up condition of a

flow through reactor in which the (outlet) concentration is maintained

while mass transport performance increases due to metal powder development.

In addition, the mass transport to developed rough deposits is comparable

to that in an 'Eco-Cell' R.C.E.R., although the metal powder surface is

normally controlled in thickness by a mechanical scraper in this case.

Under potentiostatic control at -1000 mV M.M.S. (corresponding to limiting

current operation) in a fixed concentration solution(0.014 M $CuSO_{4}$), the

current transient for various rotational speeds is shown in Fig.10.39 . The

curve may be divided into three regions. Initially, and at short times, the
(limiting) current is reasonably constant and comparable with the value
obtained from the corresponding polarisation curves for a smooth cylinder.
A gradual transition then occurs to higher currents. Eventually, the
current tends towards a reasonably constant 'saturated' value. These regions
may be approximately identified with deposition to a smooth cylinder,
roughness development and 'saturated' roughness formation. In practice, the
situation is more complex, as roughness development is known to take place
almost as soon as the R.C.E. is made cathodic at potentials near the
limiting current (as shown in the following sections; I2.6 and I2.7). Metal
deposition is still actively occurring at long times, but presumably, the
continued growth is such as to maintain a reasonably constant mass transport
by contributions from surface area and roughness factors.

The 'initiation' time for growth of current is seen to decrease markedly as
the rotational velocity (and hence the mass transport) is increased. At
high rotational speeds, this region almost disappears. The transition to
saturated roughness becomes shorter and the I/t curve more steep as
rotational speed is increased, resulting in higher final values of current.
As with the decay curves, a degree of scatter was always obtained for the
I/t curves at constant C, despite careful surface preparation. Fig.I0.40
indicates that the limits of reproducibility for fresh, smooth electrodes
increased at higher rotational speed, suggesting an increase in the random
nature of growth at higher mass transport. Reproducibility was reasonable at
short times i.e. for smooth electrodes and low growth conditions, suggesting
again an inevitable degree of randomness in roughness formation.

A log-log plot (Fig.I0.4I) of I_L vs. U for initial and final currents on
Fig.I0.39 reveals a different relationship for smooth and roughened deposits.
For initial results,

$$I_L \propto U^{0.74} \qquad \qquad \text{Equation I2.23}$$

(in accordance with earlier smooth cylinder data), while at long times,

$$I_L \propto U^{\sim 0.90} \qquad \qquad \text{Equation I2.24}$$

The exponent for rough deposits is not well established, however, due to

scatter, and the relatively restricted range of velocity.

The increase in (limiting) current due to roughness development under the

experimental conditions varied from $\times 7.6$ at I80 r.p.m. to $\times 8.6$ at I230

r.p.m.

The above results concerned a constant potential. The effect of varying this

parameter is shown in Fig.I0.42 . The transition time for a discernable

increase in current appears to progress as the potential is lowered towards

values which represent a lower mass transport contribution. A 'saturation'

current is not seen at long times. It is interesting to note that at potentials

markedly below those corresponding to limiting current operation, some

increase in current (i.e. a certain degree of roughness development) still

occurs given a sufficient time. At particularly low cathodic potentials,

~ -0.750 V. M.M.S. and less, no significant increase in current occurs,

indicating the continuance of substantially smooth deposition and an

insignificant contribution from mass transport control.

The above trials serve to illustrate the importance of potential rather than

current density per se. For example, potentials of -I.I00, -I.000 and -0.950

V. M.M.S. all correspond to limiting current plateau operation, but the

current-time behaviour is markedly different, especially at longer times.

This may be attributed to significantly different growth of rough deposits

over such an apparently small potential range. Thus a potentiostatic

approach may yield improved information compared to a galvanostatic study.

Much of the work to date on mass transport and the development of powdered

deposits has been galvanostatic, particularly the works by Ibl et al.[193,194],

380, and by Robinson[68]. There is evidence of an increasing awareness of the importance of the potentiostatic approach, however, as is clearly shown in the recent works by the research groups of Calusaru[357] and Popov et al.[372-375, 382]. The remaining importance of constant current trials should not be overlooked, as this represents a frequent industrial mode of operation. Previous studies of roughness formation have already been reviewed in Chapter 5, and a general comparison of techniques employed is made in Table I2.4 . The potentiostatic work by Calusaru[357] et al. deserves more attention as, in common with the present studies, a wide variety of techniques are employed to study roughness formation. Additionally, the quantum mechanical treatment of the subject by Calusaru et al.[357,363-366] is in many ways complementary to the mass transport approach by Ibl et al.[193,380].

The overall polarisation behaviour for copper deposition to roughened electrodes was similar to that for their hydrodynamically smooth counterparts. Fig.I0.52 shows a progressive increase in the limiting current plateau for deposits grown at various times. The plateau value corresponds approximately to that seen on the relevant I-t curves.

It is interesting to examine the effect of rotational velocity on developing rough deposits. Assuming a control potential of -I000 mV M.M.S. to correspond to mass transport controlled deposition at I00% cathode current efficiency, Fig.I0.53 shows steady (limiting) currents observed for deposits of 0 - I00 mins. growth. At $t=0$, the velocity exponent in the expression $I_L \propto U^n$ is approximately 0.73, as expected for a hydrodynamically smooth electrode. For deposits grown over the first I0 mins., this slope increases, being approximately I.0 for higher times. This is in accordance with known works involving hydrodynamically rough (knurled) cylinders, where the observed limiting current is directly proportional to peripheral velocity[190].

It may also be noted that at short times and deposits of developing

roughness ($\equiv$ 10 mins. in this case) the average slope obtained is apparently

intermediate between that for a hydrodynamically smooth electrode and a

saturated rough one. This 'indicator' technique of mass transport measurement

at a single potential corresponding to limiting current operation is rapid

and convenient , as previously noted, but lacks the precision of a

polarisation curve determination.

In industrial 'Eco-Cell' R.C.E.R.'s for metal powder production, the

cathode is continuously scraped to remove a stream of powder. It is important

to substantially preserve the surface roughness and enhanced area of the

powdered deposit, however, to maintain reactor performance. For this

reason, a small portion only is scraped at a given time, by means of a

'reciprocating point scraper' technique. The disastrous effect of a full

length, flat blade scraper is clearly shown in Fig.10.54 . Here a static

'tufnol' blade was allowed to contact the rotating,rough-deposit cathode

surface after 180 mins. In the absence of scraping, the current progressively

developed from a smooth cylinder value as described in early parts of this

section. After some 120 mins., the current tended to stabilise due to the

formation of a saturated condition of roughness. At t = 180 mins., the

scraper blade was engaged, the current rapidly falling to a value only just

in excess of the original, smooth cylinder value. The powdered deposit was

almost completely removed, leaving a substantially smooth electrode. The

enhanced mass transport due to rough deposit formation is also shown in

Fig.10.54 by a comparison of mass transport to a knurled R.C.E. of peak to

valley roughness 0.3 mm. (according to Kappesser et al., equation 6.6[190]).

A limiting current of 1.2 A, equivalent to that of a knurled cylinder of

such roughness was reached after 35 mins., the current then steadily

increasing to a value of 5.8 A, some 4.8 times greater. The maximum current

shown for the powdered rough deposit is equivalent, in terms of the

Kappesser et al. equation, to a peak to valley roughness > 7 mm. This

clearly demonstrates the special enhancement of mass transport characteristic

of rough electrodeposits.

The reasons for such enhancement are severalfold. Firstly, scanning electron

microscopy and electrode capacity and impedance measurements[68,84,380] have

shown an appreciable surface area increase compared to smooth electrodes.

While the electroactive area for powder formation is appreciably less than

the actual one[68], it is considerably larger than the projected geometrical

area. Secondly, the hydrodynamic roughness of the deposits will result in a

considerable thinning of the convective diffusion layer, due to hydrodynamic

shear near the electrode. This bulk effect may be reinforced by the local

production of severely turbulent micro-eddies around marked protuberances

on the surface of the irregular deposits.

12.6 PROFILOMETRIC MEASUREMENTS DURING THE DEVELOPMENT OF ROUGHNESS

Stylus-traverse measurements revealed that surface roughness increased

rapidly during potentiostatic deposition at -1000 mV M.M.S. (Fig.10.43). The

use of higher rotational speeds resulted in a more rapid increase and also

a higher roughness at a given time. At longer times, the roughness tended to

reach a reasonably constant, 'saturated' value. This may be attributed to

the overgrowth of copper powder, such as to preserve the average roughness

value.

Actual profilometric traces for rough deposits produced after various times

(Fig.10.44) clearly show that the development of roughness is progressive

and takes place almost immediately. The development is particularly

noticeable between 25 and 30 mins. at 340 r.p.m. (Fig.10.44 d/e). After 50

mins., the roughness increased to such a degree that change to a less

sensitive stylus was necessary: this larger stylus did not accurately

follow the surface profile.

The actual range of roughness at any time is shown to be large, particularly for the rougher (longer time) deposits. The growth of roughness at, or near, limiting current conditions has been discussed by Ibl et al.[380,411], using the following interpretation. The initial 'smooth' surface has small scale geometric irregularities. The current density tends to be greater at the peaks due to a smaller solution resistance there, giving rise to the 'primary current distribution'. Activation overvoltage tends to counteract the electrolyte resistance resulting in the 'secondary current distribution'. The relevant parameter for current distribution consideration is $K \, d\eta/d \, i$, where K is the specific conductivity of solution and $d\eta/d \, i$ the slope of the potential/current curve. If this 'polarisation parameter' is large compared to the profile length h, the current distribution will be uniform, despite the irregular geometry. Only activation polarisation smoothes the current distribution, while concentration polarisation has the opposite effect. The diffusion layer thickness, d_N is then appreciably larger than h. Under mass transport control, deposition is markedly favoured at peaks leading to amplification of surface roughness.

I2.7   SCANNING ELECTRON MICROSCOPY AND MORPHOLOGY

Scanning electron micrographs provided a convenient and revealing picture of the extent and type of growth during prolonged potentiostatic deposition. Previous studies by Robinson[68] extensively examined the morphology of rough copper deposits from acid sulphate. In contrast to the present work, however, Robinson employed high copper concentrations (0.07 or 0.7 M $CuSO_4$) and a largely galvanostatic/coulostatic approach. The brief studies reported in this Thesis were intended to complement electrochemical and profilometric measurements, and were conducted potentiostatically in 0.014 M $CuSO_4$ +

$I.5$ M H_2SO_4 .

At a constant control potential of - 1000 mV M.M.S., the development of
rough deposits is shown in Fig.10.45 . At short times, ~2 mins., early
growth takes place preferentially along scratch marks (Fig.10.45.i),
resulting in miniature parallel rows of nodules. After 5 mins., certain of
the nodules have grown preferentially (Fig.10.45.b). This situation
continues for some time (Fig.10.45.c and j). Multinodular growth at many
sites over the entire surface is evident by 20 mins.(Fig.10.45.d and k).
After 45 mins. (Fig.10.45.e and l), certain nodules are seen to have grown
preferentially, so as to stand proud of the surface. The wide variety of
nodule sizes is also evident from Fig.10.45.l and m . After 60 mins., the
predominant nodular growths have formed clusters (Fig.10.45.f) and overgrowth
occurs at longer times (Fig.10.45.g). The multinodular fine structure of a
single nodule,is shown clearly in Fig.10.45.n . At long times ($\geqslant$ 90 mins.),
the deposits were truly powdery in the sense that the deposit was disperse
and easily separated from the rotating cylinder cathode.

The markedly different morphology of deposits after 60 mins. for various
potentials is shown in Fig.10.46 . At low potentials, - 750 mV M.M.S., the
surface is rough but not powdery, while at more negative potentials near or
on the limiting current plateau, extensive powder formation is seen. The
use of potentials beyond the limiting current plateau (i.e. corresponding
to some hydrogen evolution) e.g. - 1200 mV M.M.S., resulted in very fine
powder particle size (Fig.10.46d).

The effect of rotational speed after a fixed time (60 mins.) is illustrated
in Fig.10.47, where the use of high speeds (i.e. high mass transport) is
seen to result in more extensive powder formation.

Some special features of deposits,revealed at high magnification, may be
briefly mentioned. Fig.10.48 shows a multiple layered growth, where the tips

of nodules are evidently being extended in one predominant direction.

Occasionally, star-shaped multinodular growths were observed (Fig.IO.49), as

opposed to the more normal spherical forms. Such growths were rare at the

low temperature $(22^{o}C)$ used, as were dendritic, feathery growths. Fig.IO.45.k,

however, indicates a tendency towards the formation of a branched,

dendritic growth. Finally, the 'rosette' type structure of an individual

branched nodule from Fig.IO.49 is shown in Fig.IO.50 .

I2.8   INFLUENCE OF THIOUREA ON ROUGHNESS DEVELOPMENT

The effect of thiourea on the development of rough copper deposits has been

previously studied by Ibl et al.[380] and Gabe and and Robinson[84] (Table I2.5).

Both of these investigations involved rather concentrated copper solutions,

however, and the studies by Ibl et al.[380] involved natural convection to a

static electrode. The present studies are concerned with more dilute, 0.OI4M

Cu solutions, polarisation behaviour and reactor performance.

Thiourea had a marked effect on the rest potential of a copper R.C.E. (Table

IO.8), a more negative value being generally recorded with increased thiourea

additions. There was relatively little change at low $(\leqslant 10^{-4}$ M) additions,

but the influence was marked at higher $(\geqslant 10^{-3}$ M) levels. At particularly

high levels $(\sim 10^{-I}$ M), the open circuit potential became unstable, the

copper being coated with a dark grey/brown film.

The polarisation behaviour for copper deposition in the presence of thiourea

was somewhat complex (Fig.IO.58), and perhaps better viewed in terms of

overpotential vs. current curves (Fig.IO.59). The well-defined limiting

current plateau evident at potentials in the range of cathodic overpotentials,

0.45 to 0.60 V, was no longer seen for the thiourea containing solutions.

Small concentrations of thiourea $(10^{-4}$, 10^{-3} M) appeared to slightly

polarise the deposition reaction, while higher levels (10^{-2} and 10^{-I} M) appeared to effect marked depolarisation. Concentrations of 10^{-5} M resulted in polarisation behaviour which was broadly comparable with pure solutions. 10^{-3} M solutions gave a shortened inflection at $\eta = 550$ mV rather than a, well -defined plateau. Polarisation behaviour at high thiourea levels was highly irreproducible, presumably due to the irreversible formation of surface films and the poisoning of the copper deposition reaction.

The effect of thiourea was examined in two modes: batch decay and constant copper concentration. Batch decay trials (Fig.10.60) showed that low concentrations of thiourea (10^{-5} M) gave a performance roughly comparable to 0 M solutions, the development of roughness occurring in much the same way. Higher concentations (10^{-4} M) resulted in a longer effective initiation time for an increased rate of decay; the decay at higher times was no longer semi-logarithmic. The suppression of roughness at 10^{-3} M levels was such that the decay behaviour was broadly similar to solutions without thiourea, no increased rate being apparent. The suppression of roughness at 10^{-2} and 10^{-I} M levels was severe and the copper deposition reaction was effectively poisoned, little change in copper concentration occurring.

Similar considerations applied to the case of constant copper concentration. The current growth at 10^{-5} M thiourea concentrations was just below that for pure copper solutions. 10^{-4} M levels tended to suppress growth somewhat, while 10^{-3} M solutions resulted in a relatively constant current and substantially smooth deposition. Some increase in current was apparent at longer times, possibly as the thiourea level in solution was effectively decreased due to mass transport adsorption at the R.C.E. High thiourea levels (10^{-2}, 10^{-I} M) once again poisoned the copper deposition reaction, resulting in partially conductive film formation and low currents.

These results are relevant to the treatment of certain industrial effluent

solutions in powder producing reactors such as the 'Eco-cell'. In the case

of electroplating bath dragouts, for example, the copper concentration may

build up to I000 p.p.m., while thiourea based additives may gradually

increase to the range studied. In addition, the results show convincingly that

roughness formation during mass transport controlled deposition may be

suppressed by the correct concentration of electroactive additive. This is in

striking contrast to the results of Robinson and Gabe[84] where, at the 0.7 M

Cu level (which is typical of plating baths), thiourea additions were not

effective in roughness suppression.

. The mechanism of levelling by thiourea is reasonably well understood[43].

Thiourea is codeposited, under mass transport control, with the metal,

preferential deposition taking place near asperities. The resultant local

increase in overpotential at peaks favours deposition in the recess. Thus

both discharge of cupric ions and thiourea adsorption are mass transport

controlled. Depending on the relative concentrations and reactor conditions

(potential and degree of mass transport), either process may dominate, giving

rise to rough deposits or smooth ones for extreme cases.

The studies by Ibl et al.[308] showed that in 0.I N $CuSO_4$ solutions and high

thiourea concentrations ($\sim 2.6 \times 10^{-2}$ M), prevention of roughness was possible,

as with the present studies. At higher Cu concentrations (I N $CuSO_4$),

substantial roughness development occurred despite thiourea additions, in

accordance with the results of Robinson and Gabe[84].

I2.9   MASS TRANSPORT TO KNURLED ROTATING CYLINDERS

The previous sections have considered mass transport to rough deposits. Such

surfaces are difficult to characterise, regarding both surface area and the

range and type of roughness. The study of such surfaces is important,

however, for a variety of reasons:

(i)   the formation of rough surfaces represents an extreme limit for the

       production of electroplated deposits,

(ii)   random roughness formation is common to corrosion and other dissolution

       processes,

(iii) the production of powdery deposits (Chapter 7) is one of the essential

       preparative techniques for the powder metallurgy industry,

(iv) the high mass transport to rough deposits results in enhanced reactor

       performance and facilitates

(v)   fast, efficient and sometimes selective removal of metals from dilute

       solutions in the industrial 'Eco-cell'.

The study of electrochemical mass transport to surfaces of well-defined,

reproducible, uniform roughness provides a basis for comparison. Knurling is

an obvious machining technique for the production of a standard roughness. It

has the advantage that the peak to peak spacing may be altered (by choice of

tools) somewhat independently of the depth of knurling (which may be

controlled by pressure on the tool). Regarding practical reactors, the

knurling of a rotating cylinder cathode may introduce the advantages of a

faster development of deposit roughness during initial start up, together

with a more adherent powder deposit due to mechanical 'keying'.

In contrast to rough deposits, knurling normally results in only modest

increases in surface area compared to a geometrically projected smooth surface.

Indeed, this increase has normally been disregarded in mass transport studies

190,191. Before a consideration of results on copper deposition to knurled

R.C.E.s, it is useful to consider alternative methods for the production of

standard roughnesses:

(i)   grooving[317] - the machining of grooves or slots is tedious and care

       must be taken not to gretly increase the surface area or depart from a

basic rotating cylinder geometry. Grooves may be machined along the
dimension of the axis, or circumferentially. Alternatively a helical
('screw thread') groove may be cut. Clearly, the direction of the groove
relative to both the cylinder dimensions and the rotation sense may be
all important.

(ii) wire overlay[413] - a technique which has proved useful in levelling
studies has utilised the wrapping of wire around a cylindrical former.
This has the advantage of producing a very regular, predetermined,
pseudo-sinusoidal profile. The technique could prove useful in cases
where the active material must be minimised e.g. platinum. The depth
of profile is readily altered by employing wires of different diameter.

(iii) sand casting[9] - this produces a very irregular, 'saturated' roughness,
which resembles that from sand blasting.

(iv) abrasives - emery cloth or wire brushing also produces a non-uniform
roughness, which is difficult to characterise.

(v) finning - the use of massive projections from a R.C.E. may result in
stagnant zones around the electrode, and a radically different geometry.

Results for copper deposition are shown in Figs.I0.55 and I0.56 for I.5 cm.
and 6.0 cm. diameter cylinders which have been knurled to yield a range of
roughness values. For the corresponding smooth cylinders, the I_L vs. ω plots
indicate the normal relationship

$$I_L \propto u^n$$

Equation I2.25

where $n \approx 0.7$.

For the knurled cylinders, behaviour approximates to $n \approx I$ in all cases, an
increase in roughness yielding a higher mass transport. A composite plot of
the data as j_D' vs. Re indicates that, for a given value of relative roughness,
d/ϵ , the mass transport is appreciably higher (Table I2.6) than that predicted
by the generalised equation due to Kappesser et al.[190],

$$j_D' = \left[1.25 + 5.76 \log_{10} d/\epsilon \right]^{-2} \qquad \text{Equation } 12.26$$

which was reported for oxygen reduction to monel R.C.E.'s. In addition, it was surprising to find that all knurled cylinders acted as hydrodynamically rough surfaces. In view of the equation describing the criteria for an electrode to obey the above relationship,

$$Re_{crit} = \left(11.8 d/\epsilon \right)^{1.18} \qquad \text{Equation } 12.27$$

and in the range, of (Re) employed, the 1.5 cm. diameter, $d/\epsilon = 833$ and $d/\epsilon = 500$ cylinders should have behaved as 'smooth' systems. It should be remembered that the present results concern a very specific set of conditions however, i.e. one concentration and only a decadic range of rotational speed. It is interesting to compare the mass transport performance of knurled and rough deposit cylinders under set conditions: 0.014 M Cu, 22°C, and a cylinder of diameter 6 cm. rotating at 360 r.p.m. (Fig. 10.54).

12.10 MASS TRANSPORT TO AN ULTRASONICALLY STIMULATED R.C.E.

Ultrasound (Section 4.9) is known to have a significant effect on the deposition of metals from electroplating solutions. In particular, the application of ultrasonics may result in harder deposits of lower porosity with less hydrogen embrittlement, and the deposition rate may be increased. For example, Kochergin and Vyaseleva[242] have reported increased rates of up to 8 times for copper deposition.

Ultrasound has also been advocated for the electrowinning of copper in tankhouse operations[243]. In this case, advantages claimed included a slightly decreased cell voltage and a lower capital cost by virtue of the fewer electrodes necessary at higher current density. Overall operating costs were higher, however.

Walker[241] has briefly described an ultrasonically stimulated fluidised bed electrode, where particle agglomeration was discouraged by the vibration. The extent and mechanism of mass transport enhancement by ultrasonics is not

well understood, and several effects may be operative.. These include bulk

agitation, jet flow, micro streaming due to high velocity eddies, standing

waves and cavitation. This last effect is believed to be the most important in

disrupting the convective diffusion layer.. It is unfortunate that the effects

of ultrasonic fields on mass transport have not been studied in well-defined

hydrodynamic regimes, and this has undoubtedly lead to conflicting results.

In the brief studies reported here, ultrasonic stimulation markedly changed

the polarisation and mass transport behaviour during copper deposition to a

turbulent R.C..E. As shown in Fig.IO..63, the polarisation curves appeared to

be markedly shifted to less cathodic potentials such that the limiting current

plateaux lay in the overpotential range 0.35 - 0.50 V, rather than the normal

0.45 - 0.60 V. The potential at which hydrogen evolution occurred was also

lowered to an overpotential $\sim$0..50 V.

Mass transport results for these preliminary studies are presented in Fig.IO.64

as K_L vs. (Re). For the case of smooth cylinders without ultrasonics, the

results are reasonably well correlated by

$$K_L = U^{0.70}$$ Equation I2.28

in accordance with other works. The application of ultrasound resulted in a

set of data which could not be easily treated in the above fashion. This may

be the result of the ultrasonic transducer position and its relation to

cell geometry, or the change in relative intensity of mass transport due to

the combined effects of bulk solution turbulence and ultrasonic stimulation.

In any case, ultrasound enhanced mass transport appreciably, by factors of

approximately I.4 to 2.0 times, showing that the already high mass transport

to a smooth R.C.E. may be increased still further by this technique.

I2.II MASS TRANSPORT TO PILOT PLANT 'ECO-CELL' REACTORS

The 'Eco-cell' process[306-308] for metals extraction has largely evolved via an empirical approach due to the difficulty in correlating mass transport to irregular rough deposits. Holland[307,308] has attempted to correlate data by an equation of the form:

$$(St) = a (Re)^b (Sc)^c \qquad \text{Equation I2.29}$$

Arguing that (Sc) describes only the transport properties of the electrolyte (which are unaffected by cylinder rotational speed or roughness), 'c' was assigned a value of -0.644, as reported by Eisenberg et al.[57,58]. From literature studies, the constant 'a' appeared to have an agreed value of $0.079I$, leading to

$$(St) = 0.079I (Re)^p (Sc)^{-0.644} \qquad \text{Equation I2.30}$$

Here the (Re) exponent was changed to 'p' to indicate 'powder' growth conditions.

From experimental results on copper deposition, 'p' was calculated from mass transport experiments by means of the equation

$$i_L = 0.079I \ z \ F \ C \ U \left(\frac{Ud}{\nu}\right)^p \left(\frac{\nu}{D}\right)^{-0.644} \qquad \text{Equation I2.31}$$

It was realised that the powdered metal surfaces had time dependent characteristics, including electroactive surface area and roughness; the surface changed continuously due to growth and powder loss (by gravity, centrifugal forces or mechanical disruption). Therefore, although the effective current depositing metal (assumed to be equivalent to i_L) could be measured, the true current density was indeterminate. The practical way around this problem was to assume no change in surface area during growth, current densities referring to geometrically projected area.

An <u>averaged</u> value of the 'p' exponent was -0.08, transforming equation I2.31 into

$$i_L = 0.0791 \; z \; F \; C \; U \; (Re)^{-0.08} \; (Sc)^{-0.644} \qquad \text{Equation I2.32}$$

The enhanced mass transport in 'Eco-cells' was illustrated by comparing this

equation with an existing correlation for copper deposition at smooth

cylinders, due to Robinson and Gabe[68,84]

$$i_L = 0.0791 \; z \; F \; C \; U \; (Re)^{-0.31} \; (Sc)^{-0.59} \qquad \text{Equation I2.33}$$

The difference (which may be IO- IOO times for practical cells) was ascribed

to the decreased value of the (Re) exponent (Table I2.7). It was considered

that this equation was a reasonable description of mass transport over a wide

range of conditions, as scaleup had involved a diameter increase of 6 times

and a projected surface area increase of 29 times.

It should be realised that variation occurred in the value of 'p' calculated

in this manner (Table I2.8), and due to the form of the power law relationship,

apparently small variations may result in relatively large changes in the mass

transport.

Plots of j_D' vs. (Re) for 'Eco-cell' plants show that considerable scatter

occurs in the data. In practice, Equation I2.32 has proved to be a useful

empirical prediction of scaleup, and this is perhaps reflected in Figs. II.I5

and II.I6 where the data fall near the correlating line. It should be noted

that each of the pilot plants was somewhat different regarding design and

geometry.

In comparison to academic mass transport studies (Chapter 4), there may be

several objections to the 'Eco-cell' data:

(i)   the limiting current, as such, was not measured via a conventional

      polarisation curve; rather a 'useful current' was found (Section II.3)

      from reactor performance. As the majority of trials involved hydrogen

      evolution (current efficiency values were as low as 60%), this may

have enhanced mass transfer appreciably. Moreover, the enhancement is
is expected to be more severe at low (Re) than at higher (Re), and to
depend on surface roughness and the potential of the electrode (Sections
I2.3 and I2.5).

(ii)   the powdered metal surfaces were not characterised; neither was the
initial surface roughness, that is, whether it was a blasted, smooth,
abraded or knurled surface- this may appreciably affect the mass
transport. In addition, the growth characteristics of the powder
result in a time-dependent mass transfer, influenced by powder fall-off
and regrowth.

(iii)   the viscosity and diffusion coefficient were not measured, and may have
changed significantly in some of the impure solutions. A small change in
the (Sc) may appreciably change the mass transport predicted by a
correlation.

(iv)   pure copper sulphate / sulphuric acid solutions were not used in all the
experiments. In some cases, organics and chloride were present which may
have consumed current or stabilised the Cu (I) species.

(v)   the geometry of the rigs used was varied, and no account was taken of
flow separation or the importance of the gap width (Section I2.2).

(vi)   comparatively few data points are available when it is remembered that
the majority involve <u>one</u> solution at <u>one</u> r.p.m. and <u>one</u> concentration.
In mass transfer correlation, every effort should be made to obtain
data over a wide range of (St), (Re) and (Sc), in view of the power law
relationship between the variables.

(vii)   reproducibility of a single datum point was very poor in certain cases,
there being as much as $\pm$ 20°/o variation about a mean. In some cases,
reproducibility was not well established.

The particularly high mass transport to an 'Eco-cell' R.C.E. is shown clearly

in Fig.II.I7 , where a comparison is made with equations due to Eisenberg et al. and Theodorsen and Regier. Not only is the mass transport (as indexed by j_D') higher, but the relative difference increases at higher (Re). It may be noted that the 'Eco-cell' has normally been operated at $IO^5 < Re < IO^7$; a higher range than that of previous workers.

I2.I2   EXPERIMENTAL PERFORMANCE OF PILOT PLANT REACTORS

The general approach adopted in the pilot plant studies was as follows. Cathodic polarisation data for metal deposition was first obtained, either potentiostatically or galvanostatically. Examination of this allowed judicious selection of a control potential (potentiostatic) or a current (galvanostatic) for steady state operation. Metal powder was then produced continuously, and a mass balance performed over the system.

A general feature of the cathodic polarisation data for the pilot plant is the existence of poorly defined limiting currents (Fig.II.I) . There is an inherent problem in obtaining true polarisation curves in a reactor having a high conversion. Ideally, such potential-current curves should be generated under conditions of constant metal concentration. As the potential (and hence the current) is raised, however, for a given inlet concentration, C_{IN} , C_{OUT} ($= C_{reactor}$) declines as the fractional conversion increases. The best approach is to examine only the plateau region (Fig.II.2), where the existence of a reasonably constant mass transport encourages a uniform, invariant metal concentration.

The polarisation curves for copper deposition have a similar overall shape to those in the laboratory studies, hydrogen evolution occurring as a secondary reaction at post-limiting current potentials. Limiting current values (taken from Fig.II.2) indicate a direct proportionality to copper concentration (Fig.II.3) . The slope of this curve allowed an averaged mass transport

coefficient to be calculated as 0.262 cm s^{-1}. This is particularly high in comparison to other reactors, showing the mass transport advantage of a powdery, rough rotating cylinder under highly turbulent conditions.

Steady state electrolysis (Table II.3) indicated that K_L values were somewhat variable in the range 0.368 - 0.425 cm s^{-1}, this being partly attributable to the variation in the surface roughness and electroactive area of the powder deposit due to continuous growth and removal. The result of this variation was reflected in the conversion factor, C_{IN}/C_{OUT}, which lay in the range 1.90 to 2.04. The conversion factors here were appreciably higher than those calculated from the Holland equation (Equation 12.32). This was perhaps attributable in part to a low cylinder-to-vessel gap encouraging hydrodynamic shear. It is interesting to note that the linear speed of the reciprocating scaper was not important in the range 0.91 to 9.1 cm s^{-1}, indicating that the powder surface was maintained in a suitable manner i.e. having a satisfactory roughness and active area.

Concentration decay experiments allowed comparable mass transport data to be obtained. Fig.II.4 shows that I_L vs. C data for steady state and concentration decay conditions could be collapsed to a single plot. Fig.II.5 indicates that the reactor conversion was very sensitive to flow rate, as expected. An abrupt decrease in flow caused a rapid lowering in concentration, but the rate of decay (and hence K_L) remained similar at the constant rotational speed. The decay was essentially exponential, as expected from such a batch recirculation system (Chapter 6).

In summary, the copper deposition trials showed the 500 A pilot plant to operate satisfactorily in a single pass or batch recirculation mode, and the power requirements (Fig.II.7) proved moderate.

Cadmium deposition trials (Fig.II.8 and Table II.6) also proved successful in that cadmium powder of high purity could be electrodeposited continuously from a solution which was heavily laden with zinc. Such a separation is

important in the hydrometallurgical treatment of zinc calcine liquors, and

offers advantages over the conventional cementation process which requires

supply of quality zinc or iron powder, and subsequent separation.

The cadmium deposition may be contrasted with copper in several respects.

The limiting current plateau was less well defined for cadmium and appeared

at higher overpotentials (c.f. Figs.II.8 and II.I/2). Also, the mass transport

for cadmium deposition was much lower, this being a consequence of the

comparatively viscous zinc sulphate solution used. K_L values of $0.06-0.14$ cm s^{-1}

were obtained for cadmium, in comparison to ~ 0.40 cm s^{-1} for copper at a

similar rotational velocity.

12.13 CASCADE 'ECO-CELL' REACTORS

The concept of a cascade R.C.E.R. was introduced in Section 6.6 , and typical results from the 50 A laboratory and I KA Commercial models have been presented in Section II.4 .

Table 12.9 summarises the characteristics of cascade 'Eco-cell' reactors to date. Further details of each model are given in a recent paper[414] which considers the development and performance of these reactors for metal removal. The 50 A laboratory model was essentially a perspex model cell used to demonstrate the feasibility of cascade action, and to investigate anode positioning. The results were used to scale up to the Commercial I KA design. While the above reactors operated in a satisfactory manner, the 200 A 'second generation' design was evolved with a view to :

(i)   lowering capital costs,

(ii)   improving engineering and minimising maintenance,

(iii) facilitating routine maintenance,

(iv)   attaining enhanced electrochemical performance, and

(v)   improving the ease and efficiency of metal powder removal.

A major change has been the use of a cylindrical cathode rotated vertically about its axis, as opposed to the previous horizontal designs. This has several advantages including :

(i)   minimisation of floor space,

(ii)   improved mechanical operation, and

(iii) greater ease of product recovery.

In the horizontal designs, metal was removed from the reactor after a prolonged period of operation, the electrolytic current and normal electrolyte flow were turned off, and the reactor was backwashed with a minimum volume of nitric acid, to chemically dissolve the copper. This proved a rapid and successful method of product removal, and in the case of the commercial reactor, the resultant copper nitrate concentrate could be recycled to the

first stage 'Eco-cell', producing copper powder. One of the inherent

advantages of the 'Eco-cell', that is product recovery as metal powder, was

lost , however. An additional consideration is that certain of the nobler

metals, e.g. the platinum group, are difficult to dissolve chemically, and so

the method has a more limited range of application.

In the improved vertical design, a scaper mechanism has been included to

remove powder from the cathode at suitable intervals, say once per 8 hours. At

such times, a backwash cycle could be initiated, such that the normal flow

(bottom-to-top) could be reversed to facilitate powder removal, aided by

gravity. Product removal is also encouraged by having apertures in the baffle

plates. In normal operation, the apertures are covered by a close-fitting

scraper blade arrangement, but during the metal recovery operation the blade

is moved out of the baffle space. The provision of multiple blades (one per

compartment) results in a much smaller displacement and decreased blade wear

compared to a single blade.

Ideally, individual cathode compartments should each operate at a potential

equivalent to deposition at or near the limiting current to ensure maximum

duty and high current efficiency. Such operation may be monitored by potential

profile measurements (Tables II.27 and II.28). Correct working potentials may

be chosen with the aid of auxiliary polarisation curves over the concentration

range of interest, with due regard for iR drops inherent in the cylinder

fabrication or reference electrode assemblies.

Theoretically, the conversion over a cascade assembly may be described by

$$(f_R)_n = I - \frac{I}{(I + K_L A/N)^n}$$
Equation 6.38

This may be rearranged :

$$LN\ C_{OUT} = -n\ LN\ (I + K_L A/N) + LN\ C_{IN}$$
Equation I2.34

For a given C_{IN} , $LN\ C_{IN}$ is a constant, and a plot of $LN\ C_{OUT}$ against n has

a negative slope of $LN(I + K_L A/N)$. Plots of this nature allow performance

to be evaluated, and an averaged K_L to be calculated. In the case of the 50 A

laboratory and I KA Commercial models, reasonable straight lines are obtained

(Figs.II.I8 and II.I9), giving average fractional conversions of 0.45 and

0.33 . This is equivalent to a mass transport coefficient of 0.38 and 0.53 cm.

s^{-I}, the latter value being greatest due to the correspondingly higher

peripheral velocity (Table II.20).

The preliminary reults for the 200 A Development model (Tables II.8- II.I9)

show that performance tended to deteriorate in higher compartments. This

feature was persistent at various temperatures, flow rates and currents.

Typically (Table II.I5 ; Fig.II.20) the cascade action was destroyed by

compartment 4, and higher compartments realised little concentration decrease.

Indeed, in some cases, compartments 5 or 6 were at a somewhat higher copper

level than compartment 4. From potential monitoring, it was clear that each

compartment was functioning near limiting current conditions,and the reactor

was disassembled. This revealed a fault condition in the design of the anode

box to baffle sealing. The situation was such as to allow a small percentage

of the catholyte from compartment I (high concentration) to bypass

intermediate compartments and emerge in compartment 4, 5 or 6 . This clearly

demonstrated the need for careful design and assembly of cascade reactors

operating under high conversion conditions, and future designs were modified

accordingly. Fig.II.20 allowed an averaged fractional conversion of 0.44 to be

calculated for early compartments of the 200 A reactor, equivalent to a K_L

value of 0.40 cm s^{-I}.

A cascade of CSTR's is a powerful reactor assembly, capable of high overall

conversions, and low exit concentrations of metal suitable for effluent

discharge. A turbulent rotating cylinder electrode geometry is a particularly

advantageous combination of flow pattern and geometry. A uniform electode

surface is provided, enabling a near equi-potential electrode to be used thereby allowing potentiostatic control to be exercised, while high mass transfer rates may be realised giving rise to high rates of conversion. In addition, the mass transfer to the electrode is largely independent of the actual flow rate, being governed primarily by the rotational velocity of the cylinder, and its surface roughness and area. This is in marked contrast to plug flow reactors such as packed beds and unstirred filter press cells where the mass transfer is strongly dependent on the flow rate. Mass transport controlled operation ensures maximum reactor duty.

In comparison to other high conversion reactors, the 'Eco-Cascade-Cell' does not suffer the limitations of high pressure drops which may occur as product builds up in packed beds or filter press cells, or problems with severely uneven potential distribution. Unlike the majority of other electrochemical reactors for metal removal, metal product may be recovered directly for reuse or sale ; this is particularly important in the case of precious metals. Despite the importance of cascade electrochemical reactors, there has been a surprising paucity of published work in this field. Sudall[200,201] and Pickett[120] have considered theoretical aspects of a cascade arrangement with respect to electrolyte flow and electrical connections. The first author has attempted to utilise experimental data from a single impeller-stirred CSTR in order to forecast, by computer, the behaviour of a cascade of similar elements. Conventional filter press plate cells are often designed on the basis of a number of CSTR compartments in hydraulic series, the CSTR model being a more reasonable approximation in the case of low throughput of electrolyte and thorough gas stirring.

A reactor often employed in larger scale photographic silver recovery, the 'Hickman Cell', employs a number of carbon plate anodes and interleaved stainless steel cathodes, with a paddle agitator moving between the plates. While this system has been considered as a cascade cell, in practice

considerable bypassing and non-uniform electrode potential result in non-idealised performance. In addition, mechanical disassembly, followed by scraping is necessary to remove silver.

Returning to the 'Eco-Cascade-Cell' reactor, it is interesting to note that if an infinite number of elements were provided, the system might be expected to approximate to a plug flow reactor (PFR), with an enhanced overall conversion. If each compartment behaves according to the plug flow model, the conversion over each element would be given by :

$$f_R = I - \exp \left(-K_L A/N \right) \qquad \text{Equation I2.35}$$

Assuming identical values of K_L, A and N, to the CSTR example, a value of $f_R = 0.632$ is obtained, which is somewhat greater than the 0.5 in the comparable CSTR case. In the case of a cascade of n identical plug flow elements, the overall conversion is given by :

$$(f_R)_n = I - \exp \left(-nK_L A/N \right) \qquad \text{Equation I2.36}$$

Table I2.IO compares CSTR and PFR conversions for a hypothetical cascade. It may be seen that as n increases, the difference between the two models diminishes.

Another interesting comparison may be made by removing the baffles from a cascade reactor. In this case, the reactor behaves as one compartment, with an increased surface area of n A. Table I2.IO examines this case for a ten compartment cascade, the fractional conversion being given by :

$$f_R = I - \frac{I}{nK_L A/N} \qquad \text{Equation I2.37}$$

and this result is equivalent to operating the n elements in series electrical connection and parallel flow. A consideration of Table I2.IO reveals that an overall conversion 0.875 may be attained by a three compartment reactor, in contrast to the seven undivided compartments of an unbaffled reactor.

Clearly the practical cascade reactors only approach the hypothetic or

theoretical models and despite careful control of flow, rotation rates,
temperature and concentration etc., a variable conversion factor was found
from compartment to compartment (see Tables 11.27- 11.32). Although this
must partly be attributed to imperfect construction of the cascade cell
compartment dividers thereby allowing bypassing to occur, it is also
attributable to a degree of randomness in the powder electrodeposit, and to
some redissolution of copper at low concentrations. Thus the great virtue of
potentiostatic control on the single compartment 'Eco-cell', which may ensure
near I00°/o efficiency, becomes much more difficult for the multi-
compartment cascade cell and efficiency is consequently lower. Notwithstanding
this deficiency it is quite clear that the cascade cell acts as a very
effective 'stripping' or 'polishing' stage in the removal of metal from
process effluent.

I2.I4 CLOSURE AND RECENT PUBLICATIONS

In the author's opinion, the rotating cylinder electrode offers a versatile
geometry offering scope for both fundamental and applied studies. While
knowledge and use of the device has been somewhat restricted in comparison to
the rotating disc, there is evidence of continued and growing interest in the
literature.

Regarding fundamental studies, it is interesting to note the recent contribution
of Billings and Ritchie[401] who have provided a brief note on the laminar flow
regime. A group of Indian[400] workers have utilised the R.C.E. as a tool for
the applied study of non-Newtonian flow.

Undoubtedly, much work remains to be done on characterisation of the flow
domains and the importance of electrode shape factors. The pursuance of
research here would greatly facilitate the routine use of the R.C.E.
Considering the possibilities of the rotating cylinder electrode reactor, the

recent publications of Coeuret et al.[398,399] are to be welcomed. In

particular, the latter paper[399] concerns mass transport to an inner rotating

cylinder with axial flow - a most important practical case for single pass

or batch recycle reactors. These publications, however, largely deal with the

laminar or laminar + vortex flow regimes. In practical reactors, the turbulent

regime is probably much more important; there are several complications

associated with other flow regimes:

(i)   the coupling of axial flow with mass transport renders design and

        scaleup difficult, as the production rate becomes a function of two

        interrelated (Re) values,

(ii)   in vortex flow, the local mass transport distribution varies with

        electrode length and/or diameter, and

(iii) laminar and laminar + vortex flow regimes give rise to relatively low

        mass transport rates, and hence low production rates for a given ..

        reactor size.

It appears to the author that the most practically rewarding future studies

of the R.C.E.R. should concern the case of a fully turbulent reactor with

axial flow. As this Thesis hopefully shows, the mass transport in this case

is uniform and high, facilitating selective, high rate production in a

continuous manner - the object of many industrial electrochemical processes.

MEASUREMENT POINT	RUN OUT/μm
Cylindrical surface main slip ring	11
" " potential slip ring	8
Top section of drive shaft	2
Lower section of drive shaft	4
Cylindrical mid surface of cylinder	1
" " " of foil	0.3 mm.

TABLE 8.1 RUN OUT MEASUREMENTS FOR THE AUTHOR'S
LABORATORY ROTATING CYLINDER AND DRIVE
ASSEMBLY.

TRIAL	LIMITING CURRENT I_L/A	ELECTRODE PREPARATION
1	0.680	Wet '600 Grade' Emery Paper
2	0.710	"
3	0.720	"
4	0.695	"
5	0.700	"
6	0.685	"
7	0.685	"
8	0.725	"
9	0.710	"
10	0.715	"
11	0.690	Chemically Polished
12	0.705	Electropolished

mean I_L = 0.70 A ± 0.02

for trials 1 - 10

TABLE 10.1   REPRODUCIBILITY OF LIMITING CURRENT DETERMINATION
FROM POLARISATION CURVES.

0.014M $CuSO_4$, 1.5M H_2SO_4, 22° C, 500 rpm,

d = 6.3 cm, l = 4.3 cm, 150 mV $(min)^{-1}$

POTENTIAL SCAN RATE /mV(min)$^{-1}$	LIMITING CURRENT /A
15	0.580
30	0.650
60	0.695
150	8.700
300	0.725
600	0.740
1500	0.765
3000	0.790

TABLE 10.2   EFFECT OF POTENTIAL SCAN RATE ON THE OBSERVED

LIMITING CURRENT IN THE CASE OF A DIVIDED CELL.

Conditions otherwise as for Table 1.

PERIPHERAL VELOCITY U /cm s^{-1}	LIMITING CURRENT I_L /mA	LIMITING CURRENT DENSITY i_L /mA cm^{-2}	MASS TRANSPORT COEFFICIENT K_L x 10^3 /cm s^{-1}	STANTON NUMBER (St) x 10^3	REYNOLDS NUMBER (Re)	MODIFIED CHILTON-COLBURN FACTOR j_D' x 10^3
7.9	74	2.45	0.908	0.1157	1024	16.50
15.7	115	3.81	1.411	0.0898	2049	12.80
23.6	144	4.77	1.767	0.0750	3073	10.69
31.4	183	6.07	2.246	0.0715	4098	10.19
39.3	207	6.89	2.540	0.0647	5122	9.22
47.1	240	7.96	2.945	0.0625	6147	8.91
55.0	269	8.92	3.300	0.0600	7171	8.56
62.8	291	9.65	3.571	0.0568	8195	8.10
70.7	325	10.78	3.998	0.0564	9220	8.04
78.5	349	11.57	4.283	0.0545	10244	7.77

TABLE 10.3   <u>EXPERIMENTAL MASS TRANSPORT DATA FOR COPPER DEPOSITION ONTO A SMOOTH R.C.E.</u> (Selected Data Only)

d = 1.5 cm; l = 6.4 cm; A = 30.2 cm^2; T = 22°C

0.014 M $CuSO_4$ + 1.5 M H_2SO_4 (Sc) = 1825

PERIPHERAL VELOCITY U /cm s^{-1}	LIMITING CURRENT I_L /mA	LIMITING CURRENT DENSITY i_L /mA cm^{-2}	MASS TRANSPORT COEFFICIENT K_L x 10^3 /cm s^{-1}	STANTON NUMBER (St) x 10^3	REYNOLDS NUMBER (Re)	MODIFIED CHILTON-COLBURN FACTOR j_D' x 10^3
31.4	350	2.97	1.100	0.0350	16391	4.99
62.8	525	4.35	1.610	0.0256	32782	3.65
94.3	720	5.97	2.209	0.0234	45173	3.34
125.7	905	7.50	2.776	0.0221	65562	3.15
157.1	1050	8.70	3.221	0.0205	81955	2.92
188.5	1200	9.95	3.681	0.0195	98348	2.78
219.9	1330	11.02	4.080	0.0186	114736	2.65
251.3	1415	11.73	4.341	0.0173	131129	2.47
282.7	1540	12.77	4.724	0.0167	147517	2.38
314.2	1680	13.93	5.154	0.0164	163909	2.34

TABLE 10.3 (cont'd)

d = 6.0 cm; l = 6.4 cm; A = 120.6 cm^2;   22°C

0.014 M $CuSO_4$ + 1.5 M H_2SO_4 (Sc) = 2212

TABLE 10.3 (cont'd)

MASS TRANSPORT TO SMOOTH R.C.E.

d = 6.3 cm;   l = 4.3 cm;   rpm = 500;   U = 165;

cm s^{-1};   A = 85.1 cm^2;   0.014 M; $CuSO_4$ - Effect of Temperature

TEMP T /^{o}C	LIMITING CURRENT I_L /A	MASS TRANSPORT COEFFICIENT K_L /cm s^{-1} x 10^3	REYNOLDS NUMBER	STANTON NUMBER x 10^5	MODIFIED CHILTON-COLBURN FACTOR j_o' x 10^3
22	0.700	3.044	90,391	1.845	2.630
29	0.845	3.675	103,950	2.227	2.591
35	1.010	4.392	122,294	2.662	2.478
45	1.135	4.936	143,577	2.992	2.205
60	1.390	6.045	182,689	3.664	1.879

TEMP T /^{o}C	KINEMATIC VISCOSITY ν /cm^2 s^{-1}	DIFFUSION COEFFICIENT D /cm^2 s^{-1} x 10^6	SCHMIDT NUMBER
22	0.0115	5.2	2212
29	0.0100	6.2	1613
35	0.0085	7.45	1141
45	0.00724	9.12	794
60	0.00569	12.58	452

REGRESSION TABLE

VARIABLE	COEFFT.	STD. ERROR	T-VALUE
b	-0.3143	0.0156	-20.1967
c	-0.5982	0.0269	-22.2579
LOG a	-1.0506	0.1305	-8.0487

ANALYSIS OF REGRESSION TABLE

SOURCE	SUM SQUARES	D.F.	MEAN SQUARE	F-VALUE
DUR TO REGRESSION	0.6307	2	0.3154	357.5
ABOUT REGRESSION	0.0388	44	0.0009	
TOTAL	0.6695	46		

$$\text{STD. ERR. ESTIMATE} = 0.0297$$

$$\text{MULTIPLE CORR. COEFF.}(R) = 0.9706$$

$$\text{DETERMINATION } (R^2) = 0.8420$$

$$\text{CORRECTED } R^2 = 0.9394$$

THE VARIABLES GIVEN IN THE REGRESSION TABLE YIELD:

$$(St) = a \, (Re)^b \, (Sc)^c$$

$$(St) = 0.089 \, (Re)^{-0.31} \, (Sc)^{-0.60}$$

TABLE 10.4   STATISTICAL INFORMATION FROM THE COMPUTER PROGRAMME

FOR MASS TRANSPORT CORRELATION

Input Data due to Robinson[68]

COPPER CONCENTRATION C		LIMITING CURRENT I_L/A	MASS TRANSPORT COEFFICIENT K_L /cm s^{-1}
/mg dm^{-3}	/M		
1000	0.0157	0.775	0.00300
890	0.014	0.700	0.00304
500	0.0787	0.395	0.00310
250	0.00393	0.195	0.00302
200	0.00315	0.160	0.00309
125	0.00197	0.105	0.00325
100	0.00157	0.081	0.00314
62.5	0.00098	0.051	0.00317
50	0.000786	0.046	0.00356
40	0.000629	0.038	0.00368
20	0.000315	0.018	0.00348
10	0.000157	0.012	0.00464

TABLE 10.5   MASS TRANSPORT COEFFICIENTS AT VARIOUS COPPER

CONCENTRATIONS

(corresponding to Fig. 10.10, where the averaged mass transport

coefficient is given by the slops as 0.0033 cm s^{-1})

Metal	Concentration/mg dm^{-3}	
	Solution I	Solution II
Au	14.3	830
Ag	20.4	0.09
Cu	23.0	2.2
Fe	2.6	25
Ni	25.6	0.04
Sn	18.0	-
pH	11.7	4.8

TABLE 10.6 COMPOSITION OF INDUSTRIAL CYANIDIC, MIXED METAL

SOLUTIONS.

pH	METAL CONCENTRATION/mg dm^{-3}		
	COPPER	SILVER	GOLD
11.7	23.0	20.4	14.3
5.0	22.6	20.4	14.3
4.0	22.4	19.0	14.2
3.5	21.2	12.3	14.2
3.0	5.7	4.4	14.2
2.0	3.8	2.1	14.2

TABLE 10.7   COMPOSITION OF THE INDUSTRIAL CYANIDIC EFFLUENT

SOLUTION AT VARIOUS pH VALUES.

THIOUREA CONCENTRATION /M	REST POTENTIAL OF R.C.E. /V (M.M.S.)
0	-0.447
10^{-5}	-0.449
10^{-4}	-0.445
10^{-3}	-0.503
10^{-2}	-0.570
10^{-1}	-0.860
	(unstable)

TABLE 10.8   OPEN CIRCUIT POTENTIALS FOR A COPPER R.C.E. IN
THE PRESENCE OF THIOUREA

0.014 M $CuSO_4$

1.5 M H_2SO_4

22° C.

d = 6.3 cm

rpm = 340

U = 112 cm s^{-1}

CATHOLYTE FLOW RATE (nom.)	$40 \ 1 \ (min)^{-1}$
ANOLYTE FLOW RATE	$5 \ 1 \ (min)^{-1}$
CATHOLYTE TEMP.	$60^{\circ} \ C$
ANOLYTE TEMP.	$40^{\circ} \ C$
CYLINDER R.P.M.	500
PERIPHERAL VELY.	$559.5 \ cm \ s^{-1}$
DIAM.	22.9 cm
HEIGHT	22.7 cm
AREA	$1633 \ cm^2$
MATERIAL	COPPER PLATED STEEL
ANODE MATERIAL	DSA DIAMOND SHAMROCK
ANOLYTE	$1N \ H_2SO_4$
CATHOLYTE	$1N \ H_2SO_4$ $+ \ CuSO_4, 10 \rightarrow 600 \ ppm.$

TABLE 11.1 EXPERIMENTAL CONDITIONS FOR COPPER DEPOSITION FROM ACID SULPHATE SOLUTIONS

DATA SOURCE	I_L /A	C /mg dm^{-3}	K_L /cm s^{-1}
FIG. 11.1 A	175	138	0.256
B	484	360	0.271
FIG. 11.2 A	112	95	0.238
B	218	175	0.251
C	72	59	0.246
D	54	40	0.272

TABLE 11.2   Mass Transport Coefficients for Copper Deposition

in the 500A Pilot Plant 'Eco-Cell'

k_L /cm s^{-1}	RESULT	T TEMP. /°C.	SCRAPER SPEED /cm s^{-1}	E ELECTRODE POTENTIAL /mV MMS	CELL CELL VOLTAGE /V	I CELL CURRENT /A	IN INLET CONC. /ppm	OUT OUTLET CONC. /ppm	ΔC CONC. DIFF. /ppm	IN/OUT EXPTL.	I_o USEFUL CURRENT /A	C.C.E. /%	N FLOW RATE /l(min)$^{-1}$	IN/OUT THEORY	from EQN. 6.34
0.357	A	60	0.91	-900	7.7	415	380	200	180	1.90	354.5	85.4	38.9	1.73	-0.056
0.410	B	60	0.91	-900	7.1	372	360	180	180	2.00	354.5	95.2	38.9	1.73	-0.049
0.383	C *	58	0.91	-900	6.7	359	267	138	129	1.93	261.2	72.8	36.2	1.85	-0.054
0.337	D *	58	0.91	-900	4.3	182	195	107	88	1.82	178.2	97.9	35.8	1.87	-0.062
0.374	E *	58	0.91	-900	4.0	160	130	68	62	1.91	125.6	78.5	34.3	1.96	-0.055
0.283	F *	58	0.91	-900	3.8	142	71	42	29	1.69	58.7	41.3	38.9	1.73	-0.074
0.246	G *	58	0.91	-900	3.5	112	48	30	18	1.60	36.5	30.2	38.9	1.73	-0.084
0.223	H *	58	0.91	-950	3.1	91	34	22	12	1.55	24.3	26.7	38.9	1.73	-0.091
0.378	I	60	0.91	-800	8.0	448	500	260	240	1.92	486.0	108.5	38.9	1.73	-0.054
0.381	J	60	0.91	-850	8.1	500	560	290	270	1.93	546.8	109.4	38.9	1.73	-0.054
0.378	K	60	0.91	-850	8.1	450	490	255	235	1.92	475.9	105.8	38.9	1.73	-0.055
0.425	L	60	0.91	-850	8.0	500	550	270	290	2.04	567.0	113.4	38.9	1.73	-0.046
0.410	M	60	0.91	-850	8.2	500	550	275	275	2.00	556.9	111.4	38.9	1.73	-0.049
0.403	N	60	9.1	-850	8.2	510	585	295	290	1.98	587.3	115.2	38.9	1.73	-0.050
0.402	O	57	9.1	-850	8.3	510	525	265	260	1.98	526.5	103.2	38.9	1.73	-0.050

* concentration decay

TABLE 11.4   <u>DECAY RESULTS</u>

TIME /s	CELL VOLTS	CURRENT /A	USEFUL CURRENT /A Faradaic	C_{IN} /ppm	C_{OUT} /ppm	Δ C /ppm
0	6.7	359	261.2	267	138	129
600	4.3	182	178.2	195	107	88
1200	4.0	163	125.6	130	68	62
1800	3.8	142	58.7	71	42	29
2400	3.5	112	36.5	48	30	18
3000	3.1	91	24.3	34	22	12

Control potential – 900 mV MMS/1N H_2SO_4

Catholyte Flow Rate	$9 - 18.75$ dm^3(min)$^{-1}$
Anolyte Flow Rate	5 dm^3(min)$^{-1}$
Catholyte Temperature	$52 - 61.5$ $^{\mathrm{o}}$C
Anolyte Temperature	$32 - 42$ $^{\mathrm{o}}$C
Cylinder rotational speed	500 r.p.m.
Peripheral velocity	559.5 cm s^{-1}
Diameter	22.9 cm
Height	22.7 cm
Area	1633 cm^2
Material	Cadmium Plated Steel
Anode/Anolyte conditions	as Table 11.4
Catholyte	
pH	$1.93 - 3.2$
Zn (as sulphate)	127 gdm^{-3}
Cd (as sulphate)	128 mg dm^{-3}

TABLE 11.5   EXPERIMENTAL CONDITIONS FOR CADMIUM DEPOSITION FROM ZINC CALCINE LIQUORS.

						mg dm⁻³	mg dm⁻³	mg dm⁻³	/A		
1	60	-1.160	6.6	175	18	570	300	270	139	79.4	1.90
2	61	-1.2	6.6	172	18.8	520	290	230	123	71.5	1.79
3	60	-1.13	5.5	138	18.8	560	340	220	118	85.5	2.20
4	60	-1.12	5.5	139	18.8	620	405	215	115	82.7	1.53
5	60	-1.35	6.8	180	18.8	450	260	190	102	56.7	1.73
6	60	-1.3	6.6	175	18.8	480	280	200	107	61.1	1.71
7	52	-1.30	6.4	142	18.8	460	290	170	91	64.1	1.59
8	52	-1.3	5.9	130	18.8	500	275	225	121	93.1	1.82
9	53.5	-1.28	6.8	165	18.8	510	285	225	121	73.3	1.79
10	55	-1.12	6.0	140	18	510	385	125	106	75.7	2.08
11	58	-1.3	4.2	79	9	500	245	255	66	83.2	1.35
12	60	-1.3	4.4	71	9	175	92	83	21.4	30.1	1.90
13	60	-0.36	3.7	68	16	330	245	85	57	83.8	1.35
14	61.5	-0.59	4.4	91	16	250	170	80	36.7	40.3	1.47
15	60	-0.59	3.4	47	16	185	135	50	23	48.9	1.37
16	60	-0.58	3.0	30	17	150	102	48	23.4	78.0	1.47
17	60	-0.58	3.0	30	16	130	95	35	16	53.3	1.37
18	60	-0.57	2.8	25	16	145	115	30	14	56	1.26

TABLE 11.6   PILOT PLANT ELECTRODEPOSITION OF CADMIUM

			/V	/A	/dm^3(min)$^{-1}$						
19	60	-0.57	2.8	25	16	135	90	45	20.6	82	1.50
20	60	-0.54	2.9	27	15	123	81	42	18	67	1.52
21	60	-0.54	3.0	30	16.5	105	73	32	15	50	1.44
22	60	-0.49	2.8	26	16.5	110	69	41	19.4	75	1.59
23	60	-0.46	3.0	32	16.5	128	83	45	21.3	67	1.54
24	60	-0.43	2.9	33	16.5	138	87	51	24	73	1.59
25	60	-0.42	2.9	32	16	135	85	50	23	72	1.59
26	60	-0.43	3.0	34	16	133	80	53	24.3	71	1.66
27	60	-0.44	3.0	34	16	130	81	49	22.5	66	1.60
28	61	-0.40	3.2	42	15.5	165	104	61	27	64	1.59
29	61	-0.50	3.2	40	15.5	125	82	43	19	48	1.52
30	60	-0.46	3.0	31	15.5	120	98	22	10	32	1.22
31	60	-0.48	3.0	32	15.5	125	96	29	13	41	1.30
32	60	-0.44	2.9	26	16	130	105	25	11.5	44	1.24
33	60	-0.47	2.9	26	17	125	100	25	12.2	47	1.20
34	60	-0.42	2.8	25	17	143	110	33	16	64	1.43
35	60	-0.42	2.8	25	17	137	106	31	15	60	1.29

TABLE 11.6 (CONT.)

diameter of cylinder	=	30.6 cm
ave. length of compartment	=	14.4 cm
compartmental area	=	1387 cm^2
rotational speed	=	730 r.p.m.
peripheral velocity	=	1170 cm s^{-1}
catholyte temperature	=	20-60° C
catholyte flow rate	=	0.583 to 1 dm^3 s^{-1}
catholyte concentration	=	1.0M H$_2$SO$_4$

TABLE 11.7   GENERAL OPERATING CONDITIONS FOR THE 200A
ECO-CASCADE-CELL REACTOR.

PARAMETER	COMPARTMENT NO.						
	IN	1	2	3	4	5	6
POTENTIAL, E/mV (S.C.E.)	-	-550	-582	-540	-538	-363	-309
COPPER CONCENTRATION $C/mg\ dm^{-3}$	134	80	36	23	15.1	21.2	13.5
FRACTIONAL CONVERSION, f_R	-	0.403	0.550	0.361	0.343	-0.404	0.363

Anode pair used	No. 1
Temperature of Catholyte/^{0} C.	ca. 60
Catholyte Flow Rate/$dm^3\ s^{-1}$	1
Current /A	500
Overall Cathode Current Eff./%	73

TABLE 11.8 RESULTS OF STEADY STATE ELECTROLYSIS IN THE
200 AMP ECO-CASCADE-CELL REACTOR.

PARAMETER	COMPARTMENT NO.						
	IN	1	2	3	4	5	6
POTENTIAL, E/mV (S.C.E.)	–	-583	-591	-557	-554	-377	-300
COPPER CONCENTRATION $C/mg\ dm^{-3}$	105	60	32	16.8	12.2	18.4	14.5
FRACTIONAL CONVERSION, f_R	–	0.429	0.467	0.475	0.274	0.508	0.212

Anode pair used	No. 1
Temperature of Catholyte $/^o\ C$	60
Catholyte Flow Rate $/dm^3\ s^{-1}$	1
Current $/A$	500
Overall Cathode Current Eff./%	55

TABLE 11.9   RESULTS OF STEADY STATE ELECTROLYSIS IN THE

200 AMP ECO-CASCADE-CELL REACTOR.

PARAMETER	COMPARTMENT NO.						
	IN	1	2	3	4	5	6
POTENTIAL, E/mV (S.C.E.)	-	-555	-577	-526	-544	-321	-336
COPPER CONCENTRATION $C/mg\ dm^{-3}$	112 ± 3.5	65 ± 2.8	29.9 ± 2.8	16.0 ± 3.0	12.1 ± 1.5	17.0 ± 2.5	13.3 ± 3.3
FRACTIONAL CONVERSION, F_R	-	0.420	0.540	0.465	0.244	0.405	0.218

Anode pair used	No. 1
Temperature of Catholyte/^{o} C.	60
Catholyte Flow Rate/$dm^3\ s^{-1}$	1
Current /A	500
Overall Cathode Current Eff./%	60

TABLE 11.10 RESULTS OF STEADY STATE ELECTROLYSIS IN THE
200 AMP ECO-CASCADE-CELL REACTOR.

PARAMETER	COMPARTMENT NO.						
	IN	1	2	3	4	5	6
POTENTIAL, E/mV (S.C.E.)	-	-438	-559	-546	-592	-340	-301
COPPER CONCENTRATION $C/mg\ dm^{-3}$	112 ±2.5	64 ±2.2	29.1 ±2.8	16.3 ±0.8	12.2 ±1.0	17.5 ±2.0	16.6 ±2.7
FRACTIONAL CONVERSION, f_R	-	0.429	0.545	0.440	0.252	0.434	0.051

Anode pair used	Nos. 1 + 2
Temperature of Catholyte $/^o$ C.	60
Catholyte Flow Rate $/dm^3\ s^{-1}$	1
Current $/A$	500
Overall Cathode Current Eff./%	58

TABLE 11.11   RESULTS OF STEADY STATE ELECTROLYSIS IN THE

200 AMP ECO-CASCADE-CELL REACTOR.

PARAMETER	COMPARTMENT NO.						
	IN	1	2	3	4	5	6
POTENTIAL, E/mV (S.C.E.)	-	-372	-499	-529	-546	-429	-382
COPPER CONCENTRATION $C/mg\ dm^{-3}$	118	66.1	36.1	19.4	13.2	18.4	21.9
FRACTIONAL CONVERSION, f_R	-	0.440	0.454	0.463	0.320	0.394	0.190

Anode pair used	Nos. 1 + 2
Temperature of Catholyte/^{o} C	58 - 59
Catholyte Flow Rate /$dm^{3}\ s^{-1}$	1
CURRENT /A	500
Overall Cathode Current Eff./%	58

TABLE 11.12 RESULTS OF STEADY STATE ELECTROLYSIS IN THE 200 AMP ECO-CASCADE-CELL REACTOR.

PARAMETER	COMPARTMENT NO.						
	IN	1	2	3	4	5	6
POTENTIAL, E/mV (S.C.E.)	-	-346	-448	-352	-366	-445	-571
COPPER CONCENTRATION, $C/mg\ dm^{-3}$	118 ± 3.7	68 ± 4.8	36.2 ± 1.9	23.1 ± 2.1	19.1 ± 2.1	25.3 ± 2.4	19.5 ± 1.6
FRACTIONAL CONVERSION, f_R	-	0.423	0.468	0.362	0.173	-0.325	0.229

Anode pair used	Nos. 1 + 3
Temperature of Catholyte $/^{o}$ C.	57
Catholyte Flow Rate $/dm^3\ s^{-1}$	1
Current $/A$	400
Overall Cathode Current Eff./%	75

TABLE 11.13   RESULTS OF STEADY STATE ELECTROLYSIS IN THE

200 AMP ECO-CASCADE-CELL REACTOR.

PARAMETER	COMPARTMENT NO.						
	IN	1	2	3	4	5	6
POTENTIAL, E/mV—(S.C.E.)	–	-305	-389	-330	-346	-449	-554
COPPER CONCENTRATION, $C/mg\ dm^{-3}$	126 ± 8.6	79 ± 8.1	43 ± 6	28.3 ± 3.2	22 ± 1.8	28.7 ± 3.0	22.3 ± 3.9
FRACTIONAL CONVERSION, f_R	–	0.373	0.456	0.342	0.227	-0.305	0.223

Anode pair used	Nos. 1 + 3
Temperature of Catholyte $/^{o}$ C.	56
Catholyte Flow Rate $/dm^3\ s^{-1}$	1
Current $/A$	350
Overall Cathode Current Eff. $/\%$	90

TABLE 11.14 RESULTS OF STEADY STATE ELECTROLYSIS IN THE 200 AMP ECO-CASCADE-CELL REACTOR.

PARAMETER	COMPARTMENT NO.						
	IN	1	2	3	4	5	6
POTENTIAL, E/mV (S.C.E.)	–	-306	-367	-424	-381	-407	-509
COPPER CONCENTRATION $C/mg\ dm^{-3}$	139 ±1.2	89 ±1.2	51.8 ±1.9	35.2 ±2.1	23.5 ±1.5	27.3 ±1.5	24.3 ±3.0
FRACTIONAL CONVERSION, f_R	–	0.360	0.418	0.320	0.332	-0.162	0.110

Anode pair used	Nos. 1, 2 + 3
Temperature of Catholyte $/^{\circ}$C.	55
Catholyte Flow Rate $/dm^3\ s^{-1}$	1
Current $/A$	400
Overall Cathode Current Eff./%	87

TABLE 11.15 RESULTS OF STEADY STATE ELECTROLYSIS IN THE

200 AMP ECO-CASCADE-CELL REACTOR.

PARAMETER	COMPARTMENT NO.						
	IN	1	2	3	4	5	6
POTENTIAL, E/mV (S.C.E.)	-	-472	-573	-436	-349	-240	-207
COPPER CONCENTRATION $C/mg\ dm^{-3}$	143 ±7.8	56.3 ±3.3	22.9 $\pm\ 3.2$	14.2 $\pm\ 2.4$	12.2 $\pm\ 3.1$	18.1 $\pm\ 5.5$	14.8 $\pm\ 5.2$
FRACTIONAL CONVERSION, f_R	-	0.606	0.593	0.380	0.141	-0.484	0.182

Anode pair used	No. 1
Temperature of Catholyte $/^{o}$ C.	58 - 62
Catholyte Flow Rate $/dm^3\ s^{-1}$	0.58
Current $/A$	300
Overall Cathode Current Eff.$/\%$	76

TABLE 11.16   RESULTS OF STEADY STATE ELECTROLYSIS IN THE

200 AMP ECO-CASCADE-CELL REACTOR.

PARAMETER	COMPARTMENT NO.						
	IN	1	2	3	4	5	6
POTENTIAL, E/mV (S.C.E.)	-	-319	-496	-524	-403	-484	-332
COPPER CONCENTRATION, $C/mg\ dm^{-3}$	161 +8.7	74 + 22	32.7 + 11	15.2 + 4.8	11.5 + 4.7	12.7 +5.7	11.7 + 5.1
FRACTIONAL CONVERSION, f_R	-	0.540	0.558	0.535	0.243	-0.104	0.078

Anode pair used	No. 1 + 2
Temperature of Catholyte $/^{\circ}$ C.	53
Catholyte Flow Rate $/dm^3\ s^{-1}$	0.583
Current /A	300
Overall Cathode Current Eff./%	88

TABLE 11.17   RESULTS OF STEADY STATE ELECTROLYSIS IN THE

200 AMP ECO-CASCADE-CELL REACTOR.

PARAMETER	COMPARTMENT NO.						
	IN	1	2	3	4	5	6
POTENTIAL, E/mV (S.C.E.)	-	-355	-562	-518	-564	-447	-370
COPPER CONCENTRATION $C/mg\ dm^{-3}$	104.7 $\pm$ 4.5	61.8 $\pm$ 4.1	30.6 $\pm$ 1.8	21.6 $\pm$ 1.6	23.4 $\pm$ 1.8	31.1 $\pm$ 2.4	23 $\pm$ 2.3
FRACTIONAL CONVERSION, f_R	-	0.410	0.505	0.294	-0.083	-0.329	0.260

Anode pair used	No. 1 + 2
Temperature of Catholyte $/^{o}$ C.	41
Catholyte Flow Rate $/dm^{3}\ s^{-1}$	1
Current $/A$	400
Overall Cathode Current Eff. $/\%$	62

TABLE 11.18   RESULTS OF STEADY STATE ELECTROLYSIS IN THE

200 AMP ECO-CASCADE-CELL REACTOR.

PARAMETER	COMPARTMENT NO.						
	IN	1	2	3	4	5	6
POTENTIAL, E/mV (.S.C.E.)	-	-386	-547	-543	-551	-439	-324
COPPER CONCENTRATION C/mg dm^{-3}	165.7 ± 3.9	74.3 ± 5.2	36.2 ± 3.7	21.5 ± 3.1	23.2 ± 4.1	27.9 ± 3.5	21.4 ± 4.3
FRACTIONAL CONVERSION, f_R	-	0.552	0.513	0.406	-0.079	-0.203	0.233

Anode pair used	Nos. 1 + 2
Temperature of Catholyte /^{O} C.	42
Catholyte Flow Rate /dm^3 s^{-1}	0.583
Current /A	300
Overall Cathode Current Eff./%	85

TABLE 11.19   RESULTS OF STEADY STATE ELECTROLYSIS IN THE

200 AMP ECO-CASCADE-CELL REACTOR.

PLANT	DIAMETER d/cm	AREA A/cm^2	RPM	PERIPHERAL VELOCITY $U/cm\,s^{-1}$
LAB. RIG 1	7.62	200	600 - 3000	239 - 1200
MINI-CELL	10.2	200	500 - 1500	266 - 797
500A PILOT PLANT	23.5	1690	100 - 1380	123 - 1698
2KA PILOT PLANT	45.1	5757	460	1086 - 1112

TABLE 11.20   CHARACTERISTICS OF ECO-CELL ASSEMBLIES EMPLOYED

IN MASS TRANSFER EXPERIMENTS.

PERIPHERAL VELOCITY U/cm s^{-1}	COPPER CONC. C/mg dm^{-3}	(LIMITING) CURRENT DENSITY i_L/A cm^{-2}	MASS TRANSPORT COEFFICIENT K_L/cm s^{-1}	REYNOLDS NUMBER (Re)	MODIFIED CHILTON-COBURN FACTOR $j_D^{\,\prime} \times 10^{3}$
239	391	0.142	0.120	302086	26.6
239	376	0.204	0.179	302086	39.6
239	420	0.220	0.172	302086	38.3
600	231	0.241	0.343	758376	30.4
600	223	0.238	0.351	758376	31.1
800	177	0.235	0.437	1011168	29.0
998	150	0.230	0.505	1261432	26.9
998	183	0.227	0.408	1261432	21.7
998	147	0.227	0.508	1261432	27.0
998	158	0.189	0.394	1261432	21.0
1200	98	0.177	0.595	1516751	26.3
1200	93	0.171	0.605	1516751	26.7
1200	146	0.235	0.530	1516751	23.5
1200	96	0.171	0.586	1516751	25.9

TABLE 11.21   MASS TRANSPORT DATA (FOR COPPER DEPOSITION)

IN THE 50A LAB. RIG 1 REACTOR.

PERIPHERAL VELOCITY U/cm s^{-1}	COPPER CONC. C/mg dm^{-3}	(LIMITING) CURRENT DENSITY i_L/A cm^{-2}	MASS TRANSPORT COEFFICIENT K_L/cm s^{-1}	REYNOLDS NUMBER (Re)	MODIFIED CHILTON-COBURN FACTOR $j_D \times 10$
266	200	0.206	0.339	454585	67.6
531	100	0.142	0.467	907462	46.7
531	100	0.130	0.435	658049	52.4
531	200	0.166	0.273	658049	42.9
797	100	0.172	0.566	1362047	37.7

TABLE 11.22   MASS TRANSPORT DATA : 100A MINI-CELL

PERIPHERAL VELOCITY U/cm s^{-1}	COPPER CONC. C/mg dm^{-3}	(LIMITING) CURRENT DENSITY i_L/A cm^{-2}	MASS TRANSPORT COEFF. K_L/cm s^{-1}	REYNOLDS NUMBER (Re)	MODIFIED CHILTON-COLBURN FACTOR $j_D{}' \times 10^3$
123	1552	0.229	0.049	489086	21.0
271	1071	0.394	0.121	1077580	23.7
393	680	0.386	0.187	1562690	25.2
393	525	0.310	0.194	1562690	26.2
492	494	0.258	0.172	1956345	18.5
541	385	0.333	0.285	2151184	27.9
984	277	0.373	0.443	3912690	23.9
1000	288	0.346	0.396	3976311	21.0
1000	295	0.357	0.398	3976311	21.1
1000	277	0.361	0.429	"	22.8
1000	193	0.309	0.527	"	28.0
1000	201	0.296	0.485	"	25.7
1000	204	0.299	0.483	"	25.6
1000	194	0.304	0.516	"	27.4
1000	213	0.244	0.377	"	20.0
1000	216	0.242	0.369	"	19.6
1000	197	0.272	0.455	"	24.1
1000	184	0.246	0.440	"	23.4
1000	160	0.212	0.436	"	23.1
1000	50	0.063	0.415	"	22.0
1698	98	0.228	0.766	6751777	23.9
1698	111	0.176	0.522	6751777	16.3

TABLE 11.23   MASS TRANSPORT DATA: 500A PILOT PLANT.

PERIPHERAL VELOCITY U/cm s^{-1}	COPPER CONC. C/mg dm^{-3}	(LIMITING) CURRENT DENSITY i_L/A cm^{-2}	MASS TRANSPORT COEFF. K_L/cm s^{-1}	REYNOLDS NUMBER (Re)	MODIFIED CHILTON-COLBURN FACTOR $j_D^I \times 10^3$
1086	147	0.201	0.449	8285443	21.9
1086	162	0.187	0.379	"	18.5
1086	155	0.199	0.424	"	20.7
1086	167	0.199	0.393	"	19.2
1086	120	0.163	0.446	"	21.8
1112	234	0.133	0.186	8692792	8.9
1112	293	0.148	0.166	"	7.9
1112	100	0.116	0.381	"	18.2
1112	110	0.127	0.381	"	18.2
1112	121	0.140	0.382	"	18.2

TABLE 11.24   MASS TRANSPORT DATA: 2KA PILOT PLANT.

cylinder diameter   =   7.6 cm

no. of compartments   =   10

compartment length   =   9.0 cm

compartmental area   =   215 cm^2

rotational speed   =   2000 r.p.m.

peripheral velocity   =   796 $cm\ s^{-1}$

catholyte : $CuSO_4$ in an effluent solution containing 1.0M H_2SO_4,
               urea and NaCl.

anolyte   :   ca 2MNaOH

anodes   :   nickel mesh

TABLE 11.25   DETAILS OF THE 100A LABORATORY CASCADE REACTOR.

cylinder diameter	=	32.4 cm
no. of compartments	=	12
compartment length	=	20.0 cm
compartment area	=	2036 cm^2
rotational speed	=	860 r.p.m.
peripheral velocity	=	1459 cm s^{-1}

catholyte   :   as for Table 11.25

anolyte   :   M NaOH

anodes   :   Nickel Mesh

TABLE 11.26   DETAILS OF THE 1KA COMMERCIAL CASCADE REACTOR.

					COMPARTMENT NO.						
	INLET	1	2	3	4	5	6	7	8	9	10
C_{Cu} $\pm$ ppm	107.6 7.3	73.2 9.2	42.4 8.6	21.2 5.8	14.2 6.4	11.2 7	6.5 4.4	3.9 2.3	2.8 1.5	2.0 0.9	1.5 0.6
f_R	—	0.320	0.421	0.500	0.330	0.211	0.420	0.400	0.282	0.286	0.250
Ln C	4.68	429	375	305	265	242	1.87	136	1.03	.69	.41
E / -mV(SCE) $\pm$	— —	293 5	311 53	546 79	380 104	396 130	446 145	511 110	604 42	624 15	575 32

Catholyte Flow Rate   = $0.1 \ dm^3 \ s^{-1}$

Total Current   = 40 A

Temperature   = 60° C

Anode dividing Baffles used in compartments 3 and 7

Useful Current   = 32.2 A

Current Efficiency   = 80.5%

Overall Fractional Conversion $(f_R)_{10}$ = 0.986

TABLE 11.27   DATA FROM THE 100A LABORATORY CASCADE CELL.

	INLET	1	2	3	4	5	6	7	8	9	10
C_{Cu} $\pm$ ppm	104.9 9.5	66.2 14.2	39.3 11.6	21.8 8.5	13.7 7.8	10.5 9.3	5.1 5.6	5.3 2.8	2.0 1.5	1.5 1.1	1.2 0.9
f_R		0.369	0.406	0.445	0.372	0.234	0.514	0.039	0.623	0.250	0.200
Ln C	4.65	4.19	3.67	3.08	2.62	2.35	1.63	1.19	.69	.41	.18
E / -mV (SCE) $\pm$		312 43	419 90	551 91	518 109	425 100	509 106	533 92	579 46	592 29	563 43

Catholyte Flow Rate $= 0.1 \text{ dm}^3 \text{ s}^{-1}$

Total Current $= 40 \text{ A}$

Temperature $= 60^{\circ} \text{ C}$

Shaped anodes used in compartments 1, 2 and 3 only

Baffle used in compartment 7.

Useful Current $= 31.5 \text{ A}$

Current Efficiency $= 78.8 \text{ \%}$

Overall fractional conversion $(f_R)_n$ $= 0.989$

TABLE 11.28   DATA FROM THE 100A LABORATORY CASCADE CELL.

	INLET	1	2	3	4	5	6	7	8	9	10
C_{Cu} $\pm$ ppm	102.3 2.7	79.1 2.1	55.7 2.9	35.9 3.5	21.1 4.7	11.0 2.1	5.3 1.4	3.17 1.2	1.99 1.0	1.44 .9	1. .
f_R		0.226	0.296	0.355	0.412	0.479	0.518	0.402	0.372	0.276	0.20
Ln C	4.63	4.37	4.02	3.58	3.05	2.40	1.67	1.15	.69	.36	.

Catholyte Flow Rate $\qquad = 0.1 \text{ dm}^3 \text{ s}^{-1}$

Total Current $\qquad = 4.0 \text{ A}$

Temperature $\qquad = 60^\circ \text{ C}$

Anodes used in compartments 1 to 5 only

Useful Current $\qquad = 30.7 \text{ A}$

Current Efficiency $\qquad = 76.8 \text{ %}$

Overall Fractional Conversion, $(f_R)_n \qquad = 0.989$

TABLE 11.29 DATA FROM THE 100A LABORATORY CASCADE CELL.

	INLET	1	2	3	4	5	6	7	8	9	10
C_{Cu} ± ppm	92.4 6.6	68 5.4	54.4 7.8	38.3 6.2	33.3	23.5	17.3	11.1	8.1	4.9	3.1
f_R		0.264	0.200	0.296	0.131	0.386	0.264	0.358	0.370	0.395	0.367
Ln C	4.53	4.22	4.0	3.65	3.51	3.16	2.85	2.41	2.1	1.59	1.13

Catholyte Flow Rate $\quad\quad\quad\quad\quad = \quad 0.1 \ dm^3 \ s^{-1}$

Total Current $\quad\quad\quad\quad\quad\quad\quad = \quad 40 \ A$

Temperature $\quad\quad\quad\quad\quad\quad\quad = \quad 30^o \ C$

Useful Current $\quad\quad\quad\quad\quad\quad = \quad 27.1 \ A$

Current Efficiency $\quad\quad\quad\quad = \quad 67.8 \ \%$

Overall Fractional Conversion, $(f_R)_n \quad = \quad 0.966$

TABLE 11.30   DATA FROM THE 100A LABORATORY CASCADE CELL.

COMPARTMENT NO., n	COPPER CONC. C/mg dm^{-3}	FRACTIONAL CONVERSION f_R
INLET	88.8	——
1	73.8	0.169
2	52.5	0.289
3	40.0	0.238
4	29.5	0.263
5	21.0	0.288
6	14.2	0.324
7	9.75	0.313
8	6.75	0.308
9	4.75	0.296
10	3.6	0.242
11	2.8	0.222
12	2.25	0.196

Catholyte Flow Rate $= 8.05$ m^3 (hr)$^{-1}$

$\quad\quad\quad\quad\quad\quad\quad\quad$ (2236 cm^3 s^{-1})

Cell Voltage $= 6.4$ V

Cell Current $= 900$ A

Useful Current $= 588$ A

Current Efficiency $= 65$ %

Overall Fractional Conversion, $(f_R)n = 0.975$

Temperature $= 55.5^o$ C

TABLE 11.31 DATA FOR THE 1KA COMMERCIAL CASCADE REACTOR.

COMPARTMENT NO., n	COPPER CONC., C/mg dm^{-3}	FRACTIONAL CONVERSION f_R
INLET	76.3	-
1	60.0	0.214
2	39.5	0.342
3	29.5	0.253
4	21.5	0.271
5	15.0	0.302
6	9.6	0.360
7	6.6	0.313
8	4.9	0.258
9	3.5	0.286
10	2.6	0.257
11	1.95	0.250
12	1.6	0.179

Catholyte Flow Rate $= 8.15 \text{ m}^3 \text{ (hr)}^{-1}$

$(2264 \text{ cm}^3 \text{ s}^{-1})$

Cell Voltage $= 6.4 \text{ V}$

Cell Current $= 893 \text{ A}$

Useful Current $= 514 \text{ A}$

Current Efficiency $= 58\%$

Overall Fractional Conversion, $(f_R)_n$ $= 0.979$

Temperature $= 56.0^\circ \text{ C}$

TABLE 11.32   DATA FOR THE 1KA COMMERCIAL CASCADE REACTOR.

r_0 /cm.	r_I /cm.	$r_0 - r_I$ /cm.	$\dfrac{r_I}{r_0}$	$\dfrac{r_I}{r_0}^{0.70}$
I	I	0	I	I
2	I	I	0.5	0.6156
II	I	IO	0.0909	0.1867
II	IO	I	0.9091	0.9355
IOI	IOO	I	0.9901	0.9931

TABLE I2.I   IMPORTANCE OF RADIUS RATIO FOR MASS TRANSPORT

TO A SMOOTH R.C.E..

$$i_L \propto \left(\frac{r_I}{r_0} \right)^{0.70}$$

TEMP. T /°C	TEMP. T /K	I_L PREDICTED† /A	I_L EXPERIMENTAL /A	EXPERIMENTAL IMPROVEMENT IN I_L, relative to 22°C	THEORETICAL IMPROVEMENT
22	295	0.685	0.700	1	1
29	302	0.805	0.845	1.21	1.18
35	308	0.958	1.010	1.44	1.40
45	318	1.154	1.135	1.62	1.68
60	333	1.543	1.390	1.99	2.25

† by equation $I_L = zFCUA.\ 0.079\ (Re)^{-0.30}(Sc)^{-0.644}$

TABLE 12.2 RELATIVE IMPROVEMENT IN MASS TRANSPORT DUE TO
TEMPERATURE : COPPER DEPOSITION TO A SMOOTH R.C.E.

| RPM | APPARENT RATE CONSTANT, $k / s^{-1} \times 10^3$ | |
	Smooth k_1	Rough k_2
180	0.106	0.352
360	0.180	0.568
500	0.229	0.811
680	0.295	1.12
1000	0.393	1.45

TABLE I2.3   APPARENT RATE CONSTANTS FOR BATCH DECAY OF COPPER, showing

the effect of rotational speed

AUTHOR(S)	REF.	METAL	TECHNIQUE
Ibl, Javet & Stahel	380	Copper	Galvanostatic Deposition Profilometric Measurement
Gabe & Robinson	84	Copper	Galvanostatic Deposition Polarisation and Microscopic Measurement
Popov et al.	372 - 375 382	Copper	Potentiostatic Deposition Polarisation and Microscopic Measurement
Calusaru	357	Various	Potentiostatic Deposition Polarisation, Microscopic and Differential T. Measurement
Walsh	Present Work	Copper	Potentiostatic Deposition Polarisation, Mass Transport, Surface Profilometric and Microscopic Measurement

TABLE   12.4   COMPARISON OF METAL DEPOSITION STUDIES

INVOLVING ROUGHNESS DEVELOPMENT

AUTHOR(S)	REF.	CONCENTRATIONS/M		
		COPPER	H_2SO_4	THIOUREA
IBL, JAVET & STAHEL	380	1	0.5	1.3×10^{-3}
IBL, JAVET & STAHEL	380	0.1	1.5	2.6×10^{-2}
GABE & ROBINSON	84	0.7	1.5	10^{-5} to 10^{-1}
WALSH	Present Study	0.014	1.5	10^{-5} to 10^{-1}

TABLE 12.5   COMPARISON OF STUDIES INVOLVING THIOUREA INHIBITED

GROWTH OF ROUGH COPPER ELECTRODEPOSITS

Roughness ϵ /cm	Diameter d /cm	Relative Roughness d/ϵ	Limiting Current I_L/A †		$jD' \times 10^3$ †		Predicted Re_{crit}
			Predicted*	Observed	Predicted	Observed	
$< 5 \times 10^{-5}$	1.5	$> 3 \times 10^4$	0.222		4.95		Large
0.0018	1.5	833	0.137	1.11	3.06	55.2	51448
0.003	1.5	500	0.159	1.57	3.55	78.1	28158
0.025	1.5	60	0.340	1.78	7.57	88.5	2307
$< 5 \times 10^{-5}$	6.0	$> 12 \times 10^4$	1.52		2.15		Large
0.016	6.0	375	2.74	4.90	3.87	6.8	20053
0.040	6.0	150	3.72	7.45	5.26	10.4	6802
0.060	6.0	100	4.34	19.0	6.13	26.5	4215

*by the equation $jD' = (1.25 + 5.76 \log_{10} \frac{d}{\epsilon})^{-2}$

†at 1000 rpm

TABLE 12.6   MASS TRANSPORT TO KNURLED ROTATING CYLINDER ELECTRODES

R.P.M.	PERIPHERAL VELOCITY U / cm s^{-1}	MASS TRANSPORT COEFFICIENT K_L / cm s^{-1}		RATIO A/B
		ROBINSON-GABE (SMOOTH) A b = -0.31	HOLLAND (ECO-CELL) B b = -0.08	
19	10	0.00673	0.0560	8.32
191	100	0.0330	0.466	14.1
1910	1000	0.161	3.873	24.1

TABLE 12.7 COMPARISON OF MASS TRANSFER AT 'ECO-CELL' AND

SMOOTH ROTATING CYLINDERS

Assuming: (Sc) = 1000, d = 10 cm, $\eth$ = 0.01 cm^2 s^{-1}

$$K_L = U^1 \, (Re)^b \, (Sc)^{-0.644}$$

$$= U^{1+b} \cdot \left(\frac{10}{0.01}\right)^{b} \, (1000)^{-0.644}$$

ECO-CELL PLANT	TEMPERATURE /°C	PERIPHERAL VELOCITY U /cm s^{-1}	POWDER EXPONENT p
LAB. RIG 1	60°C	239 - 1200	-0.076 -0.068 -0.085 -0.045 -0.081
	60°C	400	-0.087
MINI-CELL	40 50 60 60 60	531 531 266 531 797	-0.046 -0.032 -0.012 -0.038 -0.052
PILOT PLANT 500 A	60	123 - 1698	-0.085
PILOT PLANT 2 KA	60	1086 & 1112	0.088 0.08 0.082

TABLE 12.8. VALUES OF p OBTAINED ON VARIOUS ECO-CELL RIGS FOR COPPER DEPOSITION[412]

MODEL	Current rating /A	n	CYLINDER DETAILS			
			Diameter (cm)	Length (cm)	RPM	cmpt. area (cm^2)
1) Laboratory	100	10	7.6	100	2000	215
2) Commercial	1000	12	32.4	288	860	2036
3] Development/ Commercial	200	6	30.6	100	730	1387

TABLE 12.9   COMPARISON OF DEVELOPED ECO-CASCADE-CELL REACTORS

(Current Ratings are nominal)

n	$(f_R)_n$ ideal CSTR	$(f_R)_n$ ideal PFR .	$(f_R)_n$ single compartment unbaffled CSTR
1	0.5000	0.6320	0.500
2	0.7500	0.8650	0.667
3	0.8750	0.9500	0.750
4	0.9380	0.9820	0.800
5	0.9690	0.9930	0.833
6	0.9840	0.9880	0.857
7	0.9922	0.9990	0.875
8	0.9961	0.9997	0.889
9	0.9980	0.9999	0.900
10	0.9990	1.0000	0.909

TABLE 12.10 COMPARISON OF CONVERSIONS FOR A HYPOTHETICAL
CASCADE REACTOR (K_L A/N = 1)

with each compartment functioning as either a
CSTR or a PFR, or a large single compartment
of area nA
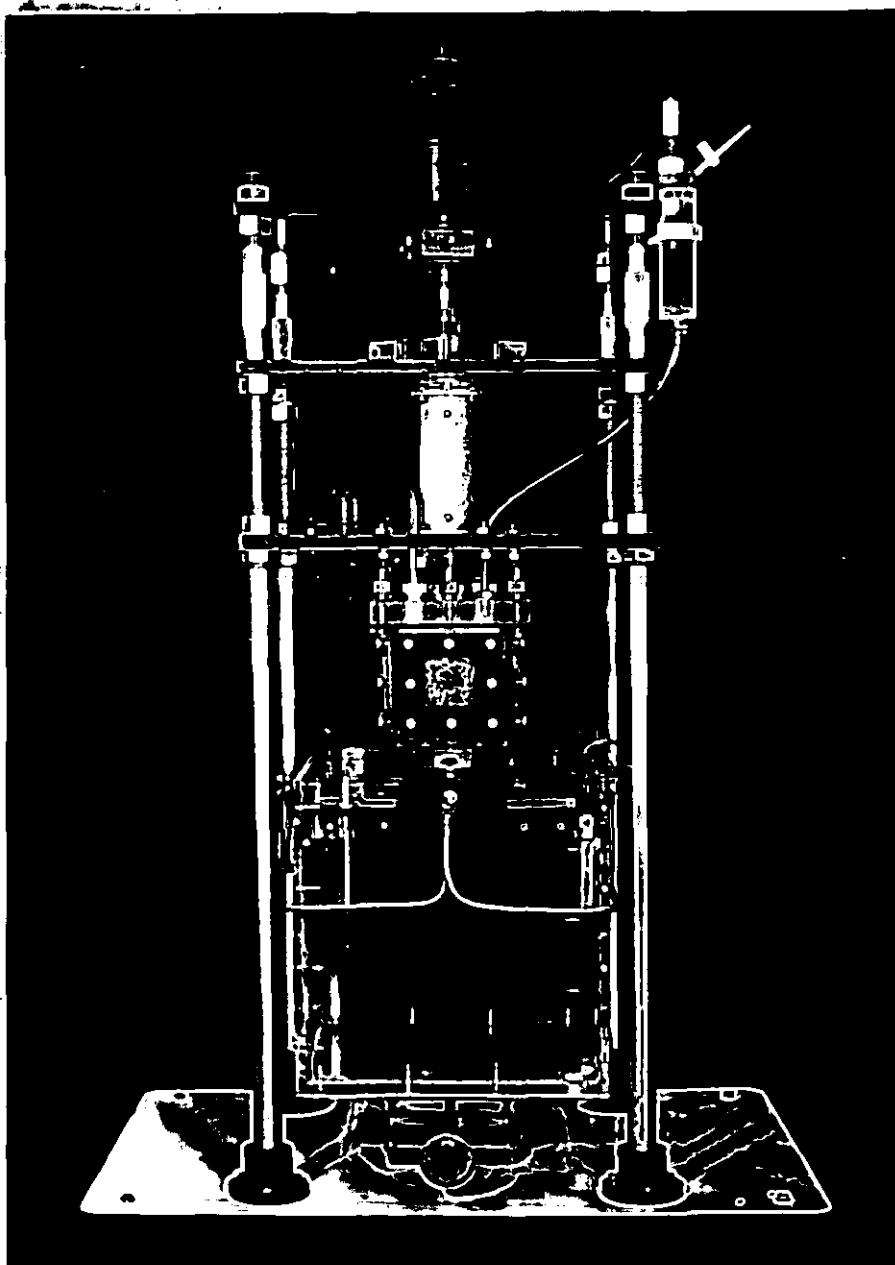
8.1 - a)

FIG. 8.1 b) THE LABORATORY ROTATING CYLINDER ELECTRODE

REACTOR ASSEMBLY

A. Electric Drive Motor

B. 'Tufnol' Support Platforms (4)

C. Salt Bridge Reservoir

D. Flexible Nylon Drive Coupling

E. Power Brushes (2) and Slip Ring

F. Bearings Housing

G. Catholyte Thermometer

H. Reference Electrode Salt Bridge

I. Potential Pick-Up Brush

J. 'Perspex' Catholyte Chamber

K. 'Perspex' Catholyte Chamber Top Plate

L. Catholyte/Rotating Shaft Seal

M. Reference Electrode

N. Anolyte Chamber Elevating Jack

O. Cation Exchange Membranes (4)

P. Catholyte Inlet

Q. Catholyte Outlet

R. 'Perspex' Anolyte Chamber

S. Anolyte Thermostat

T. Anolyte Heater (2)

U. Anolyte Stirrer

V. Plate.Lead Anode (4)

W. Anolyte Drain Tap

X. Sulphuric Acid Anolyte

Y. Auxiliary Tachometer

Z. Steel Support Rods (4)
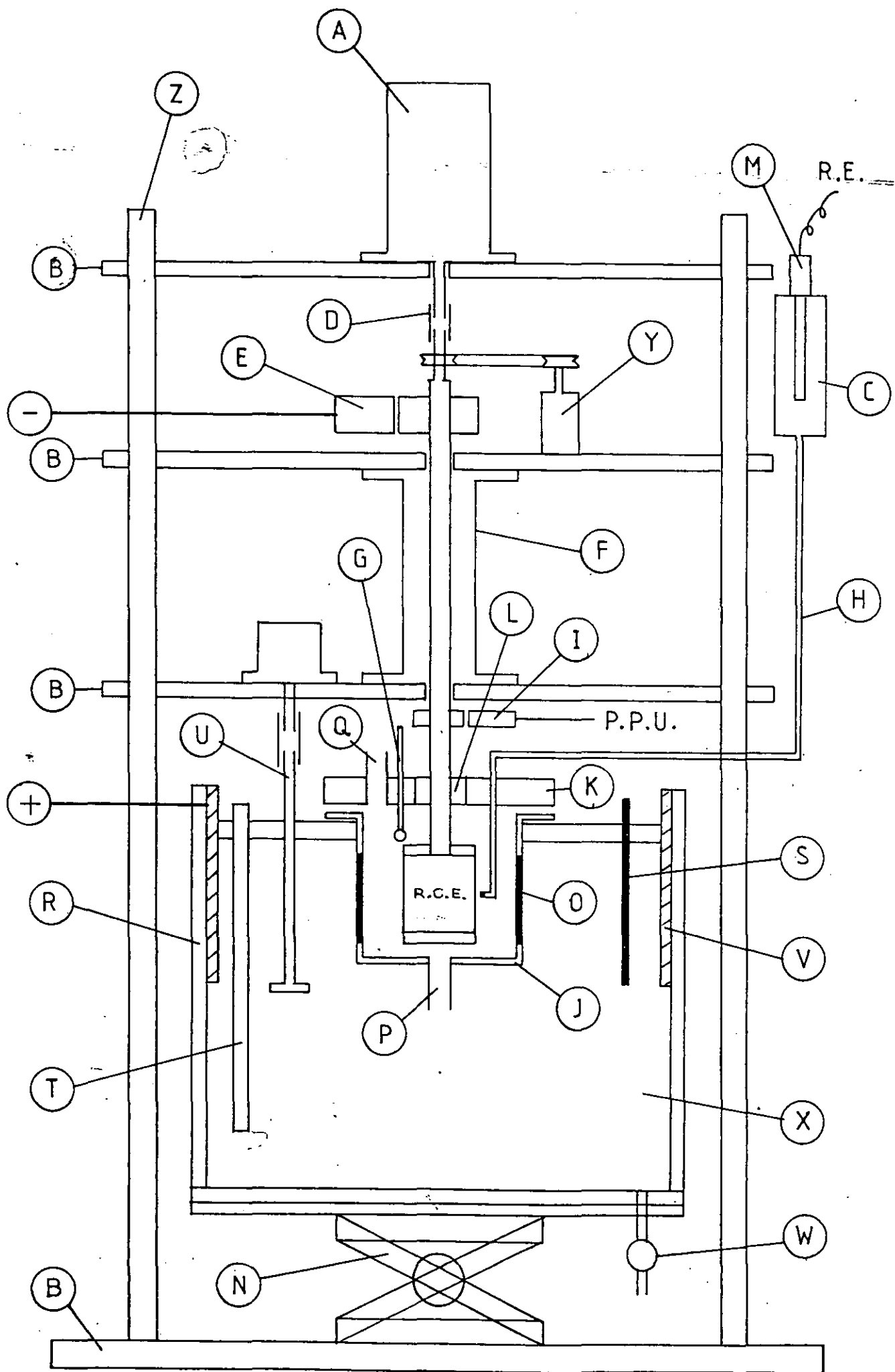
FIG. 8.1   PHOTOGRAPHS OF THE LABORATORY R.C.E.R. ASSEMBLY

c)   Anolyte bath raised, with the Catholyte compartment immersed

d)   Anolyte bath lowered, together with the catholyte compartment,

      exposing the rotating cylinder cathode.
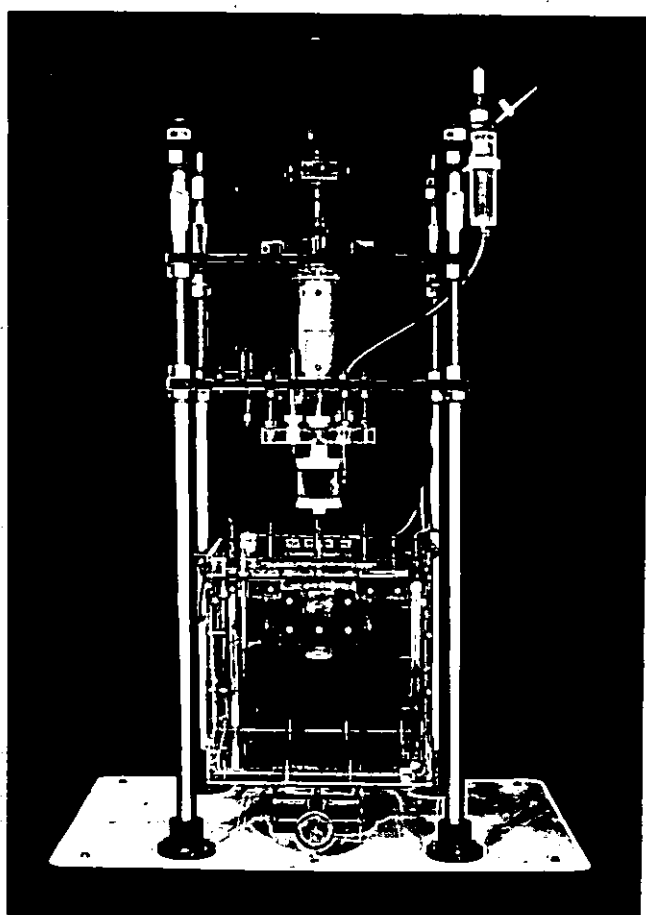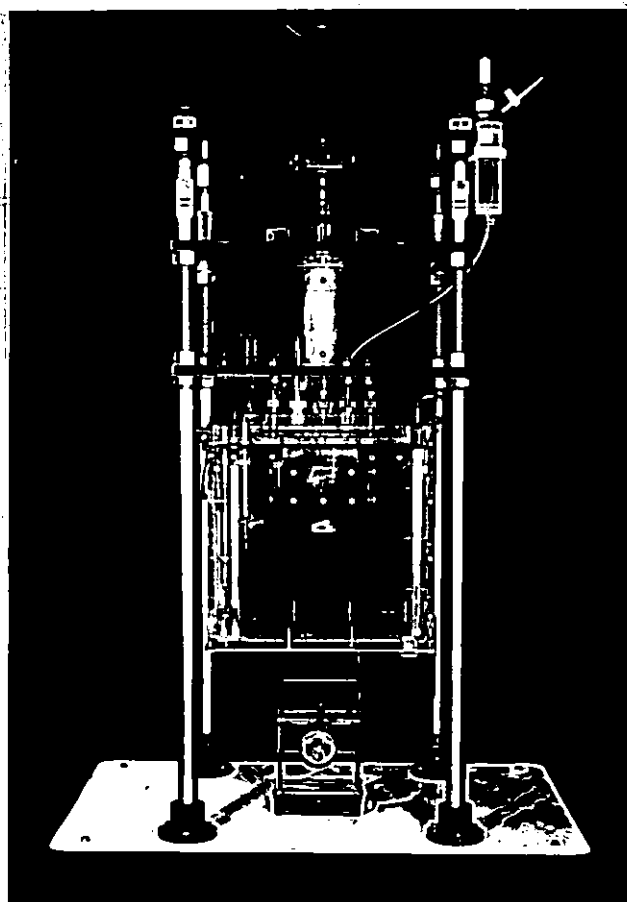
FIG. 8.2   LABORATORY REACTOR: PHOTOGRAPHS SHOWING THE
          CONSTRUCTION OF THE CATHOLYTE COMPARTMENT

a)   'Perspex' skeleton, showing the sides (with membrane apertures)
     and top flange

b)   showing membranes inserted into two of the sides

     A   ion exchange membrane

     B   rubber gasket (3 mm thick)

     C   fixing bolts (M6 polypropylene used)

c)   with top plate included

     A   shaft seal adaptor (PTFE)

     B   outlet (polypropylene)

     C   thermometer gland (PTFE)

     D   reference electrode gland (PTFE)
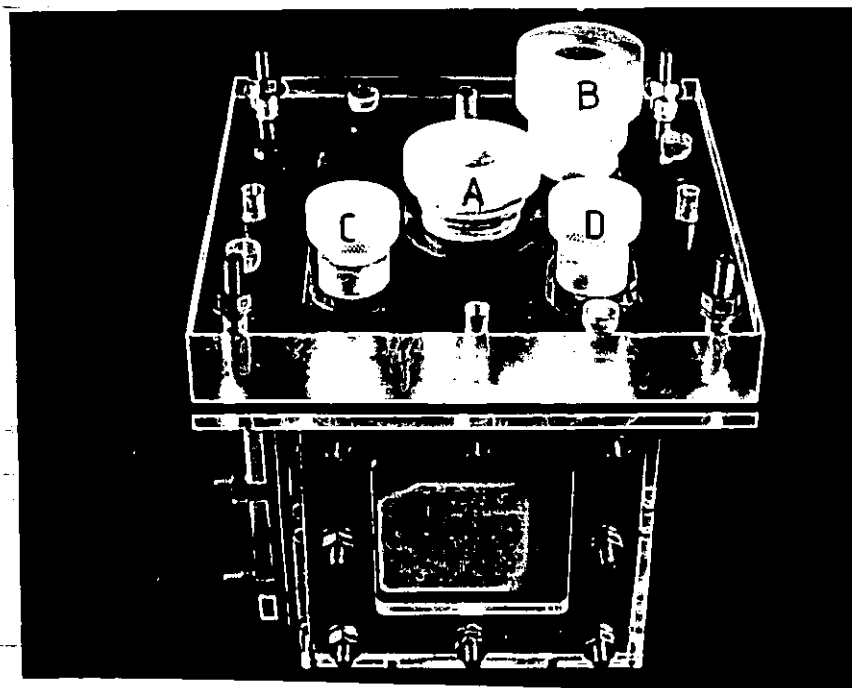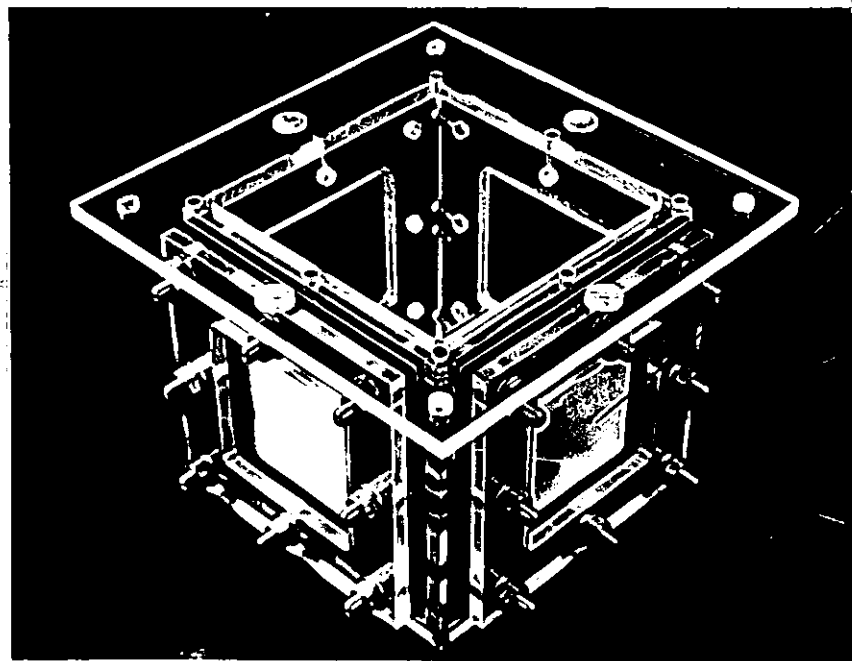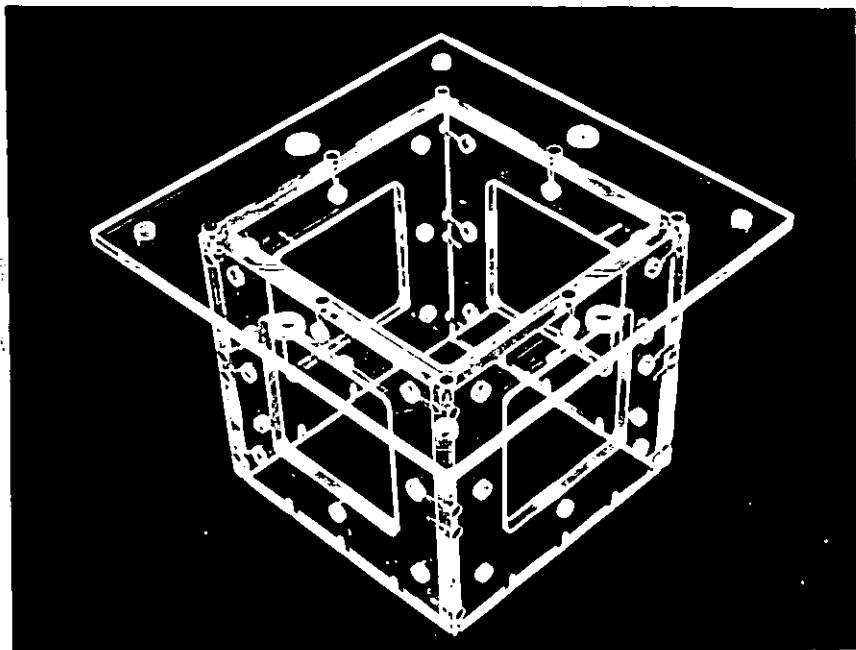
FIG. 8.3   SCHEMATIC PLAN OF THE ANOLYTE COMPARTMENT

A   'Perspex' sides (10 mm)

B   'Perspex' ledge to support lid

C   Aperture for catholyte compartment

D   anolyte stirrer

E   silica sheathed heaters

F   thermostat

G   thermometer

H   catholyte inlet aperture

I   position of R.C.E.

J   anodes (4) - lead/6% antimony plates

FRONT
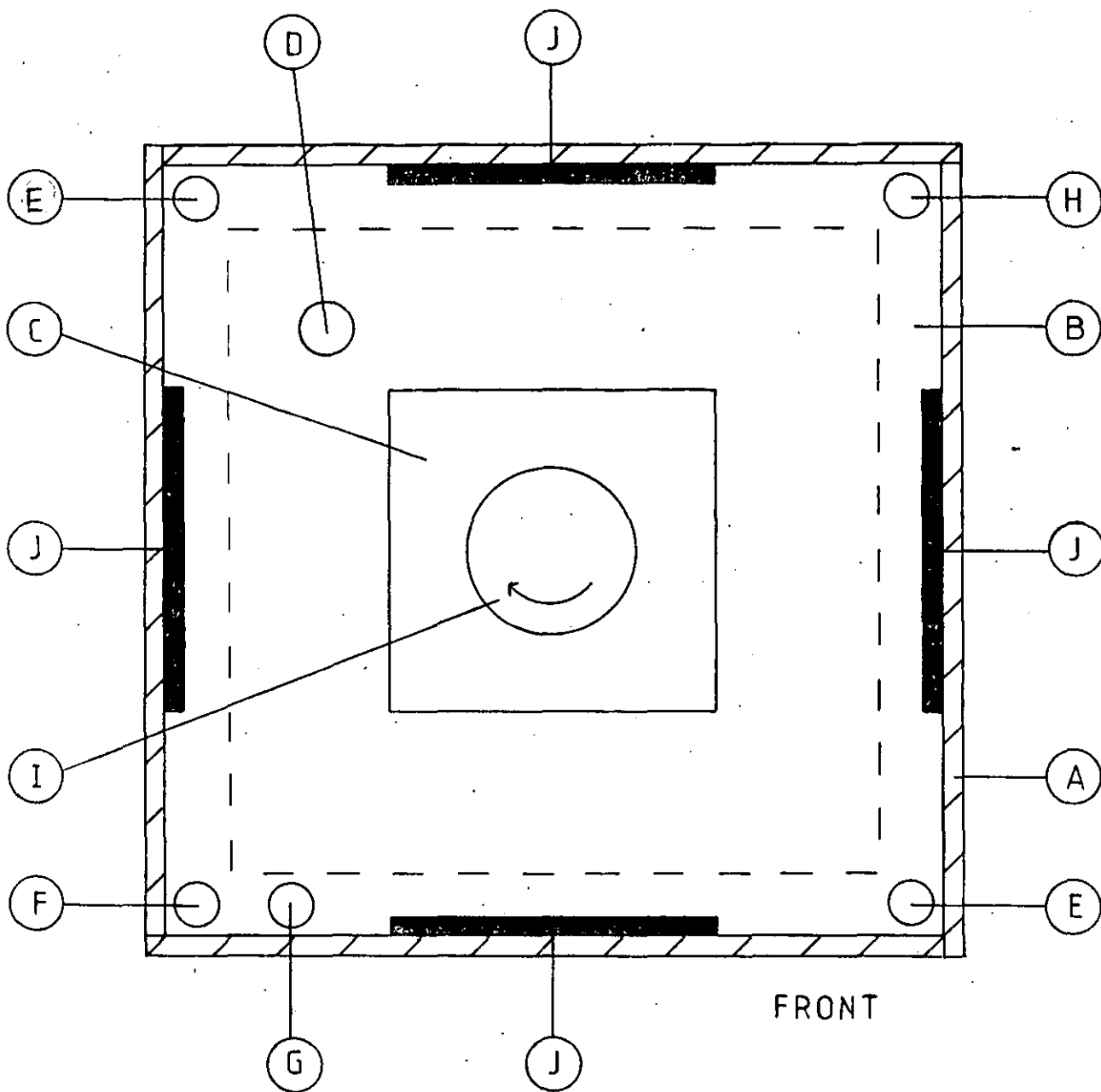
FIG. 8.4   CATHOLYTE FLOW ASSEMBLY

a) PHOTOGRAPH

b) SCHEMATIC

    A   security/drip tray (polypropylene)

    B   peristaltic pump

    C   reservoir tank (glass, 20 litre)

    D   contact thermometer

    E   stirrer

    F   silica sheathed heaters (2)

    G   PVC tube from pump (inlet)

    H   PVC tube to filter (outlet)

    I   in-line cartridge filter

    J   rotammeters (2)

    K   valves (polypropylene)

    L   reservoir lid (polypropylene)

IN

OUT

H D E F L

B

G

A

I

J J

K B

C
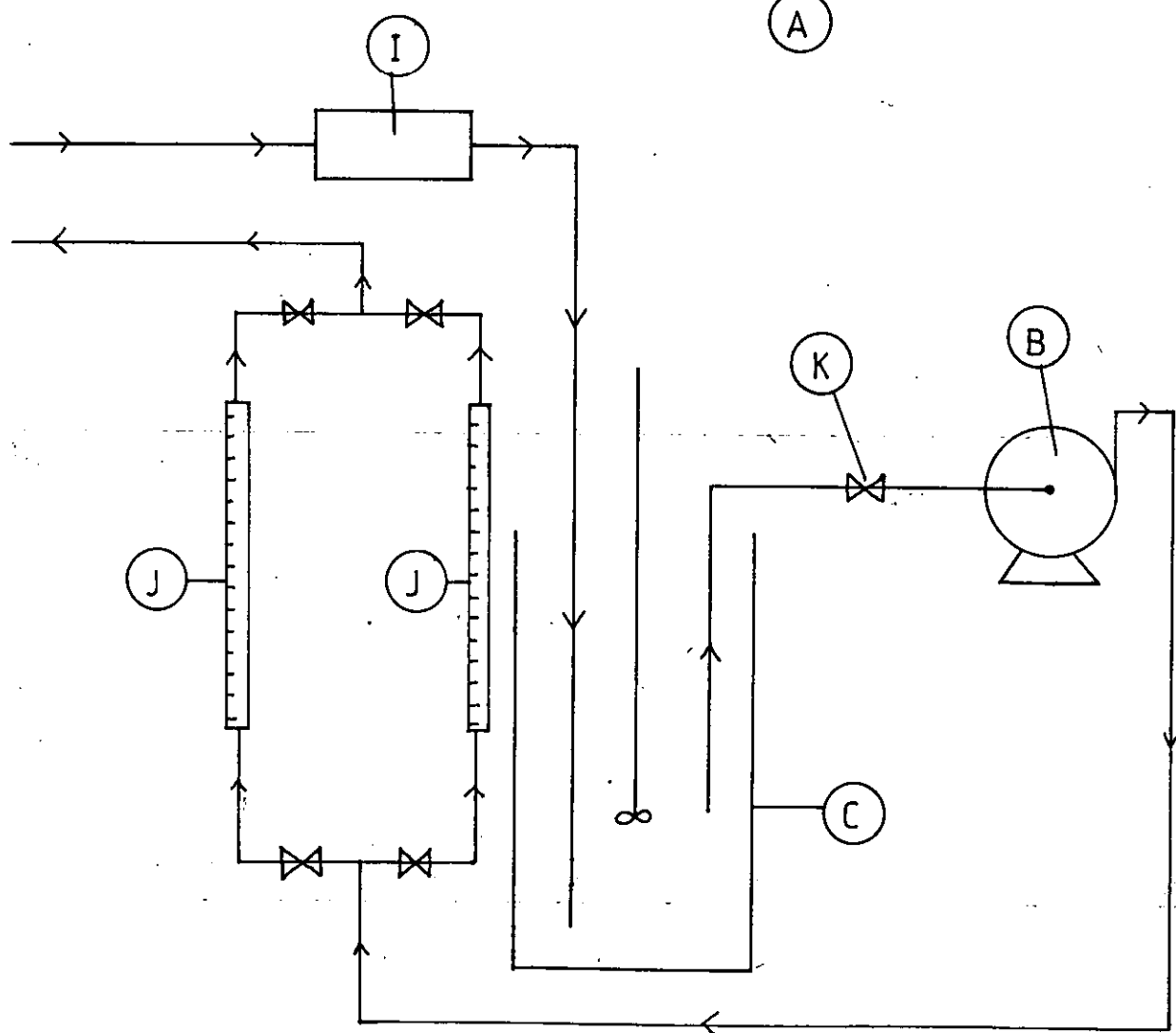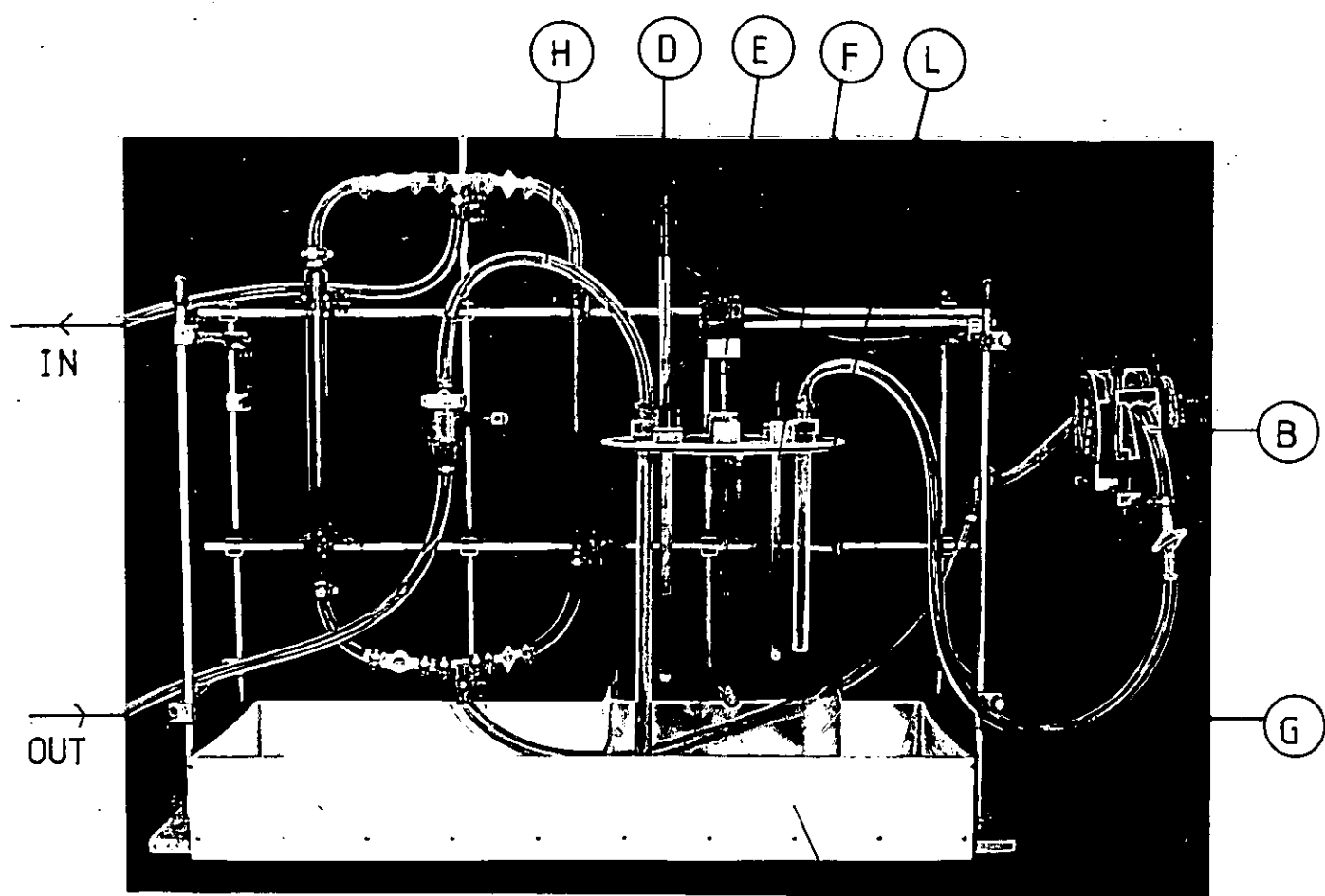
FIG. 8.5   LABORATORY INSTRUMENTATION

a)   PHOTOGRAPH

b)   SCHEMATIC

    A   Potentiostat

    B   Linear Sweep Unit

    C   Digital Coulombmeter

    D   Rotating Cylinder Speed Control

    E   Auxiliary Tachometer

    F   Catholyte temperature control

    G   Anolyte temperature control

    H   Cell Voltmeter

    I   Catholyte stirrer control

    J   Anolyte stirrer control

    K   pH/millivoltmeter

    L   input selector for K

    M   chart recorder
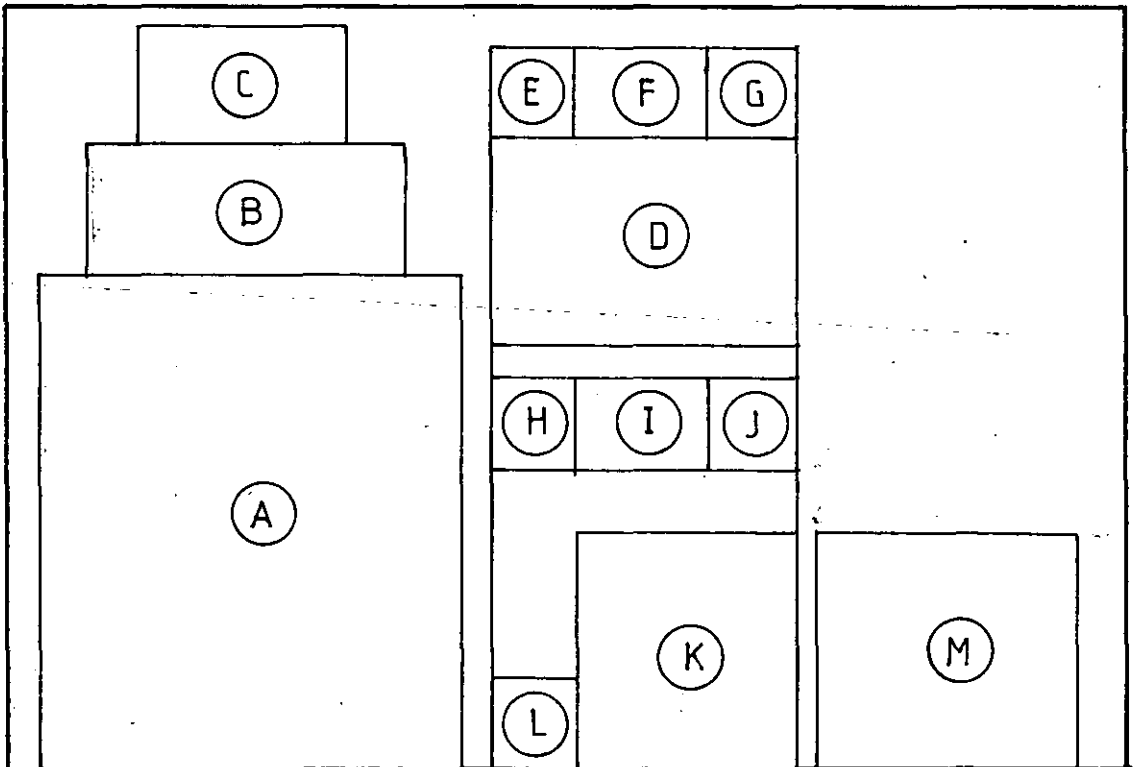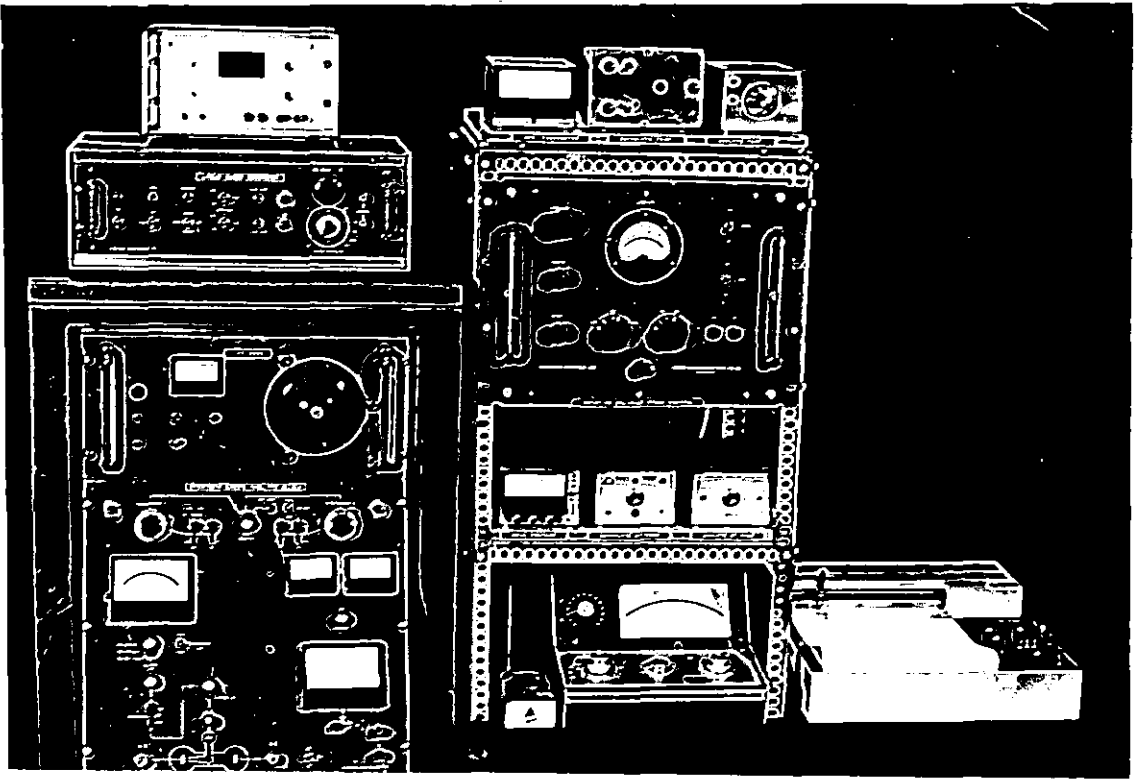
FIG. 8.6   SCHEMATIC OF THE ELECTRICAL CIRCUITRY FOR THE

LABORATORY REACTOR

A   Potentiostat

B   Linear Sweep Unit

C   Digital Coulombmeter (optional)

D   Rotating Cylinder Speed Control

E   Auxiliary Tachometer

K   High Impedence Millivoltmeter

M   Chart Recorder

N   Reference Electrode Assembly

O   Slip Rings (2)

P   Rotating Shaft

Q   Auxiliary Tachometer Sender

R   Rotating Shaft Drive Motor

S   Insulating Coupling

T   Cathode Power Brush

U   Precision Shunt

R.C.E.   Rotating Cylinder Electrode

W.E.   Working Electrode

C.E.   Counter Electrode

R.E.   Reference Electrode

P.P.U.   Potential Pick Up
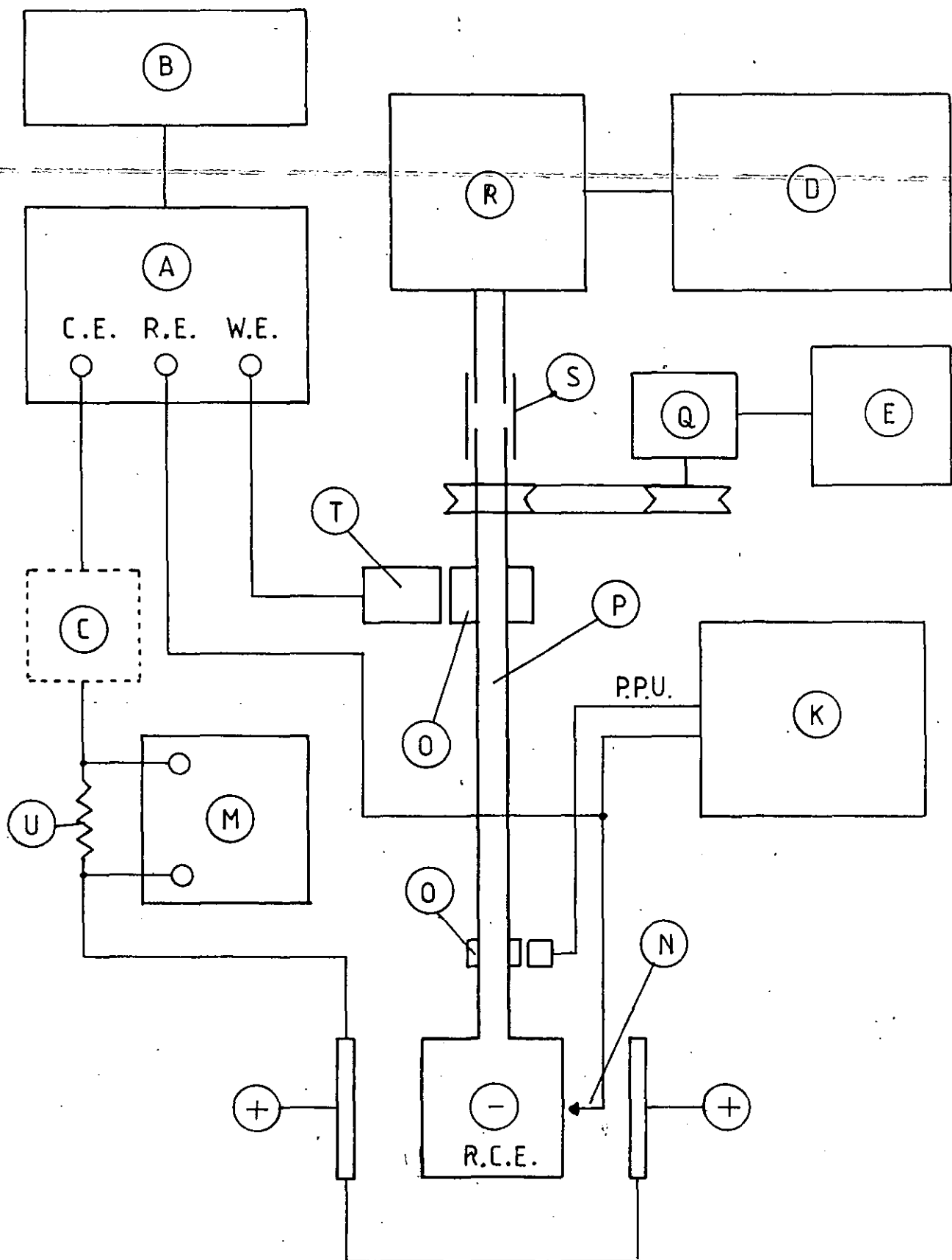
FIG. 8.7   LABORATORY REACTOR: CATHODE CHAMBER/ROTATING SHAFT,

SEAL ARRANGEMENT

A   'Perspex' Compartment Lid

B   PTFE gland (set)

C   Rotating Shaft

D . Reinforced, Sprung Lip seal

E   PTFE collar (adjustable)

F   Water pool

G   PTFE tape
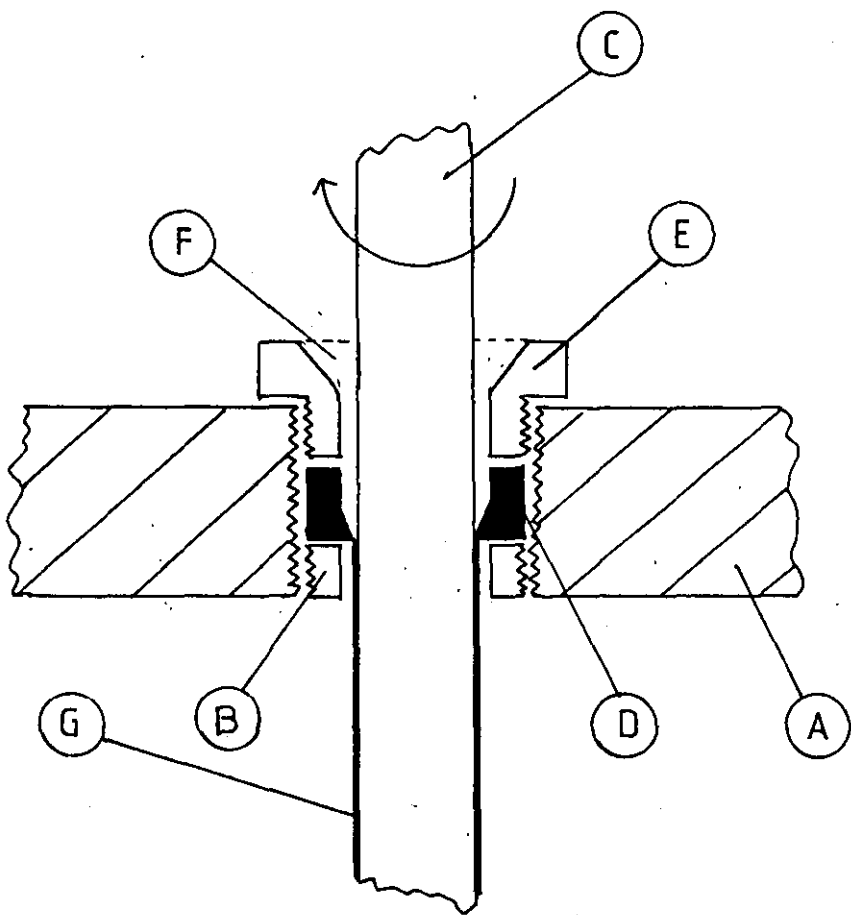
FIG. 8.8   TYPICAL LABORATORY ROTATING CYLINDER ELECTRODES

a) discrete electrode

b) incorporating foil electrodes on a former

A rotating shaft (stainless steel)

B PTFE tape

C insulating end caps (PTFE)

D solid cylindrical cathode (stainless steel)

E hollow cylindrical former (stainless steel)

F copper foil electrode

G securing screw (PTFE)
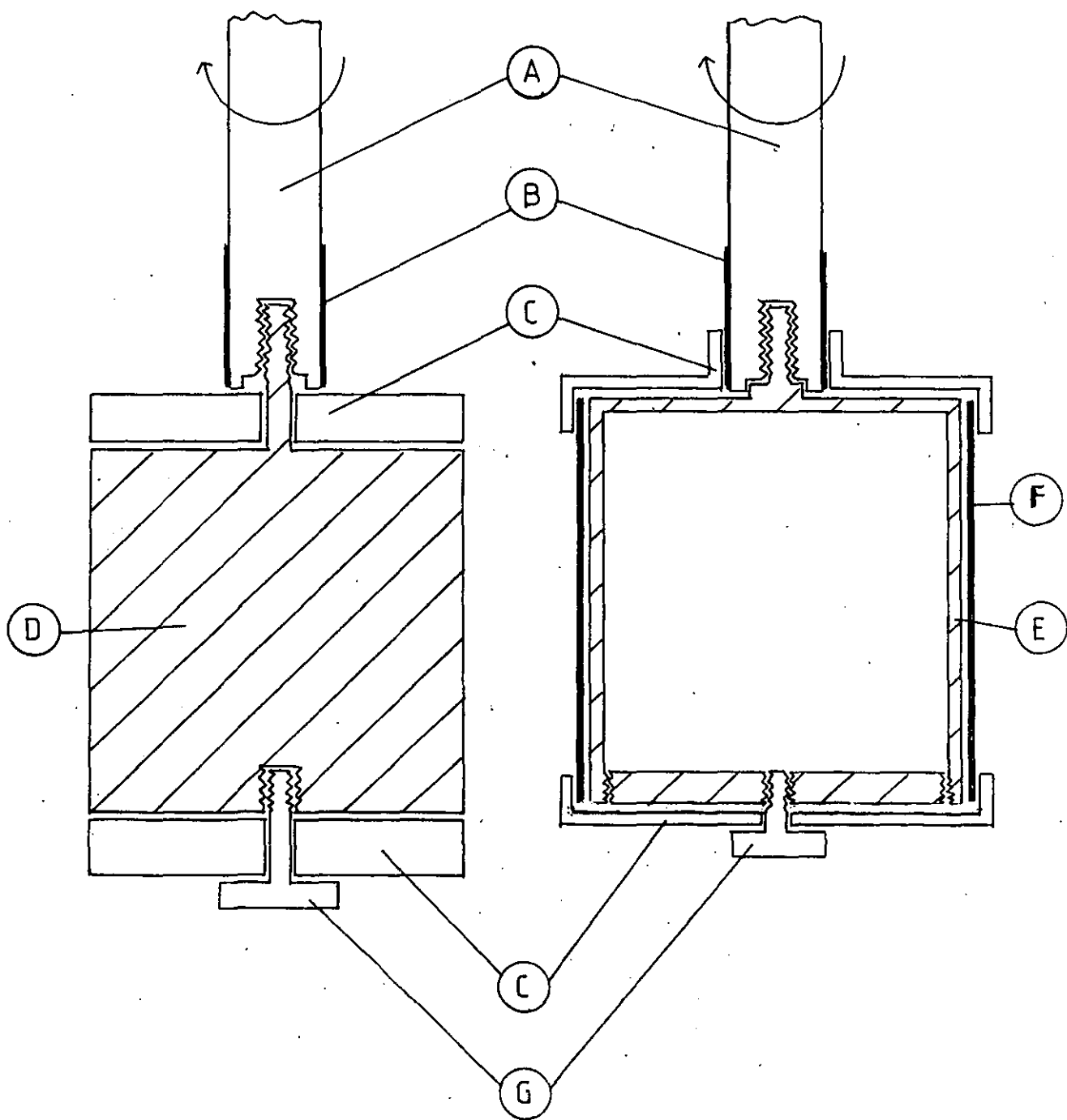
FIG. 9.1   SCHEMATIC PLAN OF THE 500 AMP PILOT PLANT REACTOR

A.   Polypropylene Body

B.   Top Flange

C.   Rotating Cylinder Cathode

D.   Cation Exchange Membranes (2)

E.   Anodes (2)

F.   Inlet Sparge Tube

G.   Outlet Tube

H.   Scraper

I.   Polypropylene Block Insert

J.   Reference Electrode, Polypropylene Probe
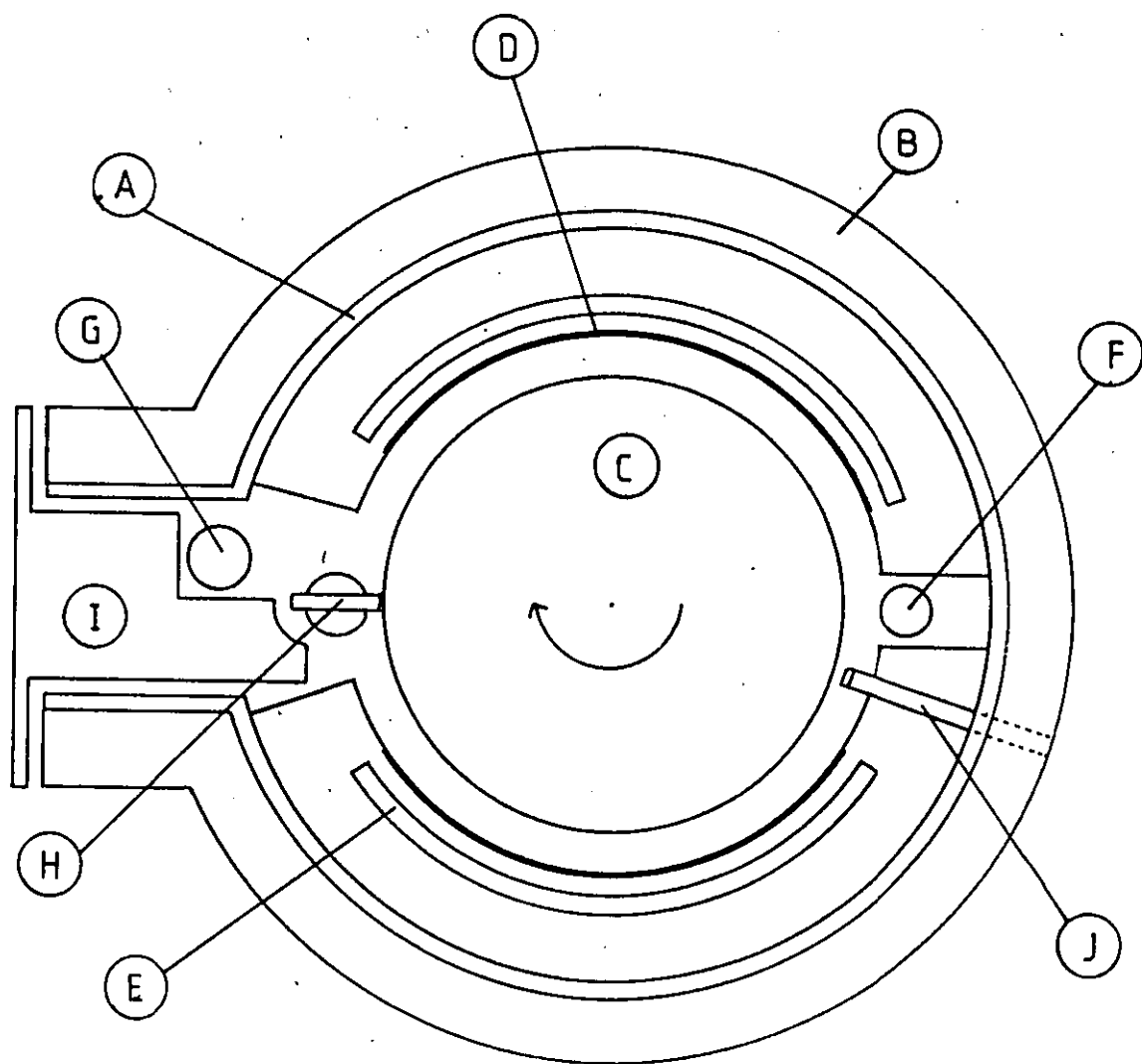
FIG. 9.2   SCHEMATIC OF THE 500 AMP PILOT PLANT FLOW SYSTEM

RC   R.C.E.R. Catholyte Compartment

RA   R.C.E.R. Anolyte Compartment

HA   Anolyte Heat Exchanger

HC   Catholyte Heat Exchanger

FM   Flow Meter

S   Gas/Liquid Separator

C   Hydrocyclone Solid/Liquid Separator

CH   Catholyte Heat Exchanger

F   Filter Tank and Tray

CM   Catholyte Mixing Tank

PC   Catholyte Pump

PA   Anolyte Pumps

PS   Separator Pump

PH   pH/reference Electrodes

ISE   Solution Bleed to Ion Selective Electrode Analyser

ADDS   Chemical Additions

A   Anolyte

CW   Cooling Water

G   Gas Vent (normally hydrogen)

D   To Drain

VALVES

$\bowtie$ normally open

◄►   normally closed
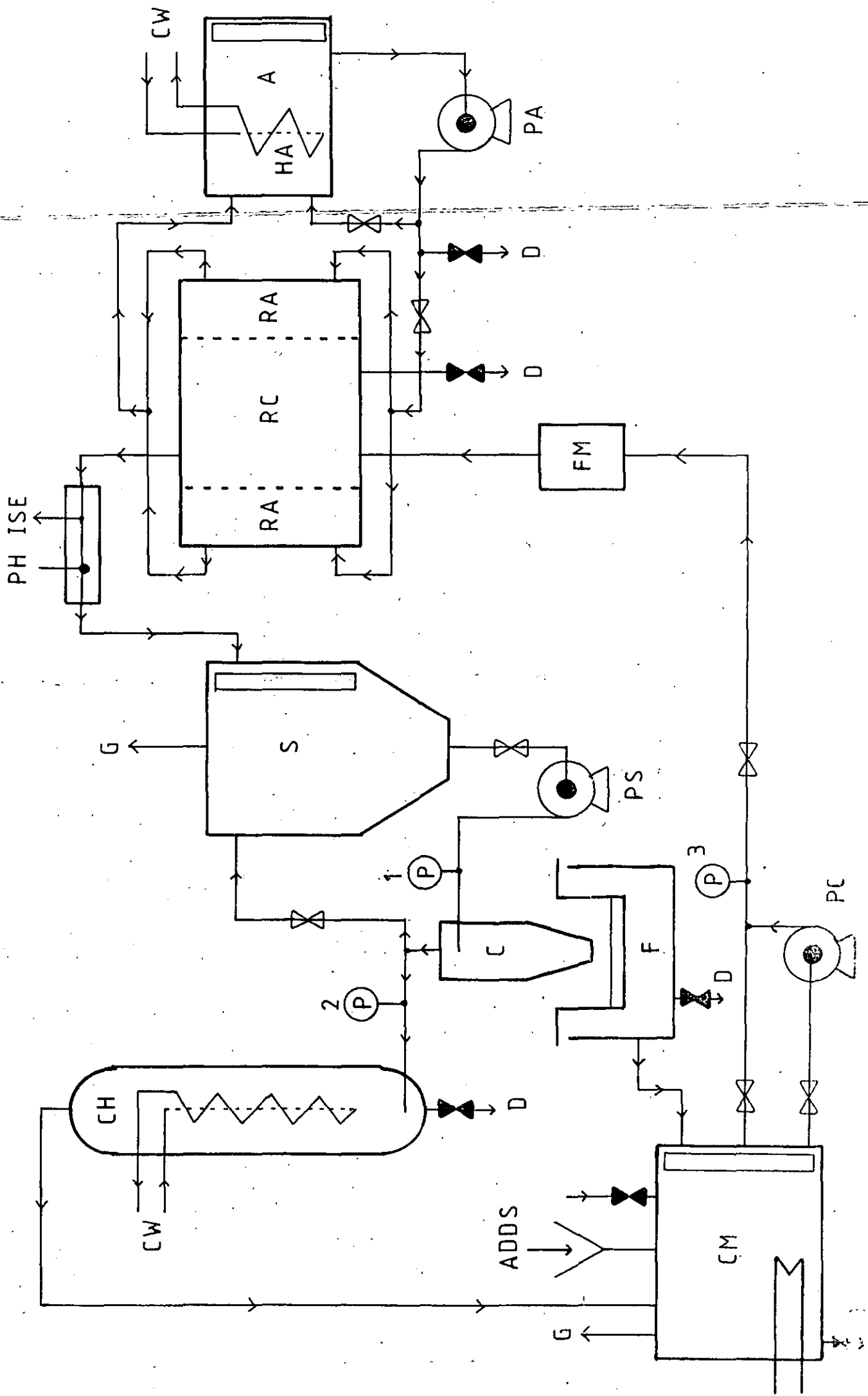
FIG. 9.3   SCHEMATIC OF THE ELECTRICAL CIRCUIT FOR THE 500 AMP

         PILOT PLANT REACTOR

P   Potentiostat Controller

R   Regulator

T   Transformer/Rectifier

MC   Motor Speed Control

M   Drive Motor

TC   Tachometer

PB   Cathode Power Brush

PPU   Potential Pick Up Brush

RE   Reference Electrode Assembly

S   Precision Shunt, 500A/50 mV

DVM(I)   Digital Voltmeter (cell current)

DVM(E)   Digital Voltmeter (electrode potential)
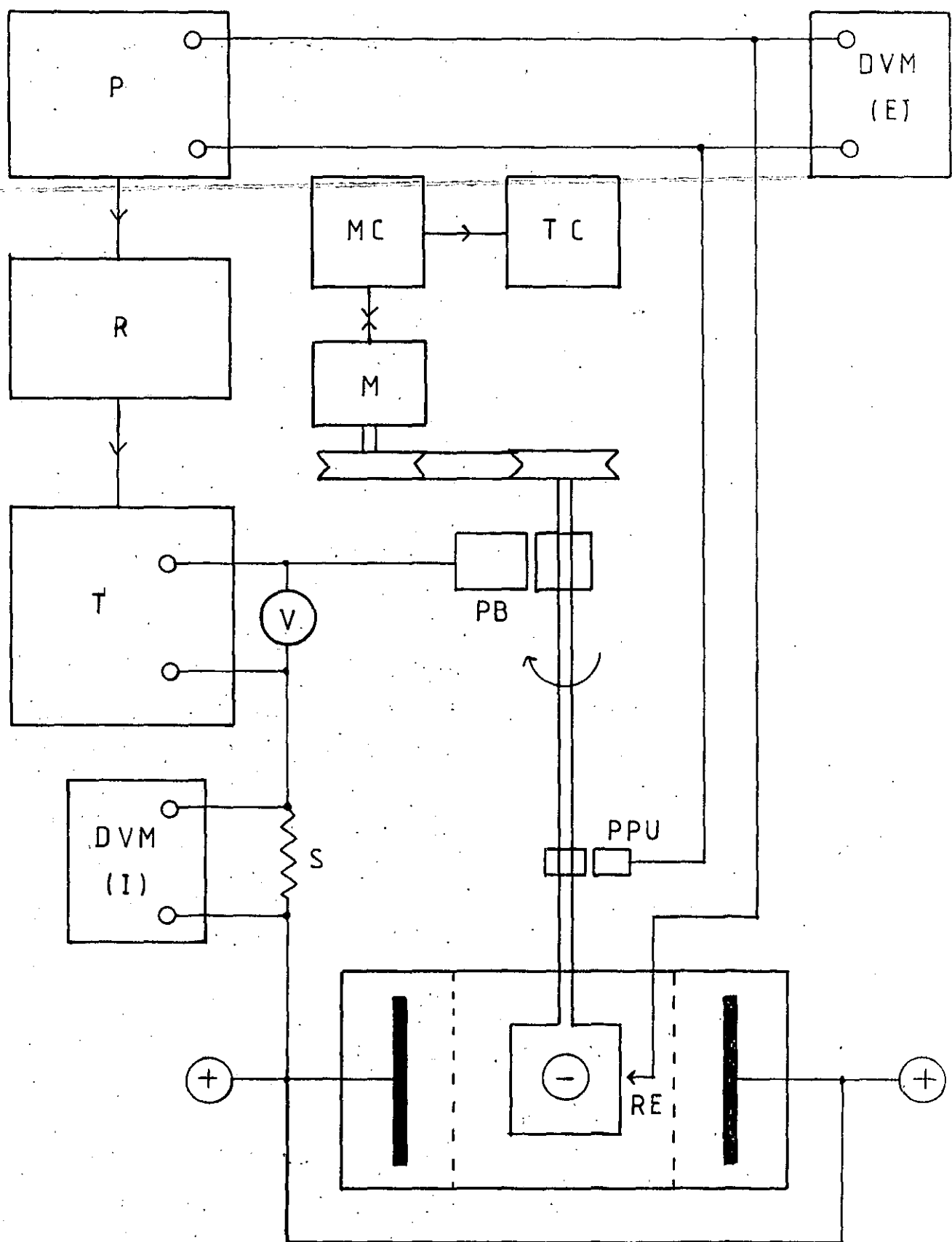
FIG. 9.4   PHOTOGRAPH OF THE 200 AMP 'ECO-CASCADE-CELL' REACTOR

A   Rubber lined, mild steel body

B   Anolyte compartment (2)

C   Anode Feeders

D   Reference electrode probes/sampling points (6)

E   Rotating Shaft

F   Scraper actuating pneumatics

9.4.
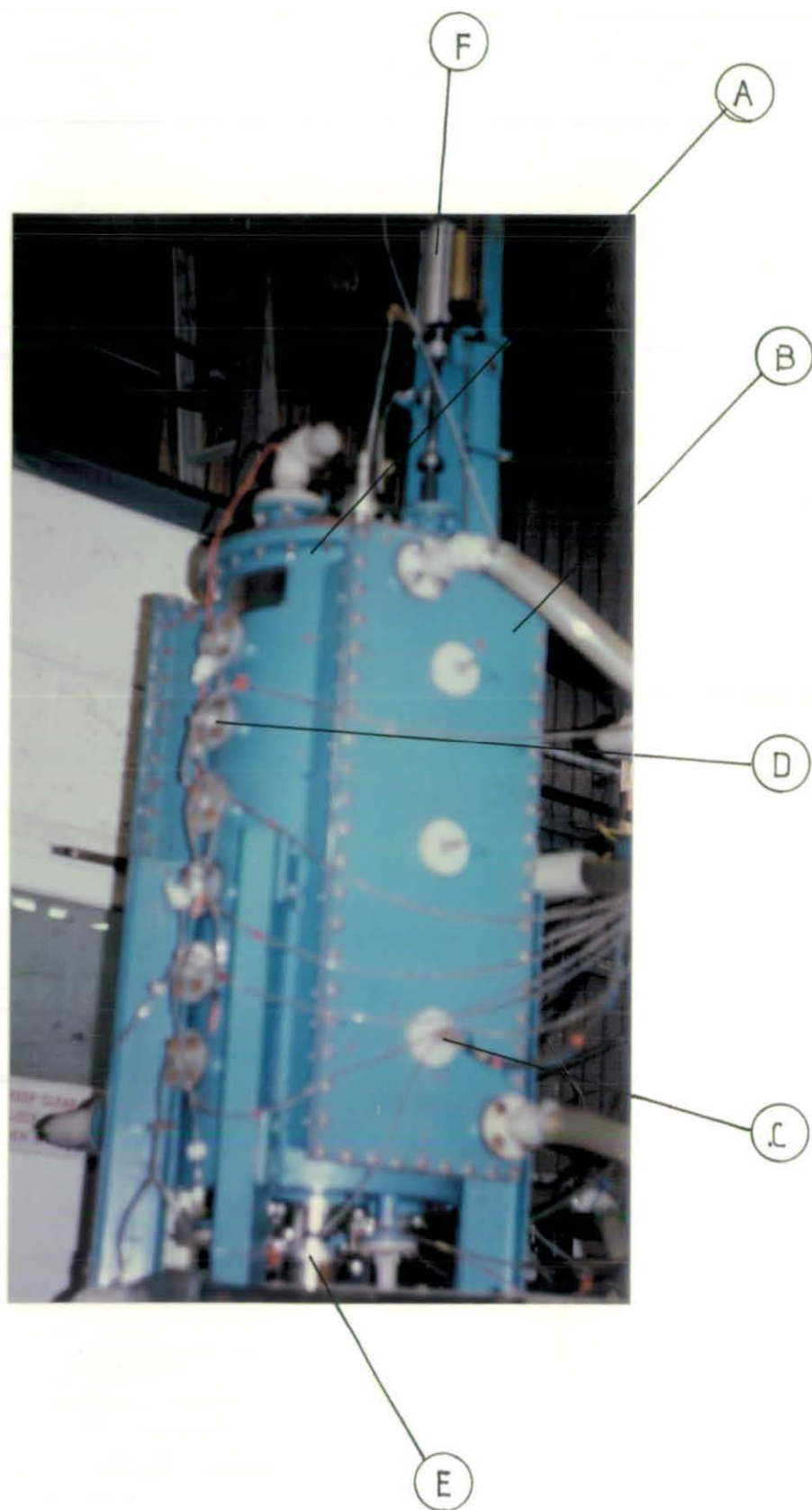
FIG. 9.5   SCHEMATIC PLAN OF THE 200 AMP 'ECO-CASCADE-CELL' REACTOR

(Upper anode box assembly omitted for clarity)

A   Anode (nickel plate)

B   Anode box securing side plate (rubber lined steel)

C   Insulating Bush (polypropylene)

D   Titanium Plate Anolyte compartment

E   Perforated Titanium Outer and Inner Plates supporting membrane

F   Membrane;   cation exchange cloth

G   Catholyte/reactor body (rubber lined steel)

H   Catholyte dividing Baffle Plate (polypropylene)

I   Baffle - cylinder space (annular)

J   Rotating Cylinder Cathode (stainless steel)

K   Scraper
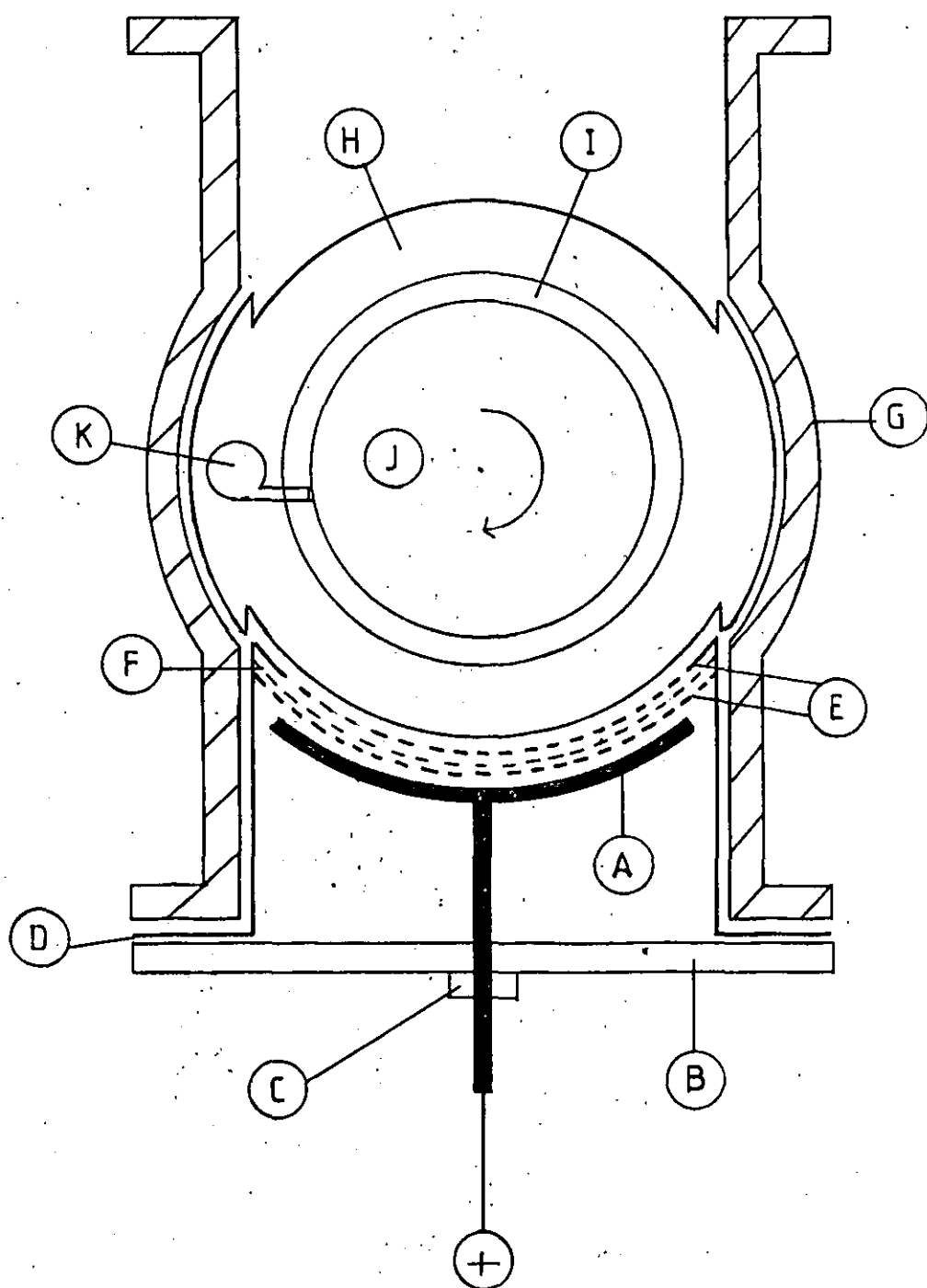
FIG. 9.6 (a)   SCHEMATIC OF THE FLOW SYSTEM FOR THE 200 AMP

'ECO-CASCADE-CELL' - showing the anolyte (bold line)

and water flush circuits

Anolyte Circuit

AT   anolyte tank

PA   anolyte pump

AC   anolyte compartment (2)

water flushes

RT   rotammeters (6)

CC   clear catholyte

R   to recycle

MW   filtered mains water

WW   waste water

F   filter

seal assemblies

ULS   upper lip seal (water flushed)

LLS   lower lip seal (water flushed)

UL   upper labyrinth (catholyte flushed)

LL   lower labyrinth (catholyte flushed)

rotammeter functions

1   clear catholyte inlet to UL

2   clear catholyte inlet to LL

3   water outlet from ULS

4   water outlet from LLS

5   water inlet to ULS

6   water inlet to LLS
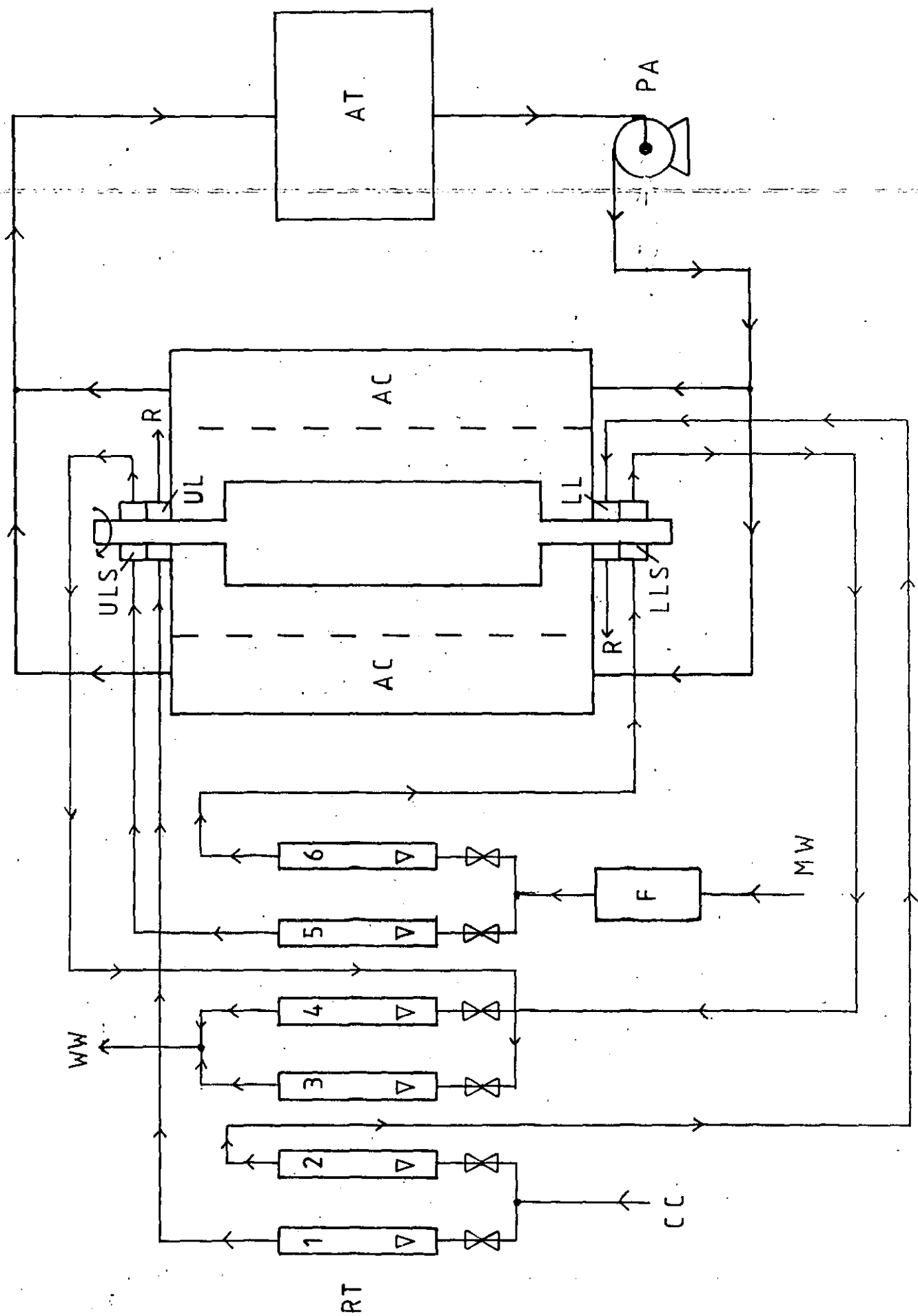
FIG. 9.6 (b) . SCHEMATIC OF THE FLOW SYSTEM FOR THE 200 AMP

'ECO-CASCADE-CELL' REACTOR - showing the catholyte

and product separation circuits

CC	Catholyte compartment
PC	Catholyte Pump
GS	Gas/Liquid Separator
G	Gas Vent
C	Hydrocyclone Solid/Liquid Separator
TH	Thickening Cone
MP	Metal Powder Slurry
CT	Catholyte Tank
PS	Separator Pump
LC	Level Control on GS

The figure shows the valves arranged for normal flow (metal removal)

i.e.   V1 open

V2 closed

V3 closed

V4 open

For product recovery, the reactor was backwashed by reversing flow through

it i.e.   V1 closed

V2 open

V3 open

V4 closed
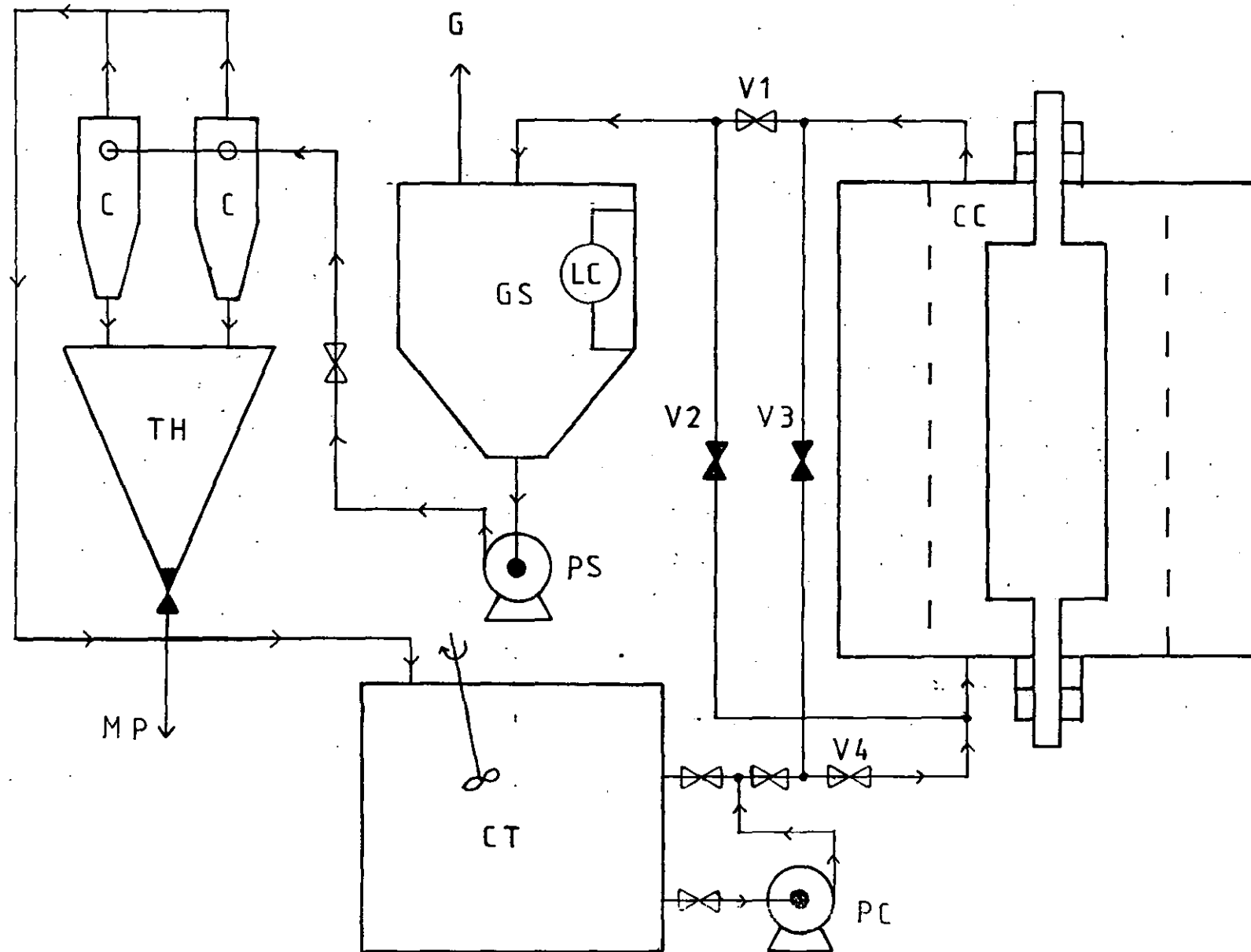
FIG. 9.7   SCHEMATIC OF THE ELECTRICAL CIRCUIT FOR THE 200 AMP

'ECO-CASCADE-CELL' REACTOR

T   Transformer/Rectifier

R   Regulator

S   Precision Shunt, 500A/50 mV

V   Cell Voltmeter

PB   Cathode Power Brush

LPPU   Lower Potential Pick Up Brush

UPPU   Upper Potential Pick Up Brush

DVM(I)   Current, Digital Voltmeter

DVM(E)   Potential, Digital Voltmeter

SWA   Switch to Select PPU Brush

SWB   Switch to Select Reference Electrode Assembly

(RHS anodes omitted for clarity: each LHS anode has a RHS equivalent
connected to it.)

UPPU

3

+

2

1

6

5

4

3

2

1

DVM
(I')

S

LPPU

PB

V

T

R

SW A

SW B

DVM
(E)
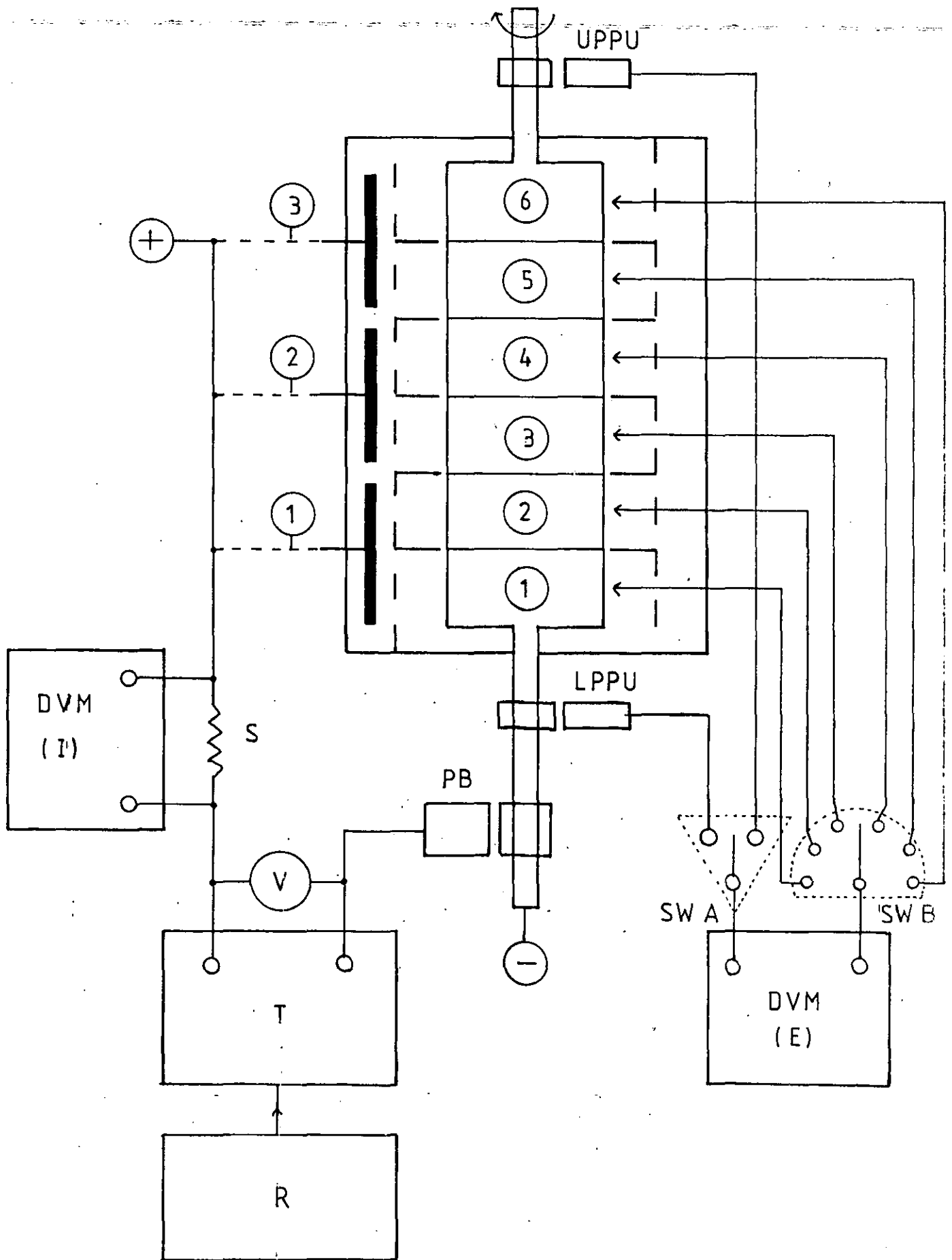
FIG. 10.1   CATHODIC POLARISATION CURVE FOR COPPER DEPOSITION

ON TO A SMOOTH COPPER R.C.E., showing the limits

of reproducibility for ten successive trials

0.014 M $CuSO_4$ + 1.5 M H_2SO_4

22° C

500 rpm

d = 6.3 cm

l = 4.3 cm

A = 85.1 cm^2

U = 165 cm s^{-1}

150 mV $(min)^{-1}$ linear sweep rate

(See also Table 10.1)
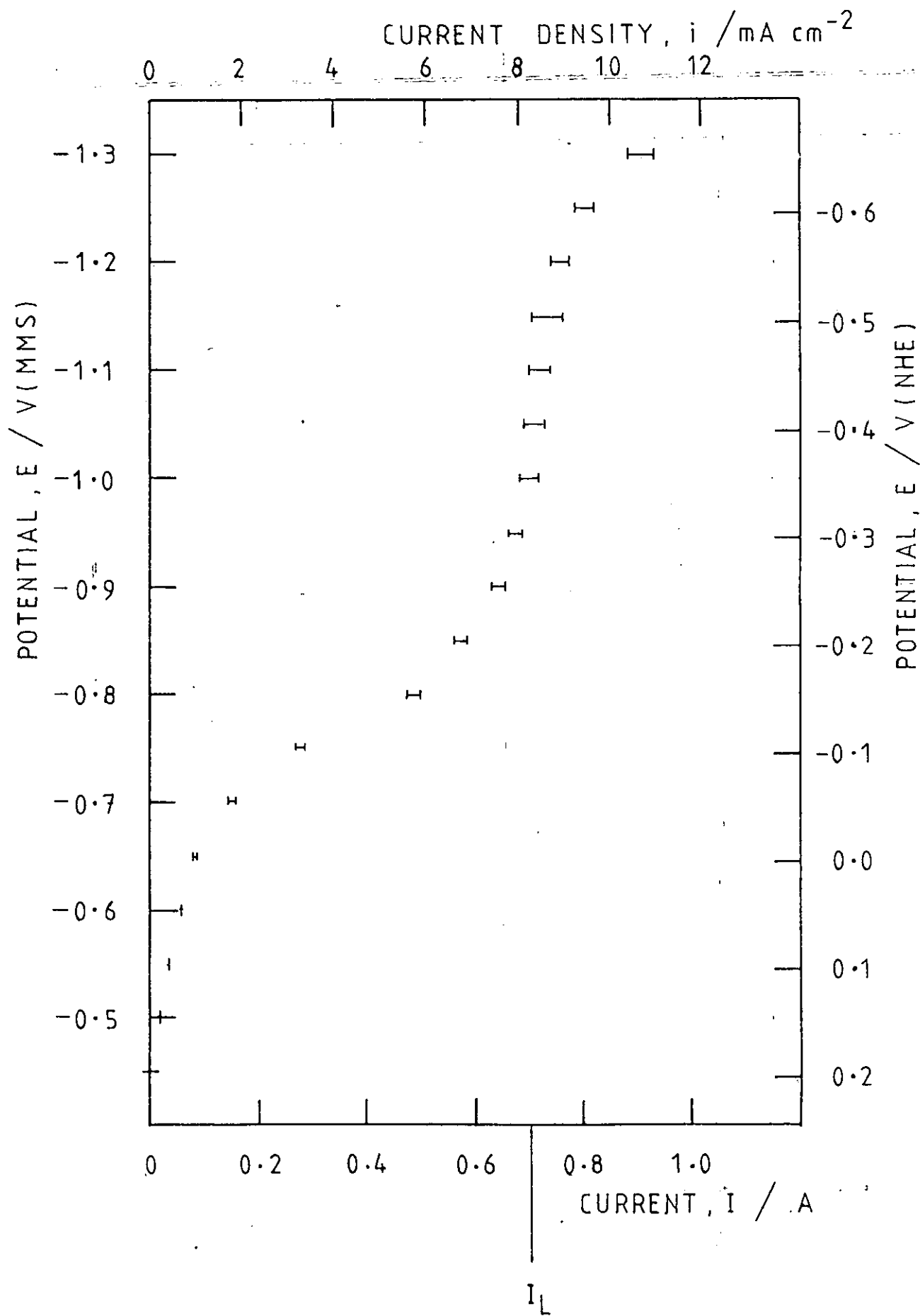
FIG. 10.2   CATHODIC POLARISATION CURVE FOR COPPER DEPOSITION

ON TO A SMOOTH COPPER R.C.E., showing the effect

of potential scan rate on the limiting current

Undivided cell; soluble copper anode. Other conditions as

Fig. 10.1
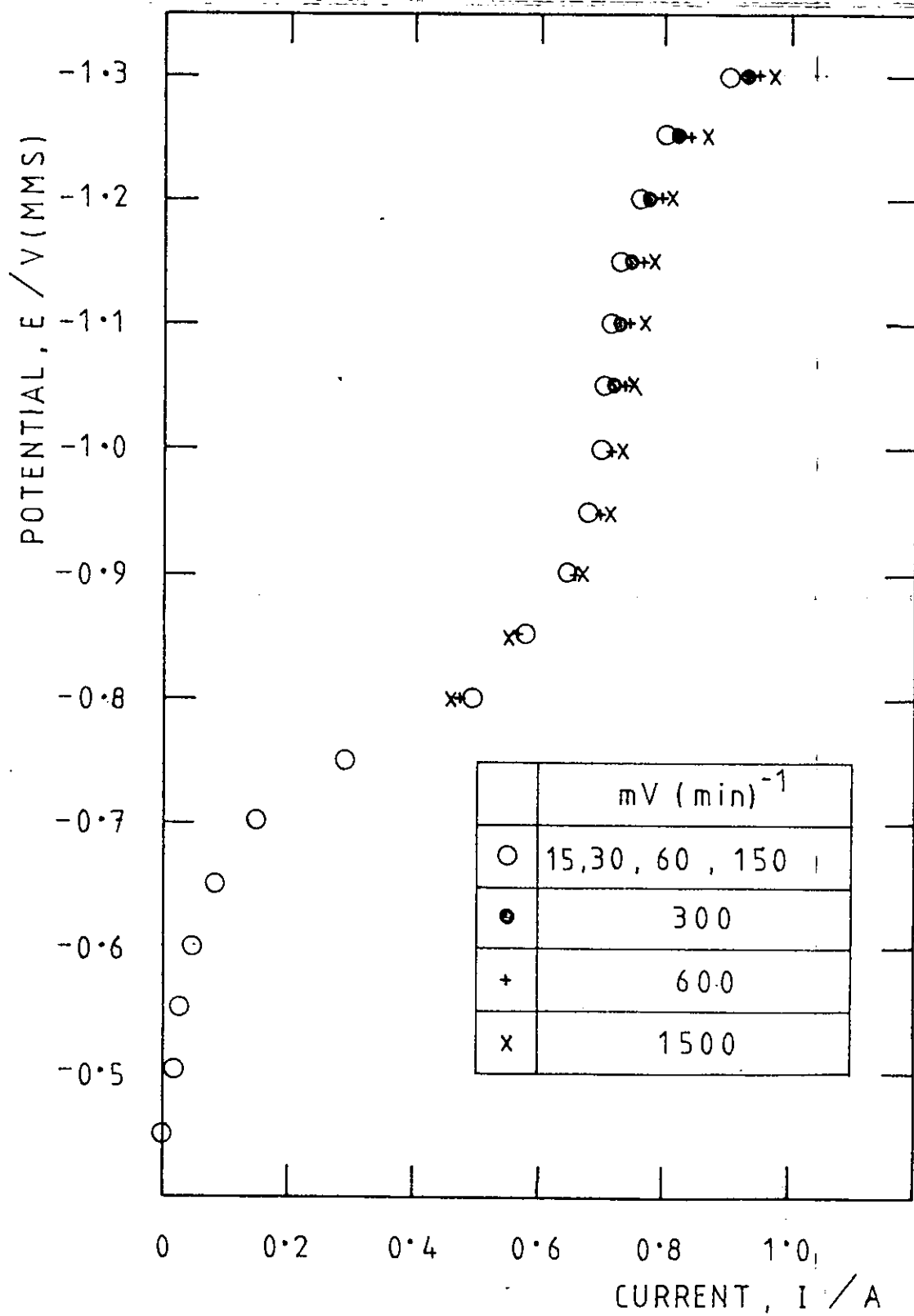
EXPERIMENTAL MASS TRANSPORT DATA FOR COPPER.

DEPOSITION TO A SMOOTH ROTATING CYLINDER

ELECTRODE : Comparison with known correlations

FIG.IO.3   Eisenberg, Tobias and Wilke Correlation :

$$j_D' = 0.079 \ (Re)^{-0.30} = (St)(Sc)^{0.644}$$

FIG.IO.4   Robinson and Gabe Correlation:

$$j_D' = 0.079I \ (Re)^{-0.3I} = (St)(Sc)^{0.59}$$

$\times 10^3$

(Re)
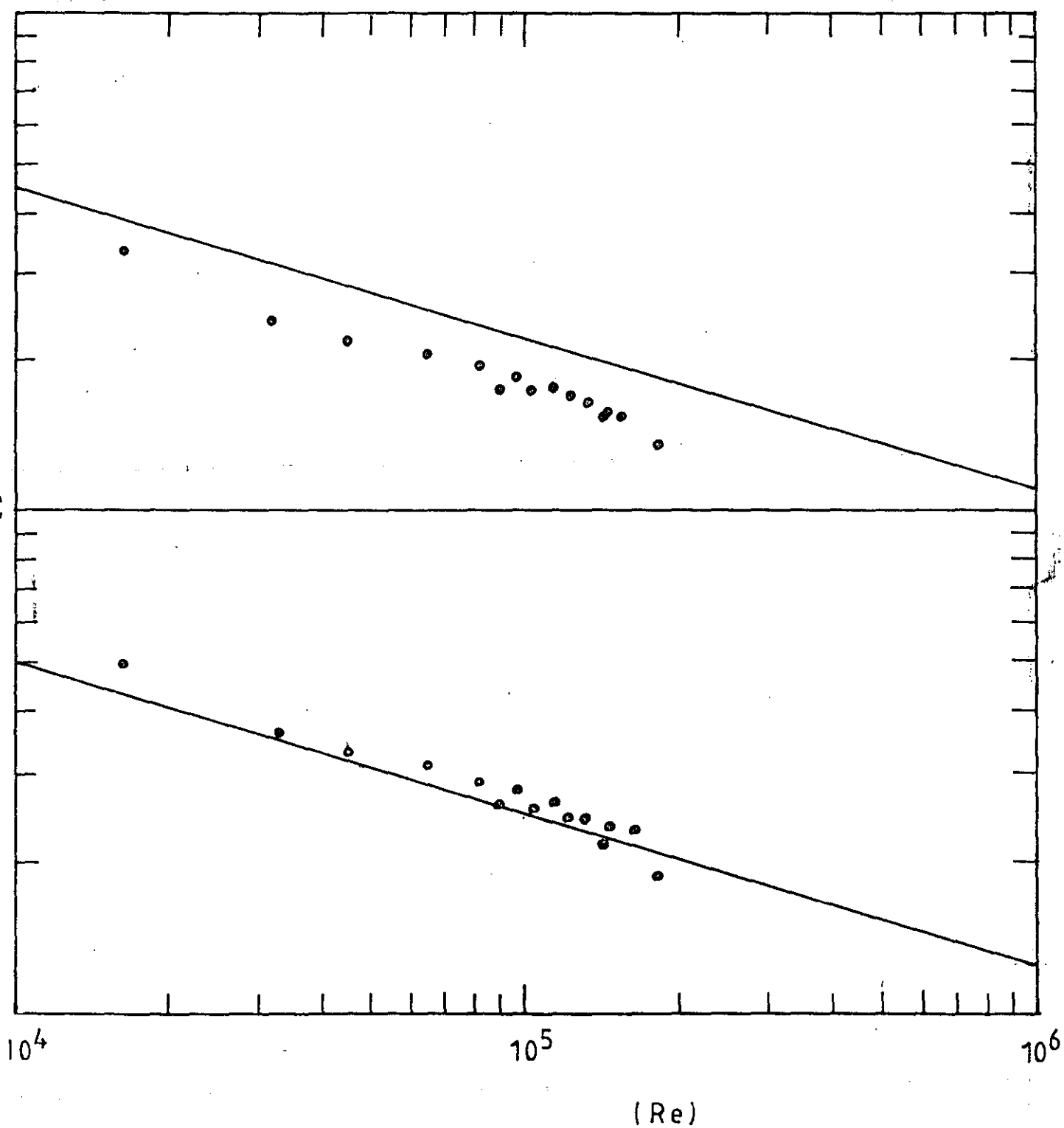
FIG. 10.5 CATHODIC POLARISATION CURVES FOR COPPER DEPOSITION

ON TO SMOOTH ROTATING CYLINDER ELECTRODES, showing

the effect of copper concentration

1.5 M H_2SO_4

22° C

500 rpm

d = 6.3 cm

l = 4.3 cm

A = 85.1 cm^2

U = 165 cm s^{-1}

150 mV $(min)^{-1}$ linear sweep rate

	Cu CONC./mg dm^{-3}
A	890
B	500
C	200
D	12 5
E	50

E / V (MMS)

I / A
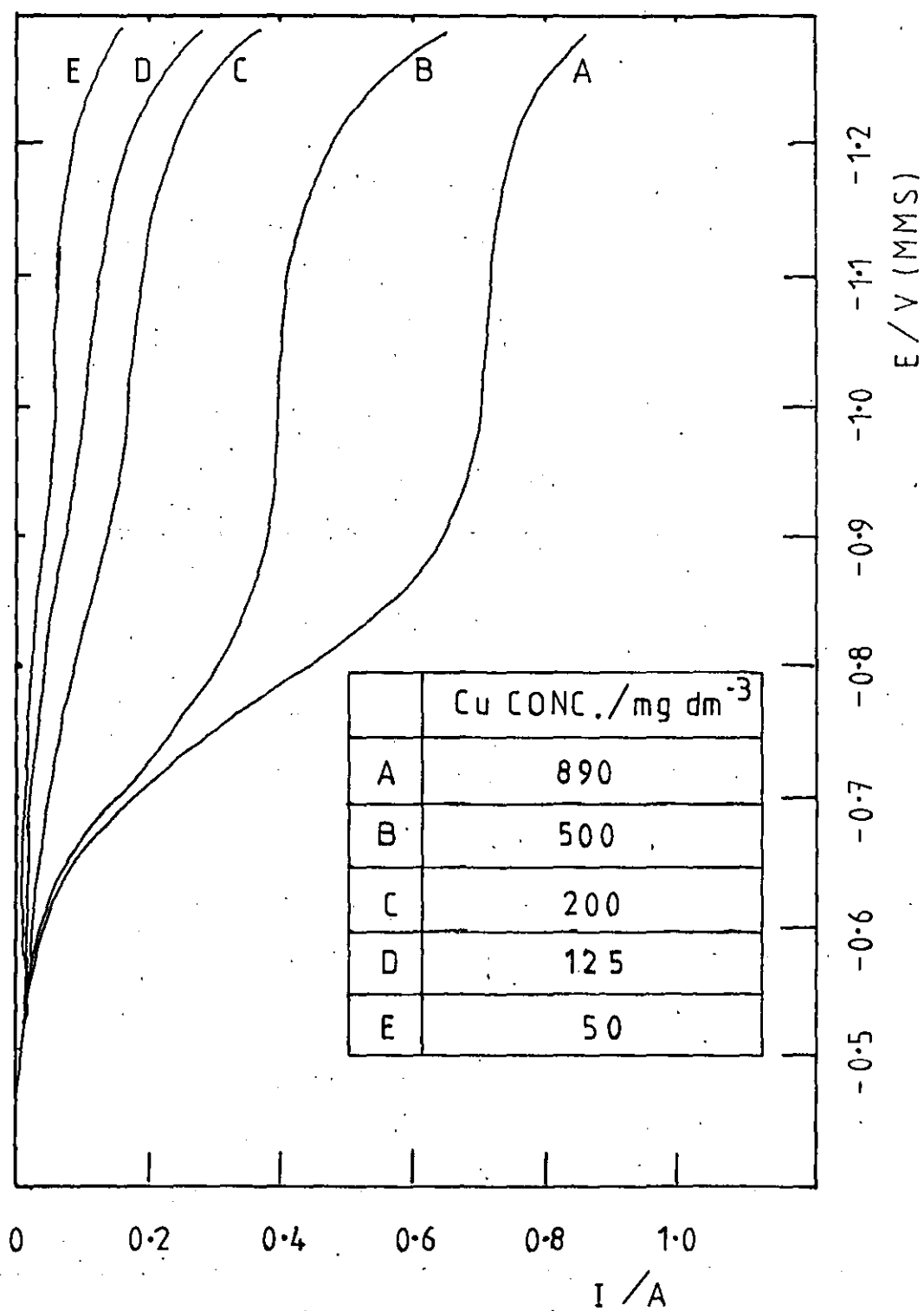
FIG. 10.6 CATHODIC POLARISATION CURVES FOR COPPER DEPOSITION

ON TO A SMOOTH R.C.E., showing the effect of

copper concentration

As Fig. 10.5, but with a logarithmic current abcissa
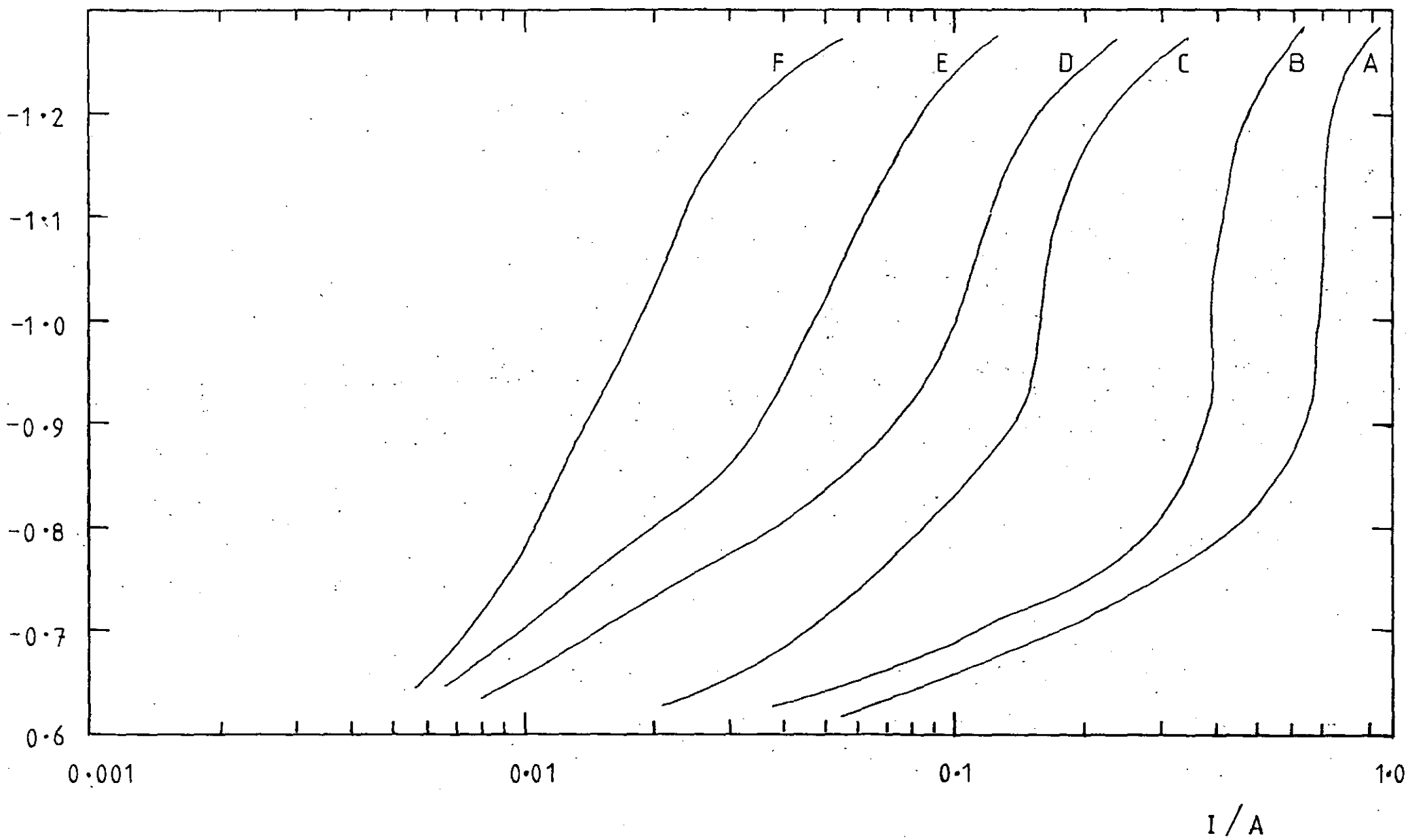
FIG. 10.7 REST POTENTIAL OF A COPPER R.C.E. AS A FUNCTION

OF CONCENTRATION

indicating a near - Nernstian response

conditions otherwise as for Fig. 10.9

22° C

500 rpm
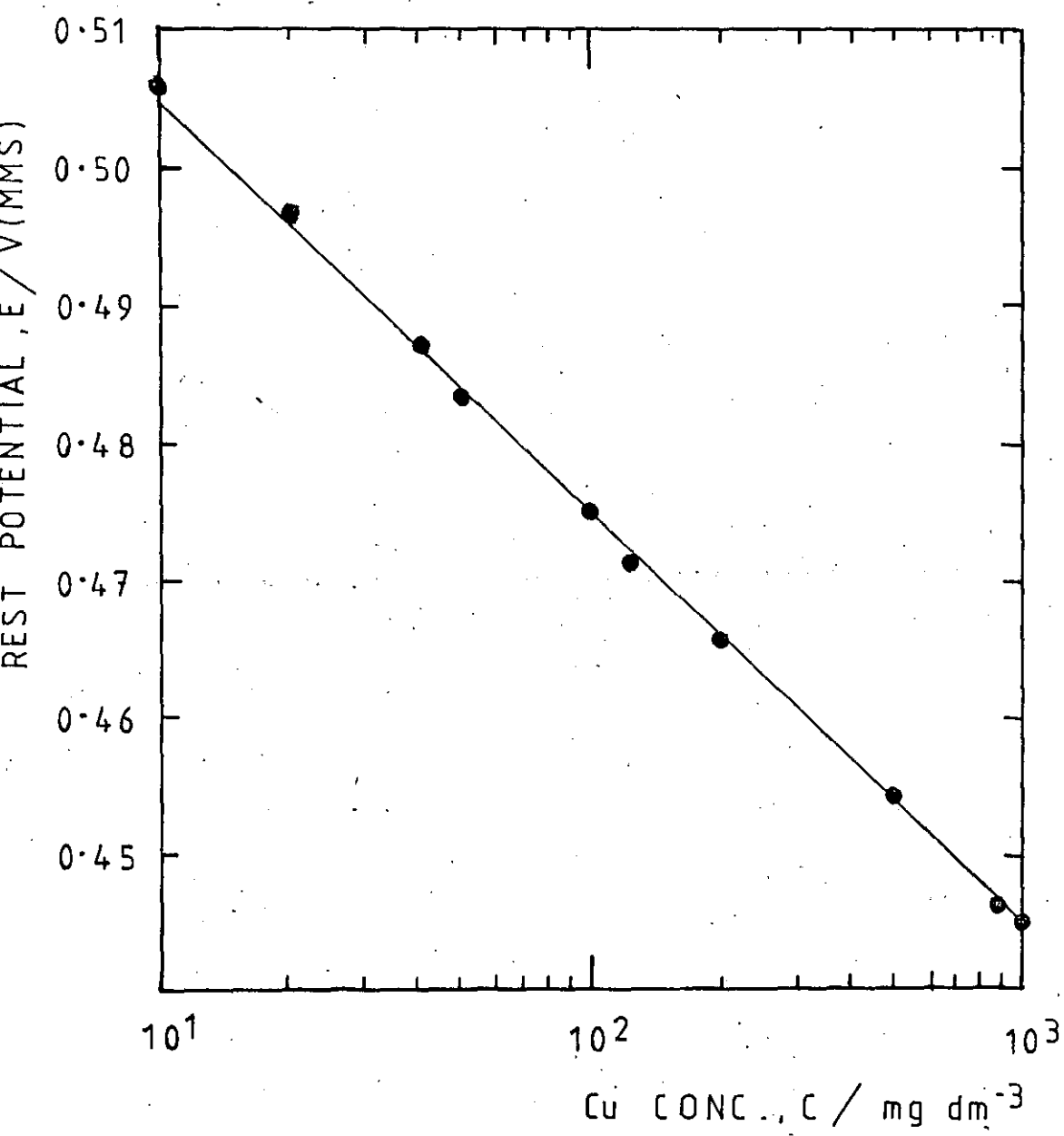
FIG. 10.8 CATHODIC POLARISATION CURVES FOR COPPER DEPOSITION

ON TO A SMOOTH R.C.E., showing the effect of

rotational speed

1.5 M H_2SO_4

22° C

d = 6.3 cm

l = 4.3 cm

A = 85.1 cm^2

150 mV (min)$^{-1}$ linear sweep rate

RPM = 100 - 1000, corresponding to

U = 33 - 330 cm s^{-1}
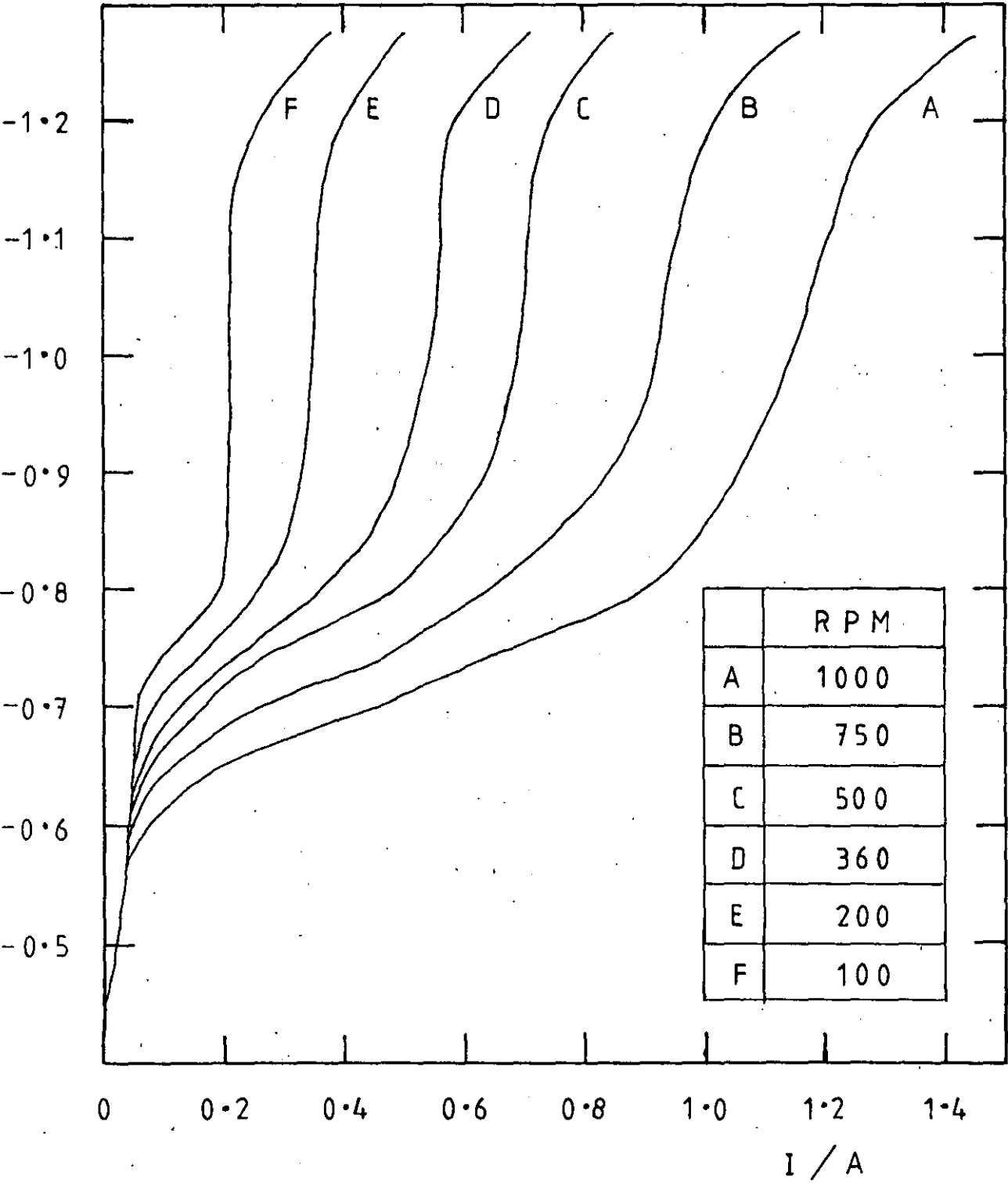
FIG. 10.9 . CURRENT AS A FUNCTION OF ROTATIONAL SPEED FOR

various potentials

LOG - LOG axes, obtained by recording steady currents at a set

potential for each rotational speed

	E / V (MMS)
+	1·200
×	1·100
•	1·000
○	/0·900
□	0·800
△	0·700
▲	0·600

I /A
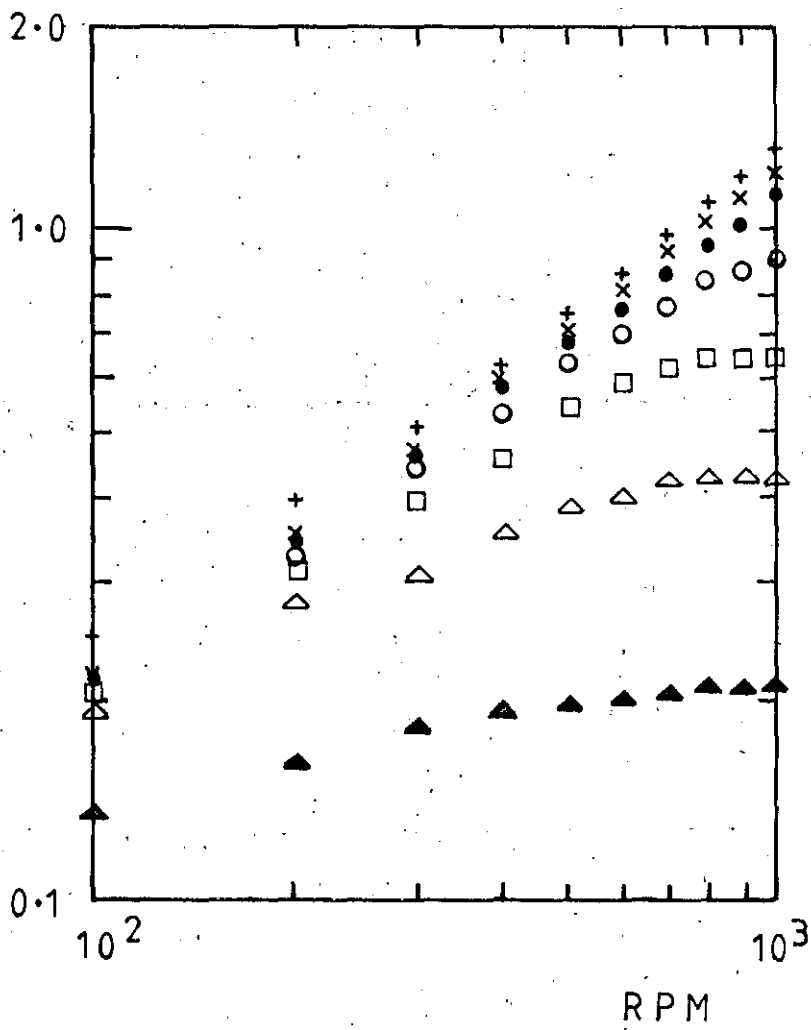
FIG. 10.10   LIMITING CURRENT AS A FUNCTION OF COPPER

CONCENTRATION

Conditions as for Fig. 10.5
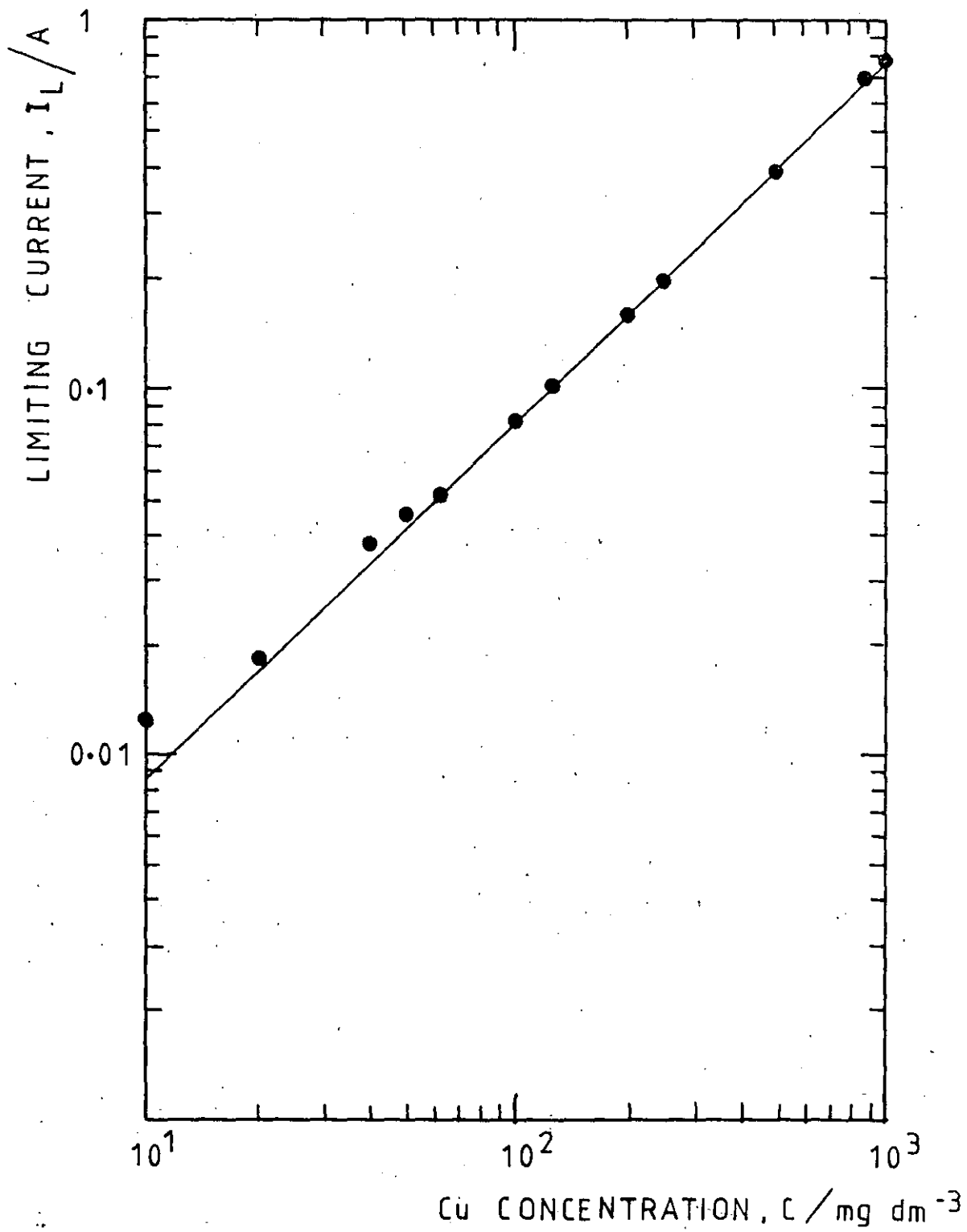
FIG. 10.11   CATHODIC POLARISATION CURVE FOR COPPER DEPOSITION

ON TO A SMOOTH R.C.E., showing the effect of

surface area

0.014 M $CuSO_4$

+ 1.5 M H_2SO_4

22° C

500 rpm

d = 6.3 cm

l = 1.1 - 5.05 cm

U = 165 cm s^{-1}

150 mV $(min)^{-1}$ linear sweep rate

A = 21.5 - 100 cm^2

E / V (MMS)

-1·3
-1·2
-1·1
-1·0
-0·9
-0·8
-0·7
-0·6
-0·5

D   C   B   A

	AREA, A/cm^2
A	100
B	85·1
C	42·6
D	21·8

0   0·2   0·4   0·6   0·8   1·0

I / A
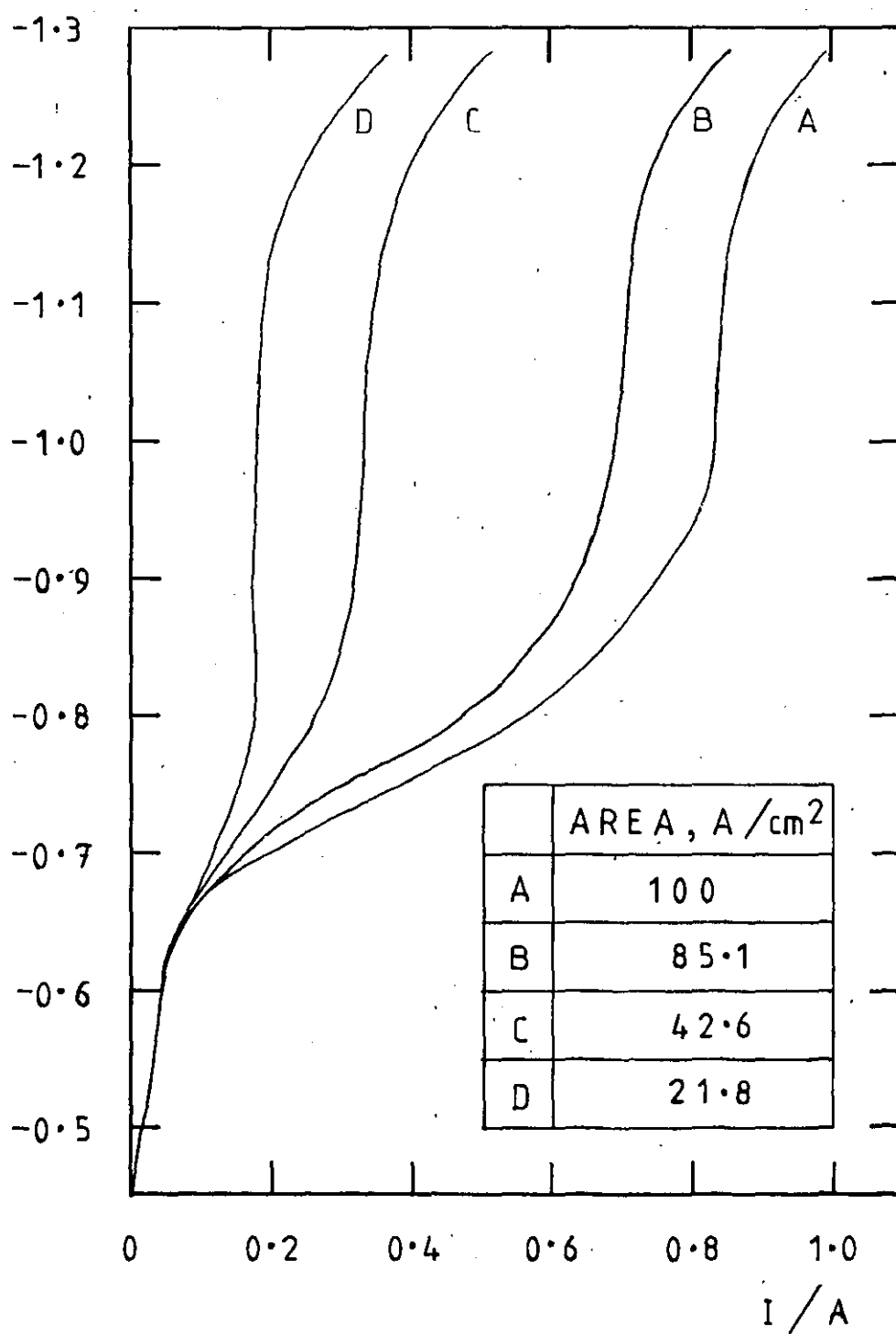
FIG. 10.12   LIMITING CURRENT AS A FUNCTION OF AREA,

corresponding to Fig. 10.11

showing a linear relationship:

$$I_L \propto A$$

The slope gives the averaged current density as 0.0081 A cm^{-2}
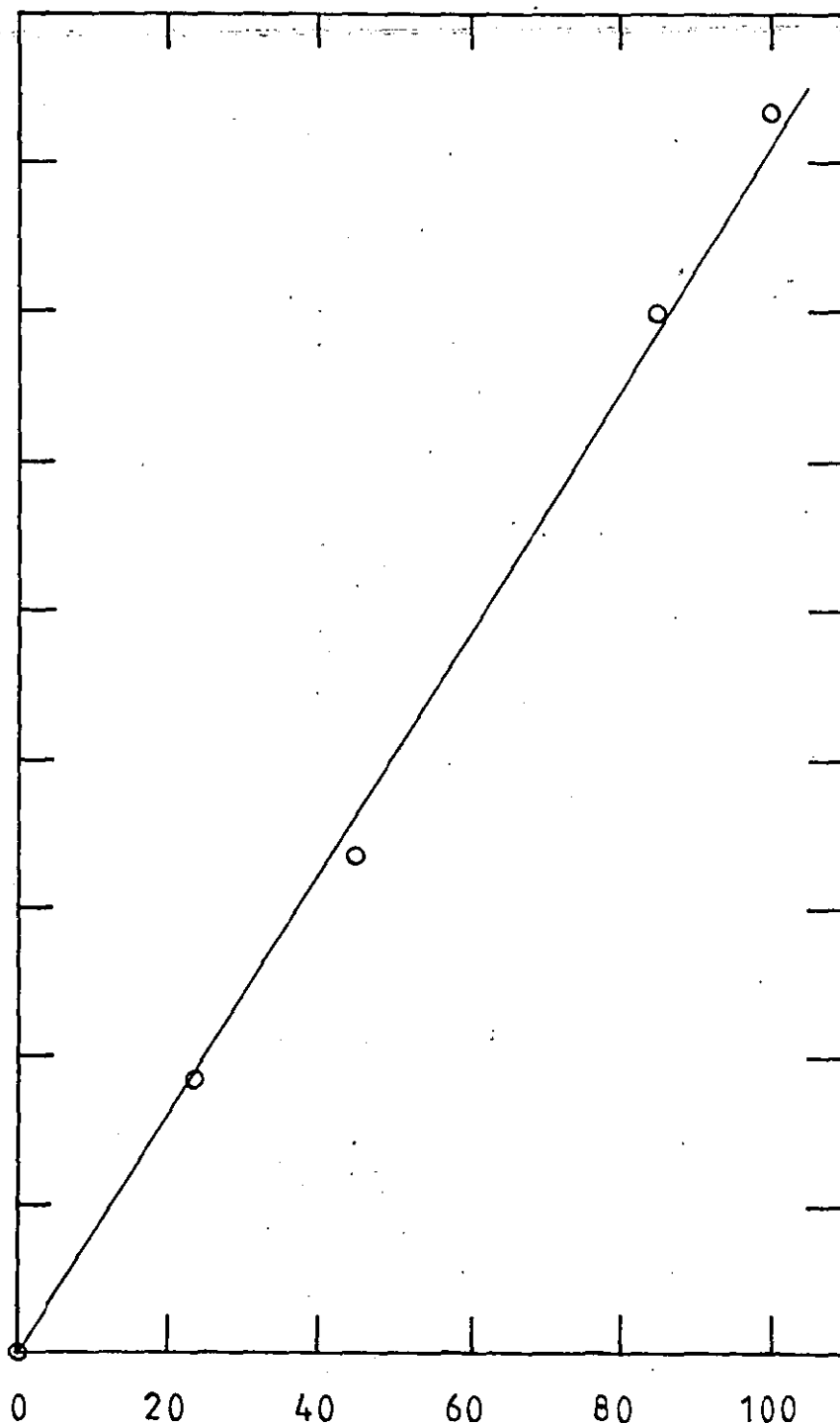
FIG. 10.13   CATHODIC POLARISATION CURVE FOR COPPER DEPOSITION

ON TO A SMOOTH R.C.E., showing the effect of

temperature

0.014 M $CuSO_4$

1.5 M H_2SO_4

22 - 60 ^{o} C

500 rpm

d = 6.3 cm

l = 4.3 cm

A = 85.1 cm^2

U = 165 cm s^{-1}

150 mV $(min)^{-1}$ linear sweep rate

E / V(MMS)

A	22 °C
B	2 9
C	3 5
D	4 5

I / A
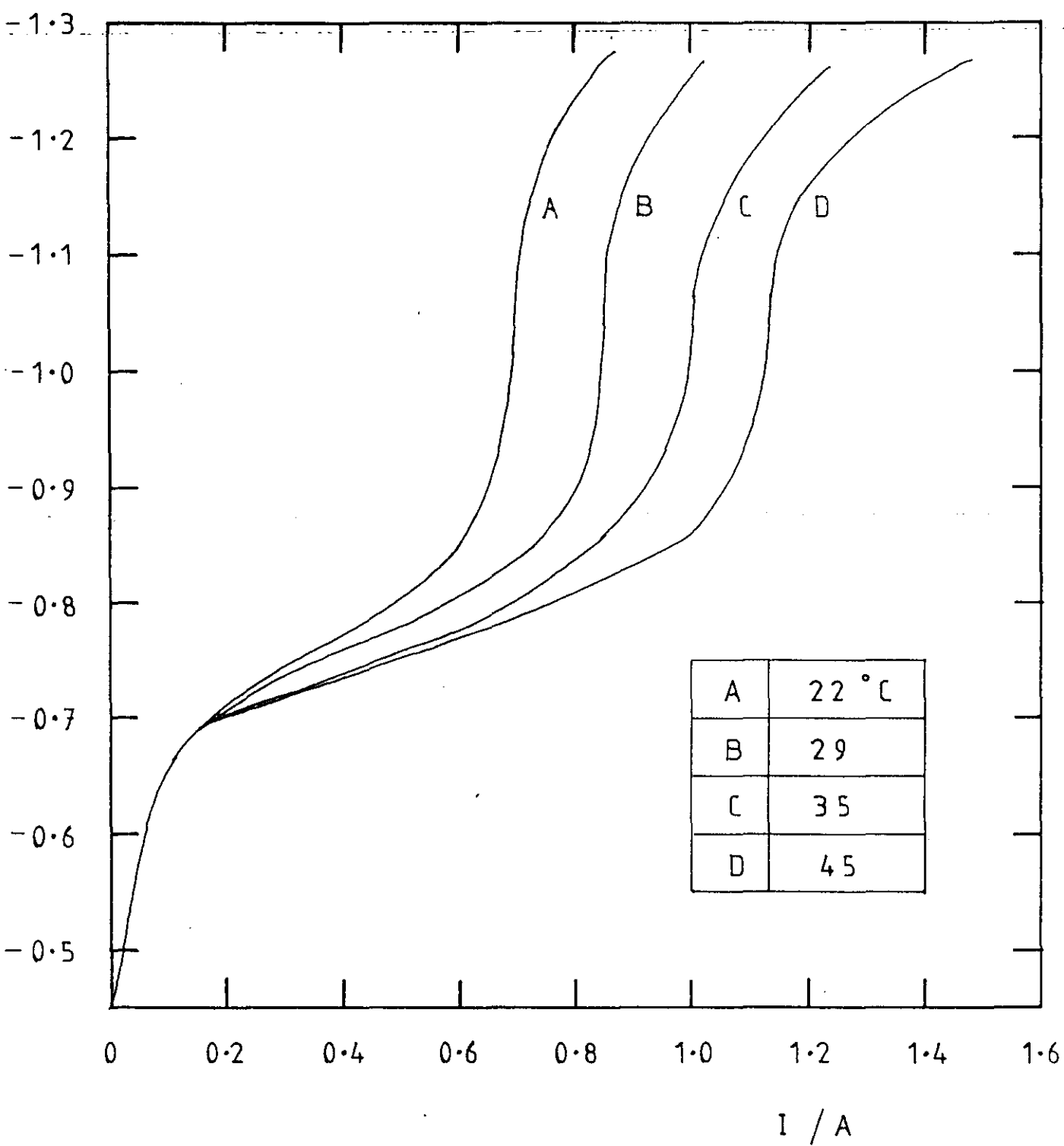
FIG. 10.14   LIMITING CURRENT AS A FUNCTION OF TEMPERATURE,

corresponding to Fig. 10.13
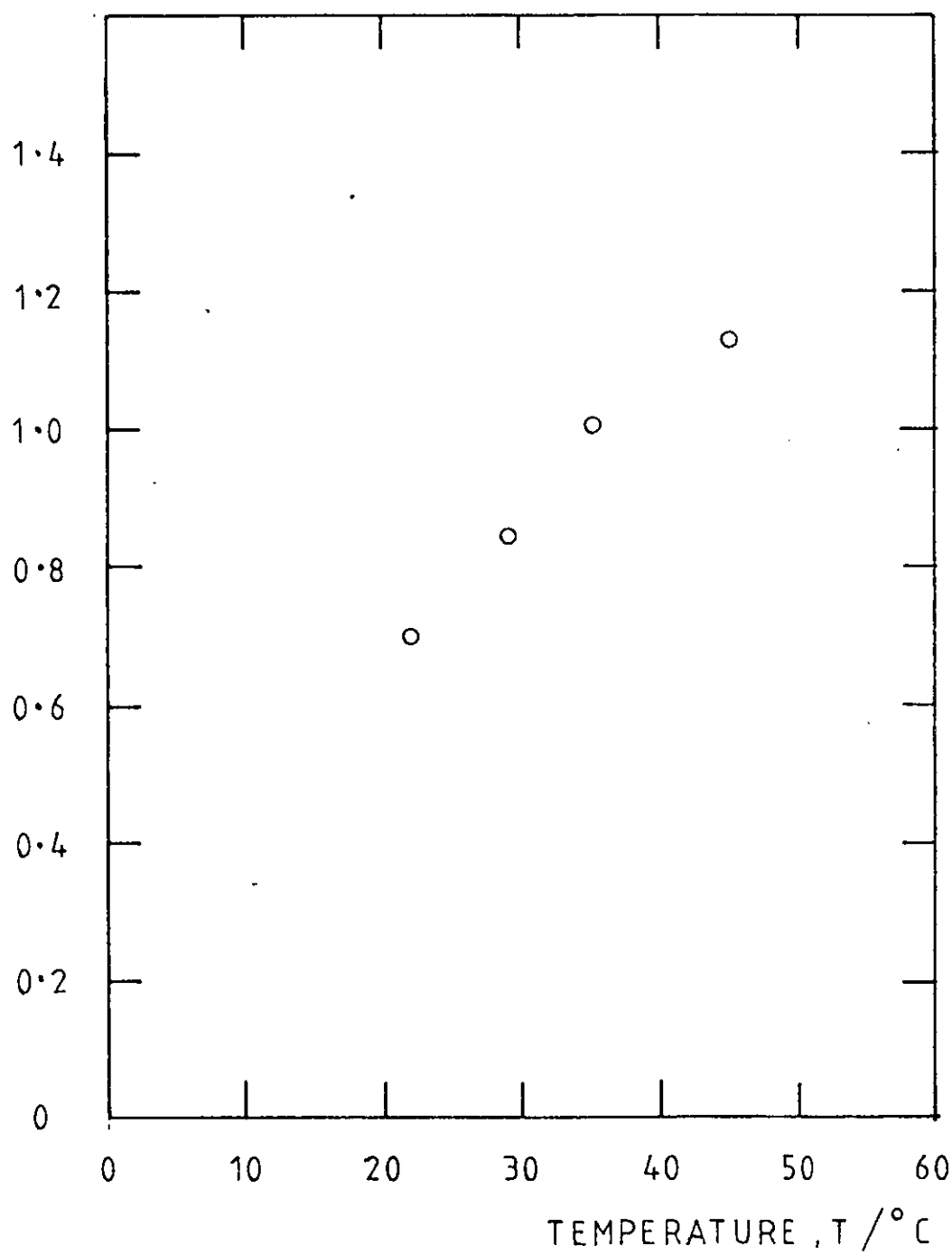
FIG. 10.15   COPPER CONCENTRATION DECAY FOR A R.C.E. DEVELOPING

ROUGHNESS

Initial concentration   0.014 M $CuSO_4$

1.5 M H_2SO_4

22° C

d = 6.3 cm

l = 4.3 cm

A = 85.1 cm^2

rpm = 340

U = 112.2 cm s^{-1}

CONCENTRATION , C / g dm⁻³ vs TIME , t / min

Legend:
- —X— EXPERIMENTAL
- ○ THEORETICAL for a SMOOTH ELECTRODE
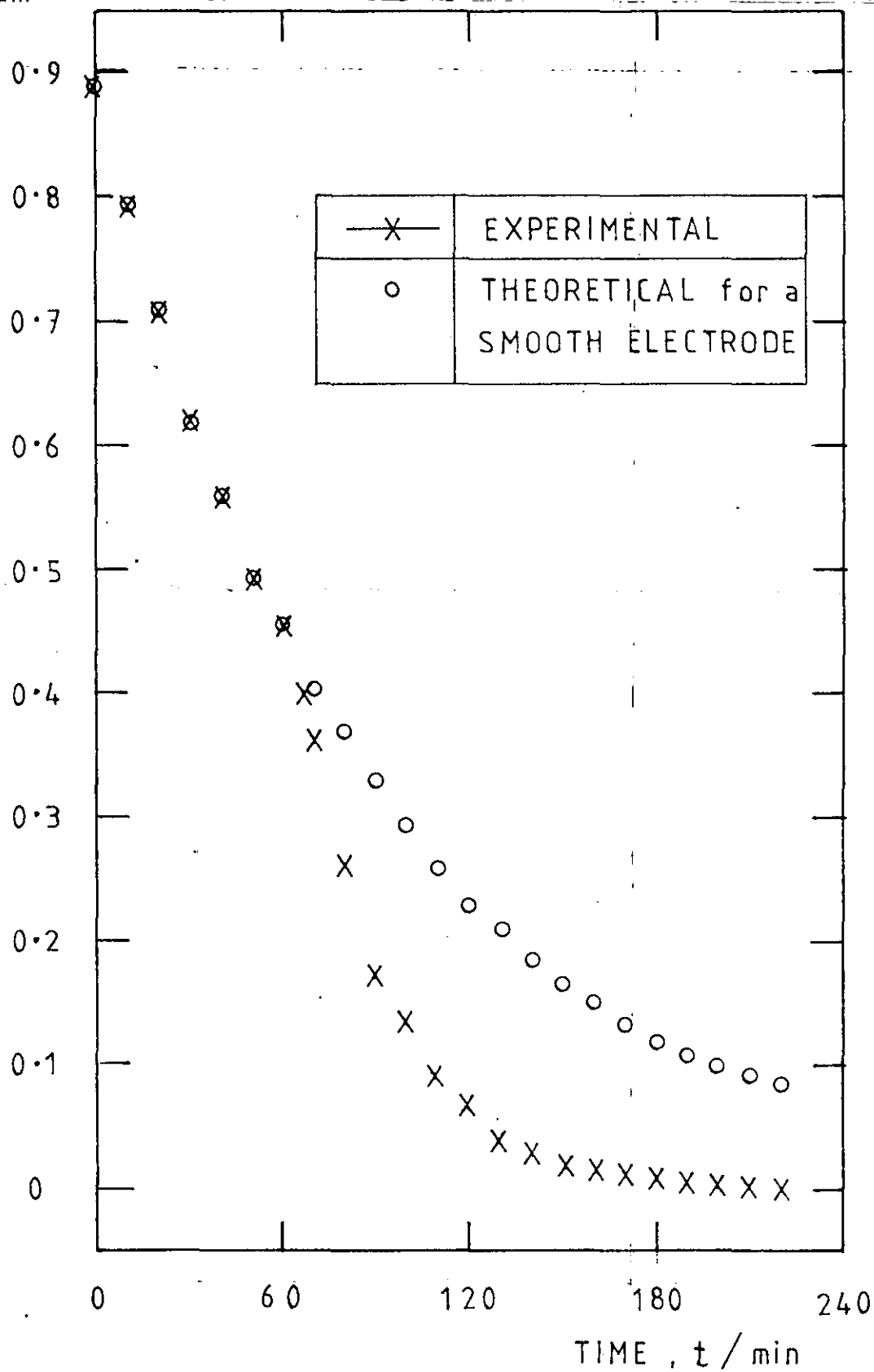
FIG. 10.16   CONCENTRATION DECAY IN A BATCH R.C.E.R.

(Fig. 10.15 plotted with LOG ordinate)

showing the limits of reproducibility for 5 trials, and typical

experimental data

conditions as for Fig. 10.15
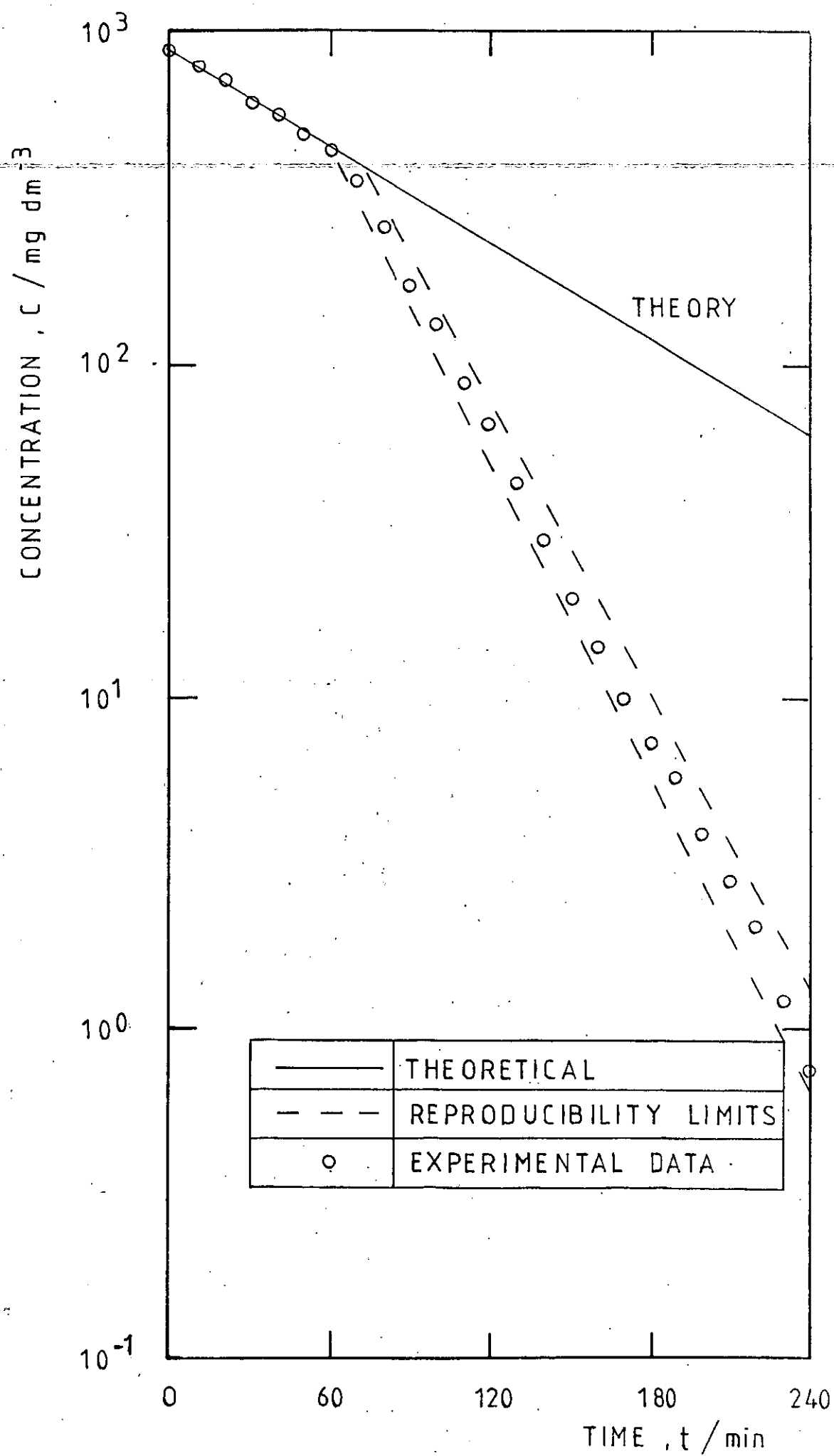
FIG. 10.17   CONCENTRATION DECAY IN A BATCH R.C.E.R.

As Fig. 10.16 but showing results for chemically

polished and electropolished copper electrodes.
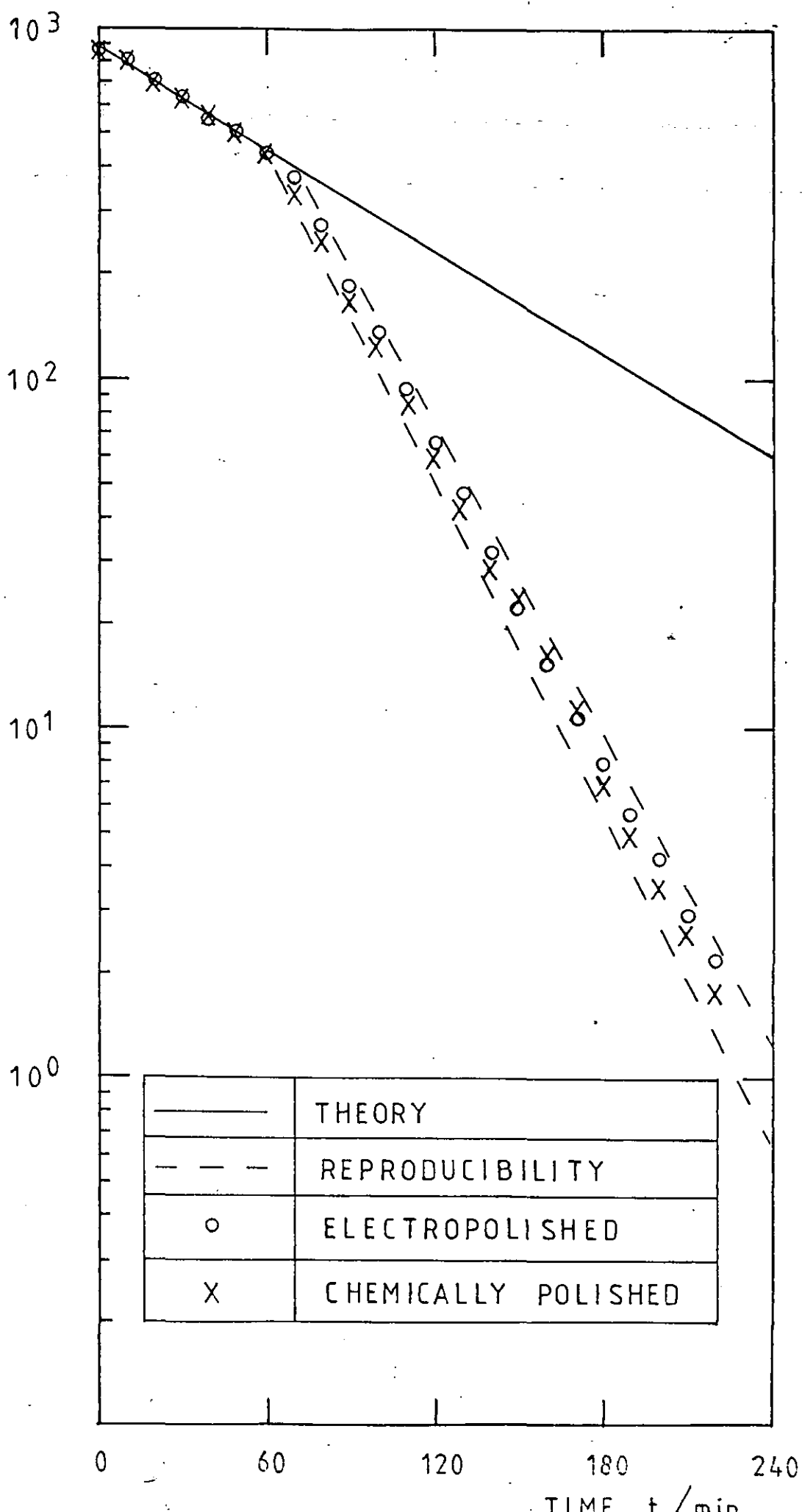
FIG. 10.18 CURRENT DECAY IN A BATCH R.C.E.R., corresponding
to the concentration decay of Fig. 10.16
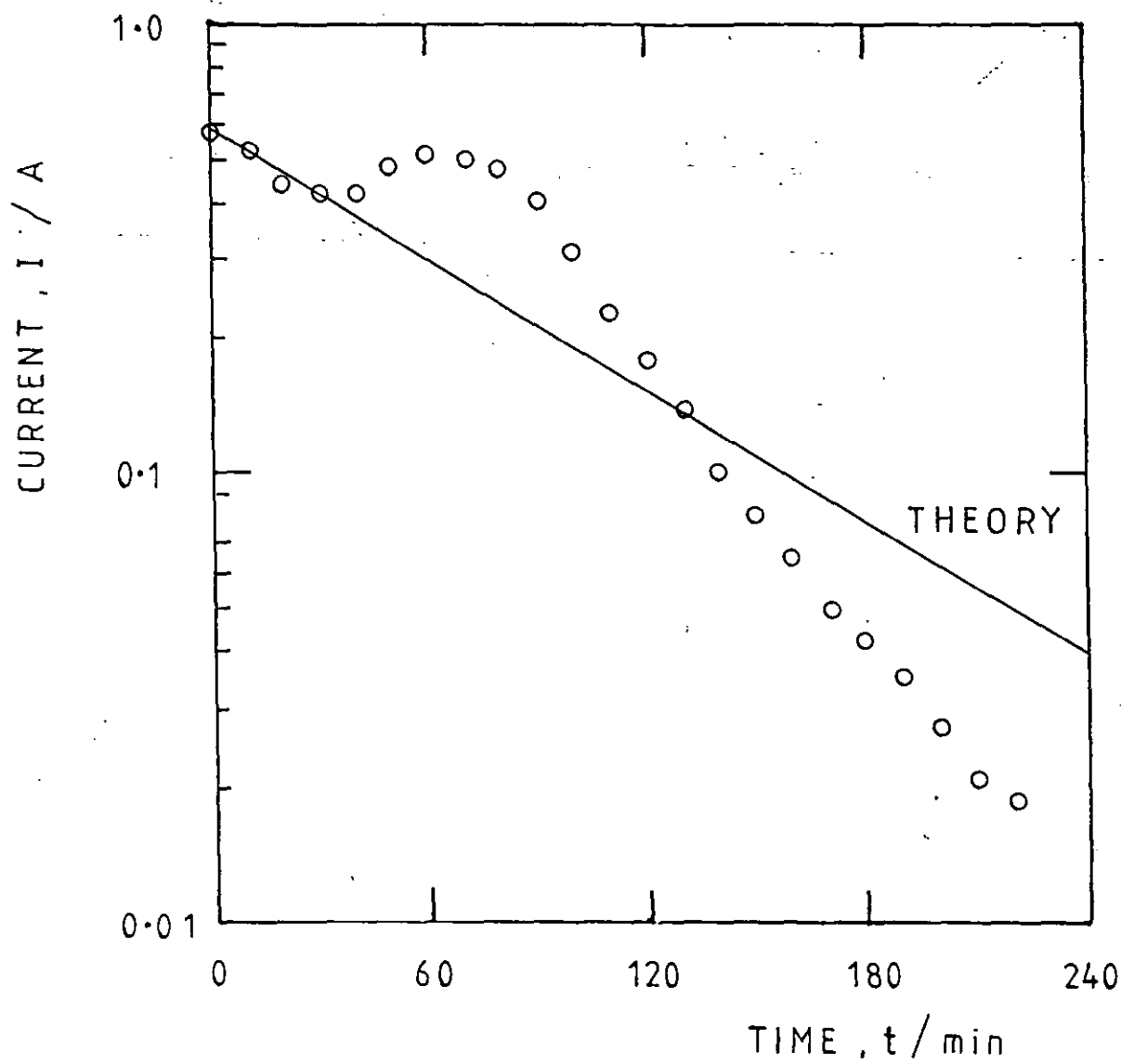
FIG. 10.19   CURRENT AS A FUNCTION OF CONCENTRATION DURING A

             BATCH R.C.E.R. DECAY, corresponding to Figs.

             10.16 and 10.18

     showing the theoretical line expected from a smooth electrode
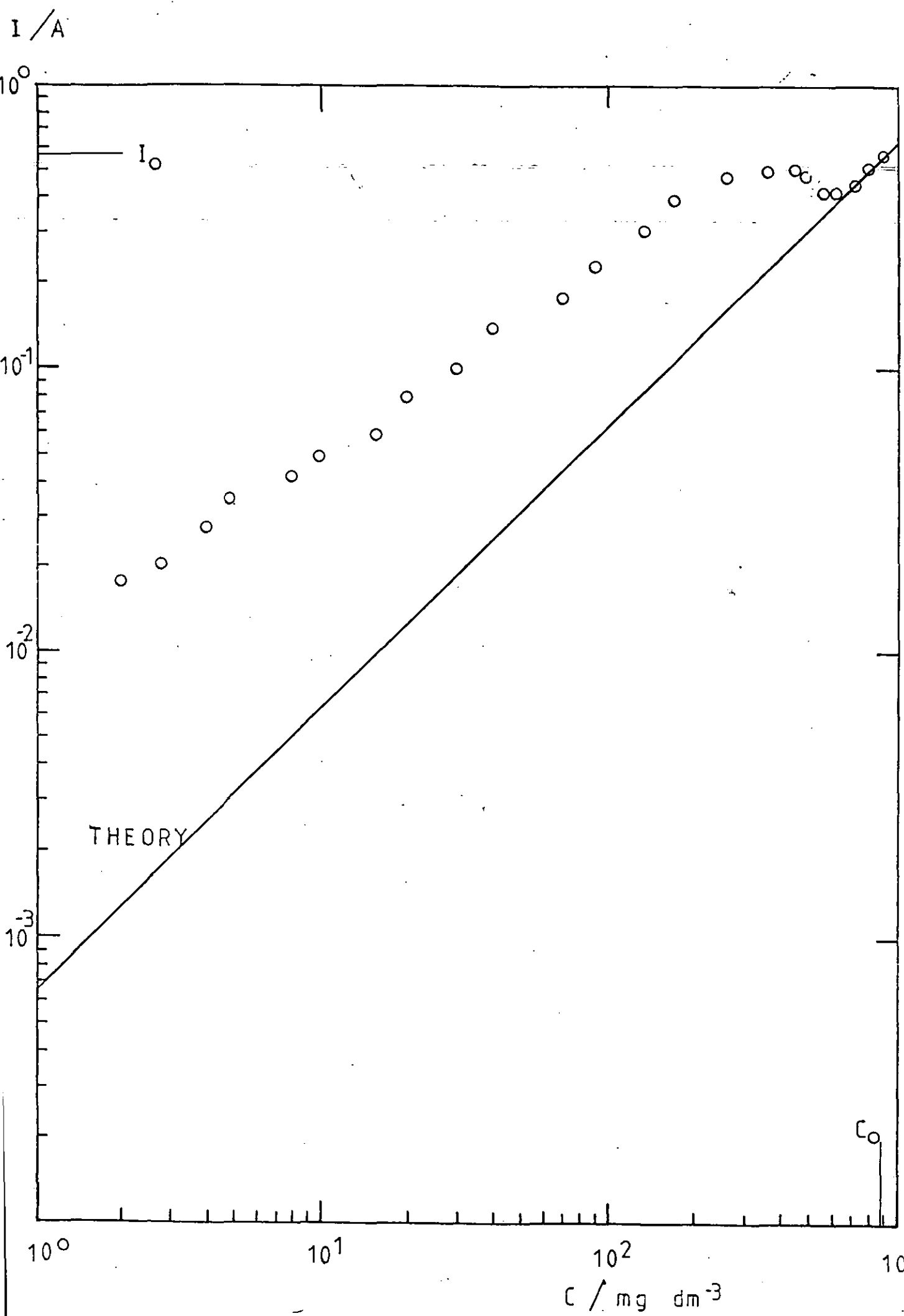
FIG. 10.20 APPARENT MASS TRANSPORT COEFFICIENT AS A FUNCTION

OF TIME corresponding to Figs. 10.16 and 10.18

showing the calculated value for a smooth R.C.E.
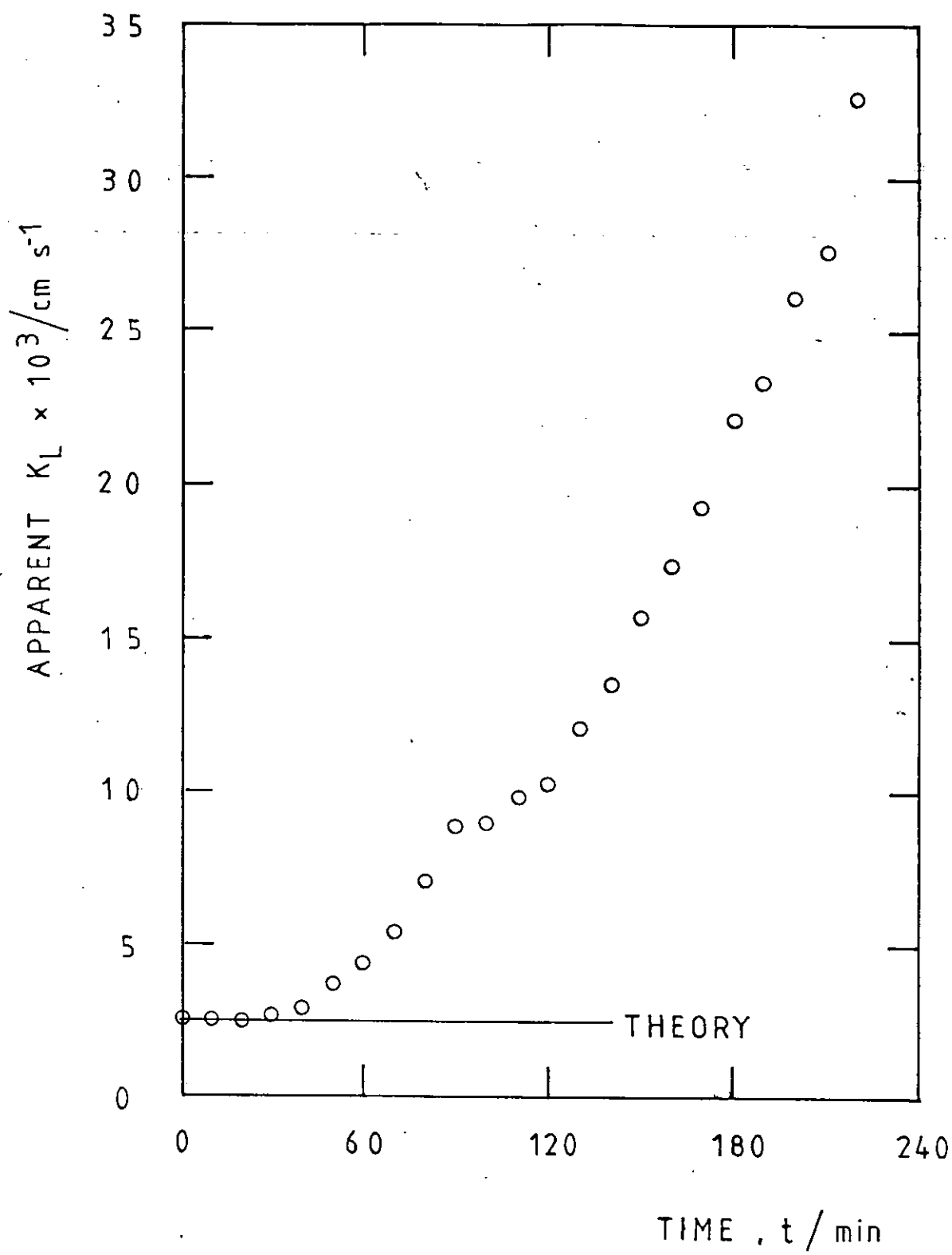
FIG. 10.21   CONCENTRATION CHANGE AS A FUNCTION OF CURRENT,

corresponding to Figs. 10.16 and 10.18

showing the theoretical line expected for a smooth R.C.E.
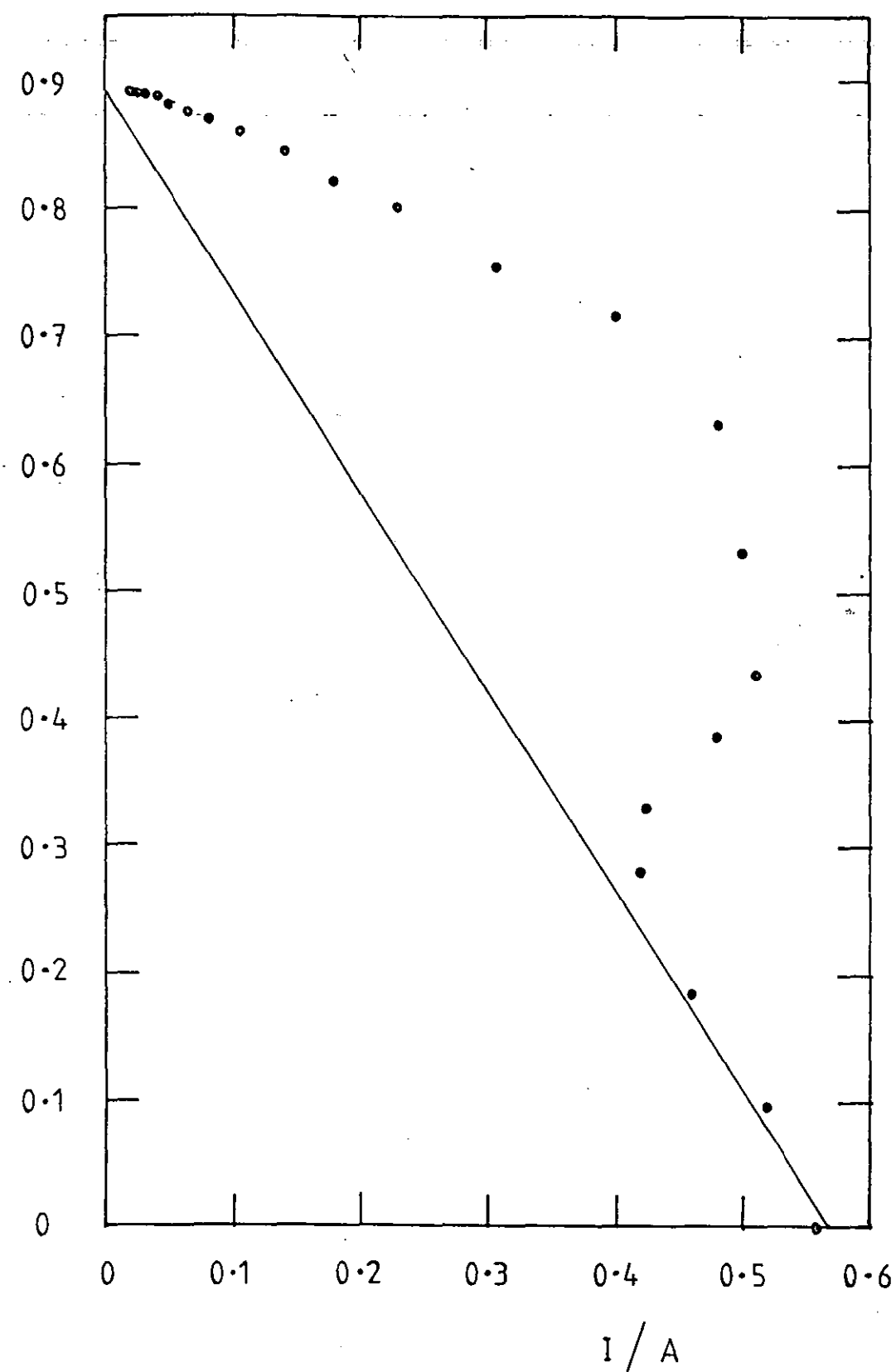
FIG. 10.22 CONCENTRATION DECAY IN A BATCH R.C.E.R., showing

the effect of cathode potential

conditions otherwise as for Fig. 10.16

some data points omitted for clarity.

cathode potentials are quoted w.r.t. M.M.S./1N Na_2SO_4

	E / mV
+	− 850
×	− 910
○	− 1000
△	− 1070
⊙	− 1150
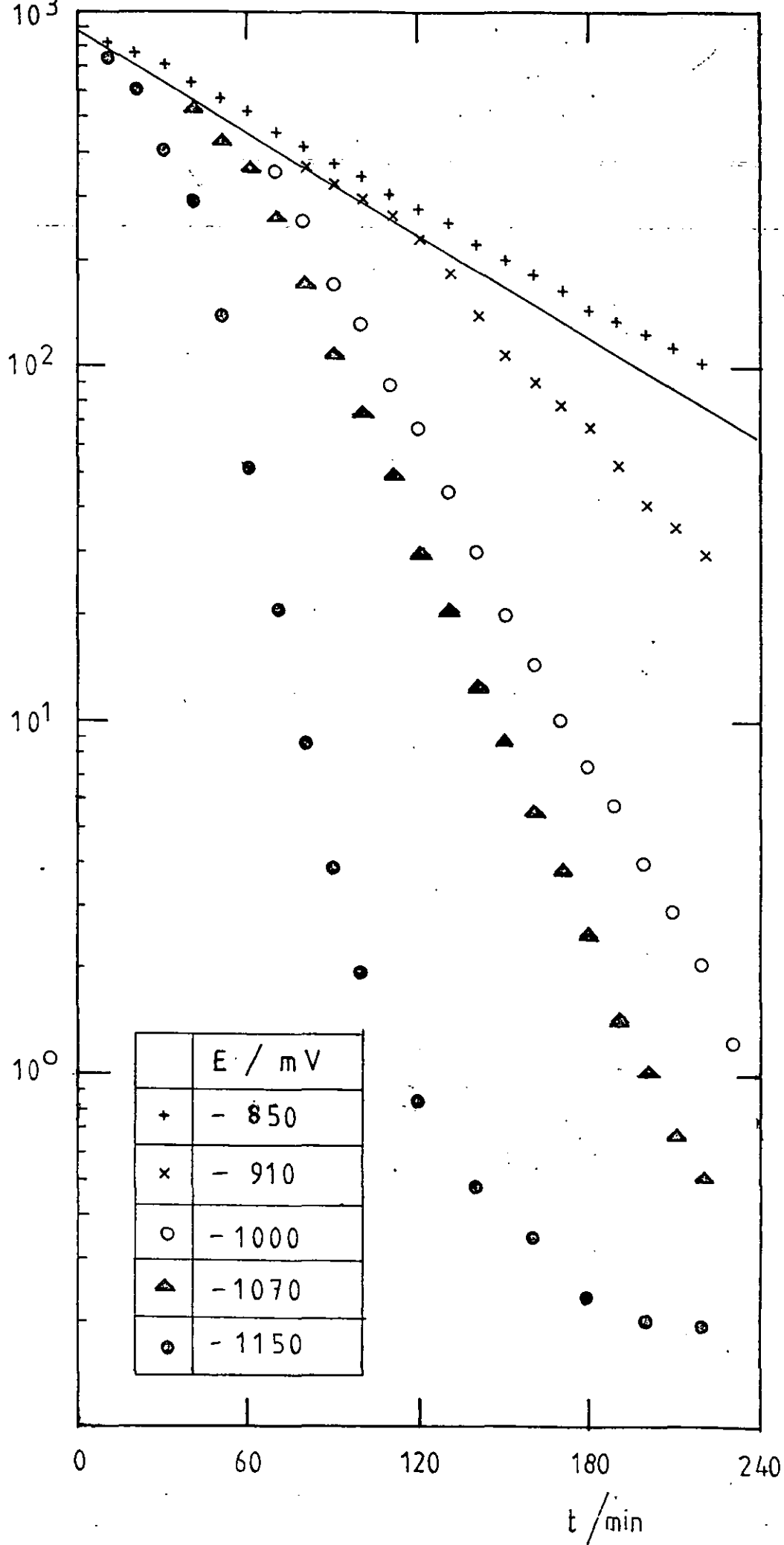
FIG. 10.23   CURRENT – TIME BEHAVIOUR IN A BATCH R.C.E.R.,

showing the effect of potential

corresponding to Fig. 10.22

	E / mV
+	- 8 5 0
×	- 9 1 0
○	- 1 0 0 0
△	- 1 0 7 0
⊙	- 1 1 5 0

I / A

10

1

0·1

0·01
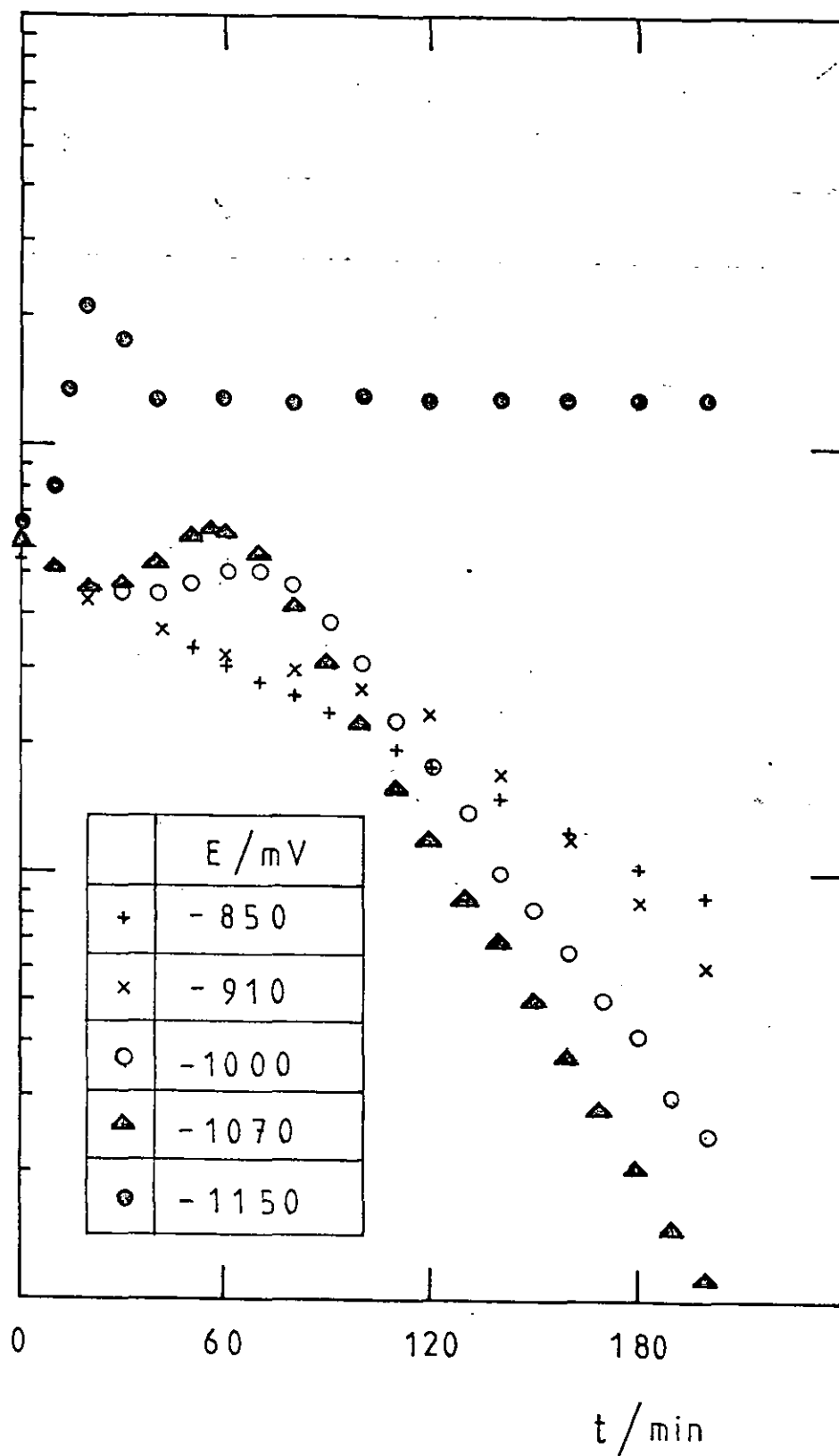
0   60   120   180

t / min

FIG. 10.24 CONCENTRATION DECAY IN A BATCH R.C.E.R., for an

initially rough (powdery) electrode

The electrode following a Fig. 10.16 trial was resubjected to
electrolysis under identical conditions
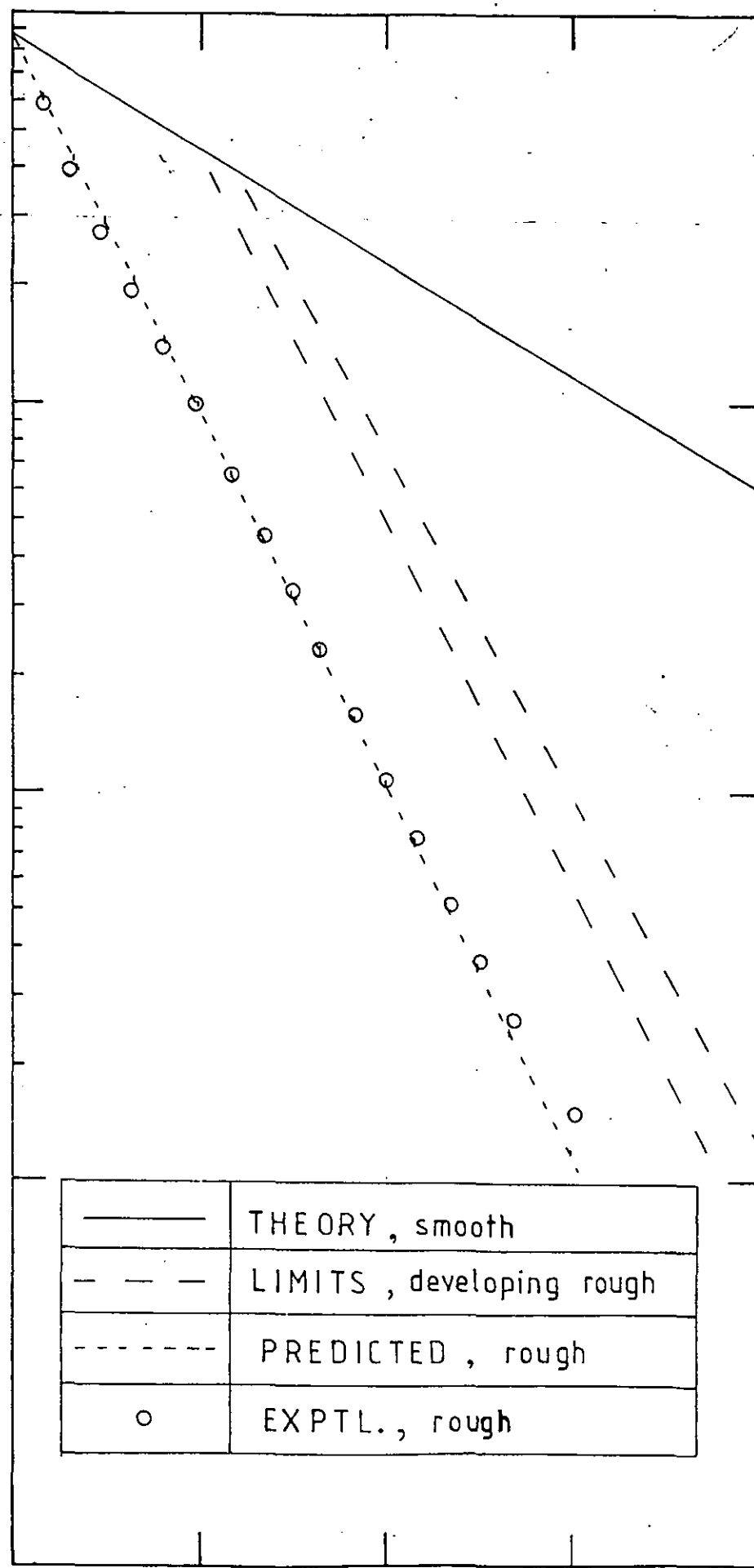
FIG. 10.25 CONCENTRATION DECAY IN A BATCH R.C.E.R., showing

the effect of rotational speed

conditions otherwise as for Fig. 10.16
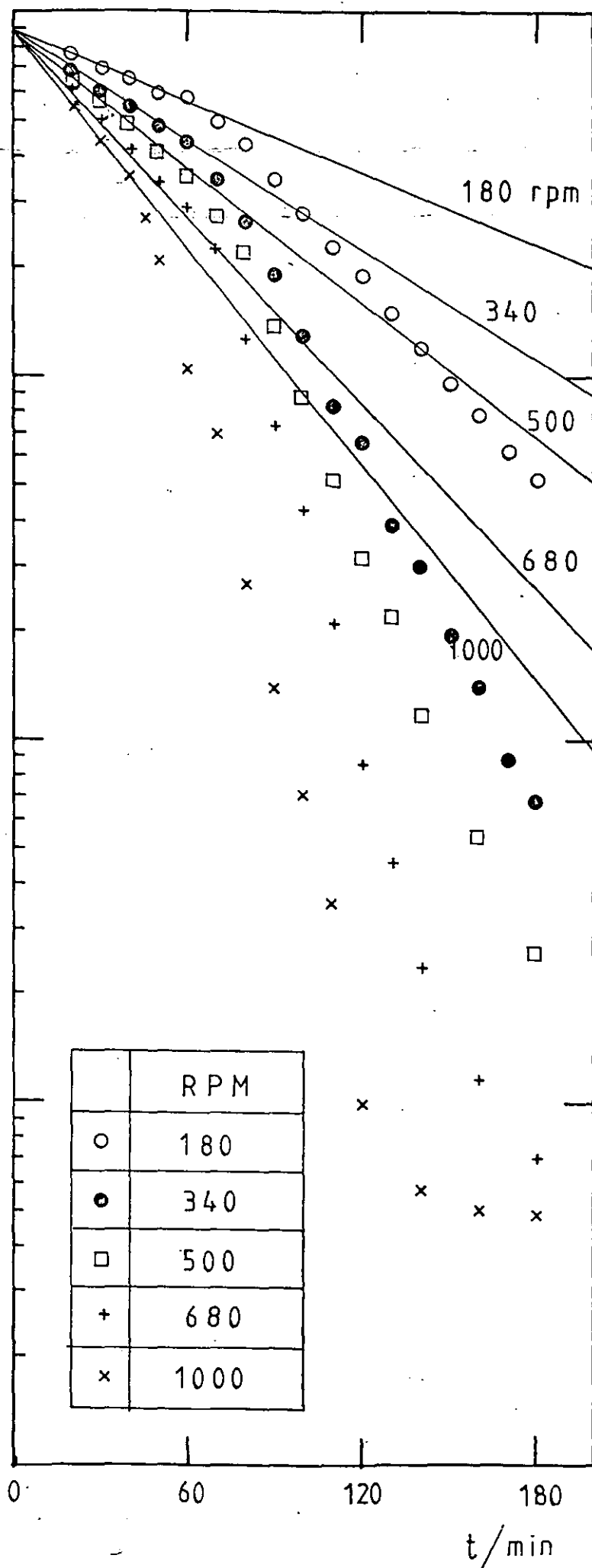
FIG. 10.25 a   APPARENT RATE CONSTANT AS A FUNCTION OF ROTATIONAL

SPEED, corresponding to Fig. 10.24

log - log plot, showing the apparent dependence of the rate constant

on the rotational speed for the initial (smooth) and final (rough)

slopes of Fig. 10.24

APPARENT RATE CONSTANT, $k \ /\mathrm{s}^{-1}$

ROUGH

SMOOTH

ROTATIONAL SPEED, ω / rev min^{-1}
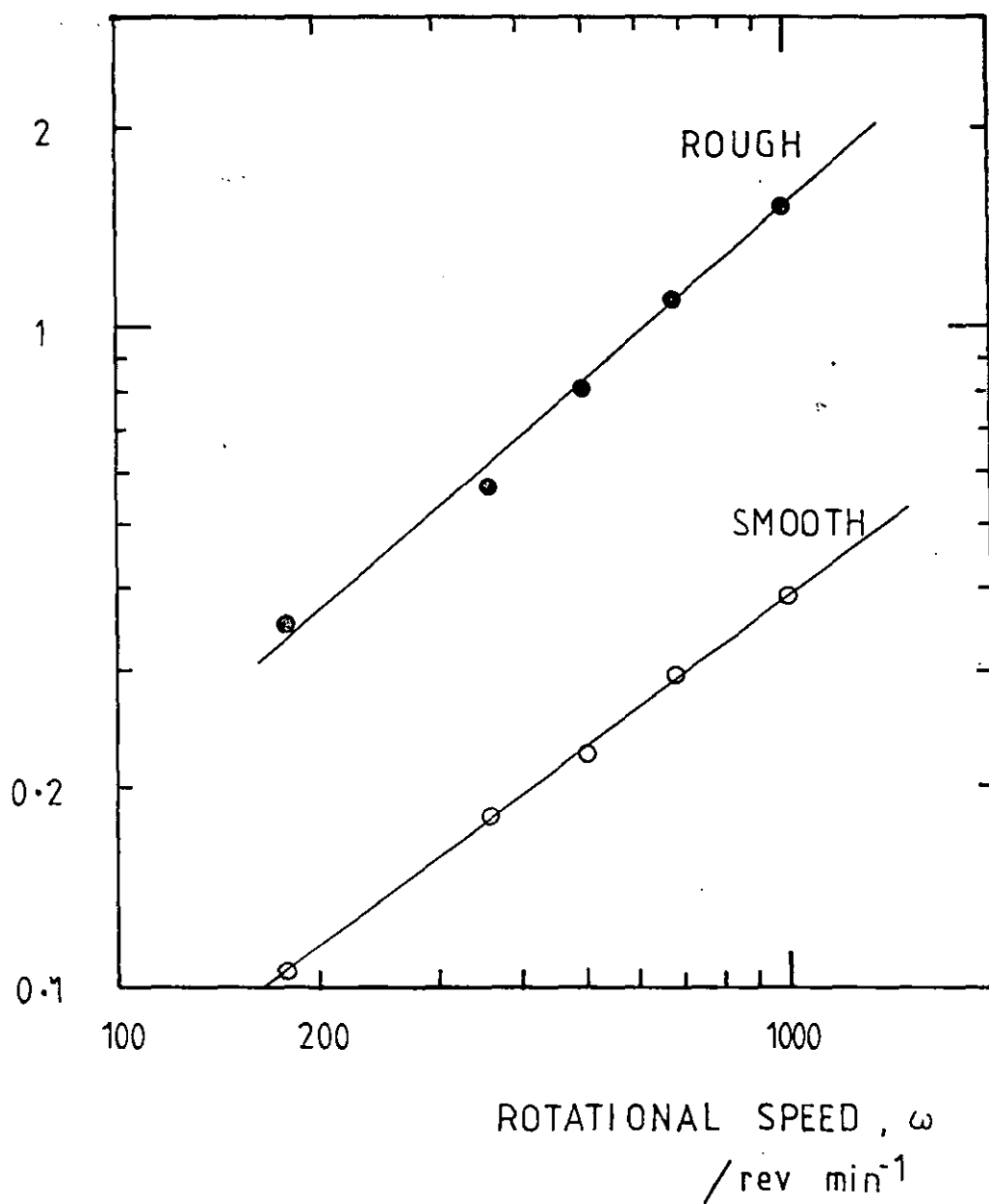
FIG. 10.26   CONCENTRATION DECAY FOR THE (SELECTIVE) DEPOSITION

OF COPPER FROM A Cu/Zn SOLUTION

Potentiostatic control at 2 different potentials

0.014 M $CuSO_4$

0.014 M $ZnSO_4$

1.5 M H_2SO_4

22° C

d = 6.3 cm

l = 4.3 cm

A = 85.1 cm^2

rpm = 340

U = 112 cm s^{-1}

V = 1000 cm^3
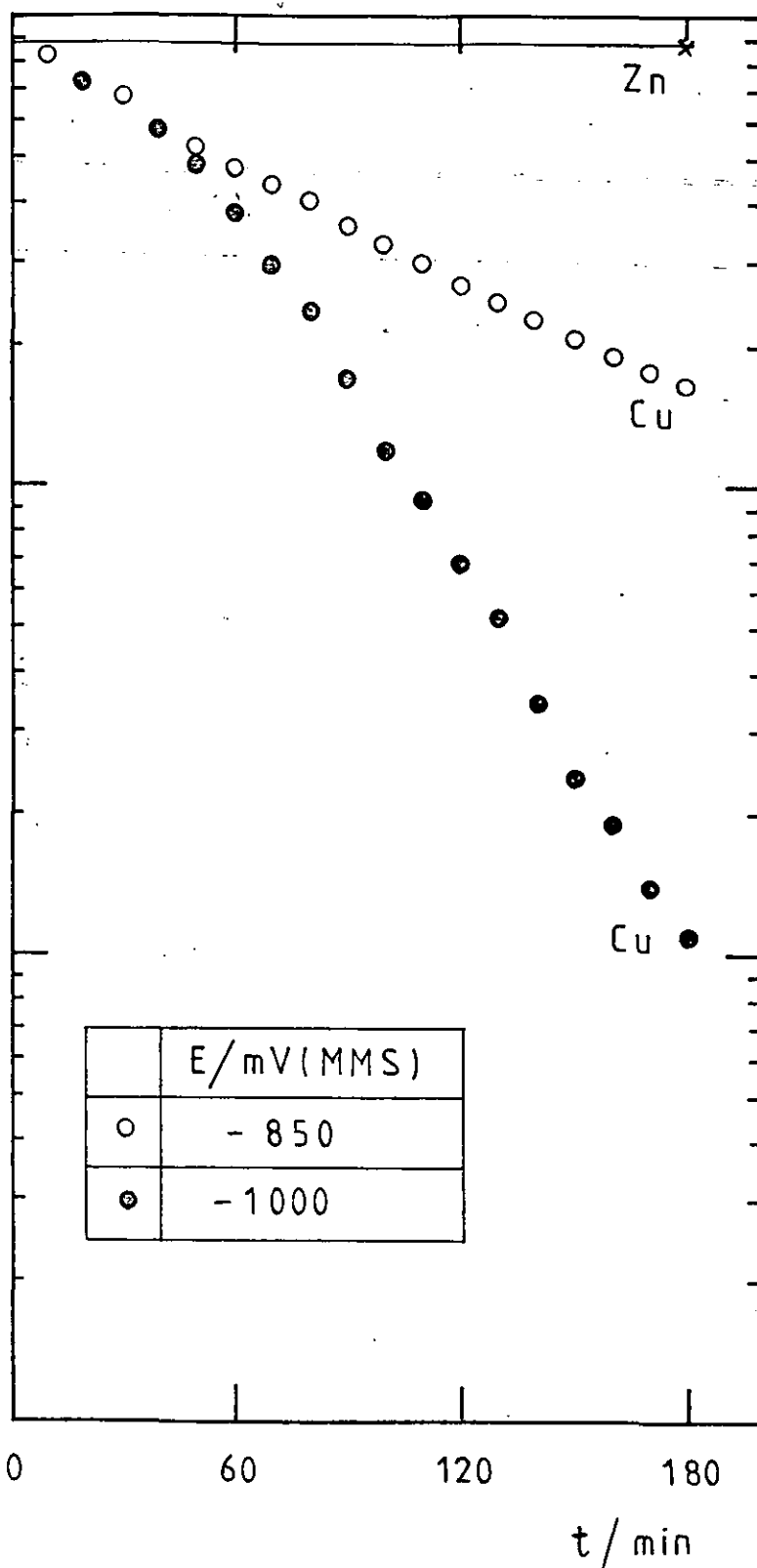
FIG. 10.27   CATHODIC POLARISATION CURVE IN A SOLUTION CONTAINING

COPPER AND ZINC SULPHATE

Conditions as for Fig. 10.26

Linear Sweep Rate = 150 mV $(\text{min})^{-1}$

indicating the control potentials used in Fig. 10.26

E/V(MMS)

Cu²⁺+2e⁻ = Cu

Iₗ

I /A
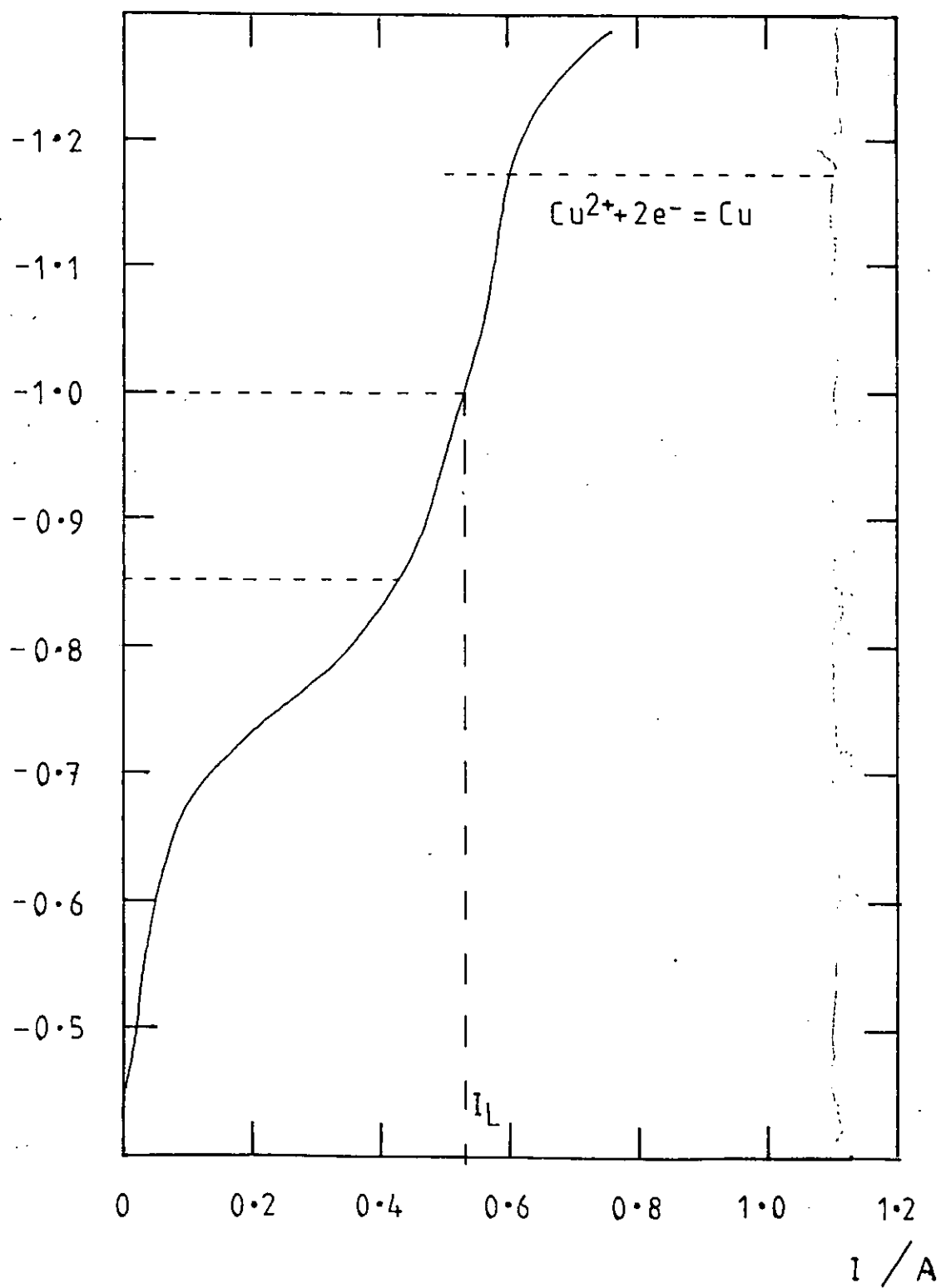
FIG. 10.28   CONCENTRATION DECAY FOR THE (SELECTIVE) DEPOSITION

OF COPPER FROM A Cu/Ni SOLUTION

Potentiostatic control at 2 different potentials

0.014 M $CuSO_4$

0.014 M $NiSO_4$

1.5 M H_2SO_4

other conditions as Fig. 10.27

$V = 1000$ cm^3
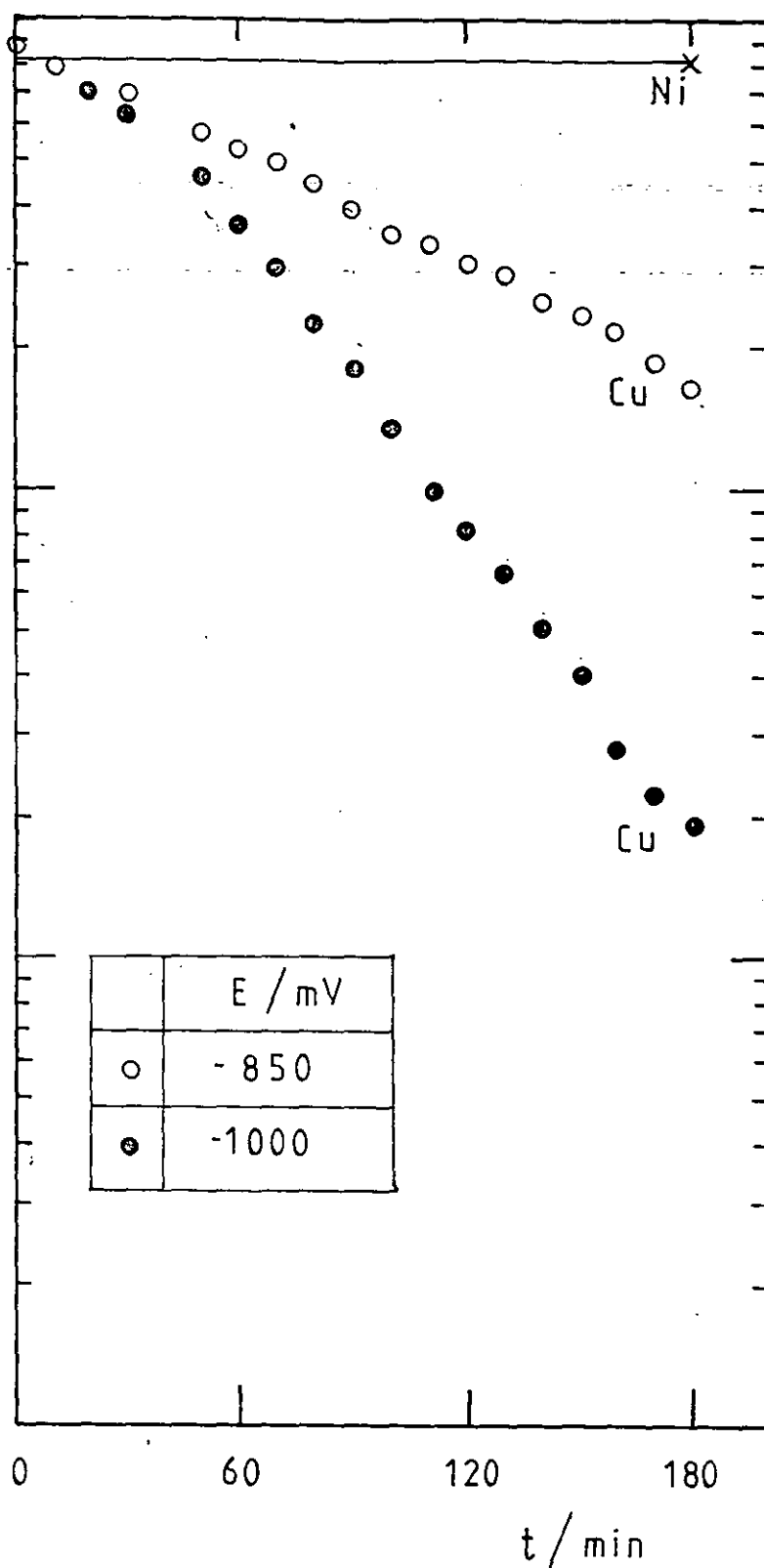
FIG. 10.29   CATHODIC POLARISATION CURVE IN A SOLUTION

CONTAINING COPPER AND NICKEL SULPHATES

Conditions as for Fig. 10.28

Linear Sweep Rate = 150 mV $(min)^{-1}$

indicating the control potentials used in Fig. 10.28
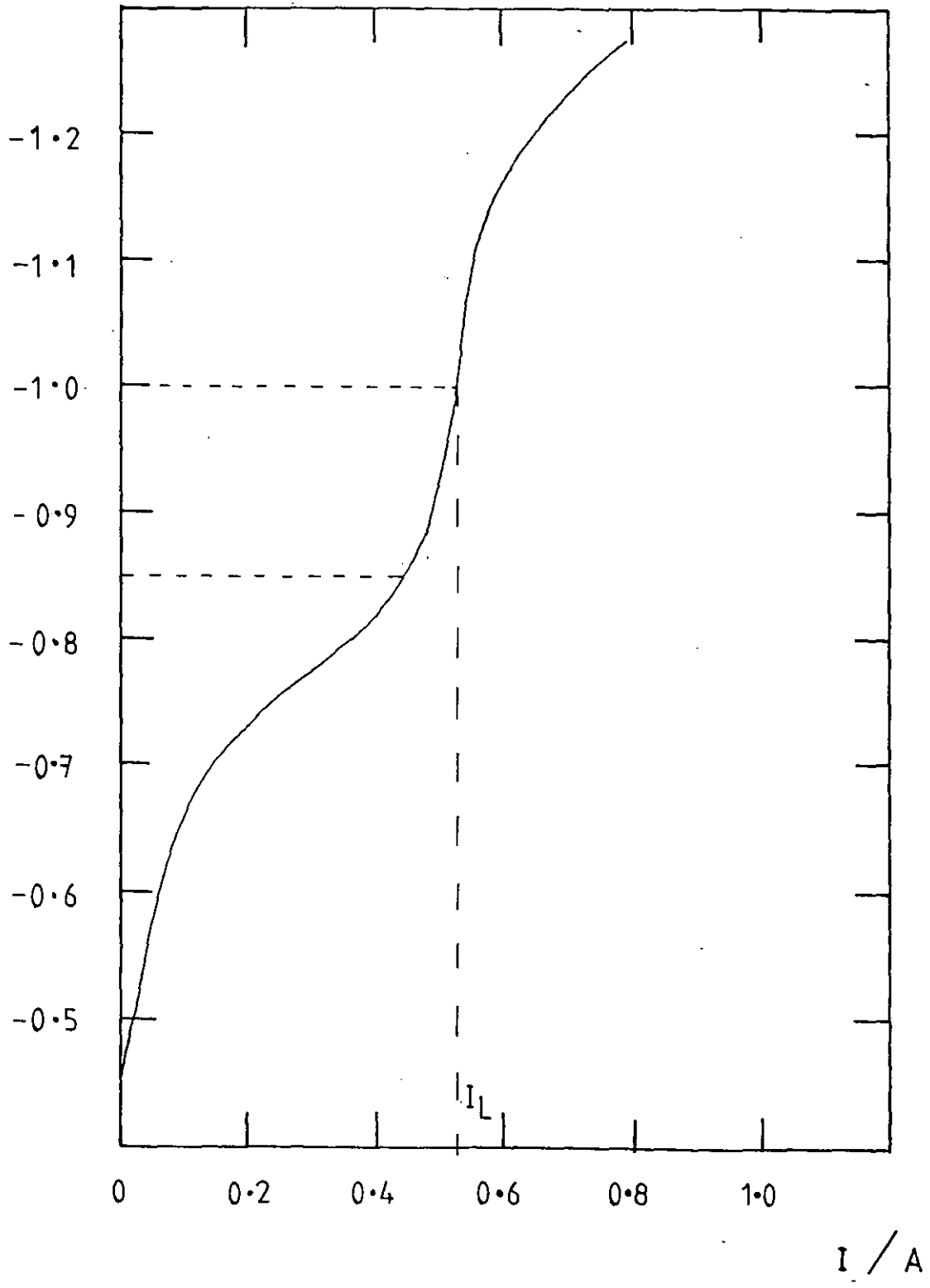
FIG. 10.30   INDIVIDUAL POLARISATION CURVES FOR COPPER AND SILVER

DEPOSITION IN NITRIC ACID SOLUTION

0.014 M $Cu(NO_3)_2$)
)
0.15 M HNO_3)

and

0.014 M $AgNO_3$.   )
)
0.015 M HNO_3)

22° C

d = 6.3 cm

l = 4.3 cm

rpm = 340

U = 112 cm s^{-1}

linear sweep rate = 150 mV $(min)^{-1}$
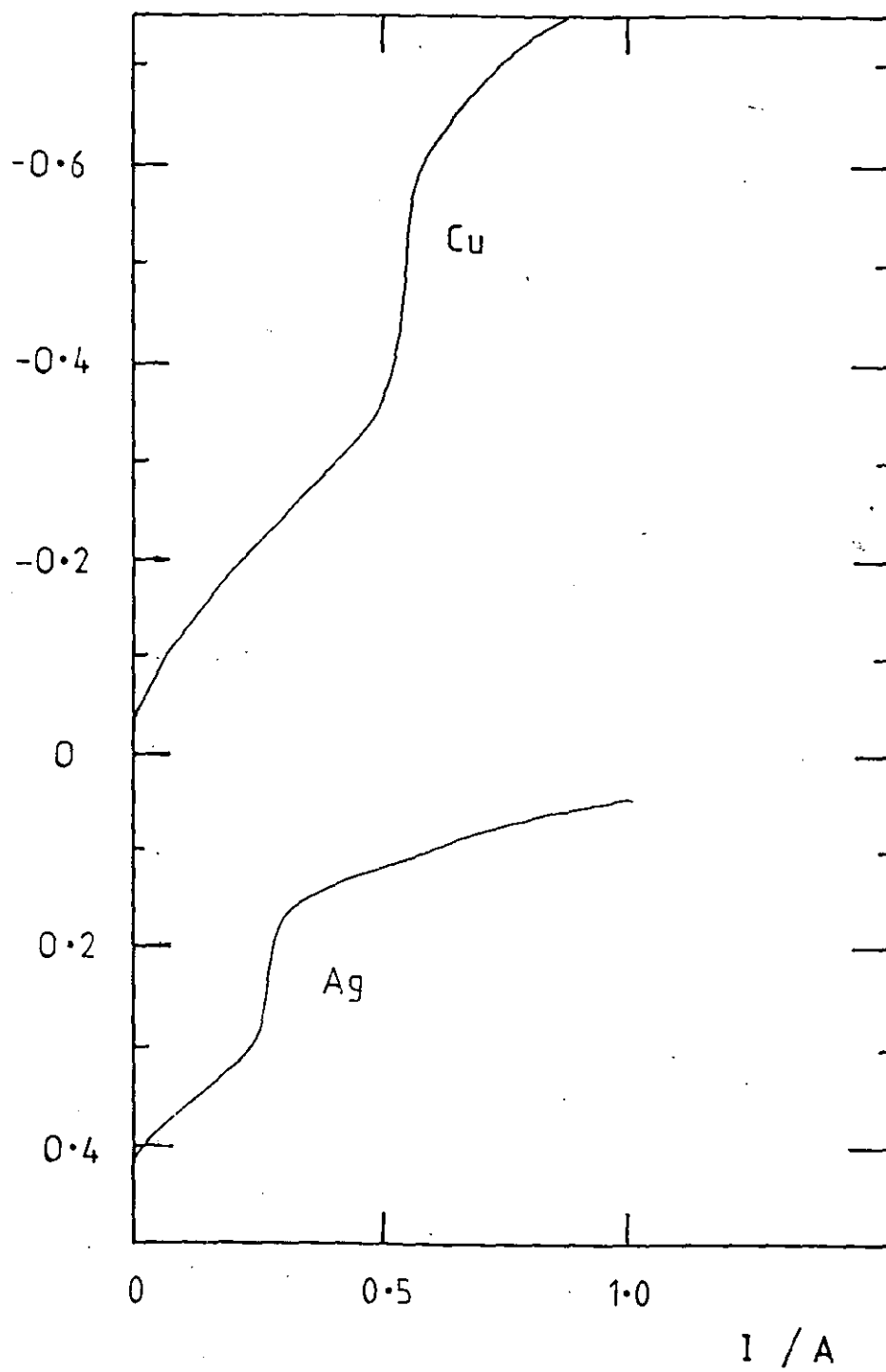
FIG. 10.31   CONCENTRATION DECAY FOR THE (SELECTIVE) DEPOSITION

OF SILVER FROM Ag/Cu SOLUTION

Potentiostatic control at a silver overpotential of - 180 mV

Conditions as for Fig. 10.30

$V = 1000 \text{ cm}^3$

Solution composition as Table 10.5 stainless steel R.C.E.

20° C

d = 6.0 cm

l = 4.5 cm

A = 85.1 cm^2

rpm = 500
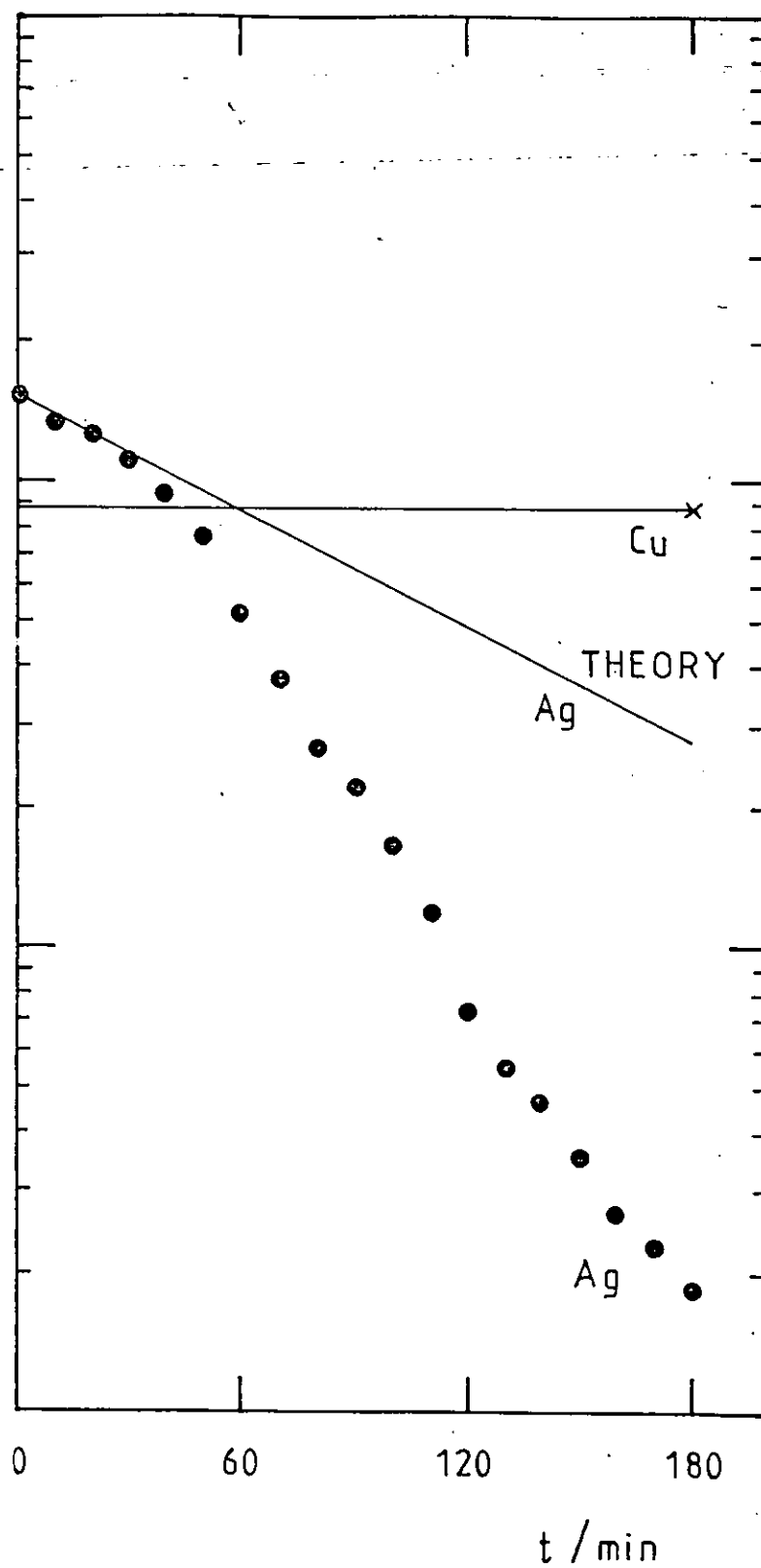
U = 157 cm s^{-1}

linear sweep rate 150 mV $(min)^{-1}$
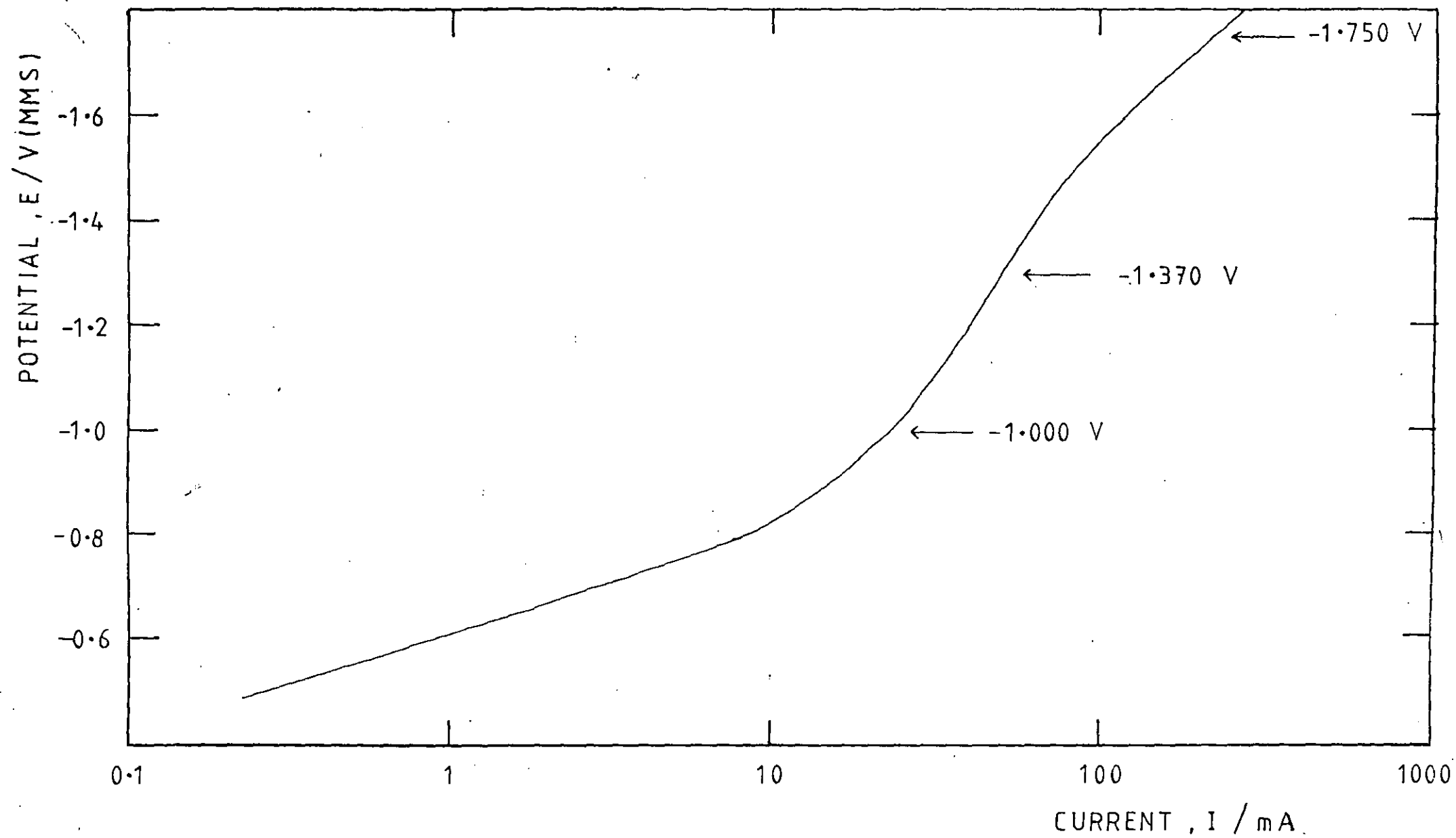
FIG. 10.33   CONCENTRATION DECAY FOR A CYANIDIC DRAGOUT

SOLUTION, showing the effect of cathode potential

Conditions as for Fig. 10.32; undivided reactor, stainless steel

anode

$V = 1000 \text{ cm}^3$

smooth deposits in all cases
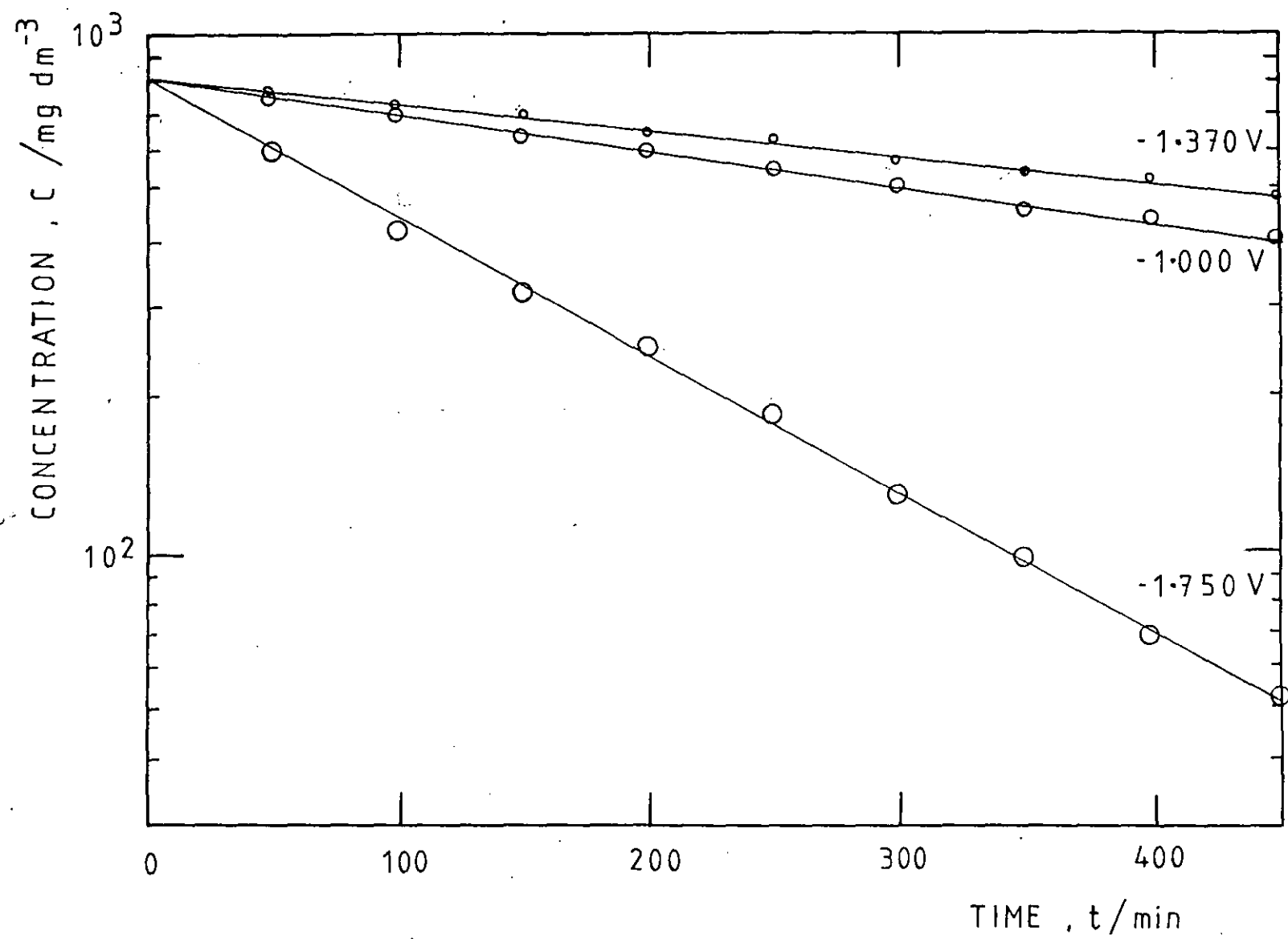
FIG. 10.34   CURRENT - TIME BEHAVIOUR FOR CONCENTRATION DECAY

OF A GOLD CYANIDE SOLUTION

Corresponding to Fig. 10.33
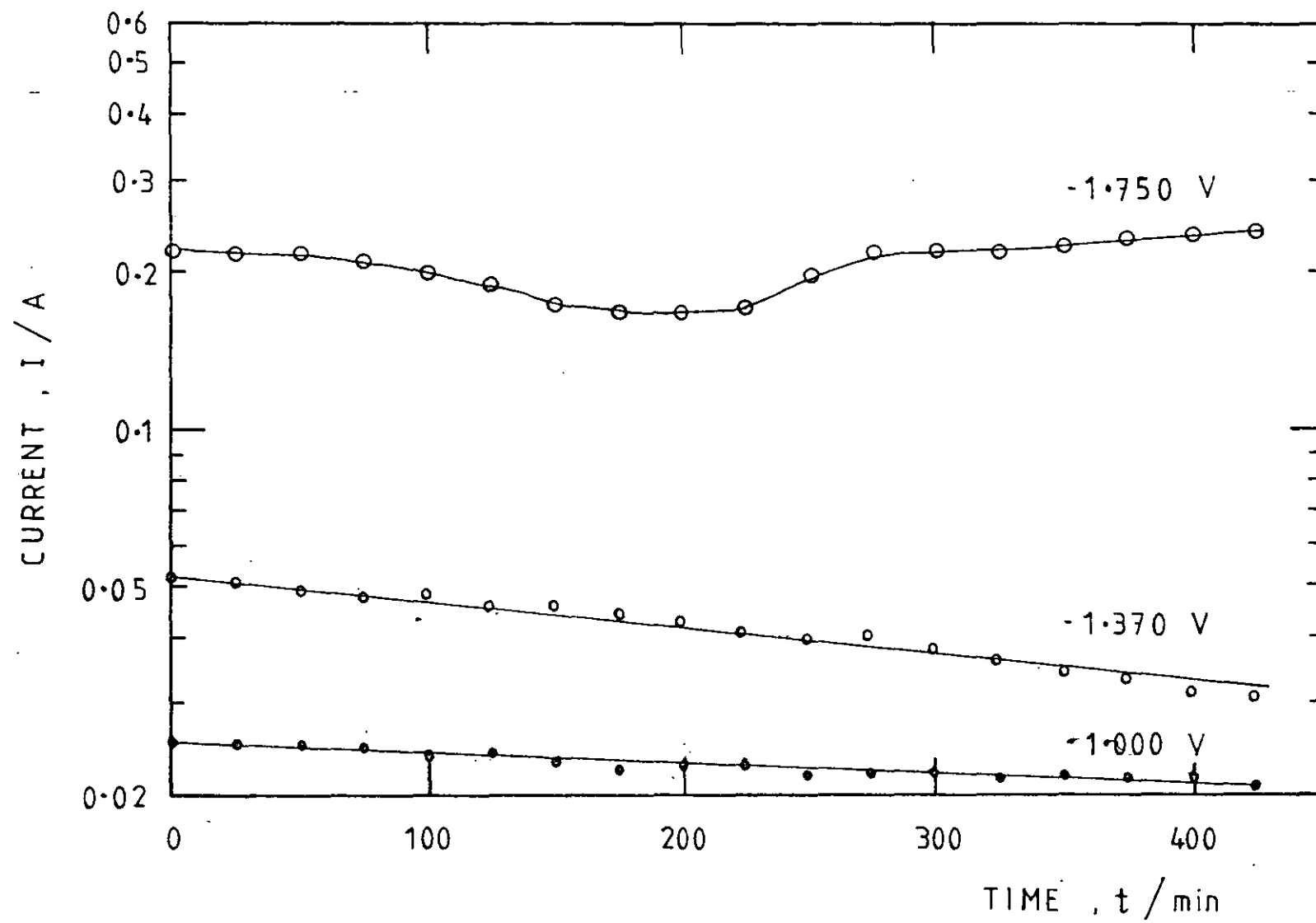
FIG. 10.35   CATHODIC POLARISATION CURVES FOR METAL DEPOSITION

IN A CYANIDIC EFFLUENT SOLUTION

Showing the effect of pH.Compositions are shown in Table 10.6

d = 6.0 cm

l = 4.3 cm

$A = 85 \text{ cm}^2$

rpm = 500

$U = 157 \text{ cm s}^{-1}$

linear sweep rate = $150 \text{ mV (min)}^{-1}$

The control potentials used in the potentiostatic electrolyses of

Figs. 10.36 - 10.38 are shown

FIG. 10.36   CONCENTRATION DECAY IN A MIXED METAL,

CYANIDIC EFFLUENT SOLUTION

Potentiostatic control at -0.550 V (M.M.S.) in a divided cell

pH = 4.0

Conditions as for Fig. 10.35

$V = 1000 \text{ cm}^3$
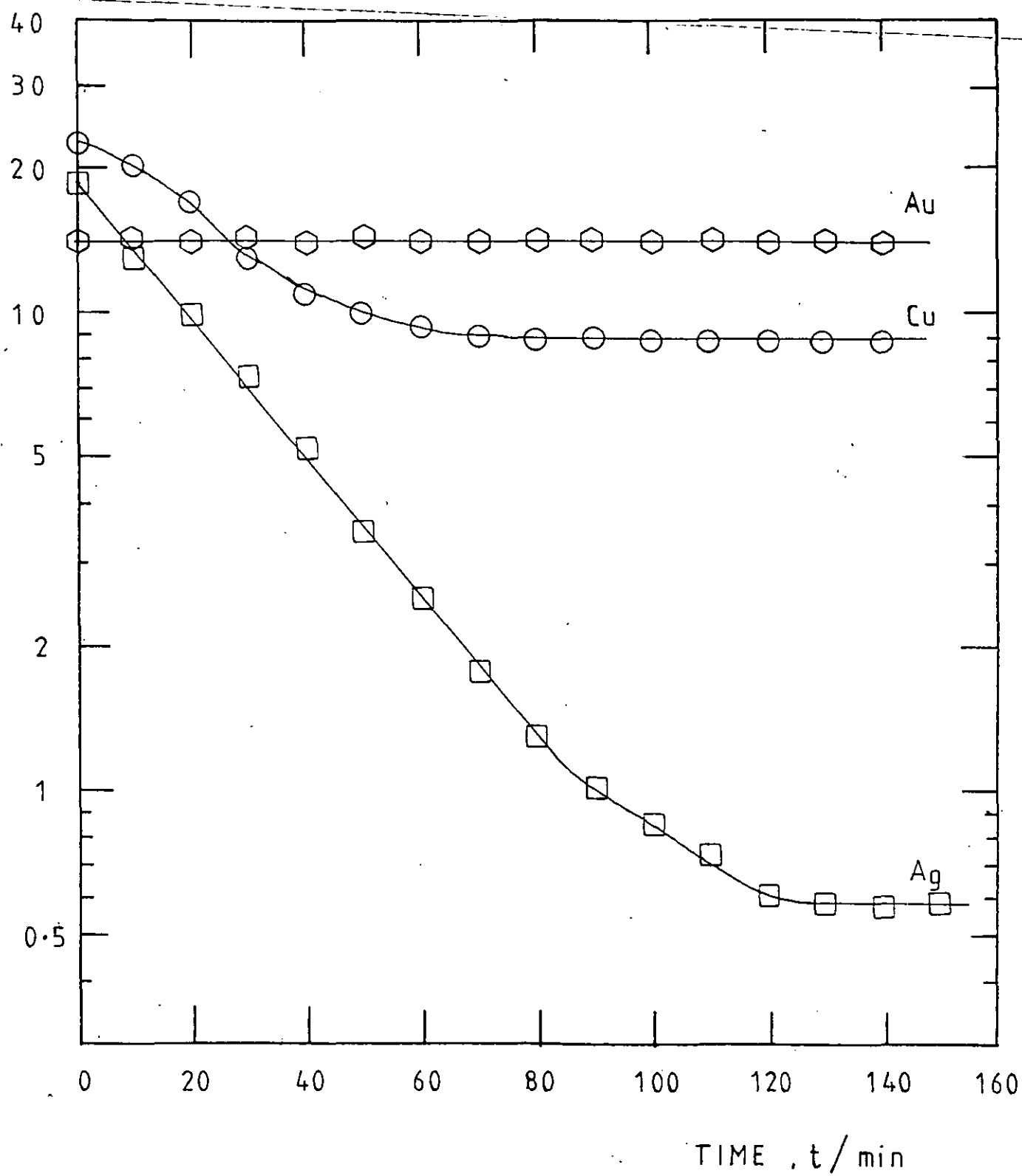
FIG. 10.37   CONCENTRATION DECAY IN A MIXED METAL,

CYANIDIC EFFLUENT SOLUTION

As for Fig. 10.36, but using an undivided cell
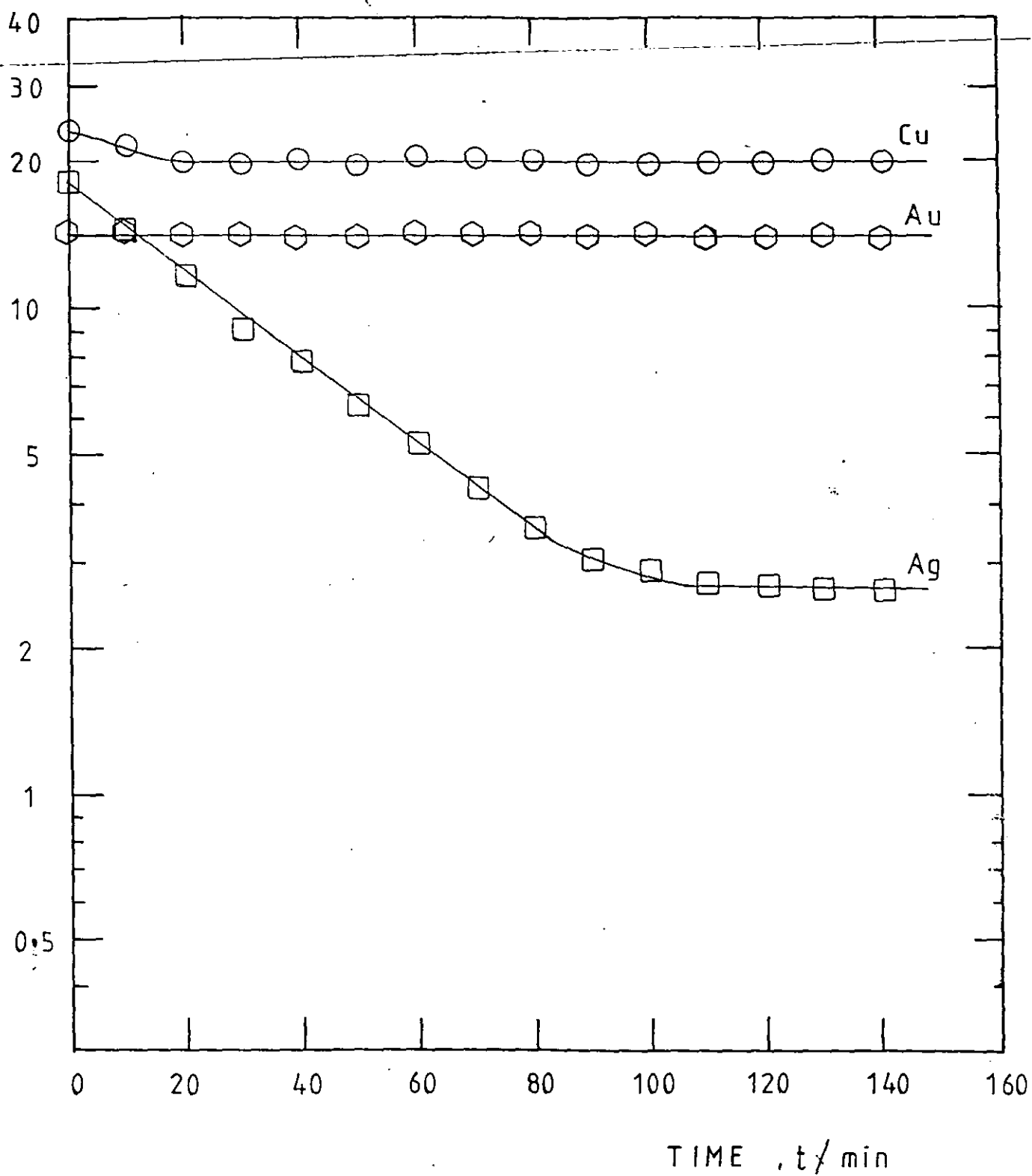
FIG. 10.38   CONCENTRATION DECAY IN A MIXED METAL,

CYANIDIC EFFLUENT SOLUTION

Conditions as for Fig. 10.37, but using a control potential of

-0.900 V (M.M.S.) and the solution following Fig. 10.37
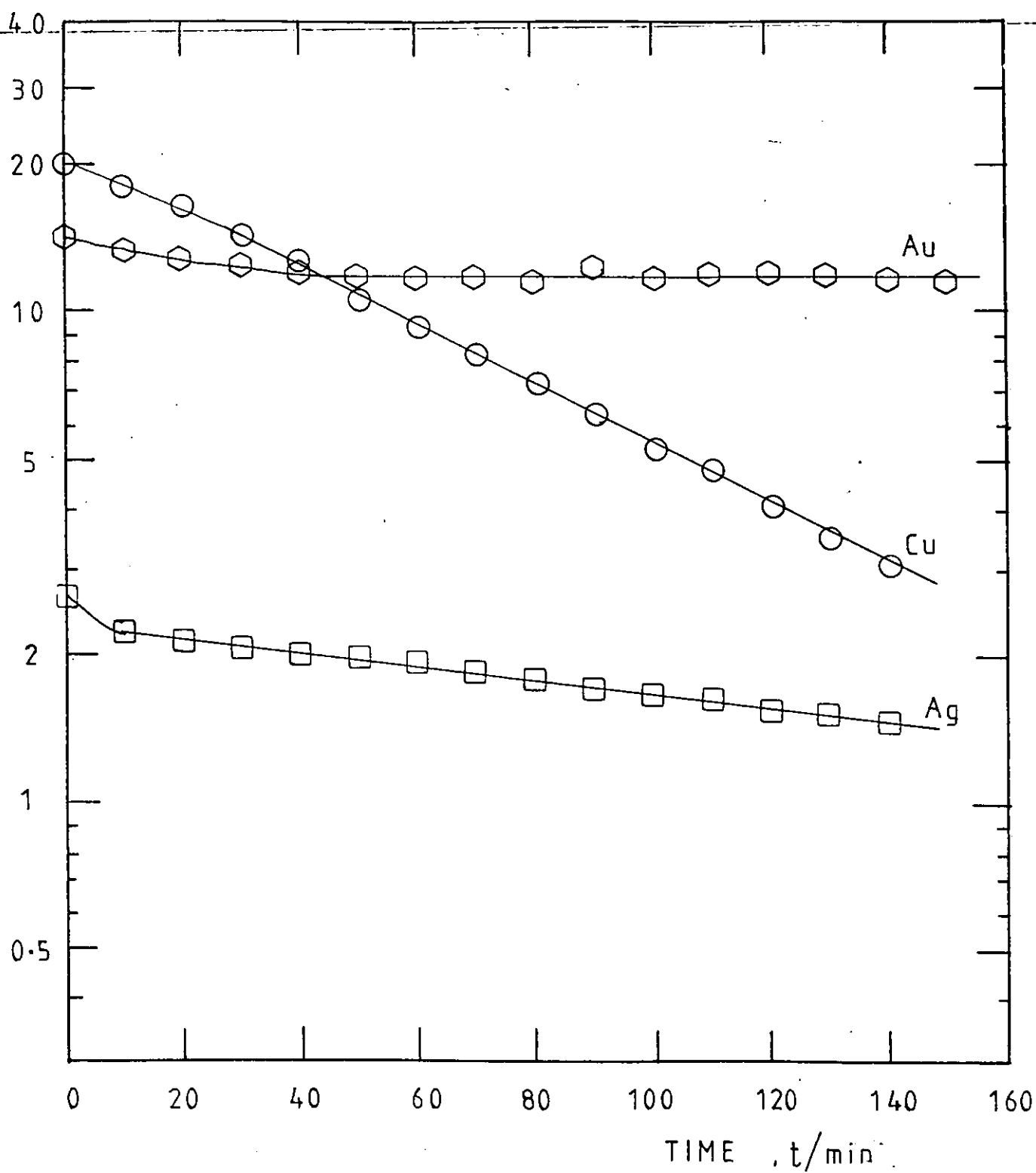
FIG. 10.39   CURRENT—TIME HISTORY FOR GROWTH OF ROUGH COPPER

DEPOSITS showing the effect of rotational velocity

Potentiostatic control at - 1.000 V (M.M.S.) corresponding to
limiting current conditions

0.014 M $CuSO_4$

1.5 M H_2SO_4

22° C

d = 6.3 cm

l = 4.3 cm

A = 85.1 cm^2

rpm = 180 to 1230

U = 59.4 - 405.7 cm s^{-1}

typical, average curves shown

(LIMITING)
CURRENT
I_L /A
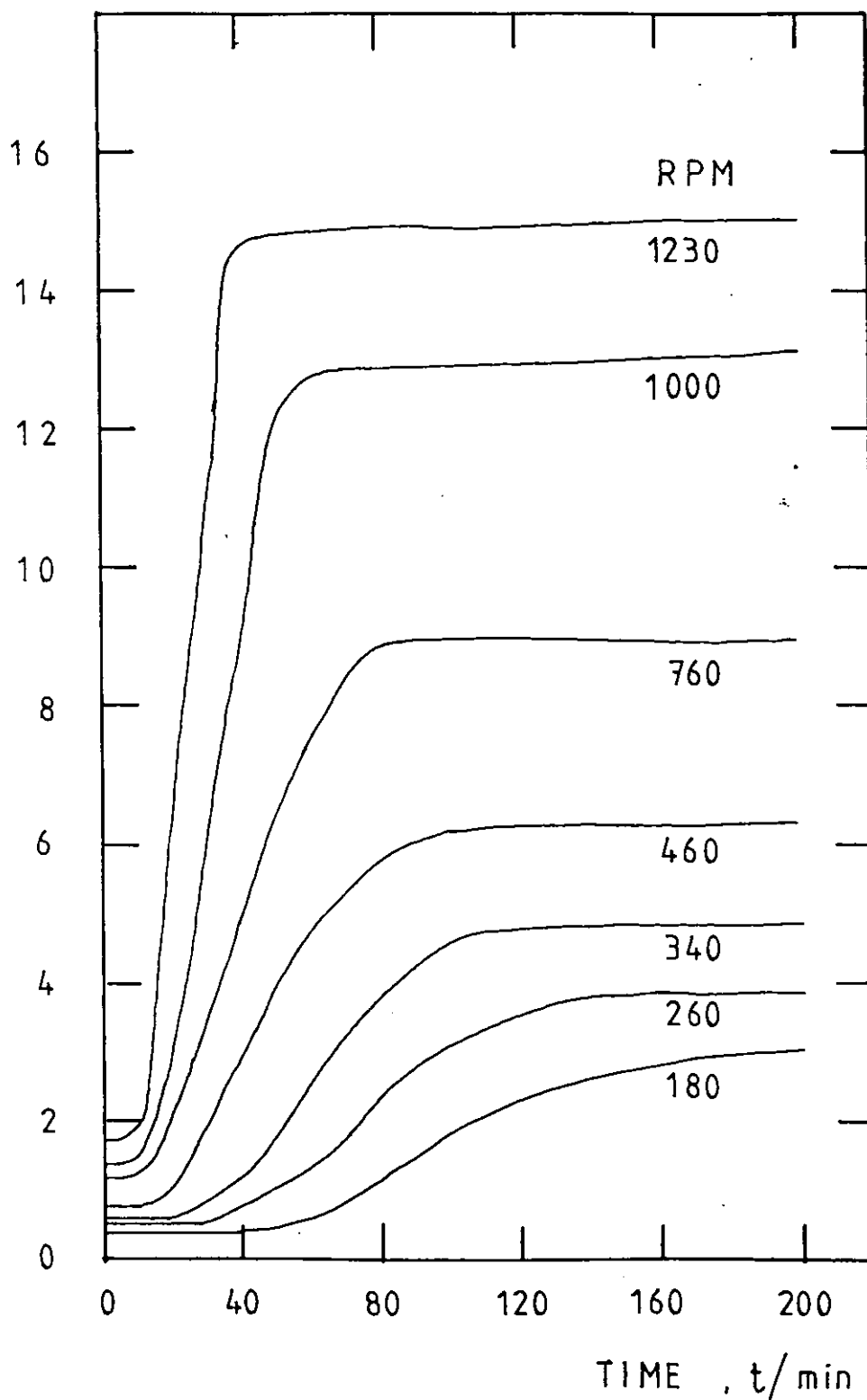
16

14

12

10

8

6

4

2

0

RPM

1230

1000

760

460

340

260

180

0   40   80   120   160   200

TIME , t/ min

As for Fig. 10.39, showing as hatched areas the limits for
reproducibility for several rotational velocities. 5 trials
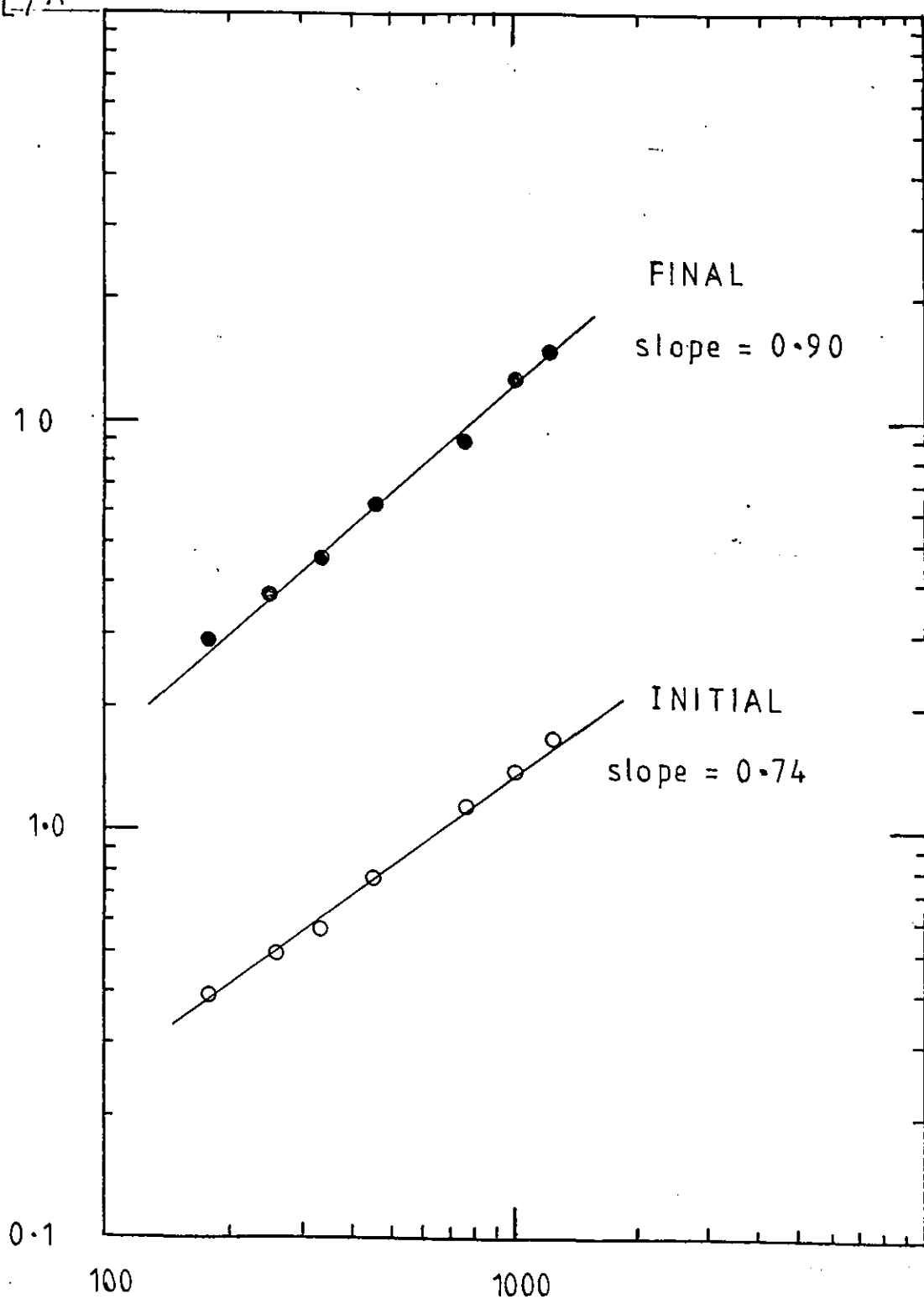were performed for each curve.
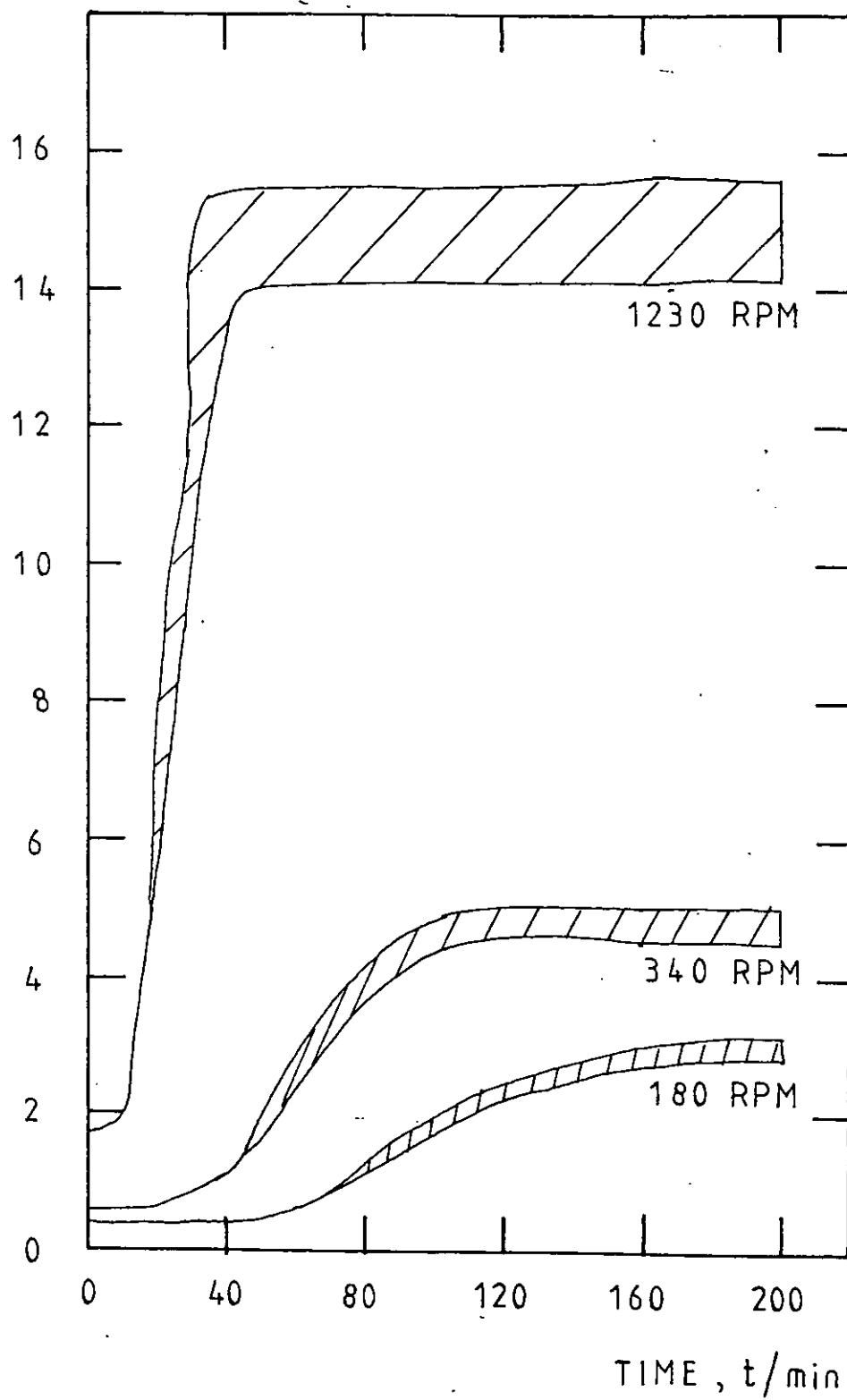
FIG. 10.41   LIMITING CURRENT AS A FUNCTION OF ROTATIONAL

VELOCITY FOR SMOOTH AND ROUGHENED COPPER

DEPOSITS

Corresponding to the initial and final values of limiting current

at a given rotational velocity from Fig. 10.39

FIG. 10.42   CURRENT-TIME HISTORY FOR THE DEVELOPMENT OF

ROUGH COPPER DEPOSITS

showing the effect of electrode potential, under potentiostatic

conditions

0.014 M $CuSO_4$

1.5 M H_2SO_4

22 ^{0} C

d = 6.3 cm

l = 4.3 cm

A = 85.1 cm^2

rpm = 340

U = 112 cm s^{-1}

	E /V(MMS)
A	− 1·100
B	− 1·000
C	− 0·950
D	− 0·900
E	− 0·850
F	− 0·750
G	− 0·700
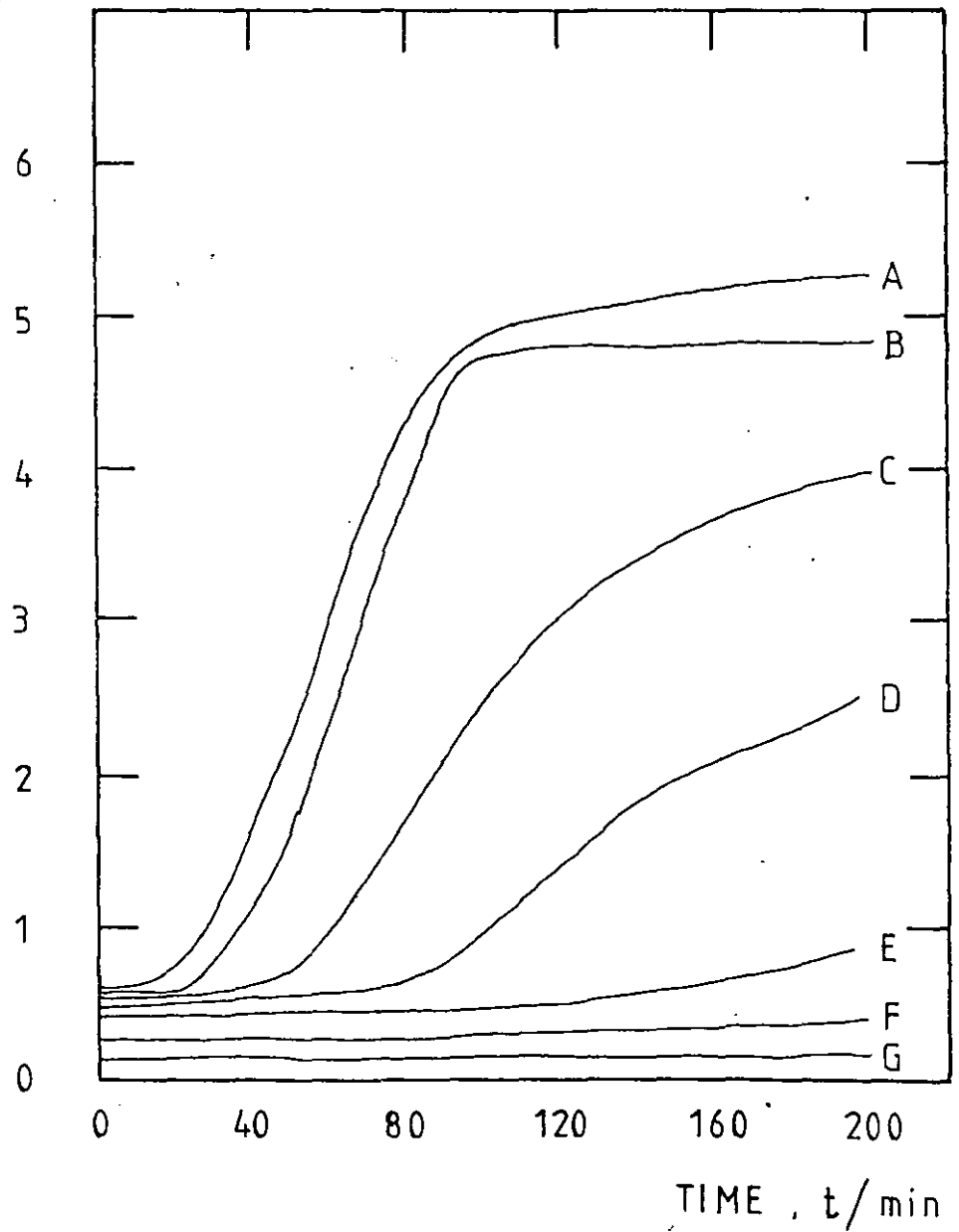
FIG. 10.43 AVERAGE ROUGHNESS AS A FUNCTION OF TIME FOR

GROWTH OF ROUGH DEPOSITS

Showing-the-effect-of-rotational-speed

Potentiostatic Growth of copper at - 1.000 V (M.M.S.)

0.014 M CuSO$_4$

1.5 M H$_2$SO$_4$

22 $^{\circ}$ C

d = 6.3 cm

l = 4.3 cm

A = 85.1 cm^2

rpm = 180 or 340

U = 59.4 or 112.1 cm s^{-1}

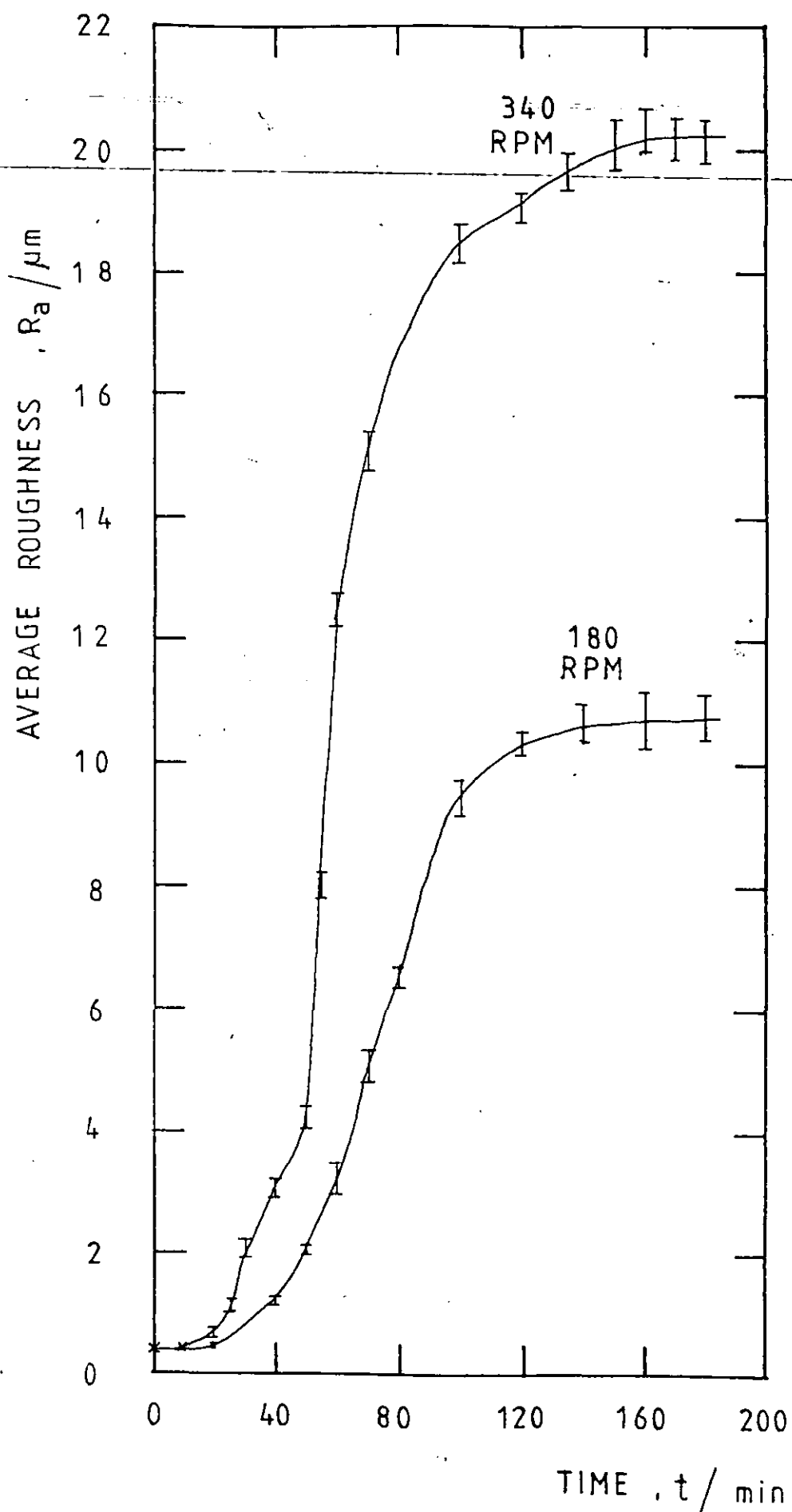The limits of variation in Profilometric R$_a$ value are shown

for each time.

FIG. 10.44   TYPICAL SURFACE PROFILOMETRIC TRACES FOR DEPOSITS

DEVELOPING ROUGHNESS

Showing the progressive development of roughness under potentiostatic
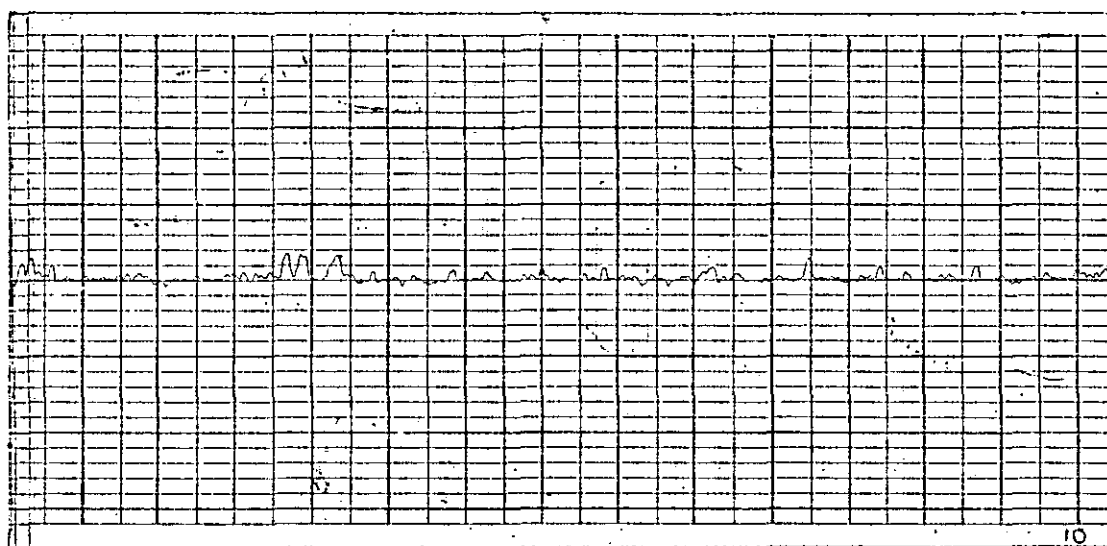control at the limiting current.

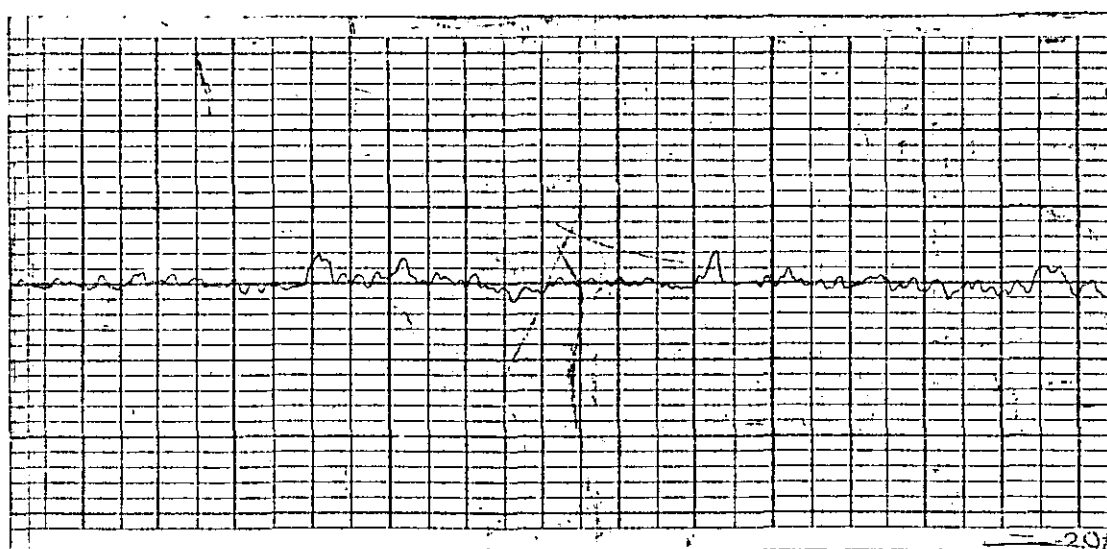Conditions as for Fig. 10.43, all traces refer to 340 rpm.

Key

a)   0 min (preplated surface)

b)   10

c)   20

d)   25

e)   30

f)   40

g)   50

h)   70
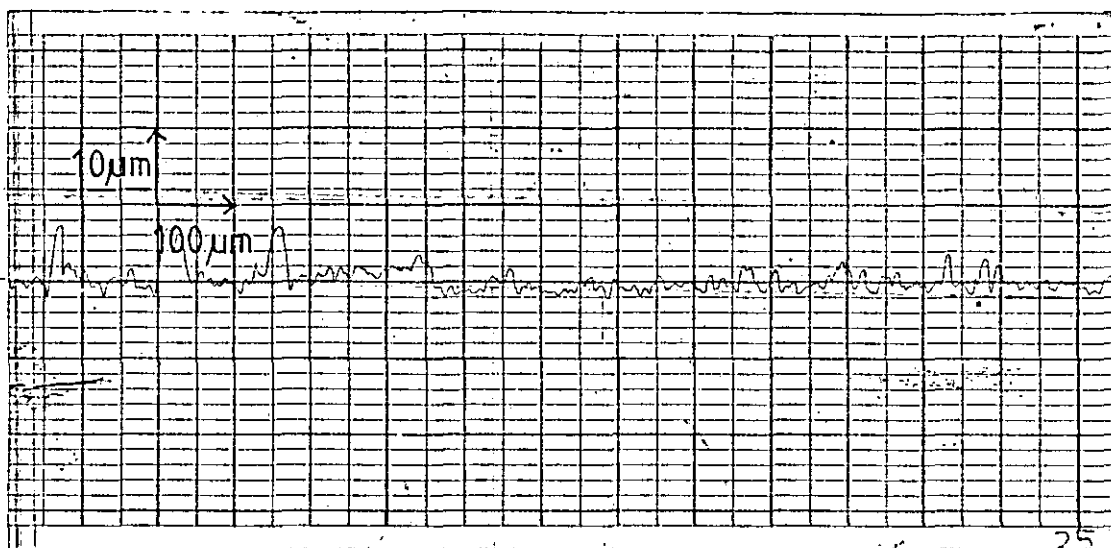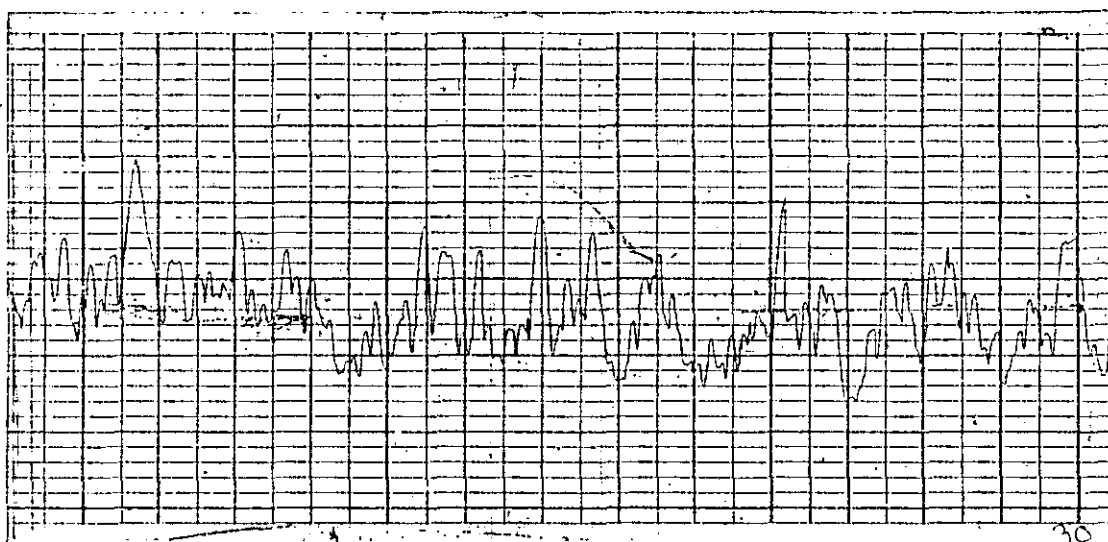
i) 120
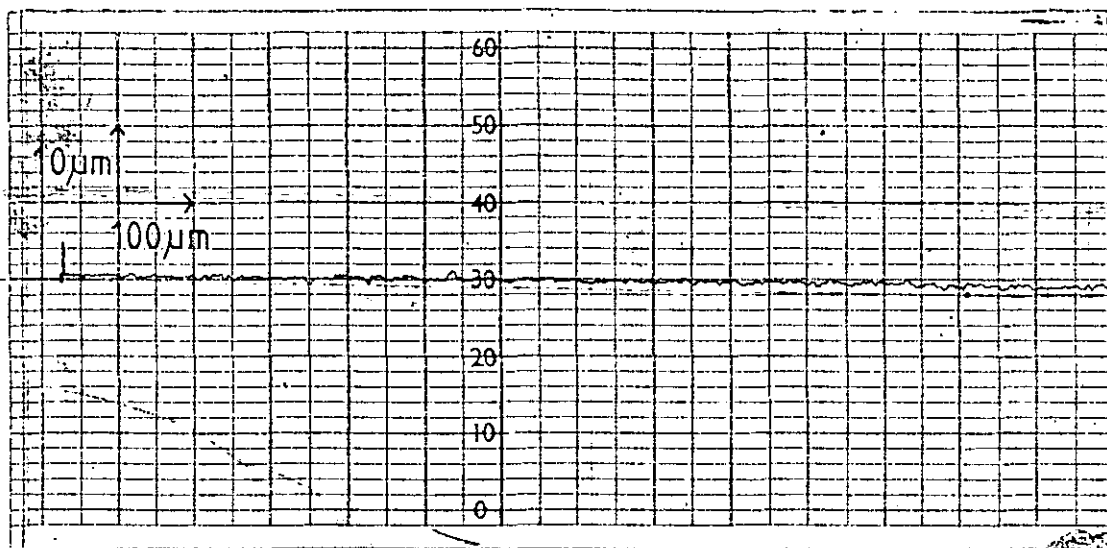
a)

b)

c)

d)

e)

f)

g)

10 μm
500 μm

h)

2 μm
100 μm

i)

2 μm
100 μm

FIG. 10.45   SCANNING ELECTRON MICROGRAPHS

showing the development of roughness

during copper deposition

MAGNIFICATION x 20

-1000 mV MMS/1N Na_2SO_4

0.014 M $CuSO_4$

22° C

d = 6.3 cm

340 rpm

U = 112 cm s^{-1}

potentiostatic growth on to a copper electrode surface
prepared by wet polishing with 600 grade emery paper, followed
by preplating.

           TIME/min.

a)   0

b)   5

c)   10

d)   20

e)   45

f)   60
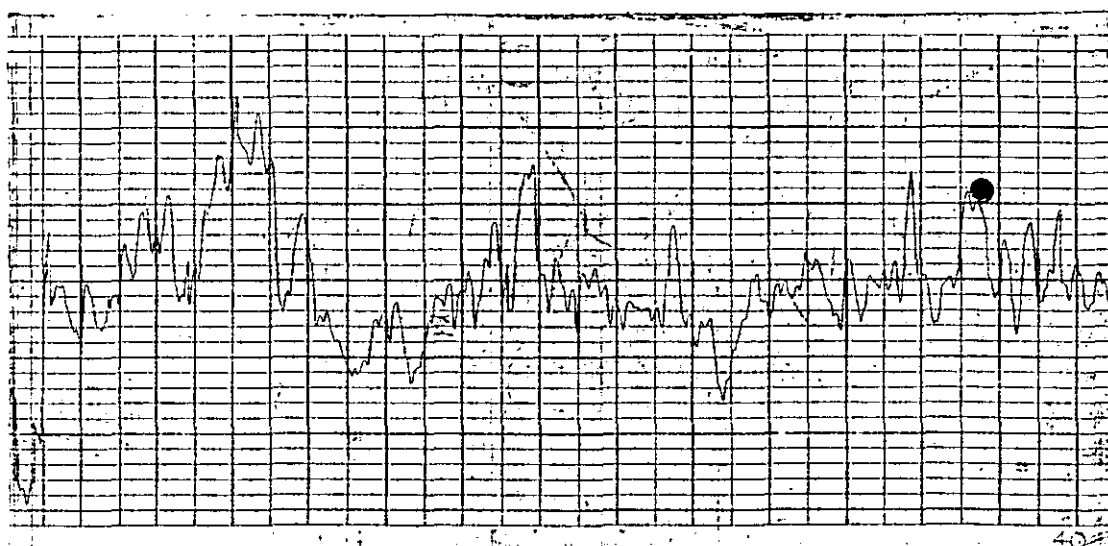
g)   90

PLAN   b) e)
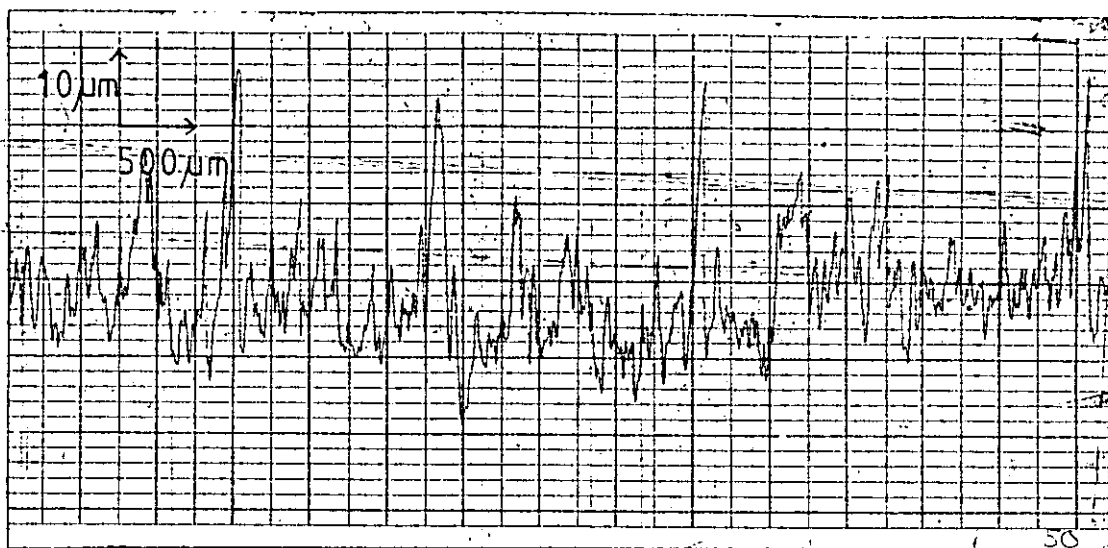
            c) f)
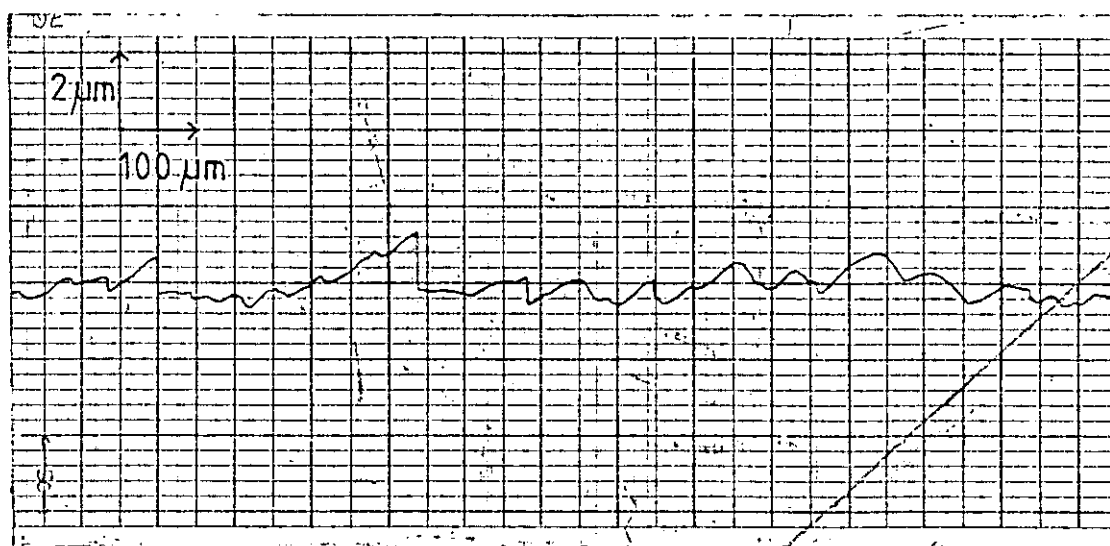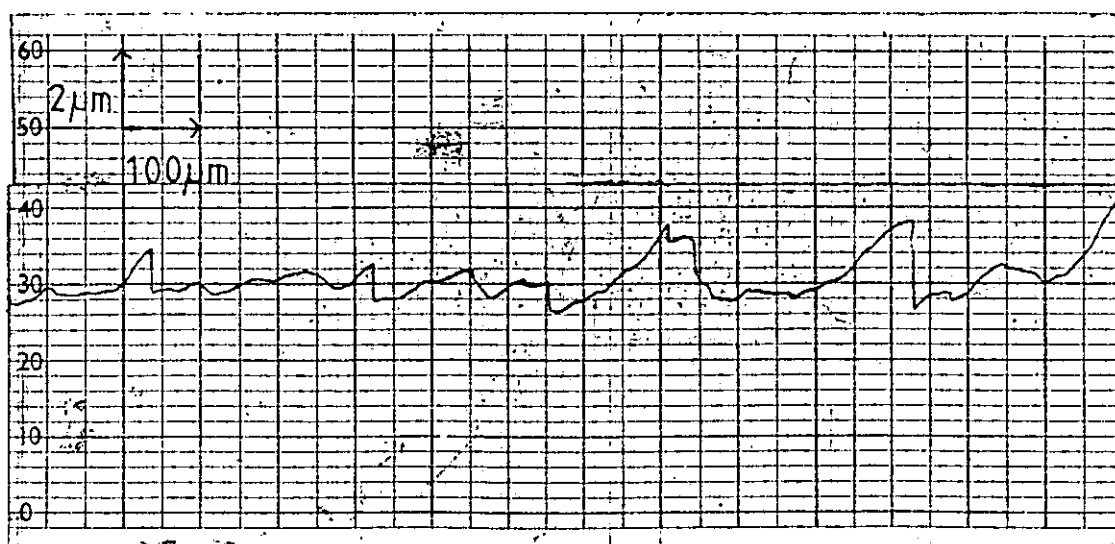
        a) d) g)
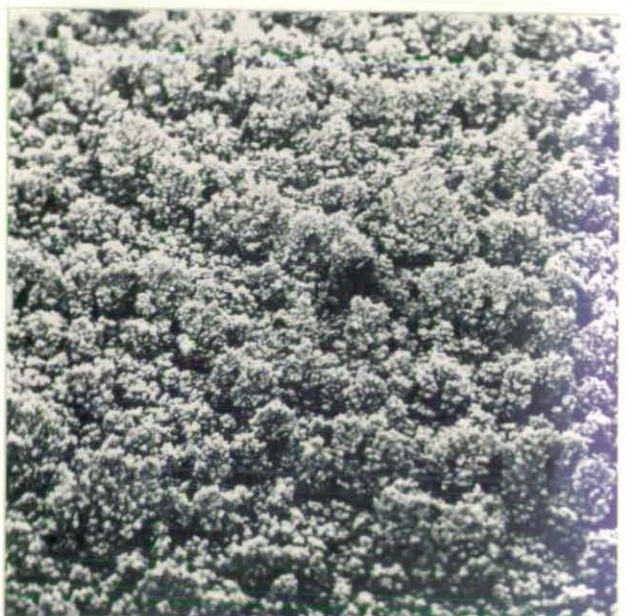
FIG. 10.45   SCANNING ELECTRON MICROGRAPHS

showing the development of roughness during

copper deposition

MAGNIFICATION x 500

Conditions as for FIG. 10.45 a) to g)

TIME/min.

h)   0

i)   2

j)   5

k)   10

l)   20

m)   45

n)   90

PLAN   i)   l)

                        j)   m)

                   h)   k)   n)
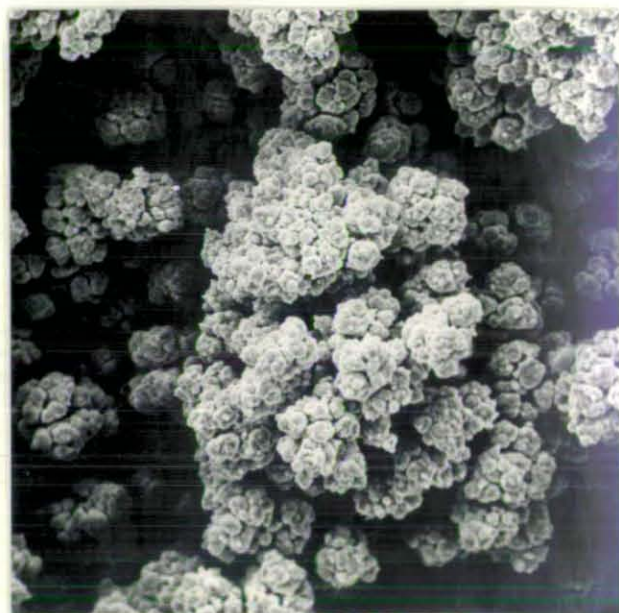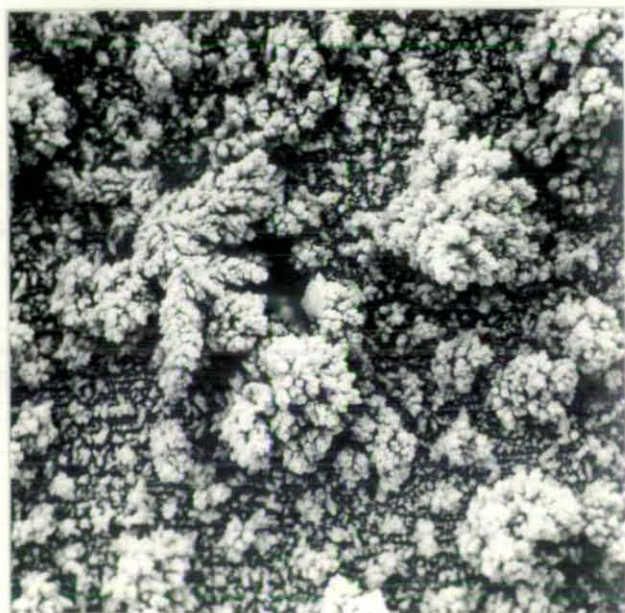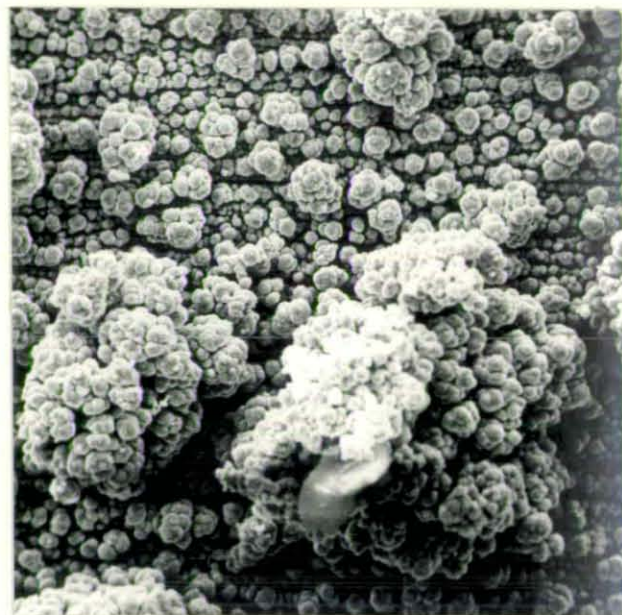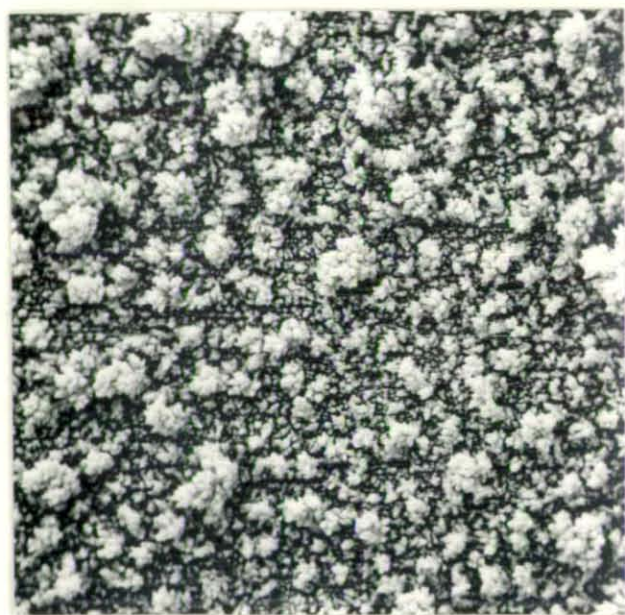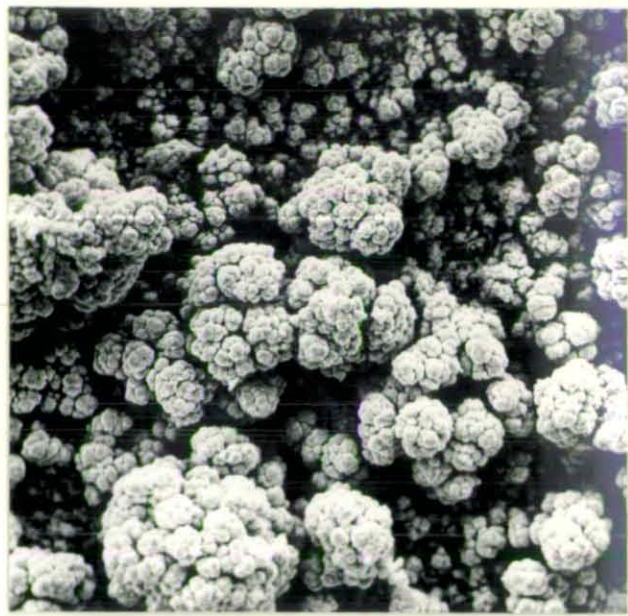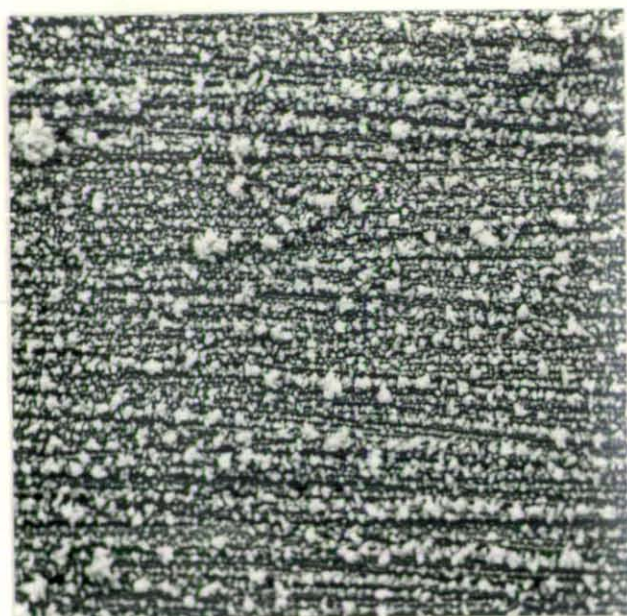
FIG. 10.46   SCANNING ELECTRON MICROGRAPHS

showing the effect of cathode potential

during copper deposition.

MAGNIFICATION x 20

0.014 M $CuSO_4$

1.5 M H_2SO_4

22° C

d = 6.3 cm

rpm = 340

U = 112 cm s^{-1}

deposition time = 60 min.

          mV (MMS/IN Na_2SO_4)

a)   -   750

b)   -   850

c)   - 1000

d)   - 1200

PLAN   a   c

                  b   d
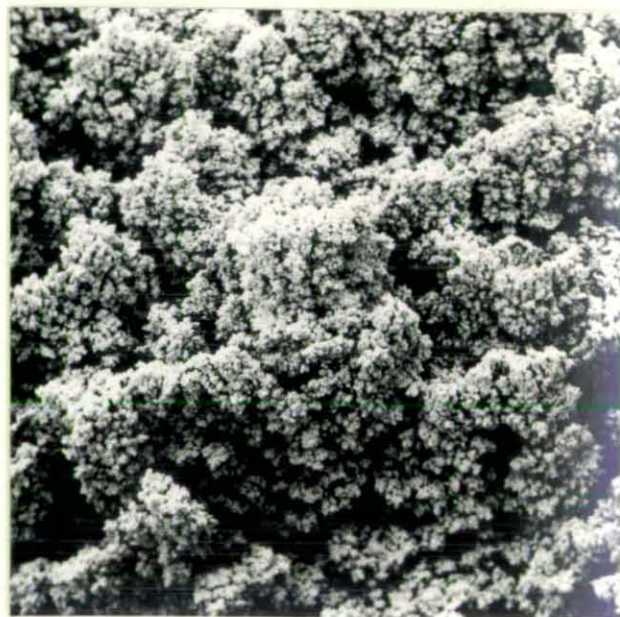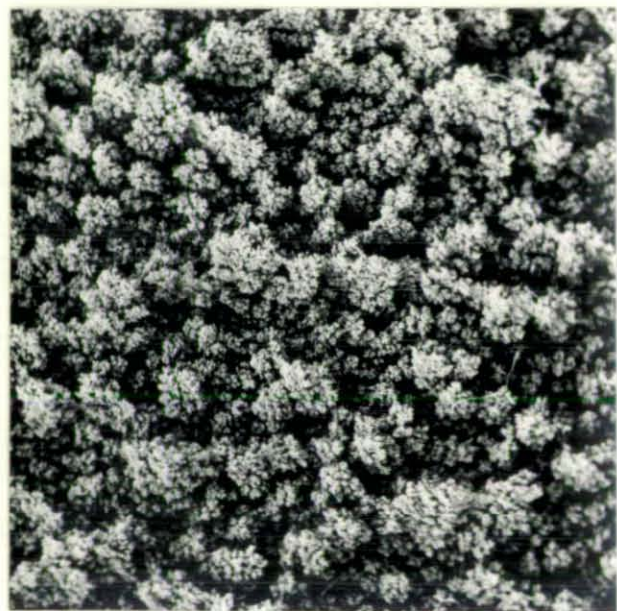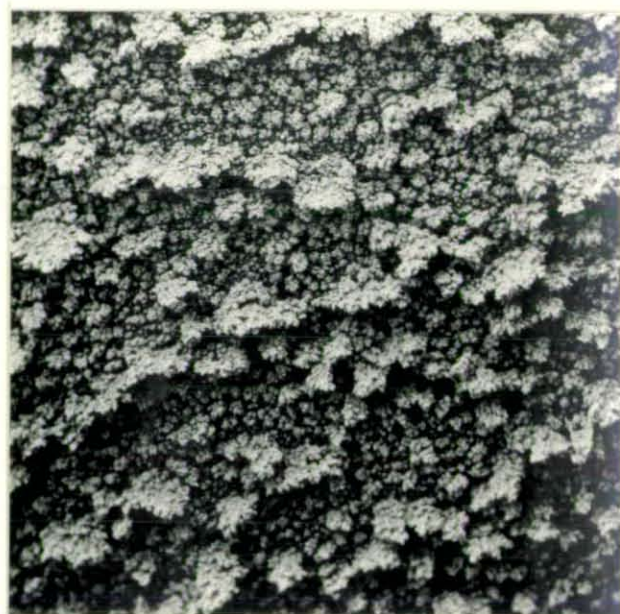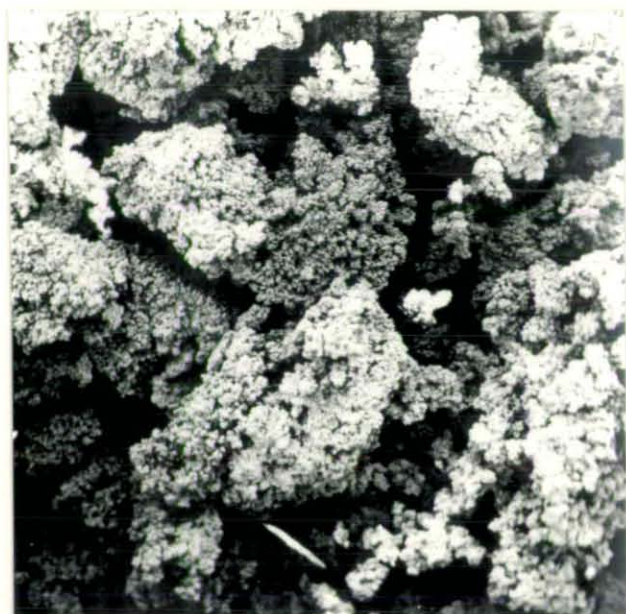
FIG. 10.47   SCANNING ELECTRON MICROGRAPHS OF ROUGH

COPPER DEPOSITS showing the effect of

rotational speed

MAGNIFICATION x 20

- 1000 mV (M.M.S./1N Na_2SO_4)

0.014 M $CuSO_4$

1.5 M H_2SO_4

22° C

d = 6.3 cm

deposition time = 60 min.

r.p.m. U/cm s^{-1}

a) 200   66

b) 500   165

c) 750   247

PLAN   a)

          b)

          c)
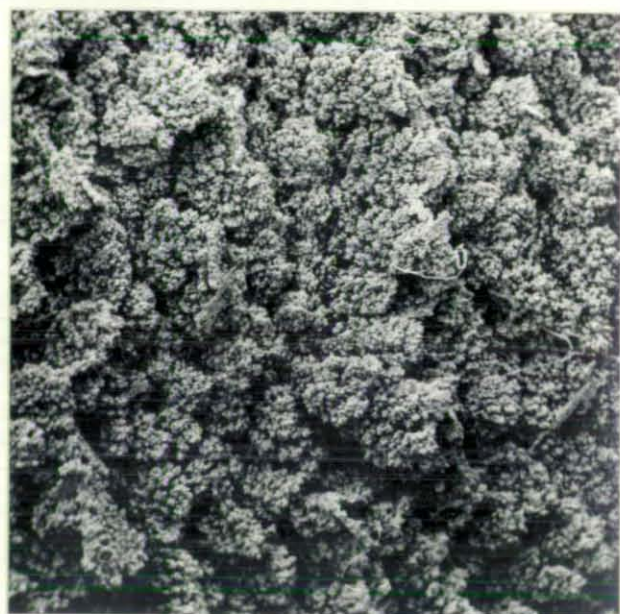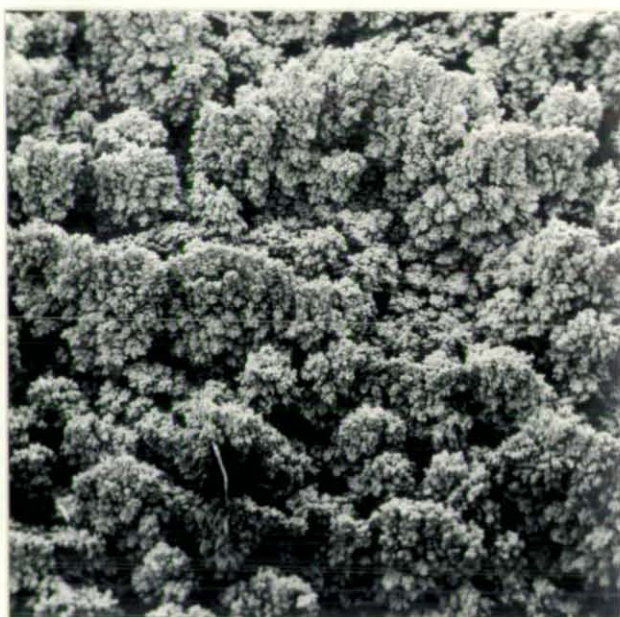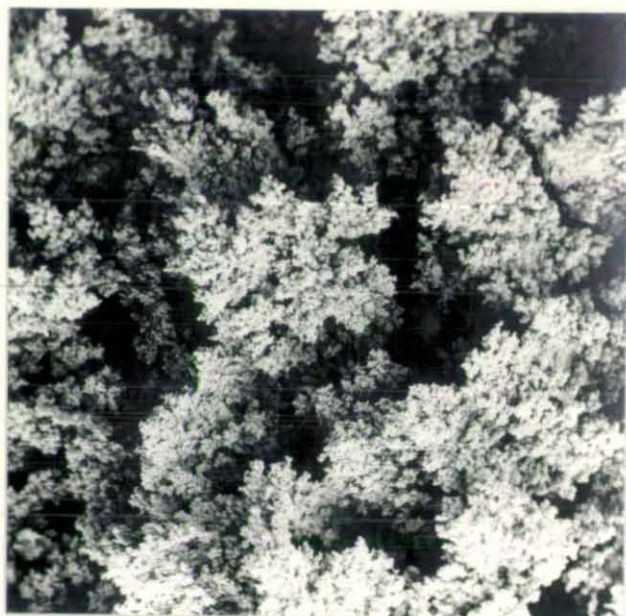
FIGS. 10.48 - 10.50   SCANNING ELECTRON MICROGRAPHS OF ROUGH

                        COPPER DEPOSITS: SPECIAL FEATURES

conditions generally as for FIG. 10.46

FIG. 10.48   MULTIPLE, LAYERED GROWTHS

                        MAGNIFICATION x 5K

                        after 5 min.

FIG. 10.49   'STAR' SHAPED DENDRITIC BRANCHES

                        MAGNIFICATION x 2K

                        after 30 min.

FIG. 10.50   'ROSETTE', LAYERED STRUCTURE

as FIG. 10.49, but at an increased time and MAGNIFICATION x 10K

                        after 60 min.
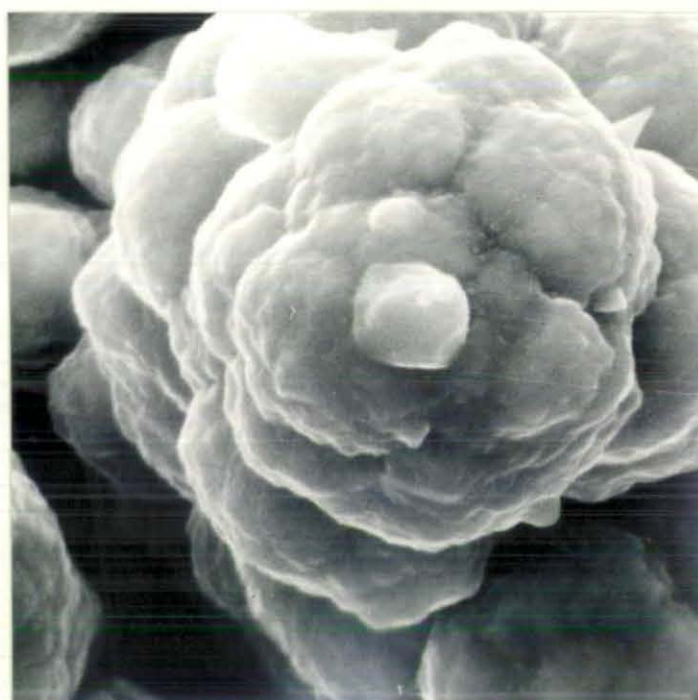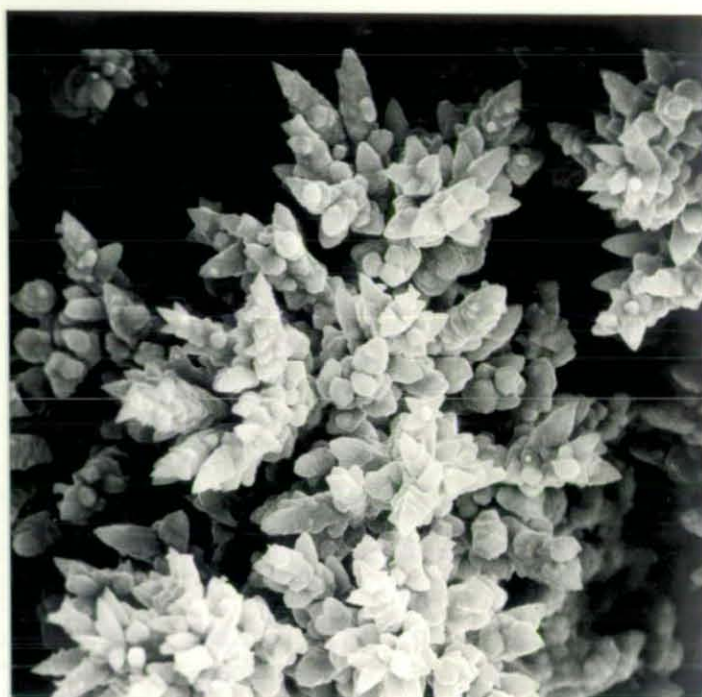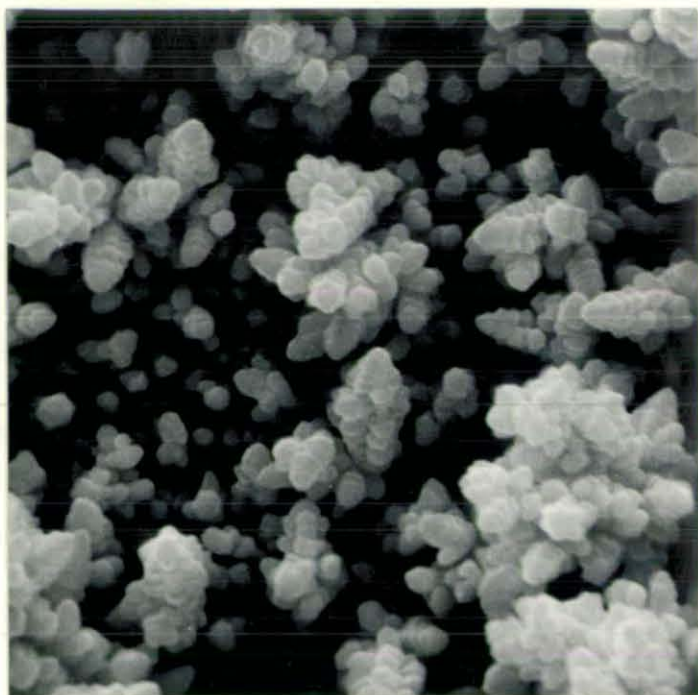
showing the effect of deposition time under the conditions shown in

Fig. 10.39

340 rpm
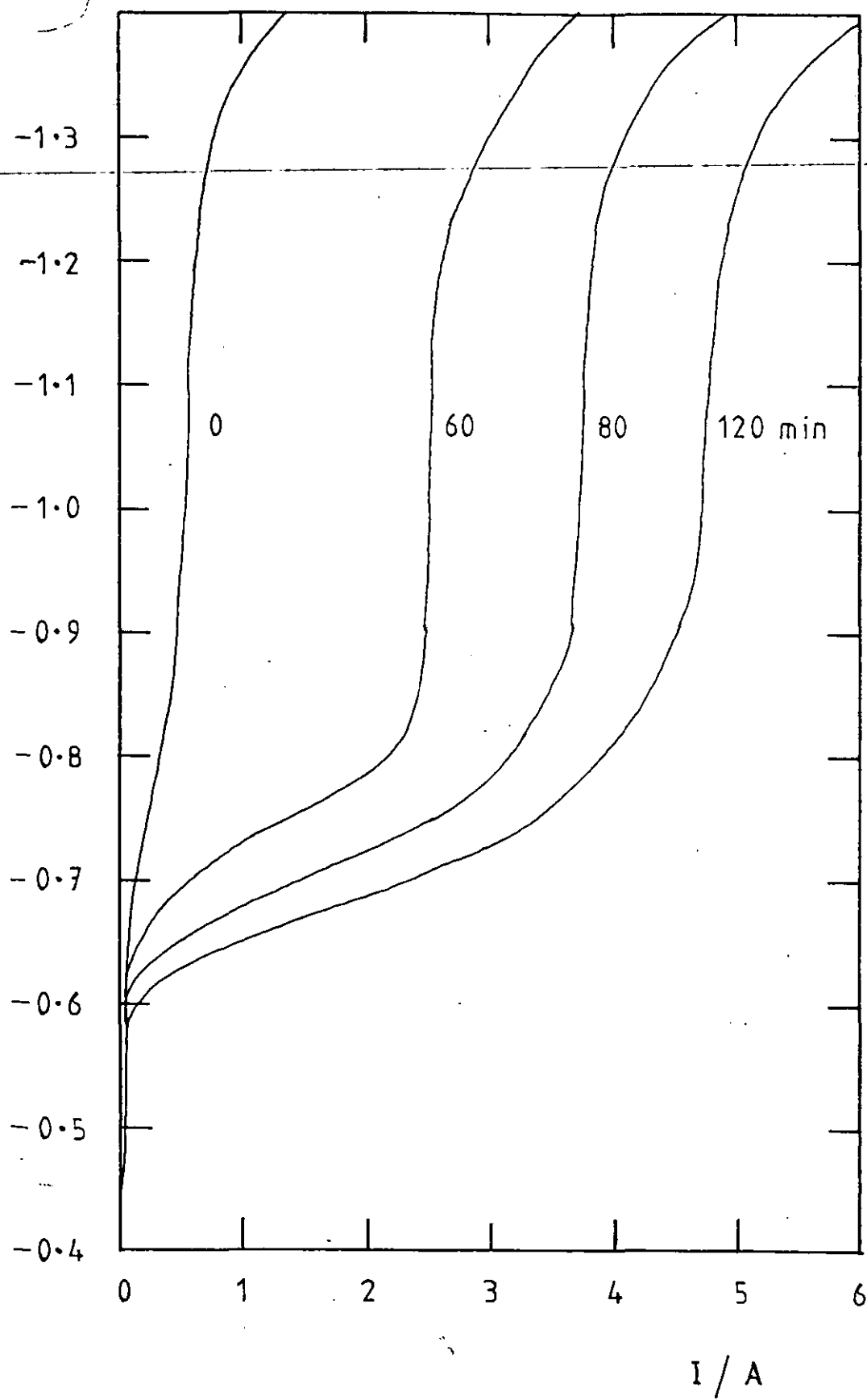
FIG. 10.53   LIMITING CURRENT AS A FUNCTION OF ROTATIONAL

VELOCITY FOR ROUGHENED DEPOSITS

deposits grown at the limiting current, under potentiostatic control
- 1.000 V (M.M.S.) for various times.

measurements obtained by recording steady currents at set
potentials.

Other conditions as for Fig. 10.52.
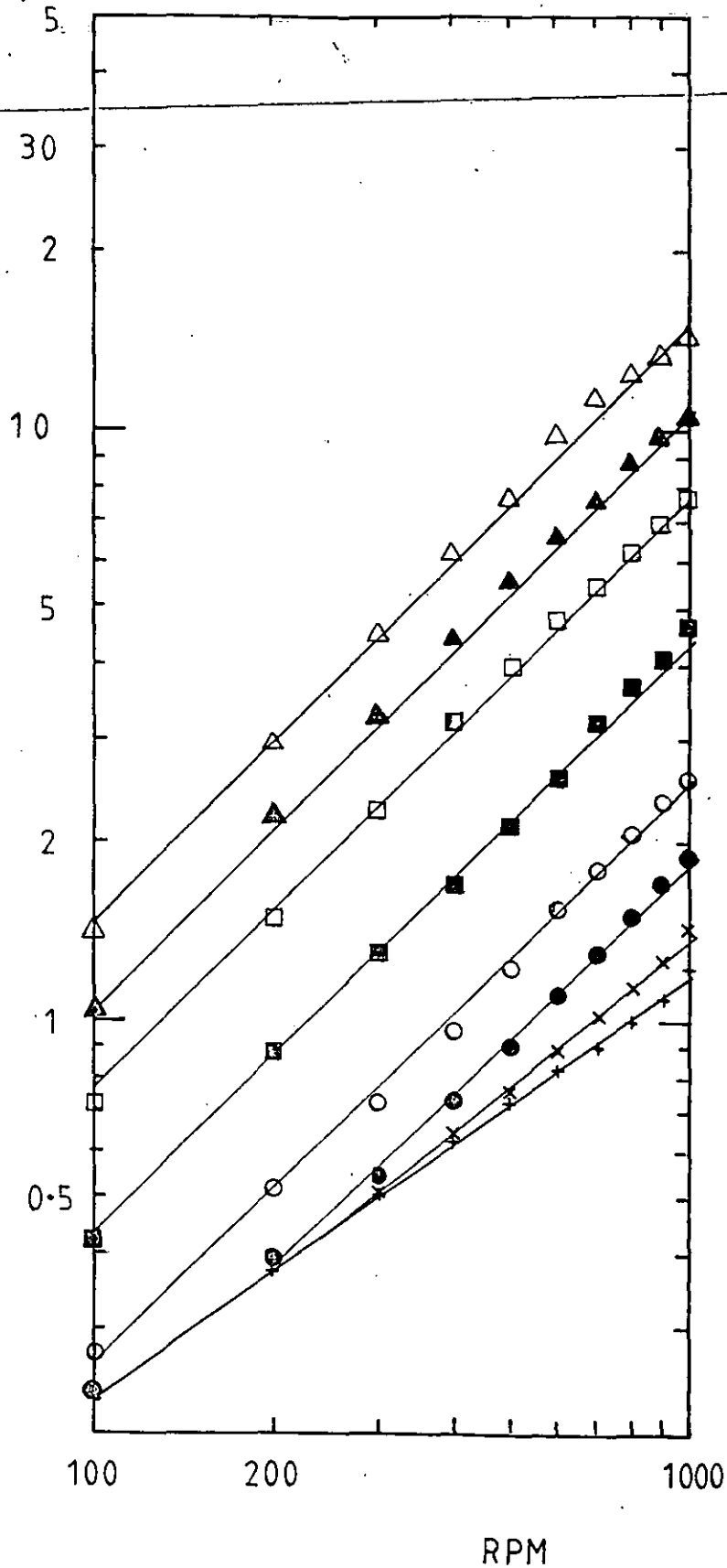
FIG. 10.54   EFFECT OF ABRUPT DEPOSIT REMOVAL ON MASS

TRANSPORT

showing the growth of (limiting) current and the effect of scraping

(by means of a full length 'tufnol' blade)

0.014 M $CuSO_4$

1.5 M H_2SO_4

22 $^{\circ}$ C

d = 6.0 cm

l = 6.3 cm

A = 119 cm^2

rpm = 360

U = 113 cm s^{-1}

ETW value predicted by the Eisenberg, Tobias and Wilke Correlation.

KCG value predicted by the Kappesser, Comet and Greif Correlation.
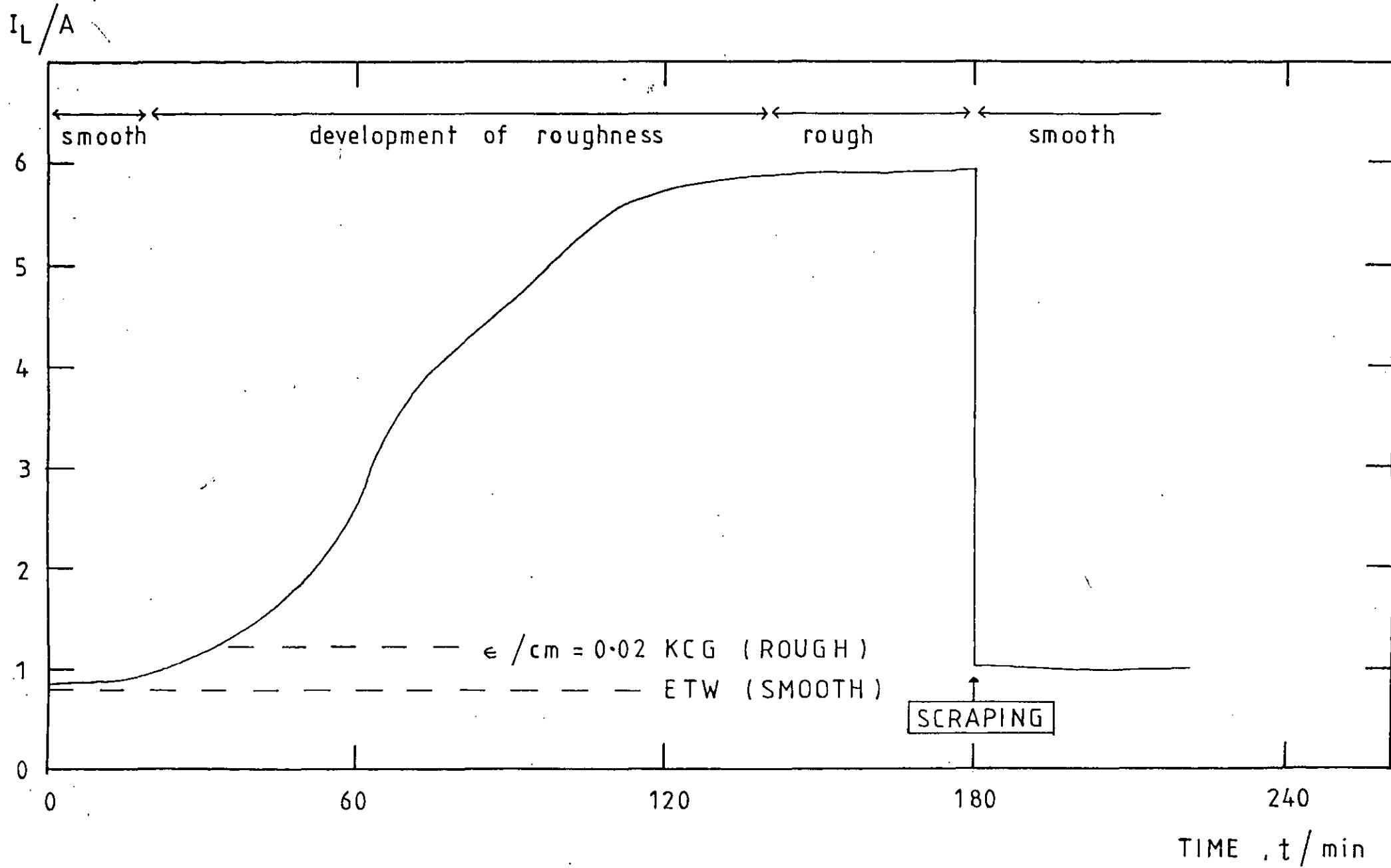
FIG. 10.55   LIMITING CURRENT AS A FUNCTION OF ROTATION VELOCITY

FOR KNURLED CYLINDERS, diameter 1.5 cm.

Copper deposition from: 0.014M Cu SO$_4$ +

1.5 M   H$_2$SO$_4$
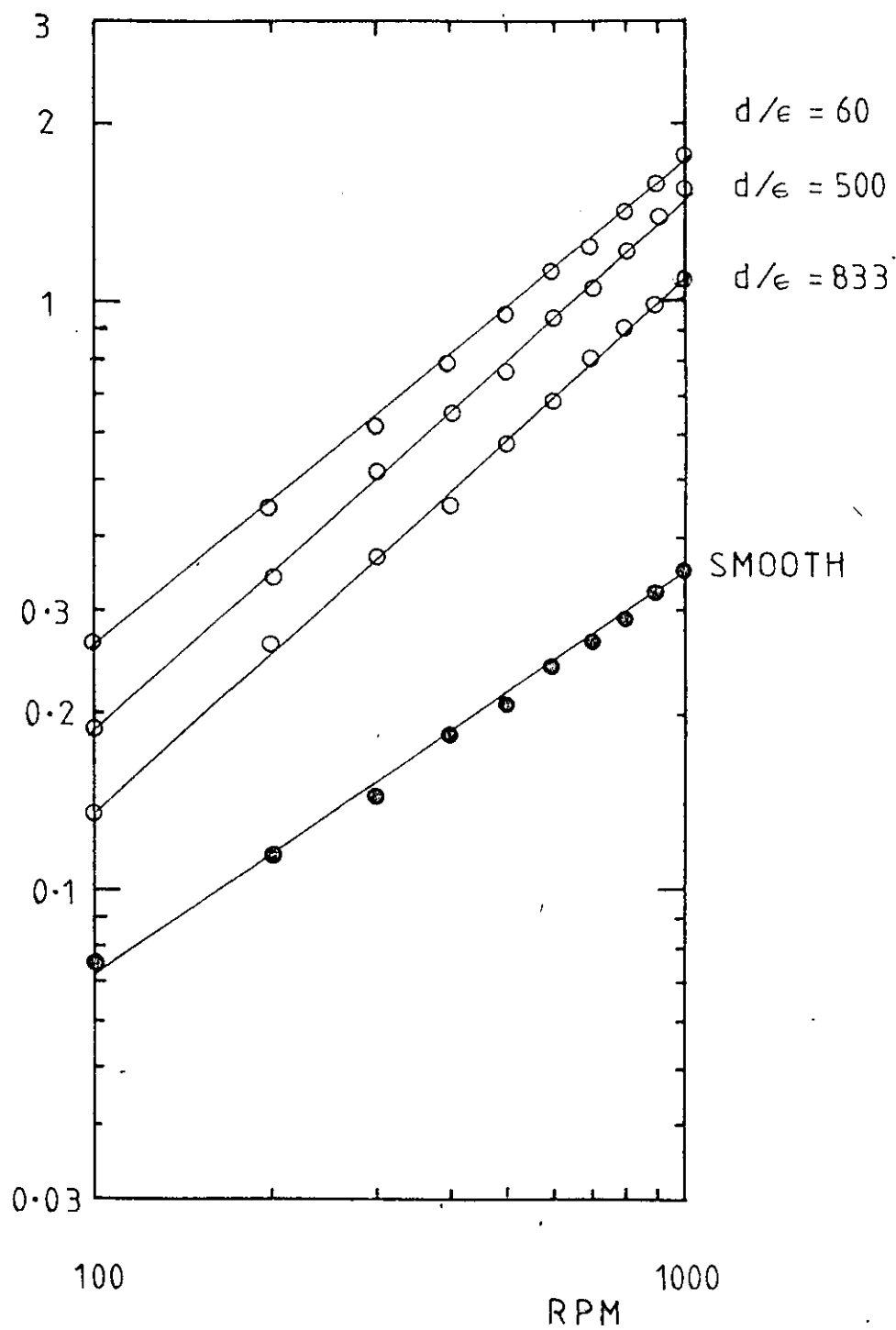
FIG.IO.56 LIMITING CURRENT AS A FUNCTION OF ROTATIONAL

VELOCITY FOR KNURLED CYLINDERS, diameter 6.0 cm.

conditions as for Fig. IO.55
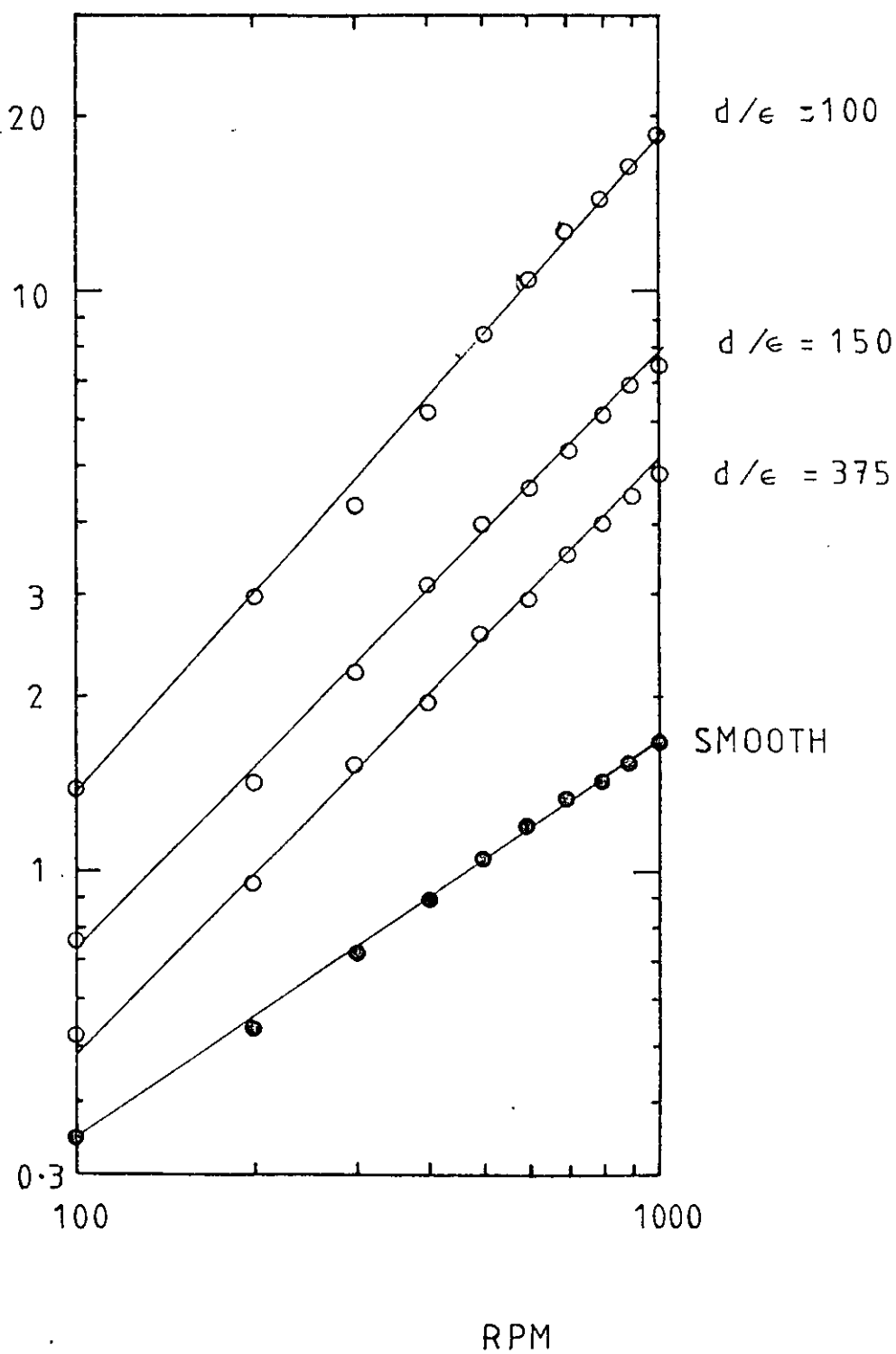
FIG. IO. 57   MASS TRANSPORT TO KNURLED ROTATING CYLINDERS,

during copper deposition.

Plots of modified Chilton Colburn factor, j_D'

against Reynolds number.

Solid line due to the smooth cylinder correlation,

of Eisenberg, Tobias and Wilke :

$$j_D' = 0.079 \ (Re)^{-0.30}$$

where $\quad j_D' = (St) \ (Sc)^{0.644}$

and $\quad (Re) = \dfrac{Ud}{\nu}$

$j_D \times 10^3$

$d = 1 \cdot 5\,cm\;;\;d/\epsilon\;=\;60$

$d = 1 \cdot 5\,cm\;;\;d/\epsilon\;=\;500$

$d = 1 \cdot 5\,cm\;;\;d/\epsilon\;=\;833$

$d = 6 \cdot 0\,cm\;;d/\epsilon =100$

$d = 1 \cdot 5\,cm;smooth$

$d = 6 \cdot 0\,cm\;;d/\epsilon =150$

$d = 6 \cdot 0\,cm\;;d/\epsilon =375$

EISENBERG et al.

$d = 6 \cdot 0\,cm;smooth$

(Re)

10^3

10^4

10^5

10^6

100

10

1
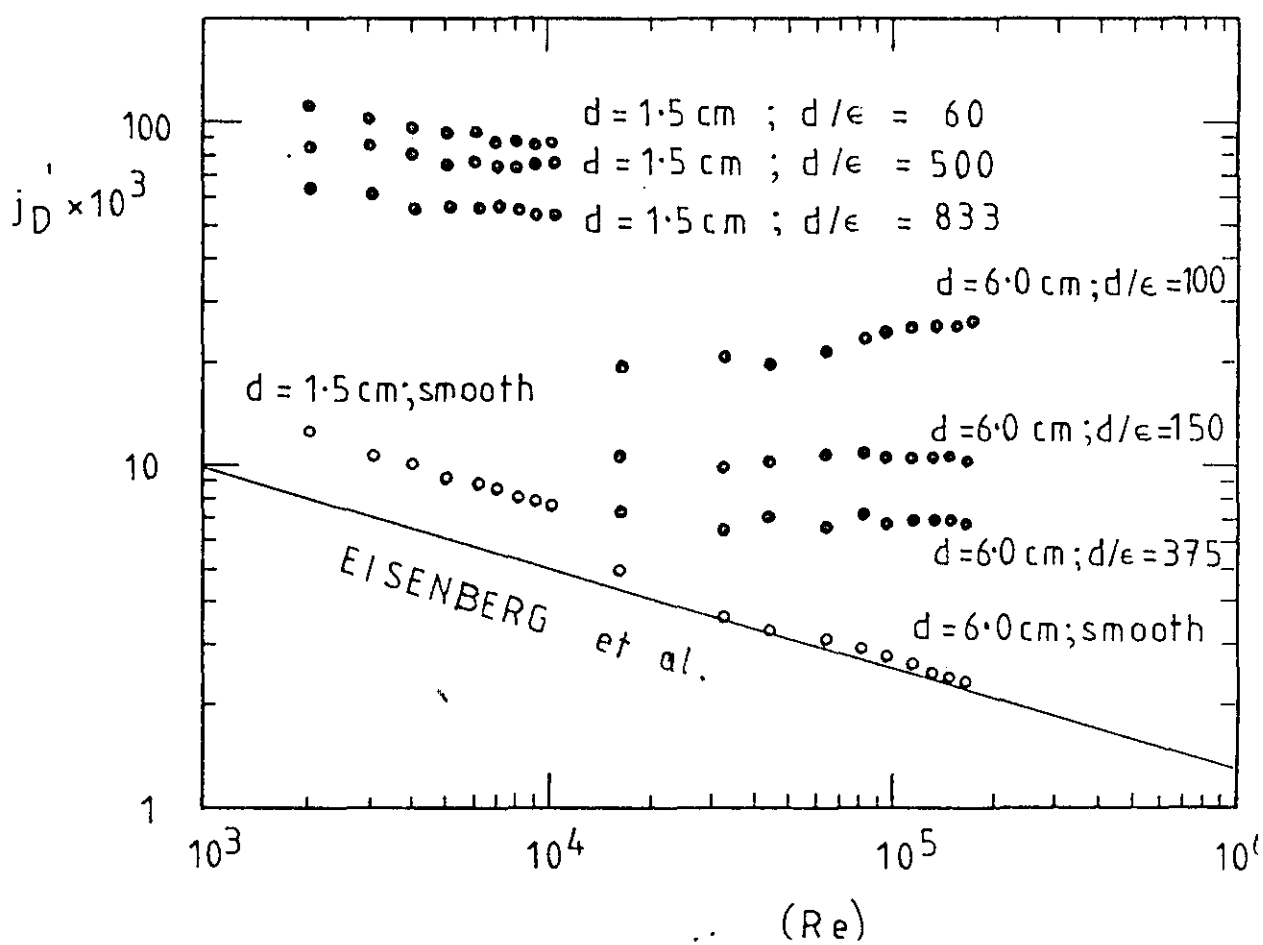
FIG. 10.58 CATHODIC POLARISATION CURVES IN THE PRESENCE
OF THIOUREA

0.014 M $CuSO_4$

1.5 M H_2SO_4

22 ^{o} C

d = 6.3 cm.

l = 4.3 cm.

A = 85.1 cm^2

rpm = 340

U = 112 cm s^{-1}

POTENTIAL , E /V(MMS)

	THIOUREA CONCENTRATION/M
○	0
●	10^{-5}
□	10^{-4}
■	10^{-3}
+	10^{-2}
×	10^{-1}
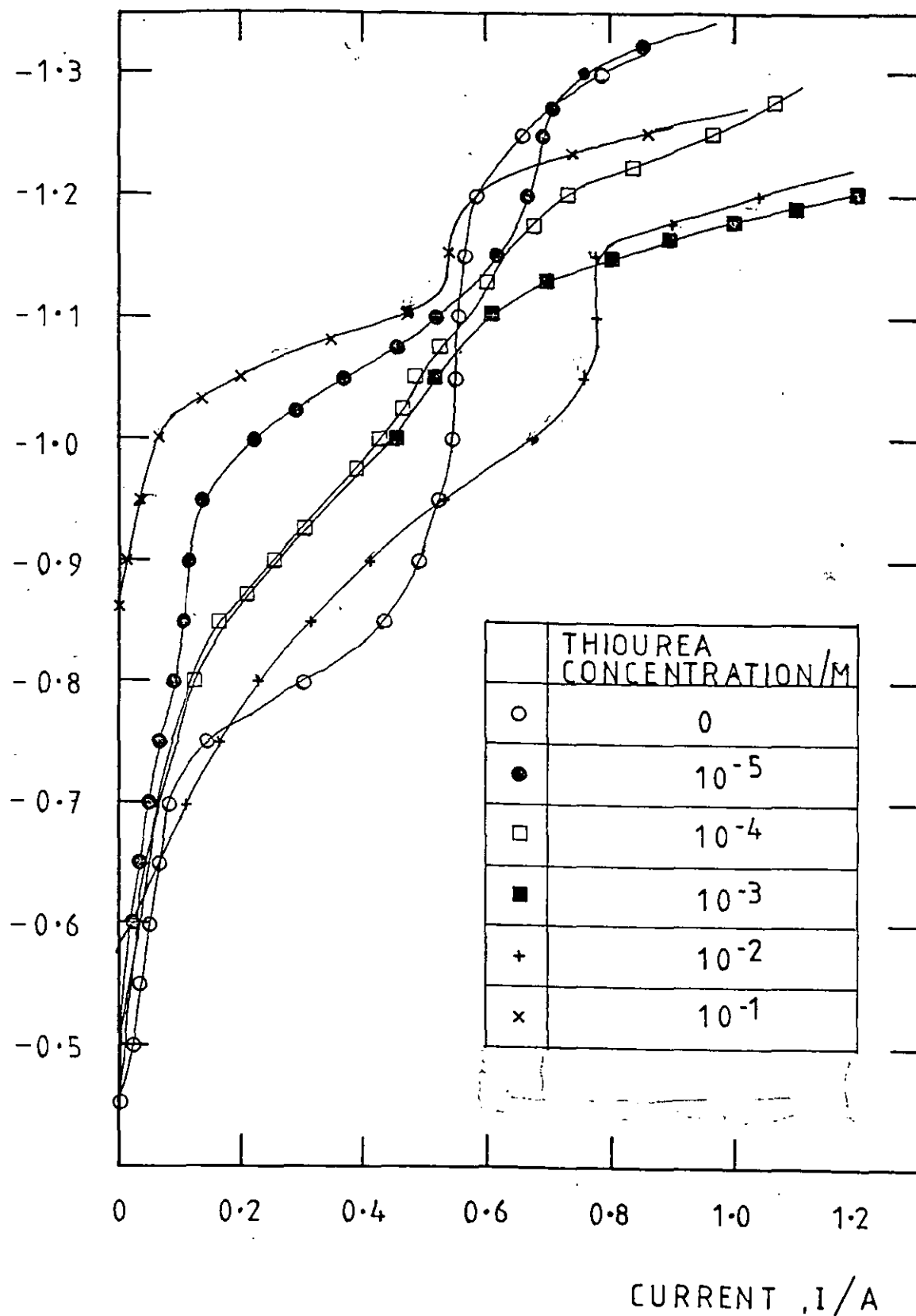
CURRENT , I/A

FIG. 10.59   CATHODIC POLARISATION CURVES (OVERPOTENTIAL AGAINST
              CURRENT) SHOWING THE INFLUENCE OF THIOUREA

As Fig. 10.58
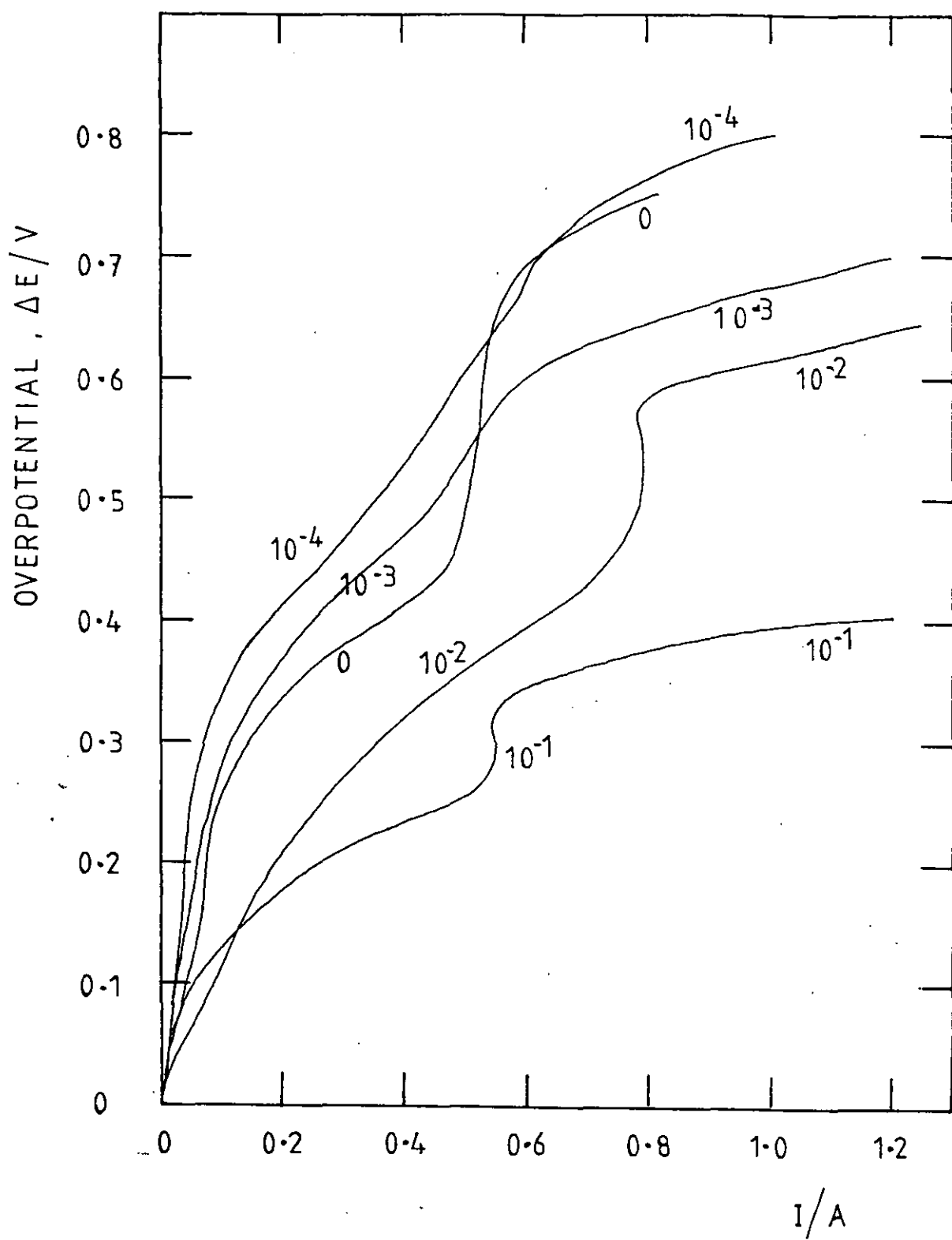
FIG. 10.60   COPPER CONCENTRATION DECAY IN THE PRESENCE OF

THIOUREA

0.014M $CuSO_4$

1.5 M H_2SO_4

22° C

d = 6.3cm

l = 4.3cm

A = 85.1 cm^2

rpm = 340

U = 112 cm s^{-1}

E = - 1.000 V (MMS)

Thiourea, 10^{-5}, 10^{-4}, 10^{-3}, 10^{-2}, 10^{-1}, 0 M

CONCENTRATION, c /mg dm^{-3}

10^3

10^2

10

1

10^{-1}

10^{-2}

10^{-3}

THEORY
0 M

10^{-4}

$0, 10^{-5}$

0   60   120   180

TIME , t/min
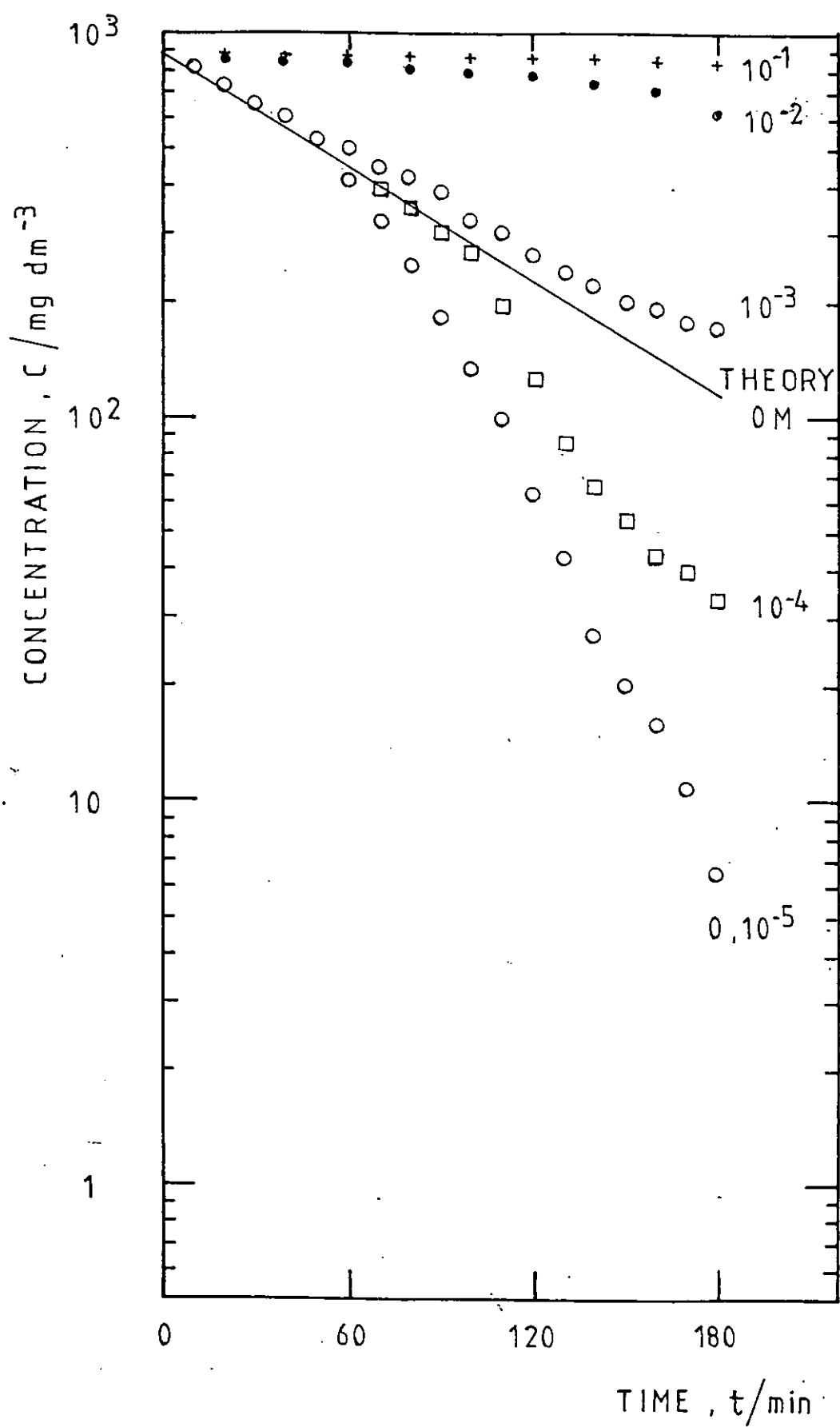
FIG. 10.61   CURRENT-TIME BEHAVIOUR FOR THIOUREA ADDITION TO
COPPER SOLUTIONS

Corresponding to Fig. 10.60

10^{-3} M   Thiourea
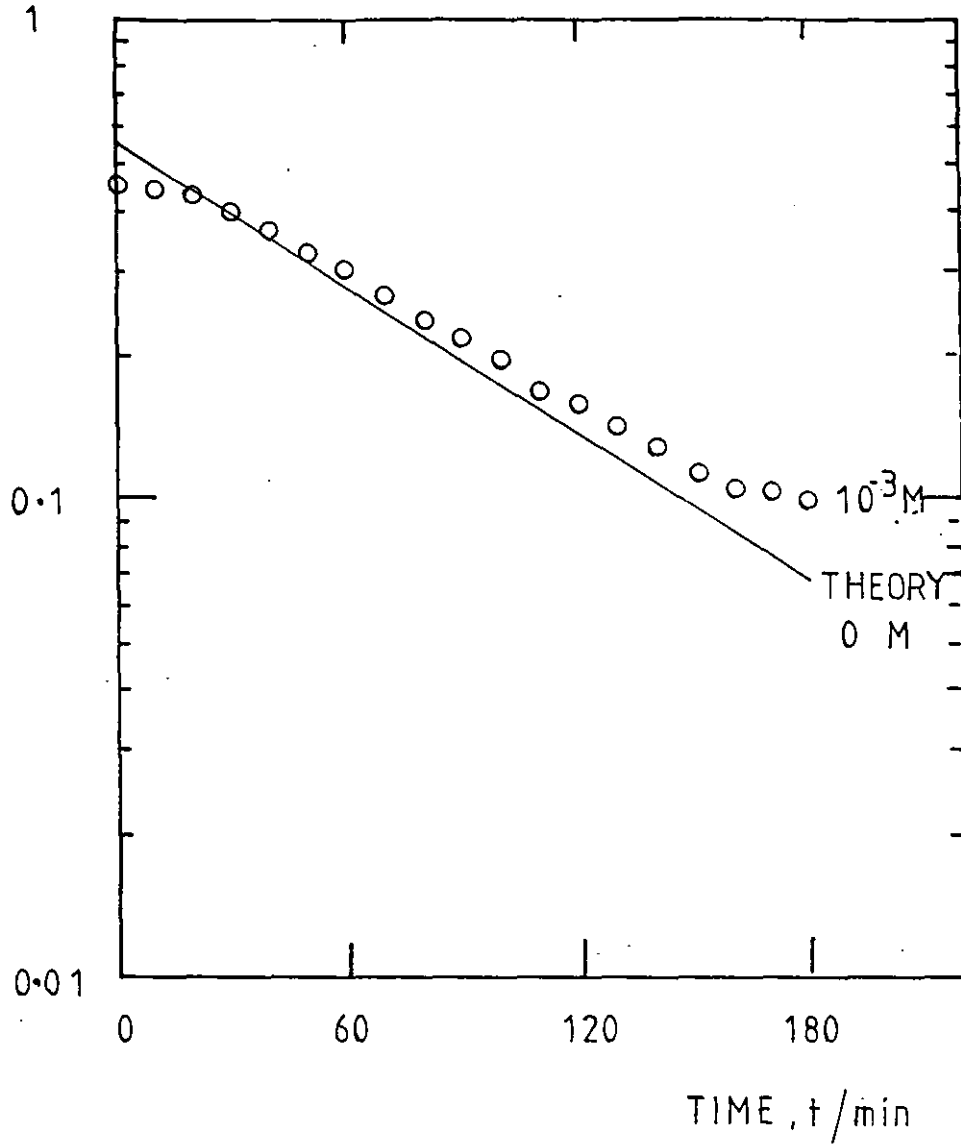
	CONC. THIOUREA / M
○	0
●	10^{-5}
□	10^{-4}
△	10^{-3}
▣	10^{-2}
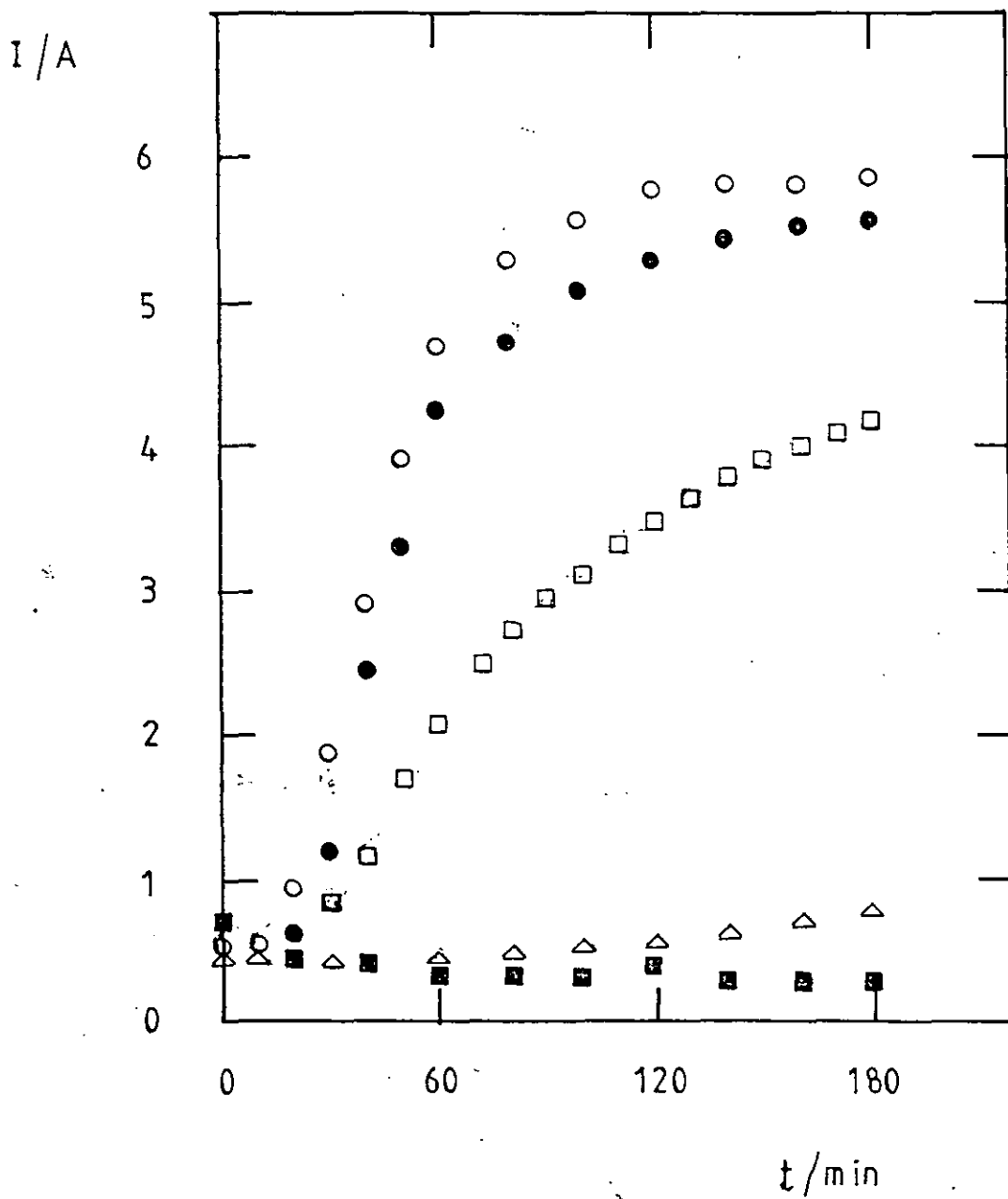
FIG. 10.62   EFFECT OF THIOUREA ON ROUGHNESS DEVELOPMENT AT
CONSTANT COPPER CONCENTRATION

Conditions as Fig. 10.39, 340 r.p.m.

FIG. 10.63   EFFECT OF AN ULTRASONIC FIELD ON THE POLARISATION

CURVES FOR COPPER DEPOSITION

Preliminary studies performed in co-operation with Mr. C. Gould.

Polished stainless R.C.E.

0.014 M $CuSO_4$

1.5 M H_2SO_4

22^0 C

150 mV $(min)^{-1}$

d = 1.03

l = 1.76

A = 5.7 cm^2

rpm = 500 - 3000

U = 27 - 162 cm s^{-1}

Ultrasonics: 25 Hz

CURRENT , I / mA

OVERPOTENTIAL , ΔE /V

- - - - ULTRASOUND + R.C.E.
——— R.C.E ONLY

		R P M
	×	500
	●	1000
	+	1500
	○	2000
	□	3000
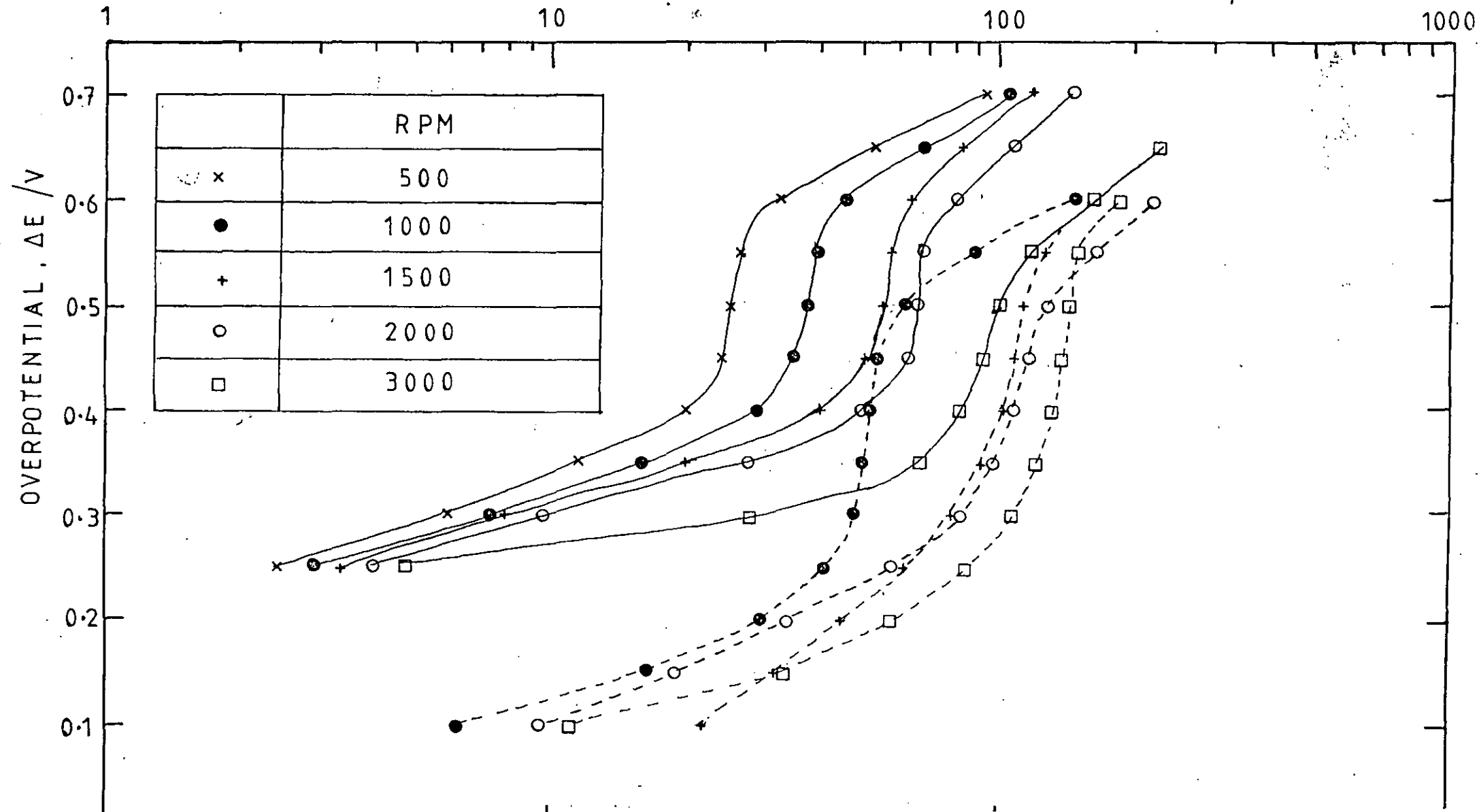
FIG. 10.64   MASS TRANSFER COEFFICIENT AS A FUNCTION OF

REYNOLDS NUMBER SHOWING THE EFFECT OF ULTRASONICS

Corresponding to Fig. 10.63.

Log - Log plot, to determine the relationship:

$$K_L \propto (Re)^n$$
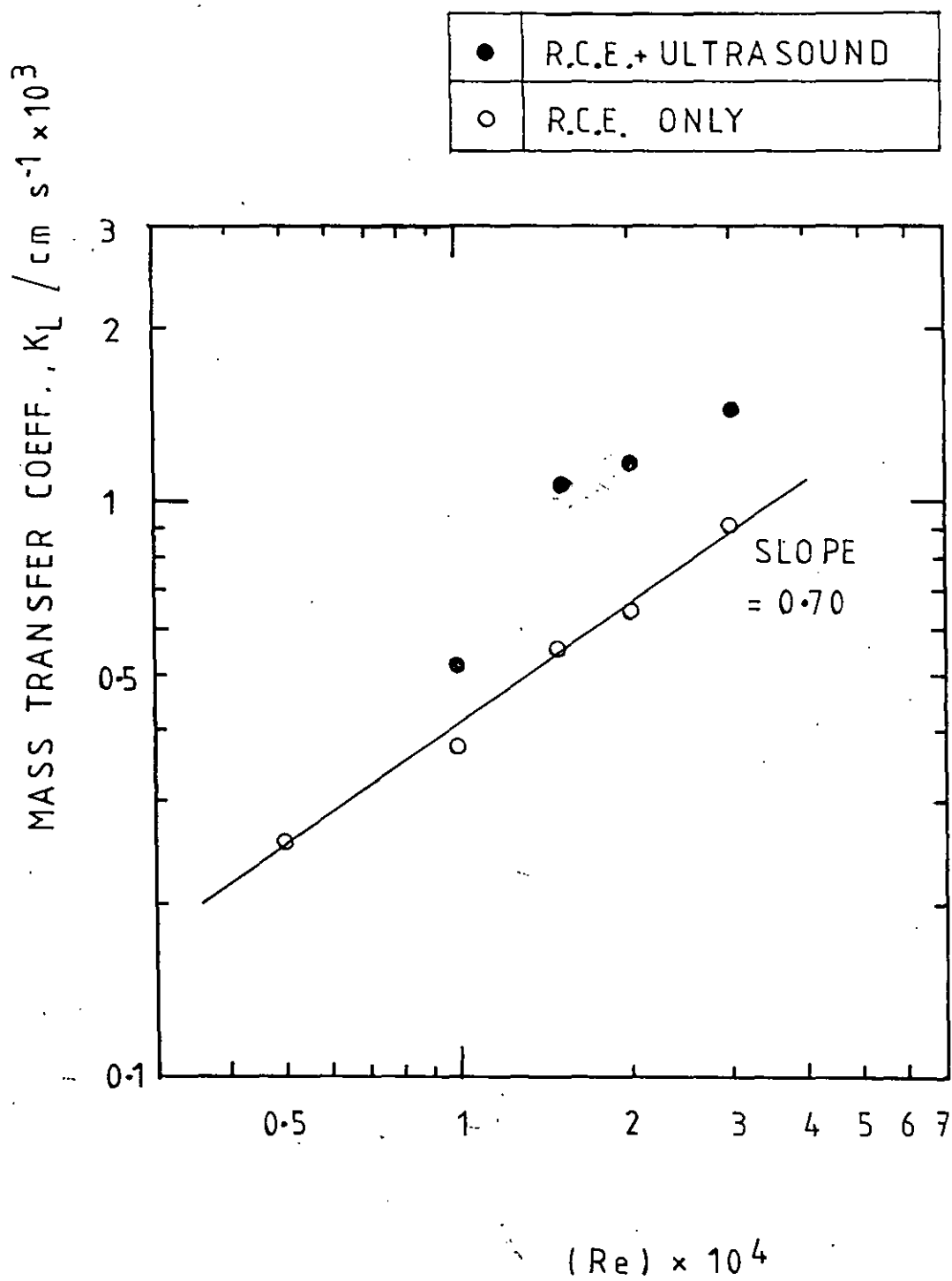
FIG. 10.65   TYPICAL CELL VOLTAGES.AS A FUNCTION OF CELL

                CURRENT

Showing the potential difference between the upper (power) brush,

and the lower (potential pick up) brush.

360 rpm
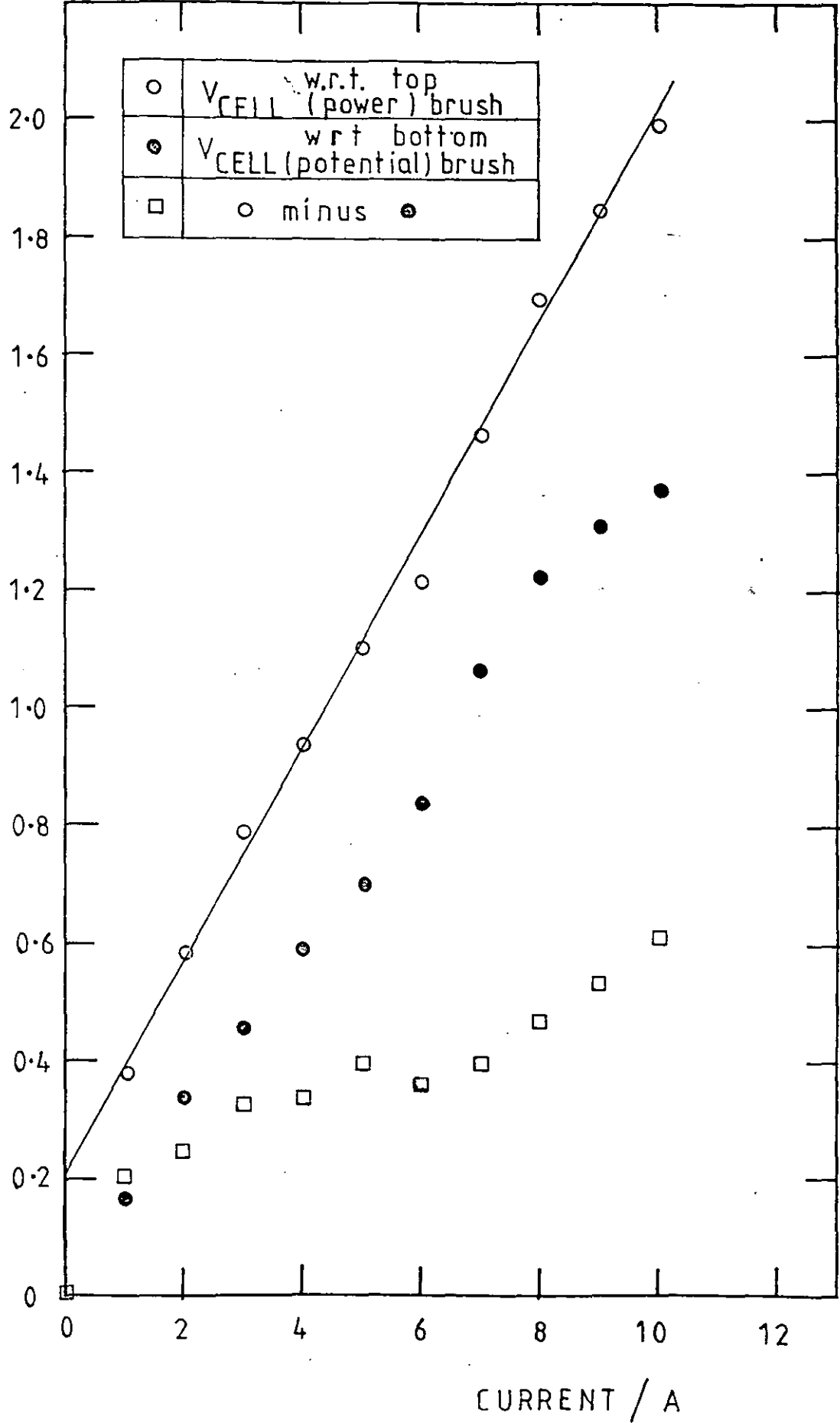
FIG. 10.66   POLARISATION CURVE FOR SMOOTH COPPER DEPOSITION

SHOWING THE (NEGLIGIBLE) EFFECT OF GAS BUBBLING

0.014 M $CuSO_4$

1.5 M H_2SO_4

d = 6.3 cm

l = 4.3 cm

A = 85.1 cm^2

rpm = 360

U = 119 cm s^{-1}

22 ^{o} C

150 mV $(min)^{-1}$ linear sweep rate

Nitrogen gas bubbled through the reactor (volume 1 dm^3) at 1 litre $(min)^{-1}$
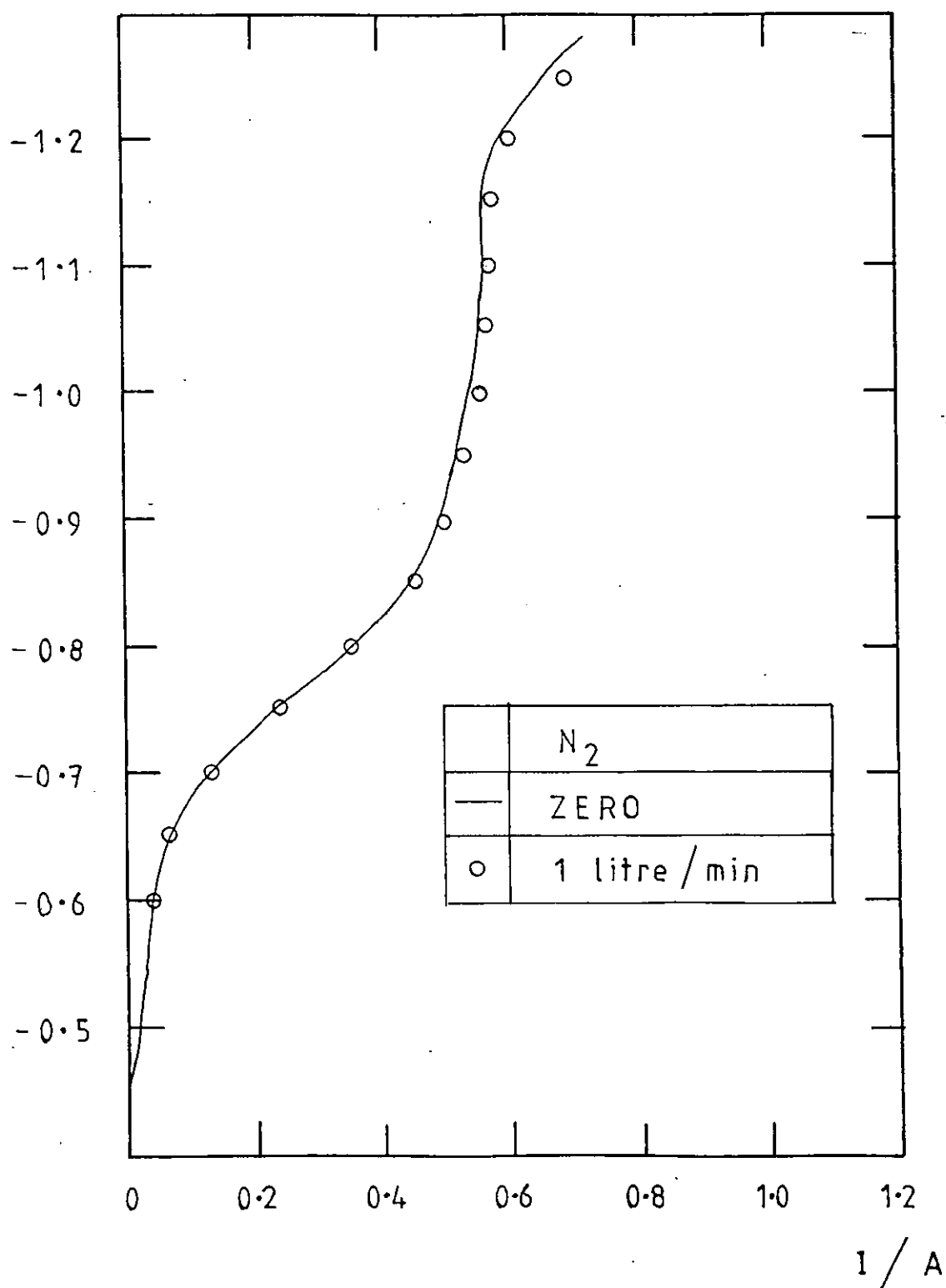
FIG. 10.67   VARIATION OF FLUID DENSITY WITH TEMPERATURE

FOR ACID COPPER SULPHATE ELECTROLYTES

1.5 M H_2SO_4

0 to 0.7 M $CuSO_4$
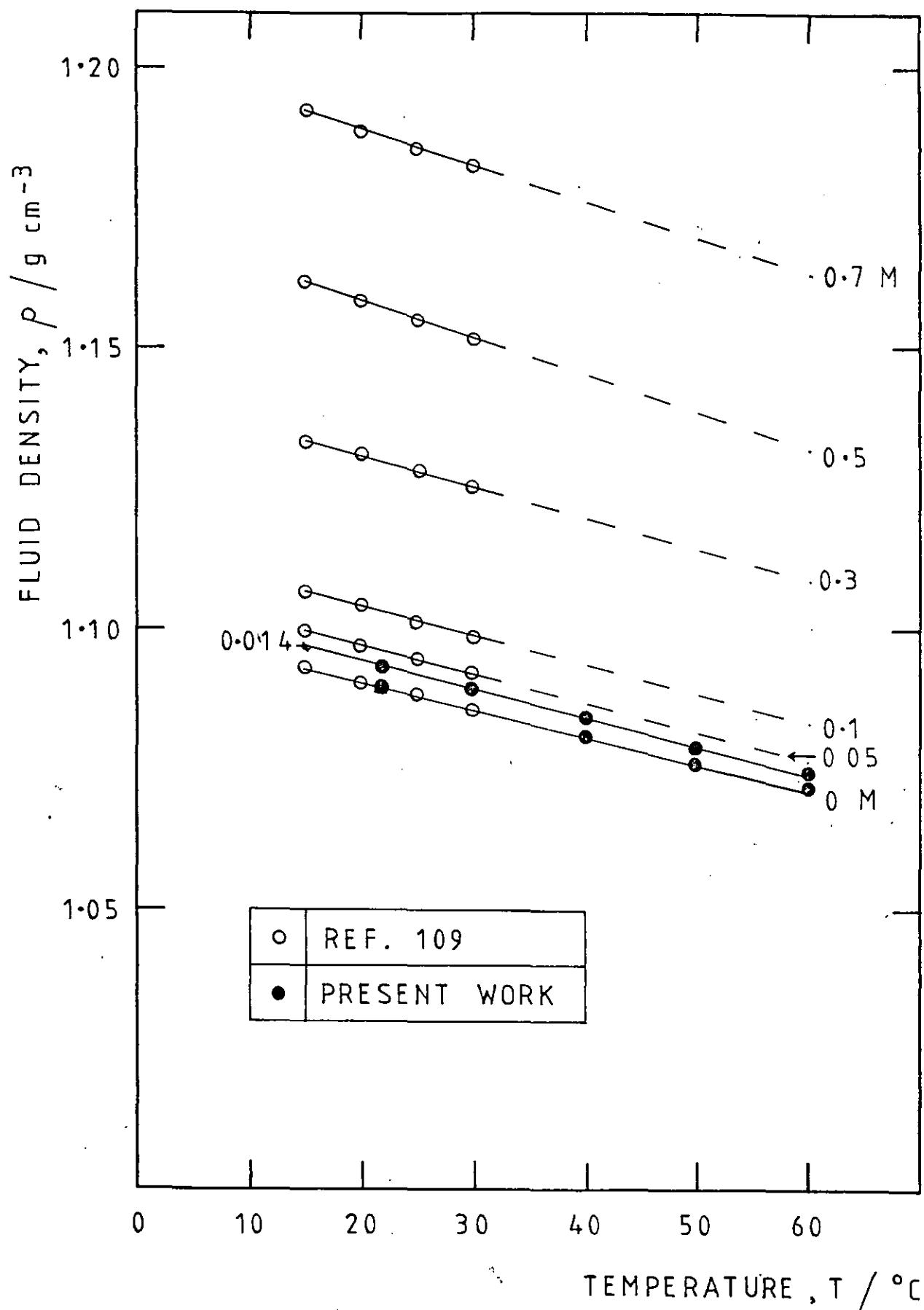
FIG. 10.68   ARRHENIUS PLOT FOR KINEMATIC VISCOSITY OF

ACID COPPER SULPHATE ELECTROLYTES

1.5 M H_2SO_4

0, and 0.014 M $CuSO_4$
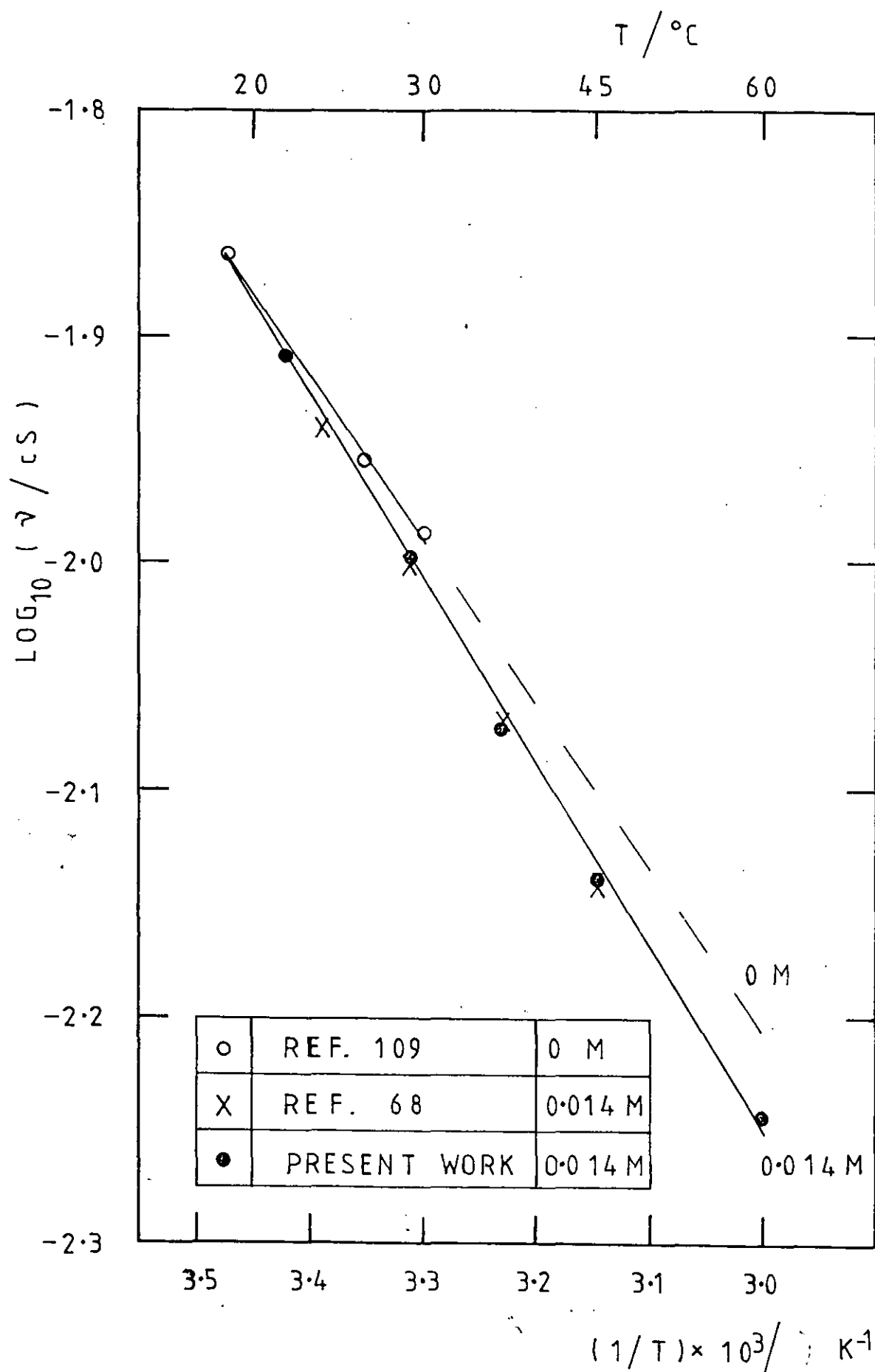
FIG. 10.69   ARRHENIUS PLOT FOR DIFFUSION COEFFICIENT OF

ACID COPPER SULPHATE ELECTROLYTES

1.5 M H_2SO_4

0.014 - 0.7 M $CuSO_4$
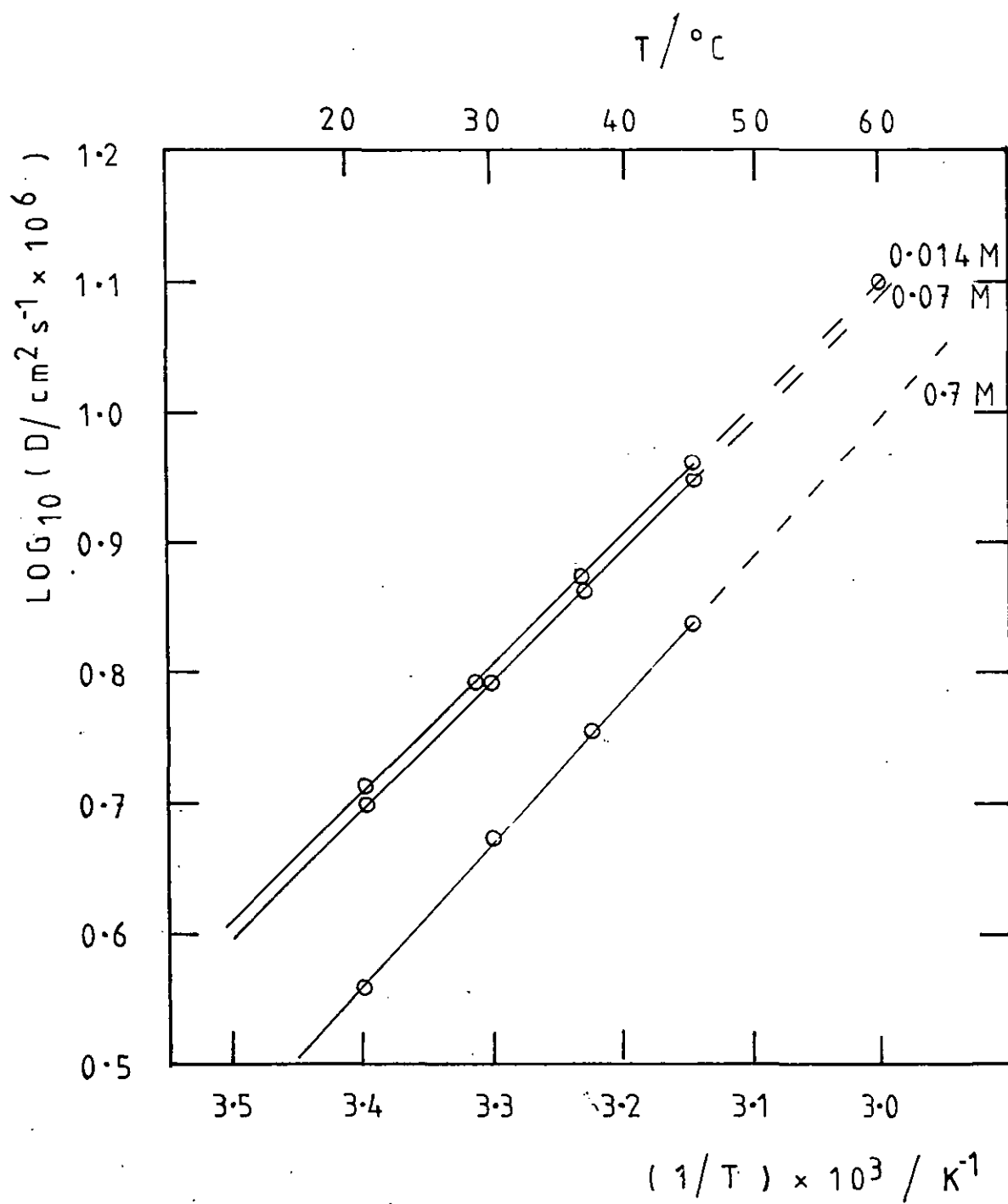
FIG. 11.1   'POLARISATION CURVES' FOR COPPER DEPOSITION IN THE

           500A PILOT PLANT

20° C

Conditions as in Table 11.1

Note: These are not steady state curves, as the effective concentration

      in the reactor decreased as the current was increased.   The

      concentration figures refer to samples taken when the current

      was ca. 200 A.

		INITIAL [Cu] /mg dm^{-3}	
		C$_{IN}$	C$_{OUT}$
A	○	233	138
B	□	625	360
C	●	—	7·1
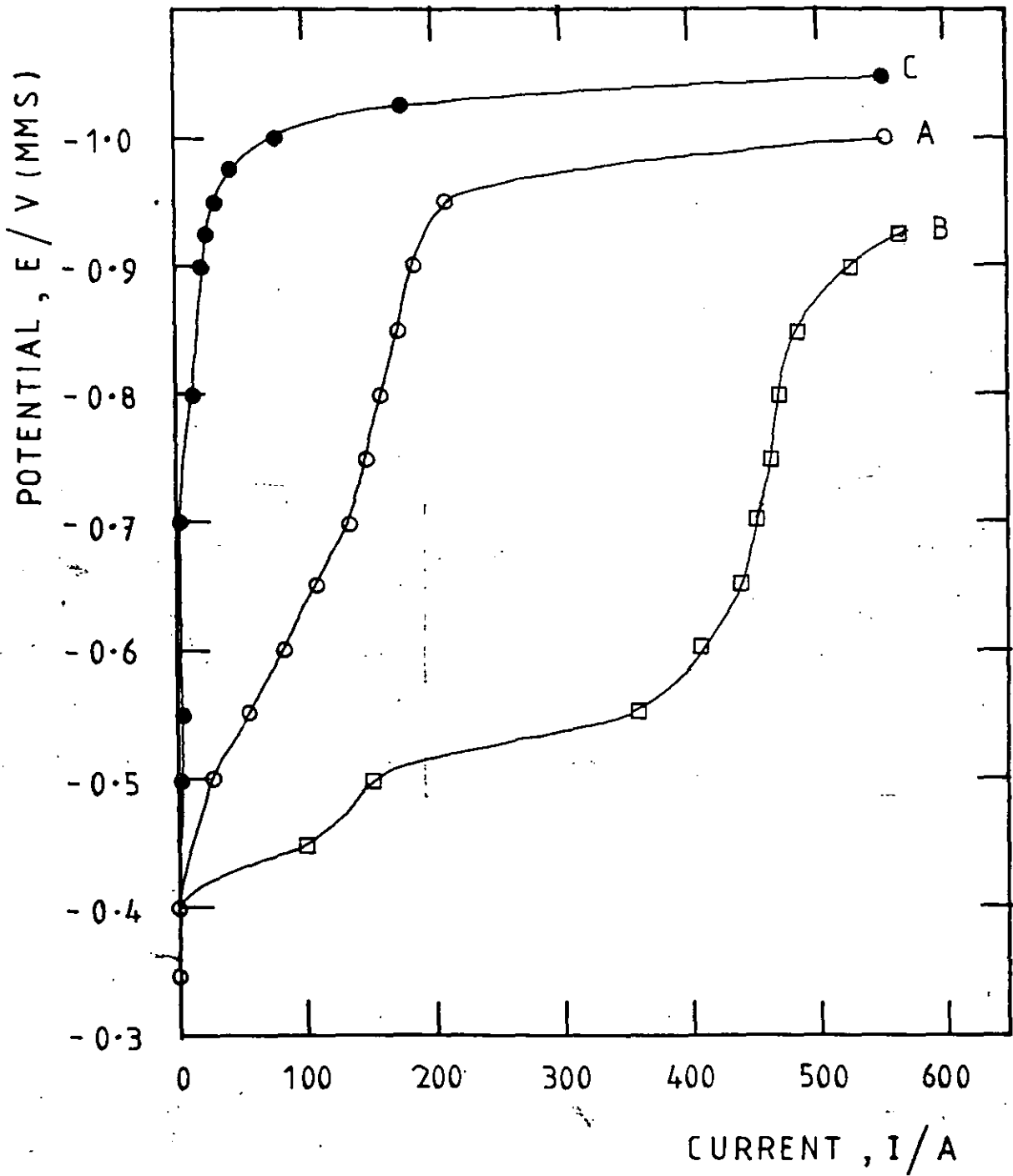
FIG. 11.2   POLARISATION CURVES IN THE VICINITY OF THE LIMITING

              CURRENT : 500A PILOT PLANT, COPPER DEPOSITION

Conditions as for Fig. 11.1.

Only currents in the region of mass transport control were used,

in order not to change the reactor conversion and hence concentration.

The concentration figures refer to samples taken from the reactor in

the vicinity of the limiting current.

	C_{OUT} , Cu
A	9 5
B	175
C	59.
D	40

E / V (MMS)
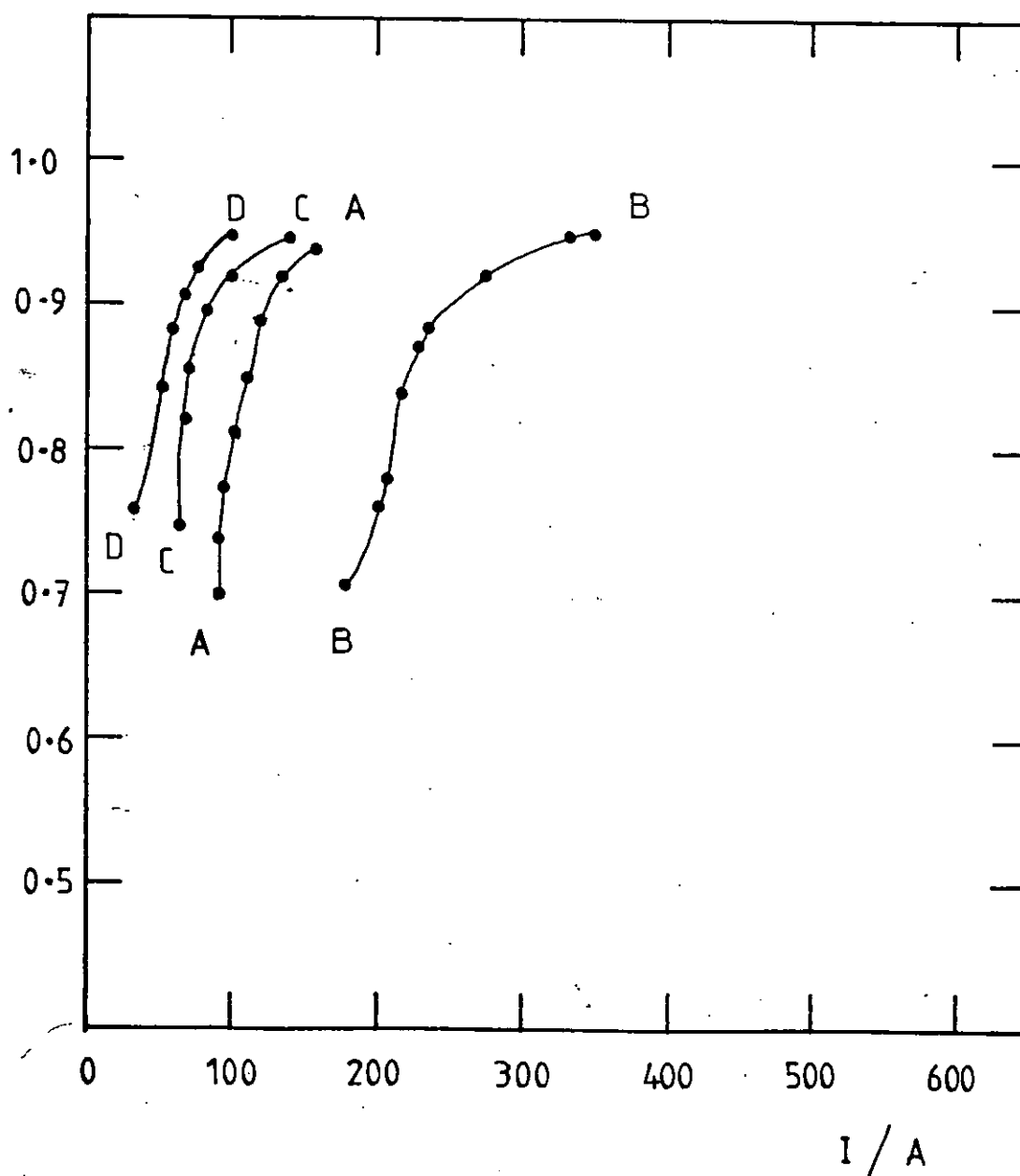
FIG. 11.3   LIMITING CURRENT AS A FUNCTION OF (OUTLET) COPPER

CONCENTRATION

Indicating $I_L \propto C_{OUT}$, approximately with the slope giving the

averaged mass transport coefficient as 0.262 cm s^{-1}.

Data from Polarisation Curves and Table 11.2.

I_L / A

500

400

300

200

.100

0

0   100   200   300

CONCENTRATION, C / mg dm^{-3}
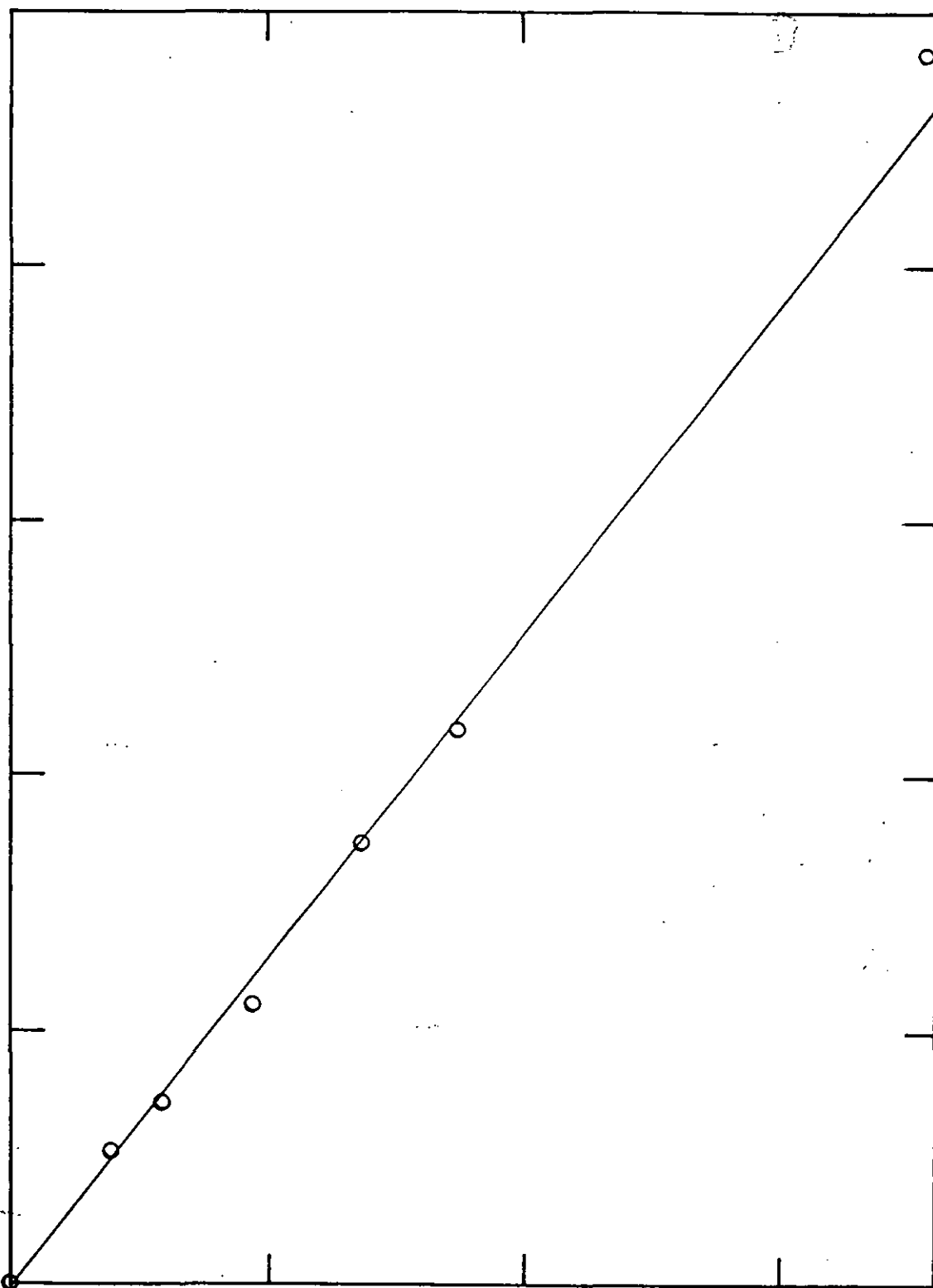
FIG. 11.4   LIMITING CURRENT – COPPER CONCENTRATION RELATIONSHIP

FOR STEADY STATE ELECTROLYSIS.

Conditions as in Table 11.1

Ideally, $I_L \propto C$,   and the line drawn gives the mass transport
coeff. as 0.393 cm s^{-1}.
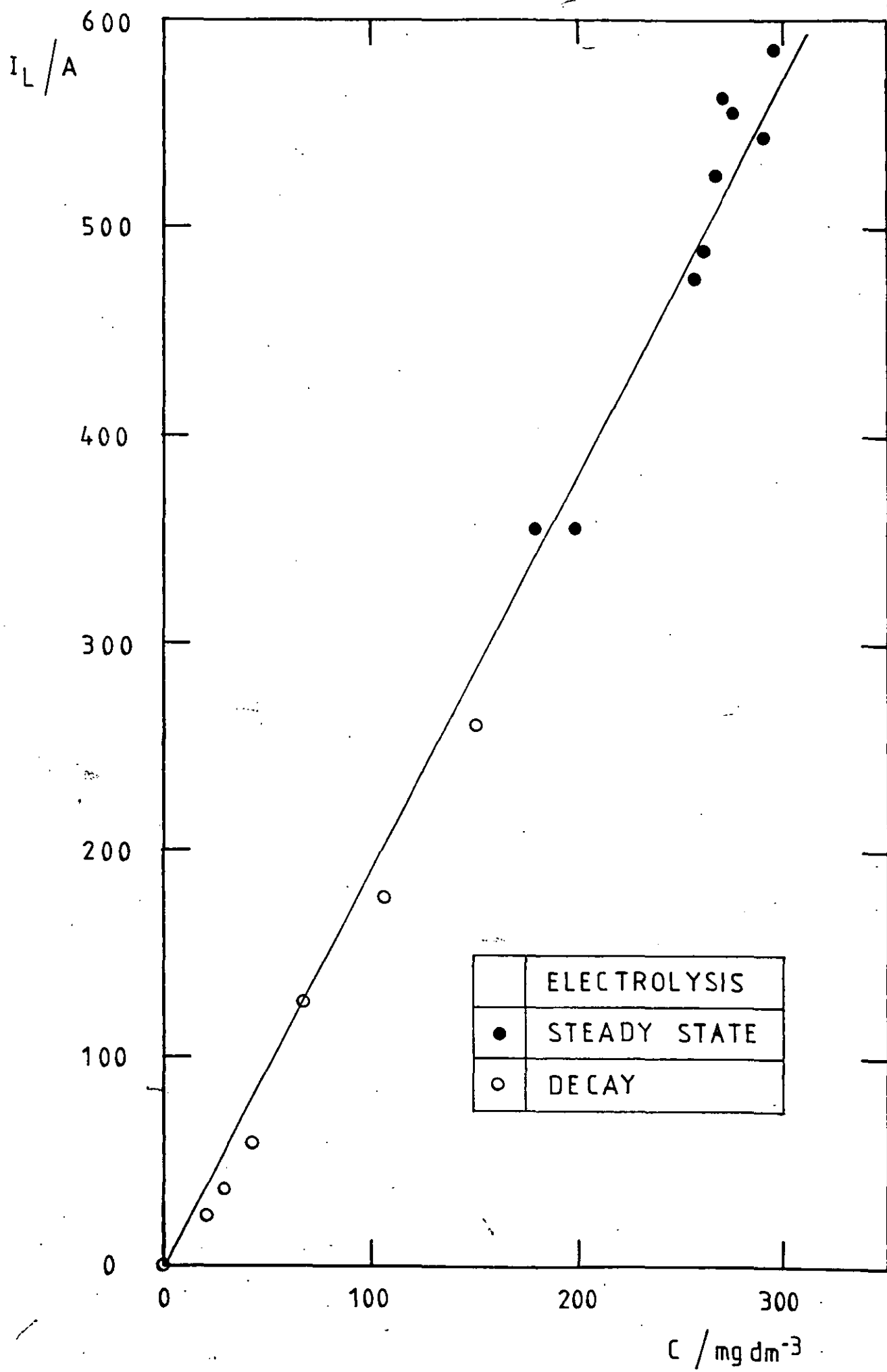
FIG. 11.5   CONCENTRATION DECAY FOR COPPER DEPOSITION

Note: The break in the curve after 20 mins. is due to an abrupt,

deliberate change in the flow rate through the reactor.
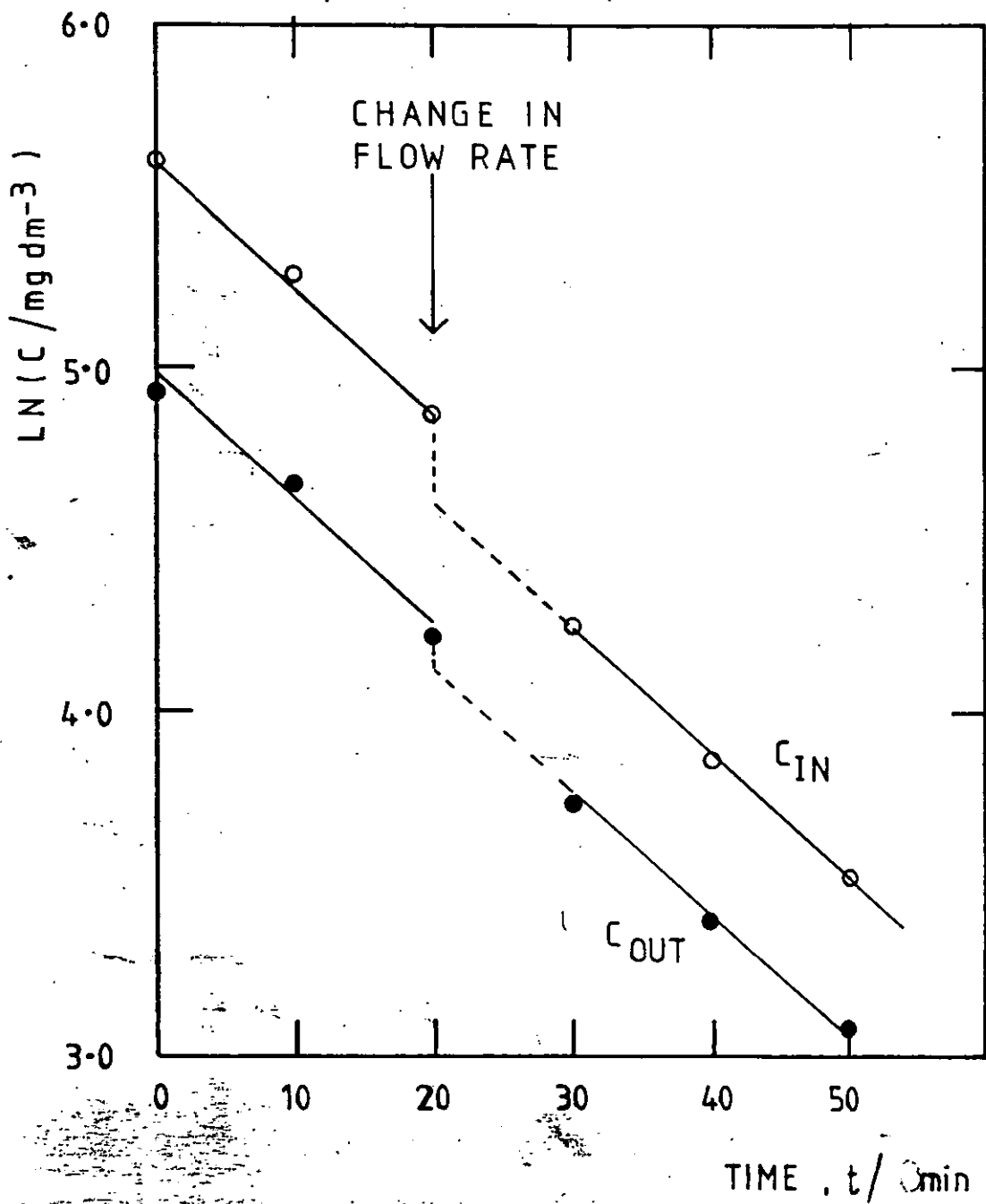
11.6 CURRENT DECAY FOR COPPER DEPOSITION

Corresponding to Fig. 11.5.

Showing both total current, I and calculated limiting current, I_L.
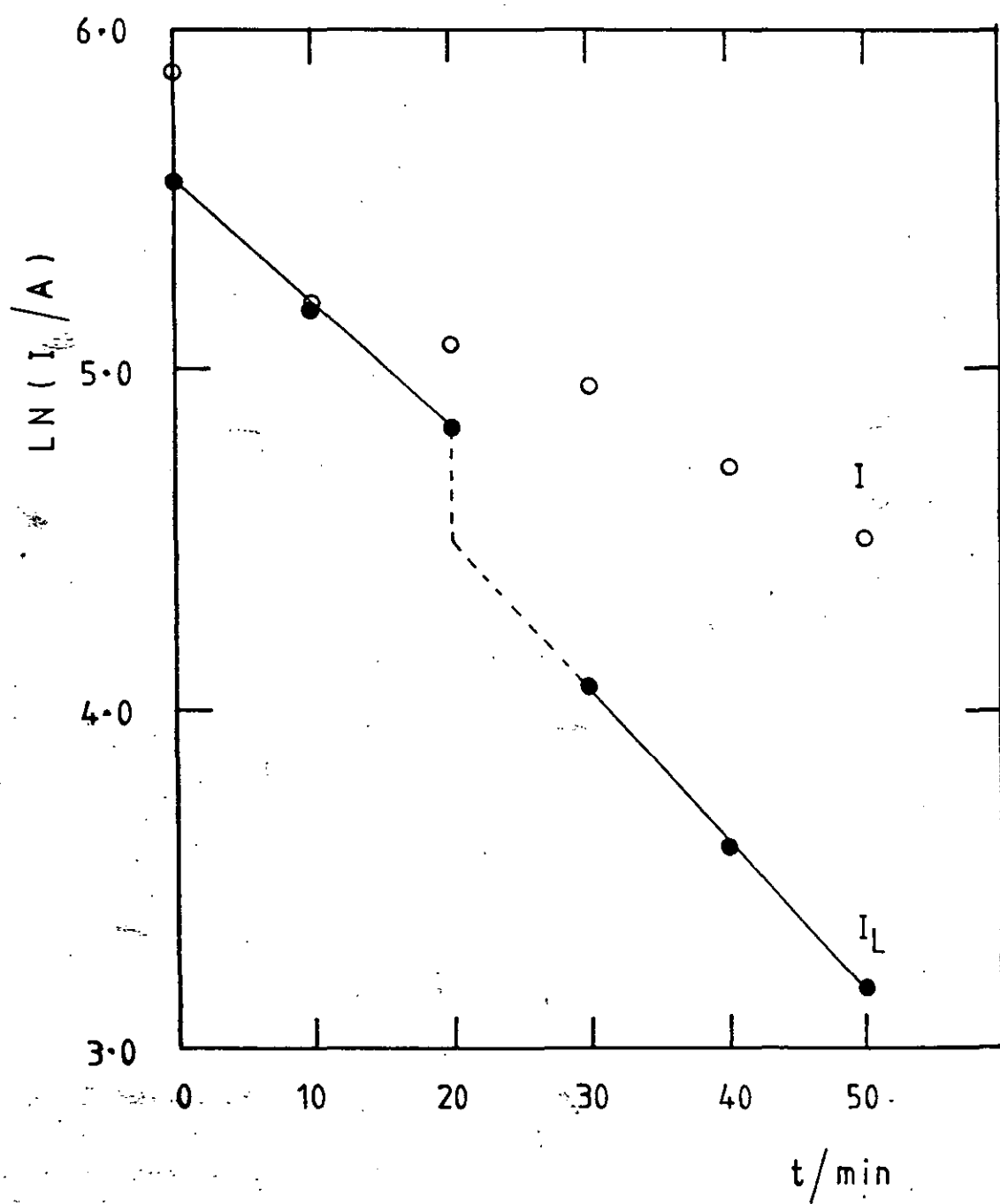
FIG. 11.7   CELL VOLTAGE AND FARADAIC POWER AS A FUNCTION

OF CURRENT for the 500A Pilot Plant

The slope of the cell voltage/current curve gives the averaged,

effective reactor resistance as 0.0138 ohm.
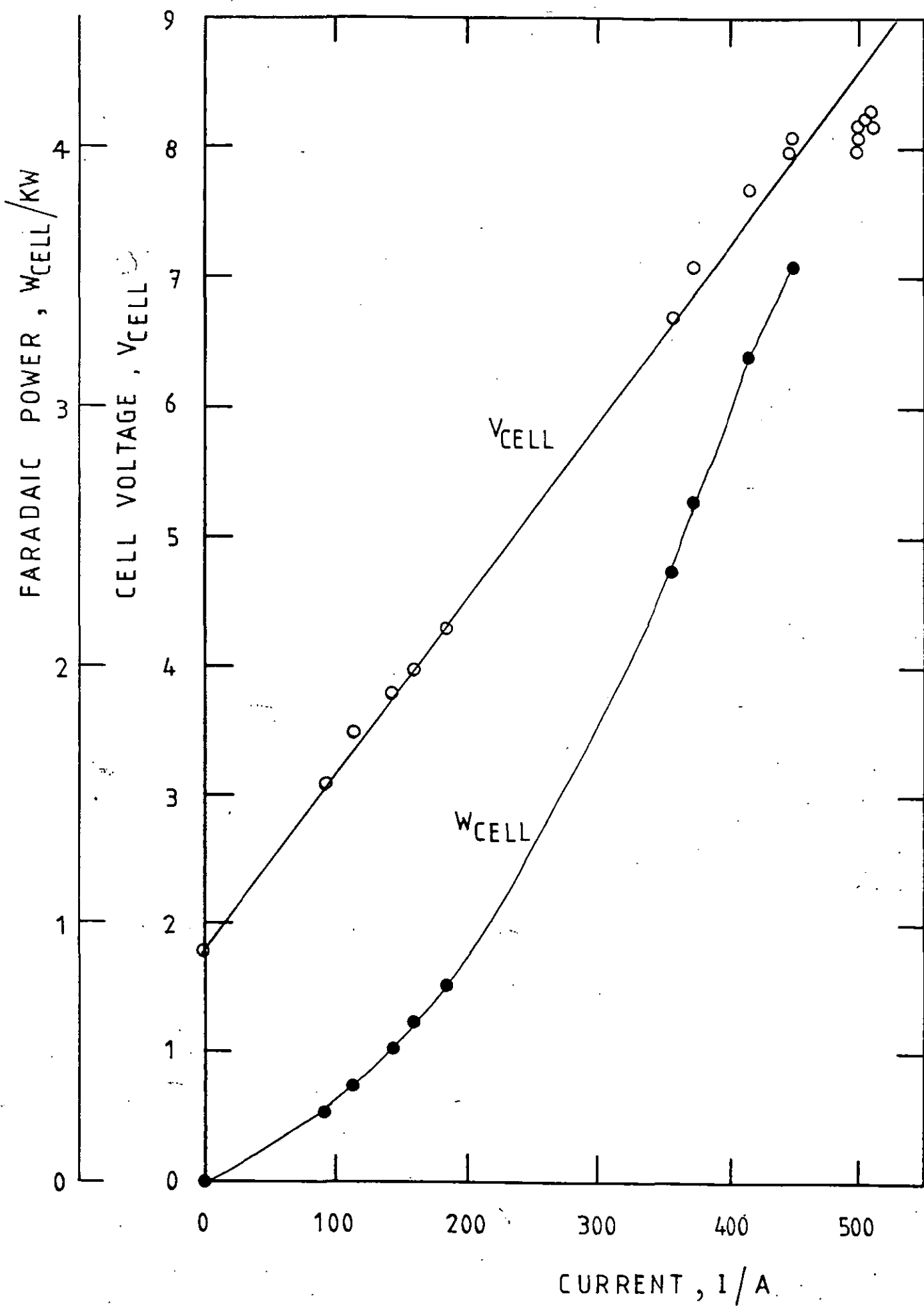
FIG. 11.8   POLARISATION CURVES FOR CADMIUM DEPOSITION FROM

ZINC CALCINE LIQUOR

112 g dm^{-3} Zn

60° C.

pH   typically   2.07 initial

2.03 final

	Cd C_{OUT}/mg dm^{-3}
A	3 0 5
B	4 0 5
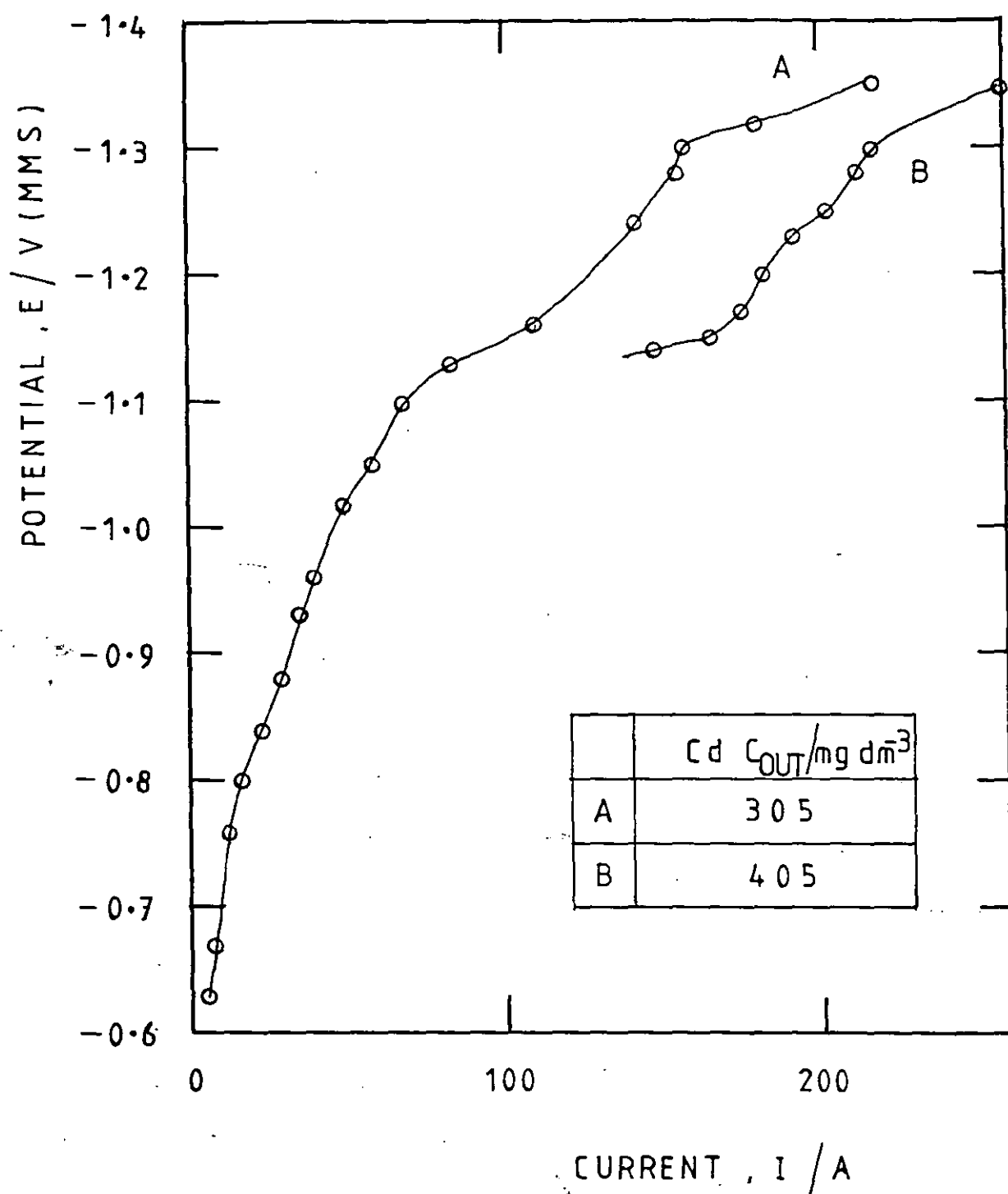
FIG. 11.9   TYPICAL HYDROGEN EVOLUTION POLARISATION BEHAVIOUR

FOR THE 200 A ECO-CASCADE CELL

Galvanostatic.

Potentials measured between a reference electrode probe near the

cylinder, in the relevant compartment and a lower brush engaging

on the rotating cylinder shaft below compartment 1.

	COMPARTMENT NO.
○	1
●	2
×	3
+	4
■	5
□	6
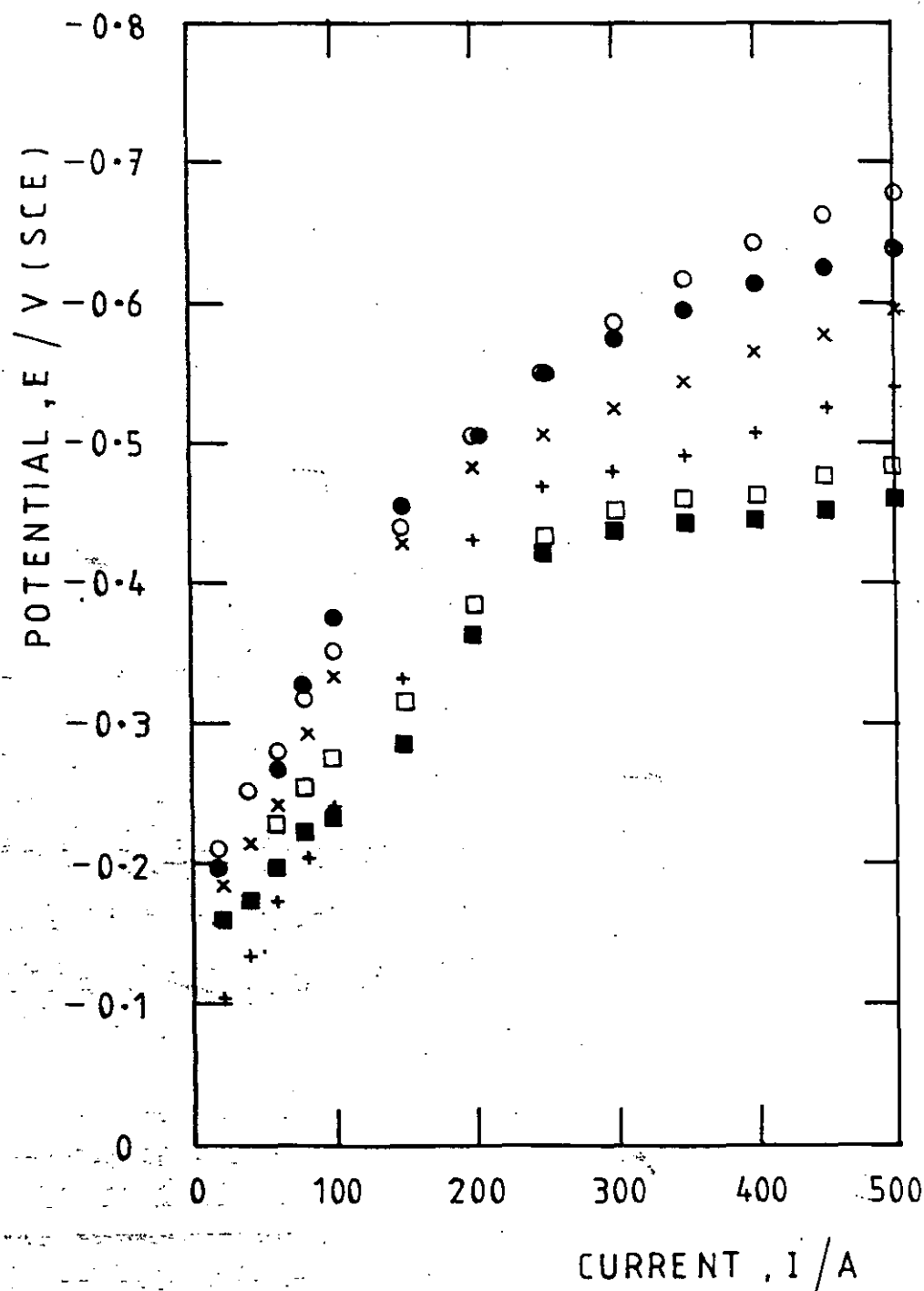
FIG. 11.10   CELL VOLTAGE AS A FUNCTION OF CURRENT:

200A ECO-CASCADE-CELL

Hydrogen Evolution

Anodes pair no. 1 only in use.
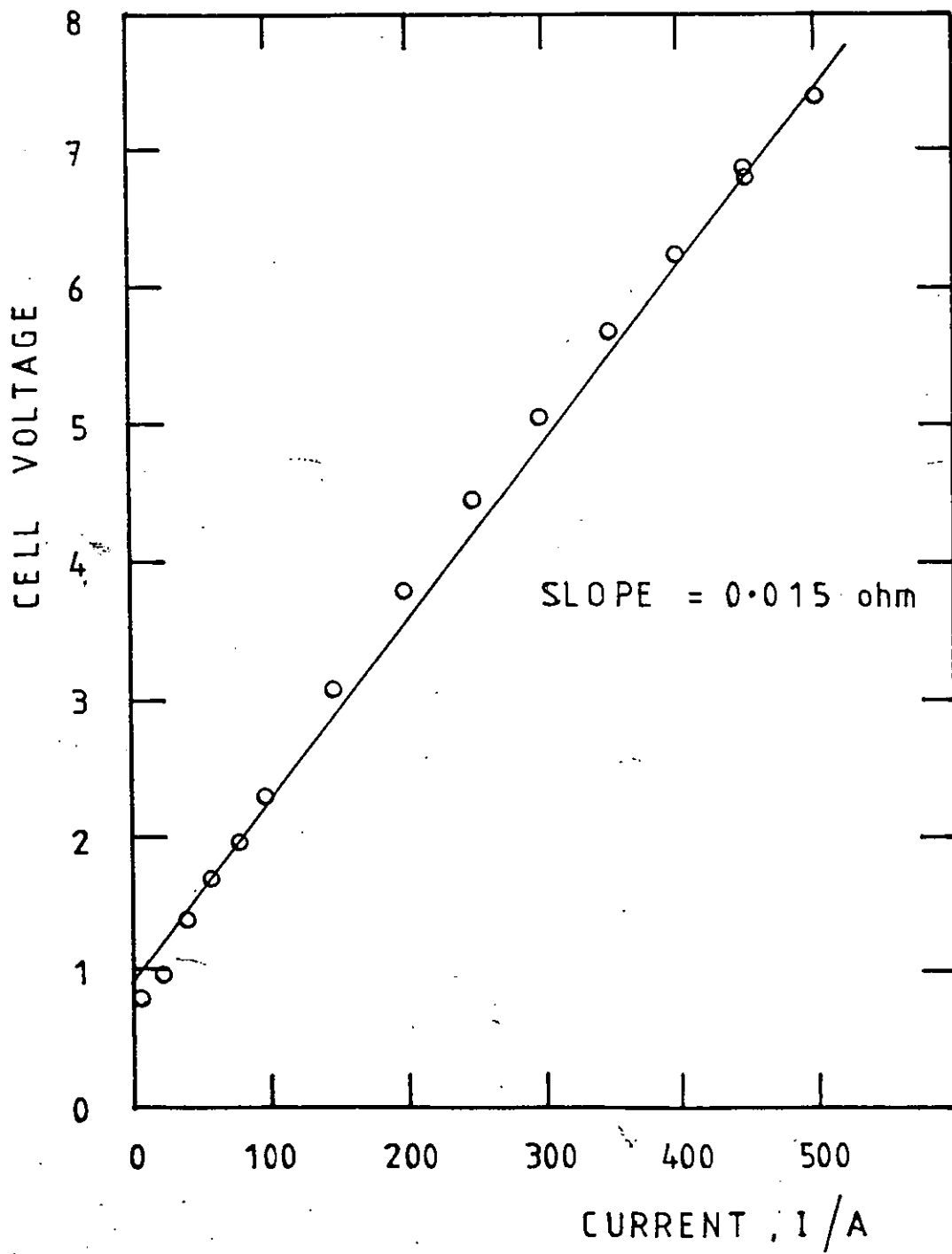
FIG. 11.11   POLARISATION BEHAVIOUR FOR COPPER DEPOSITION

IN THE 200A ECO-CASCADE-CELL

Showing potentials measured in each compartment for various

currents.

Potentials measured as for Fig. 11.10

C_{IN} = 152 mg dm^{-3} Cu

	COMPARTMENT	1
◕		
○		2
+		3
×		4
□		5
■		6
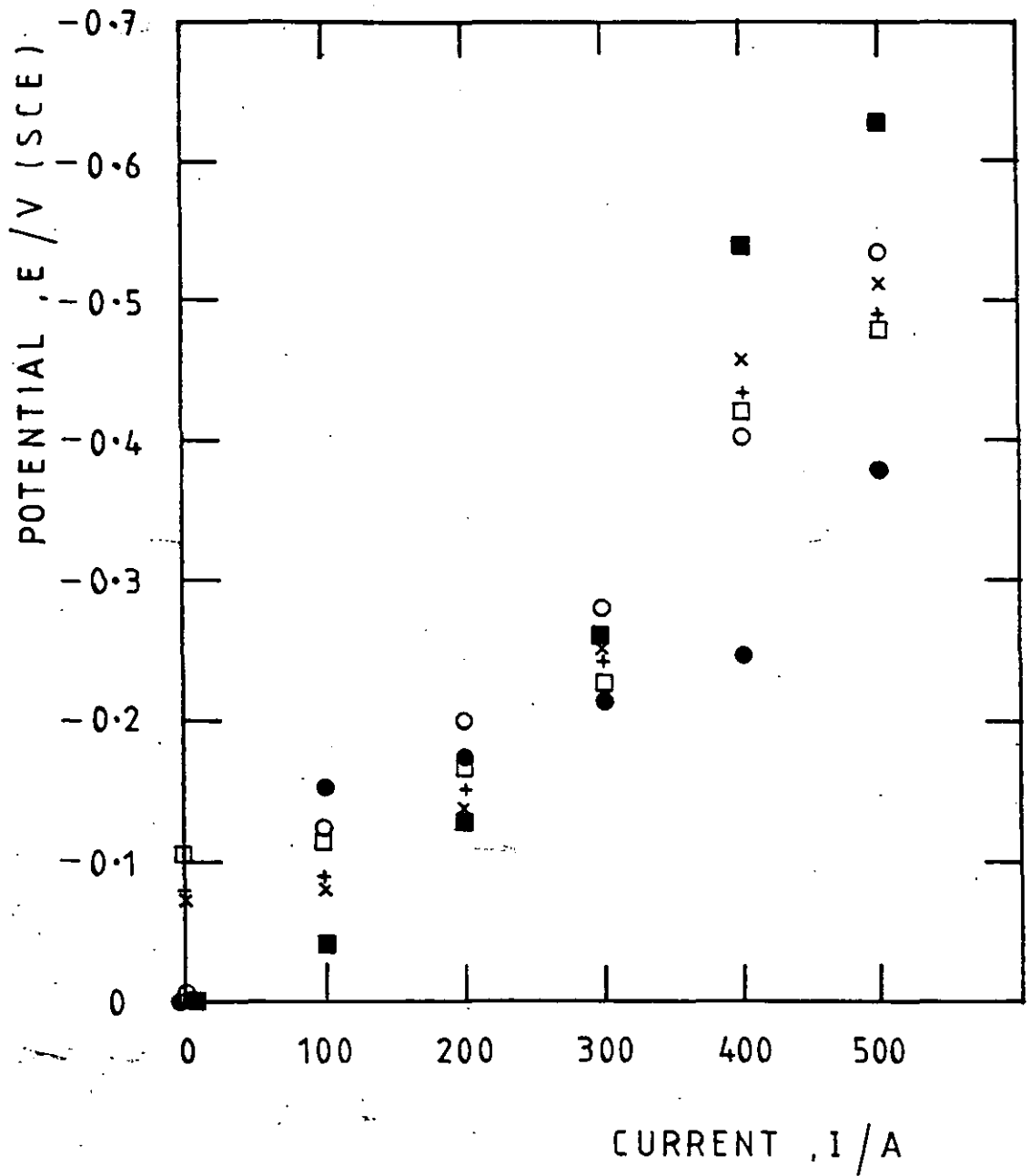
FIG. 11.12   CONCENTRATION DECAY IN THE 200A ECO-CASCADE CELL

REACTOR

Showing Concentration Profiles for the Inlet and Each Compartment

Conditions as for Table 11.7

Current = 300 A

Cell Voltage = 2.7 V
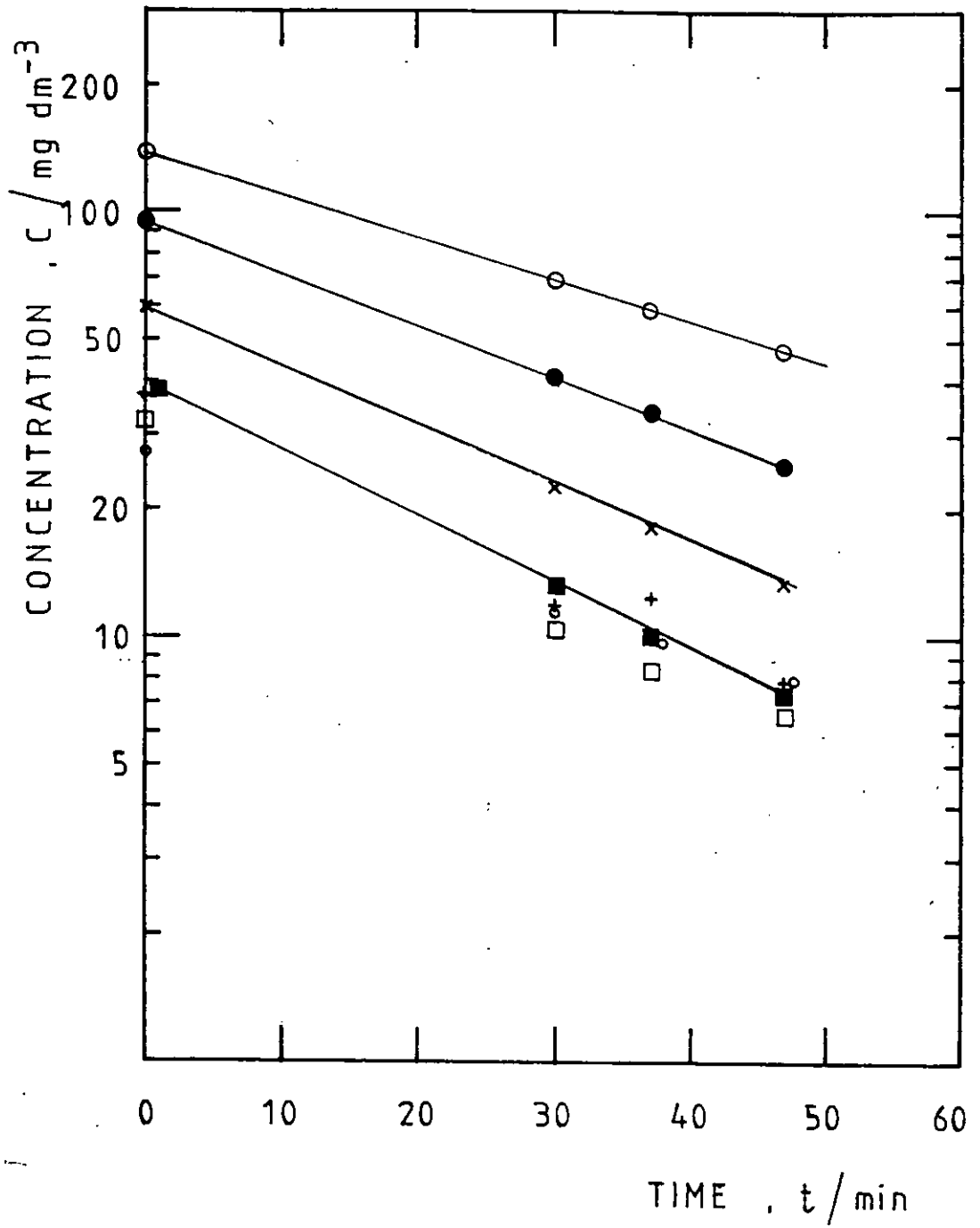
FIGS. 11.13 - 11.16   MASS TRANSPORT DATA FOR ECO-CELL PILOT

PLANTS

(Plots of Modified Chilton-Colburn factor as a function of Reynolds

Number)

11.13   50A Lab. Rig. 1

11.14   100A Mini-Cell

11.15   500 A Pilot Plant

11.16   2KA Pilot Plant

Copper Deposition from acid sulphate solutions (generally 1M H_2SO_4)

at 60° C.

Selected Data (Points) are compared to the Holland Correlation

(solid line).

$$j_D^{\;1} = St\;Sc^{0.644} = 0.0791\;Re^{-0.08}$$
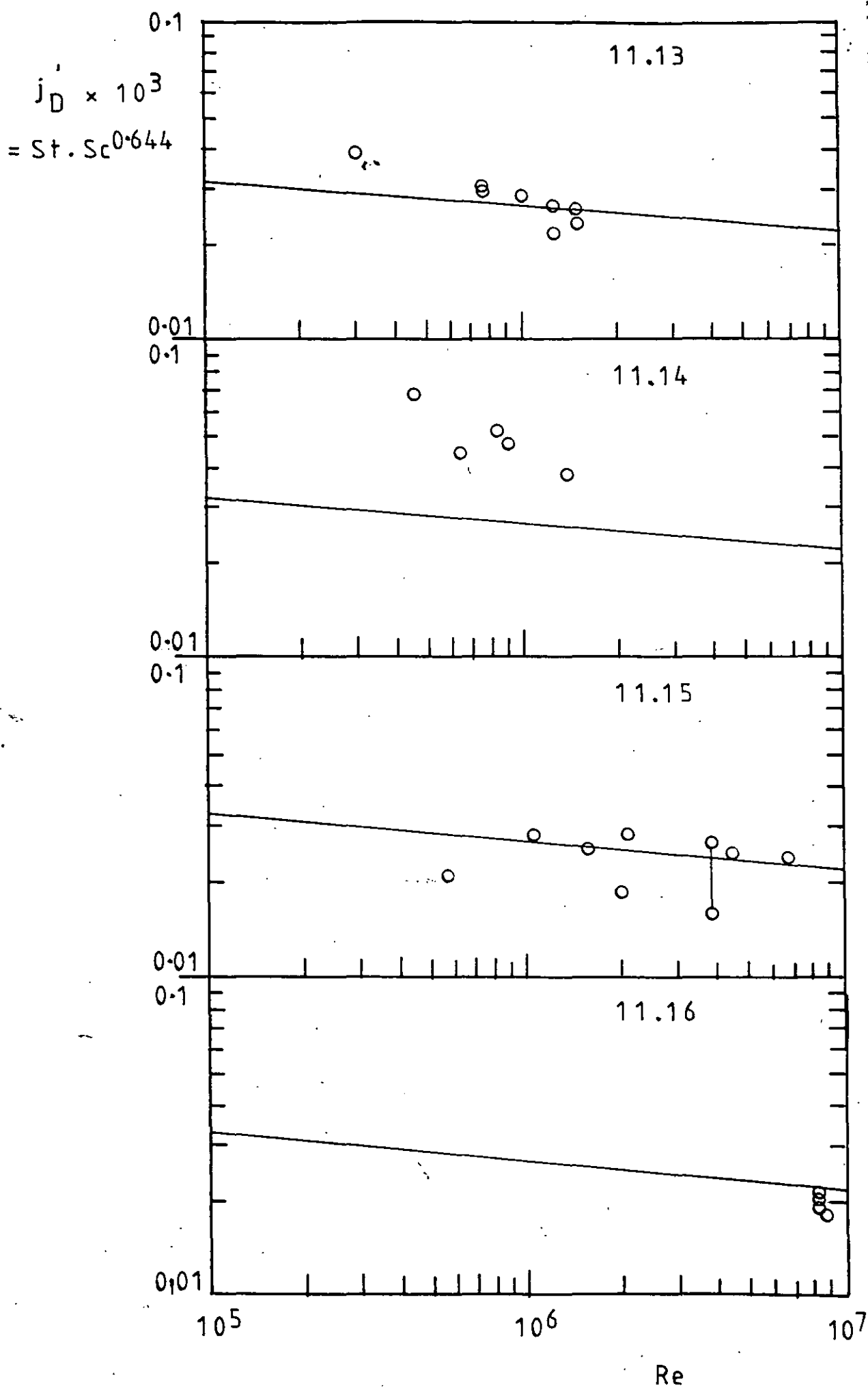
FIG. 11.17 COMPENDIUM OF MASS TRANSPORT DATA FOR ECO-CELL

Composite plot of Figs. 11.13 - 11.16

H : Equation Due to Holland:

$$j_D' = 0.0791 \, Re^{-0.08}$$

ETW : Equation Due to Eisenberg, Tobias & Wilke:

(for a hydrodynamically smooth R.C.E.)

$$j_D' = 0.079 \, Re^{-0.30}$$

TR : Equations due to Theodorsen and Regier

(for saturated roughness)

$$j_D' = \left(1.25 + 5.76 \, \log_{10} \frac{d}{\epsilon} \right)^{-2}$$

TR1 $d/\epsilon = 1000$

TR2 $d/\epsilon = 100$

TR3 $d/\epsilon = 40$
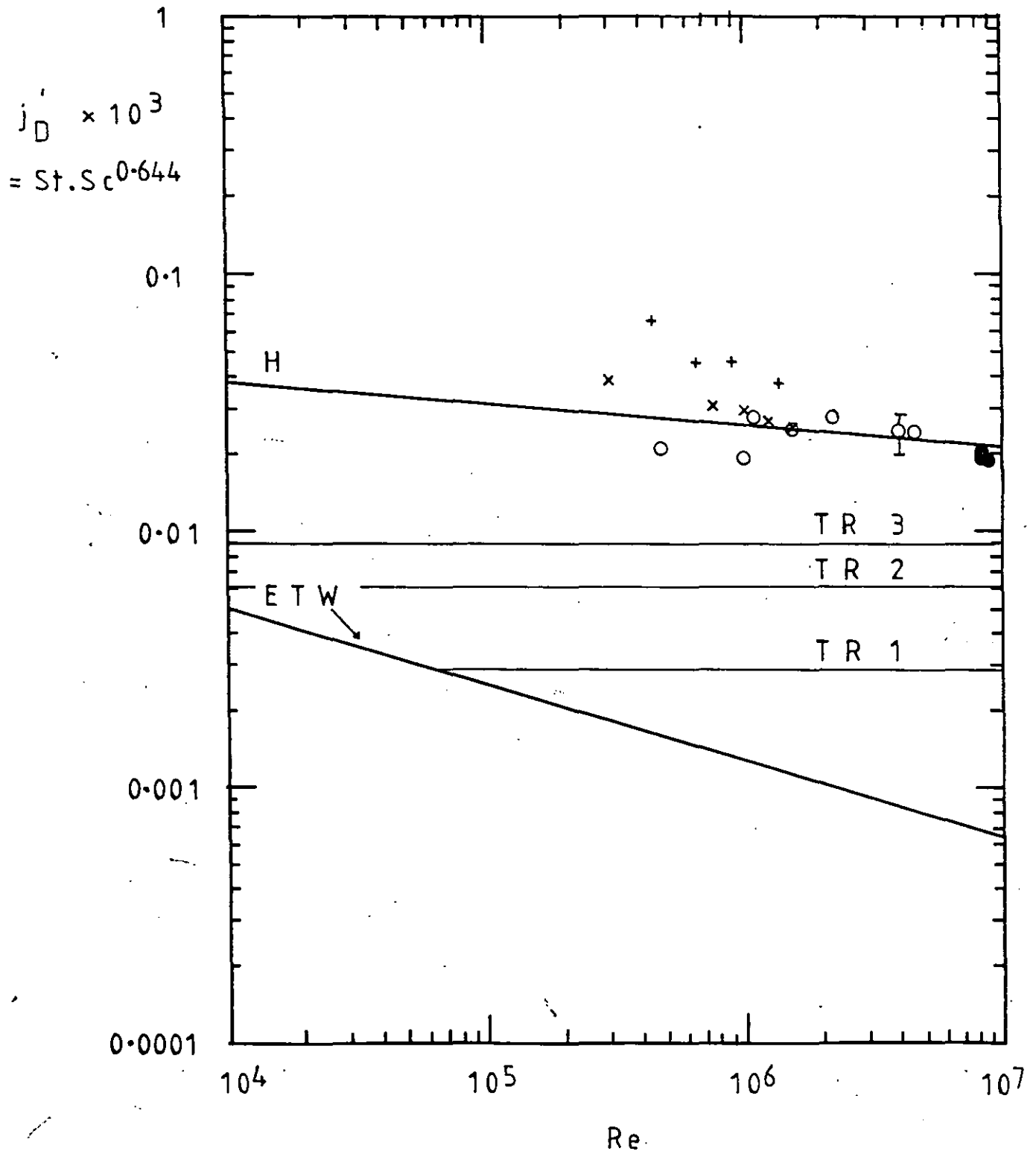
FIG. 11.18   CONCENTRATION PROFILES IN THE 100A

LABORATORY CASCADE REACTOR

slope
$= f_{r,ave} = 0.452$

CONCENTRATION , C / mg dm^{-3}

COMPARTMENT NO. , n
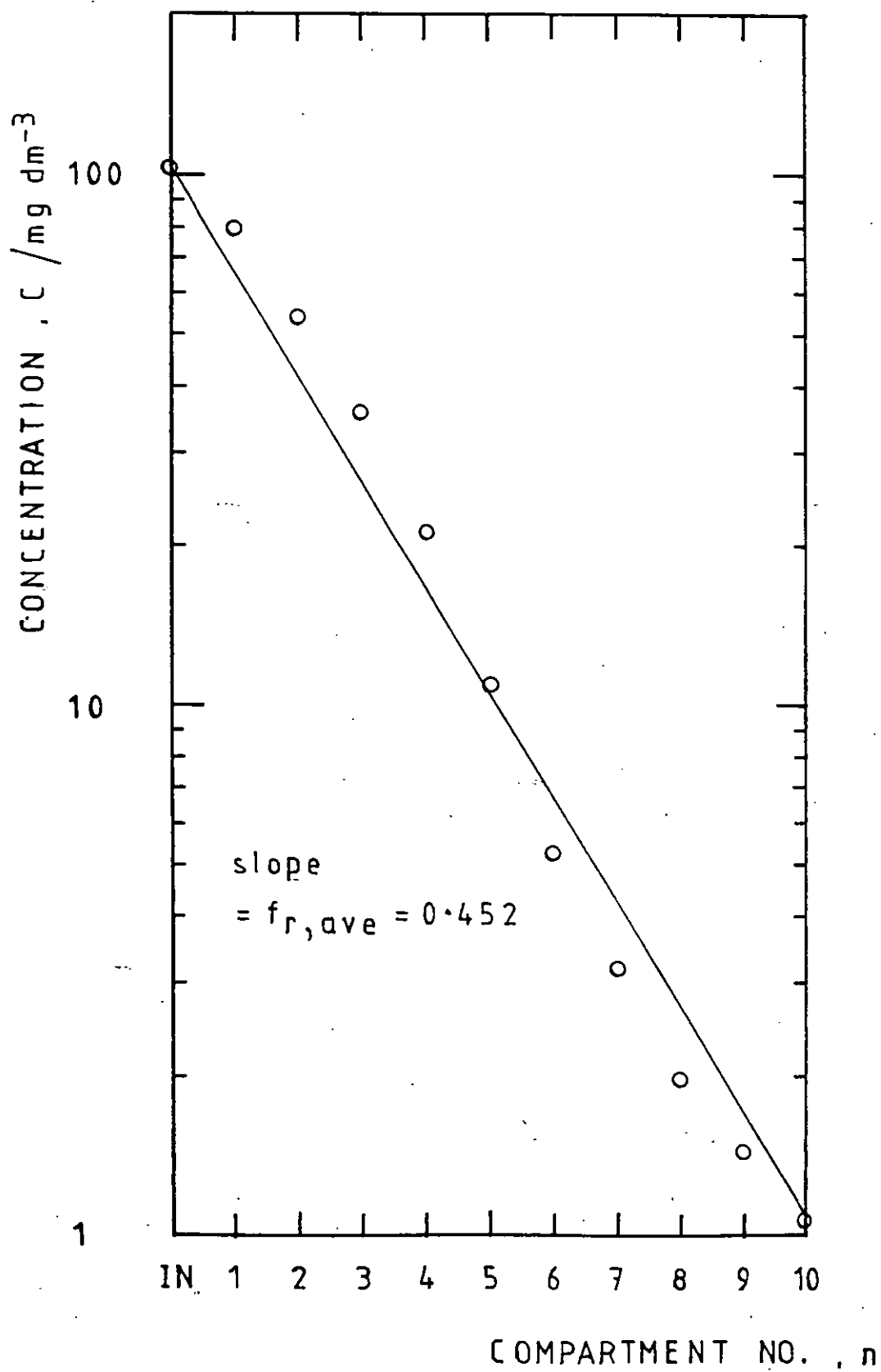
FIG. 11.19   CONCENTRATION PROFILES IN THE 1KA COMMERCIAL

CASCADE REACTOR

slope = $f_{r,ave} = 0.325$

o	≡ TABLE 11.31
●	≡ TABLE 11.32

CONCENTRATION , C / mg dm⁻³

COMPARTMENT NO., n
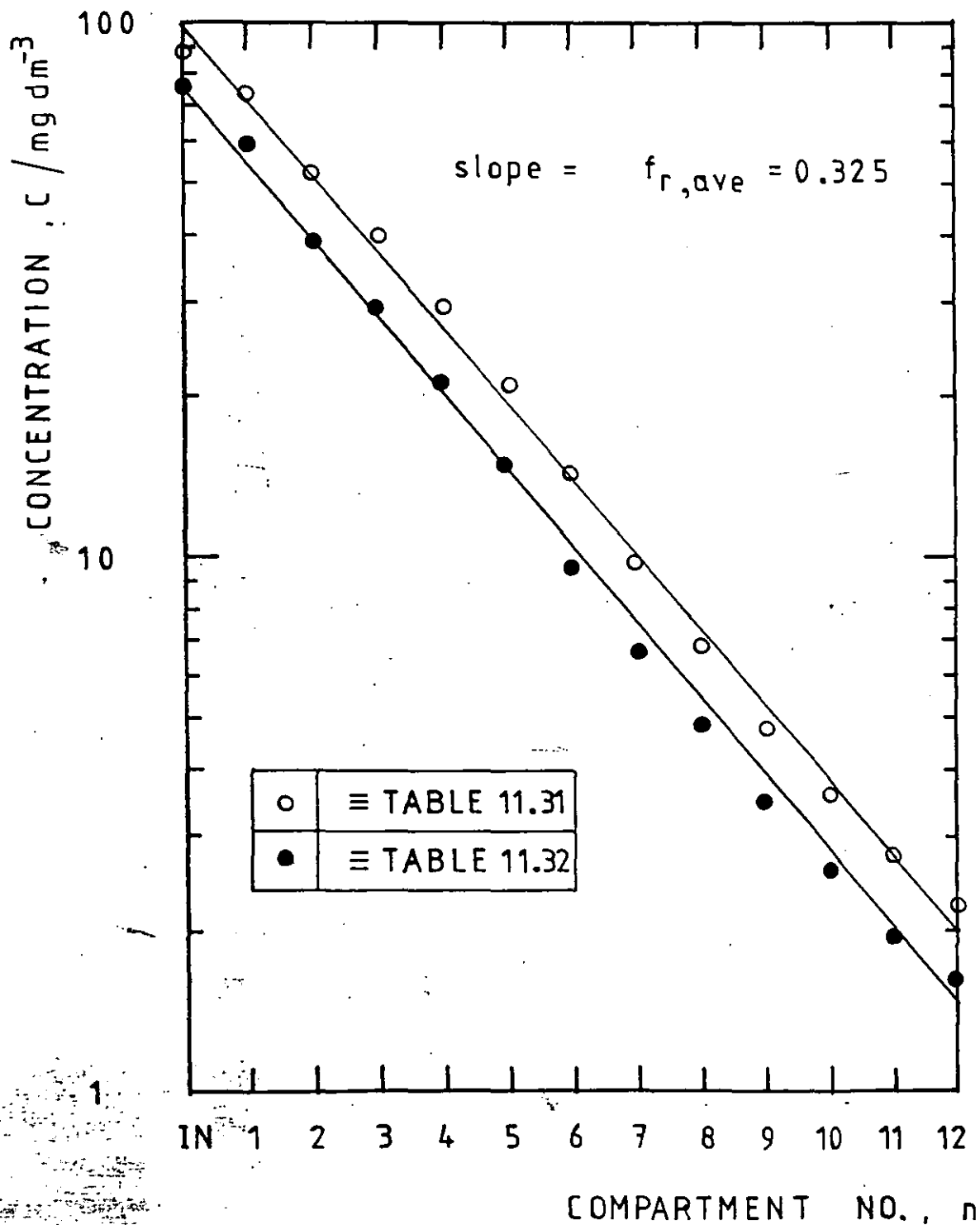
APPENDIX 1

Computer Programme 'Superspleen' for Calculation and Analysis of

Mass Transport Data

The programme devised by the author and written largely by Mr. T.C. Hopkins

receives as input data EITHER:

1) sets of (St), (Re) and (Sc)

.OR:

2) i_L, z, C, U, d, ϑ and D from which (St), (Re) and (Sc) are calculated.

To correlate the results, a power function is assumed:

$$(St) = a \ (Re)^b \ (Sc)^c$$

Taking Logarithms

$$\log (St) = b \ LOG \ (Re) + c \log (Sc) + \log a$$

A three dimensional least squares analysis is performed on log (st),

log (Re) and log (Sc) using standard 'NAG' library routines GO2BGF and

GO2CGF. These routines also output a statistical package of information

(see Table 10.2) on the constants a, b and c.

Tabular and graphical Comparison is made with literature correlations

due to Eisenberg, Tobias and Wilke:

$$(St) = 0.079 \ (Re)^{-0.30} \ (Sc)^{-0.644}$$

and Robinson and Gabe:

$$(St) = 0.079 \ (Re)^{-0.31} \ (Sc)^{-0.59}$$

A plot is also offered of $(St)(Sc)^{-c}$ against (Re) on log – log co-ordinates.

Further information is available from the programme listing, or its

accompanying notes for guidance.

APPENDIX - 2

GENERAL PROPERTIES OF PERFLUOROCARBON, CATION EXCHANGE MEMBRANES

A. NAFION type XR-400/425 (as used in the Pilot Plant Experiments)

Supplier: E. I. Du Pon de Nemours Co.,

            Plastics Dept.,

            'Nafion' Membrane Venture,

            Wilmington,

            Delaware 19898,

            U.S.A.

Properties

PROPERTY	VALUE	
Electrical resistance	3.8	ohm cm^2
Permselectivity		
(1.0NKCl /3.0N KCl)	7.0	%
Thickness at 50% R.H.	10	mils
Ion Exchange Capacity	0.83	meq g^{-1}
Tensile Strength, wet	30	lb in^{-2}
Elongation, wet	150	%
Electroosmotic transport		
(0.5N H_2SO_4, 30° C)	50	ml F^{-1}
Dimension Stability	11	%
(50% R.H. to wet)		

Description: the perfluorosulphonic acid membrane is a homogeneous
film of a completely fluorinated polymer containing pendant sulphonic
acid groups.   The membrane is reinforced by a 'Teflon' TFE Fluorocarbon
resin.

8. IONAC type MC3470 (as used in the laboratory reactor)

Supplier: Ionac Chemical Company,

                 Sybron Corporation,

                 Box 66,

                 Birmingham,

                 New Jersey 08011,

                 U.S.A.

Properties:

PROPERTY	VALUE	
Electrical Resistance		
(0.1N NaCl/1.0N NaCl)	9.6/4.8	ohm cm^2
Permselectivity		
(0.5N NaCl/1.0N NaCl)	96.2	%
Water Permeability in ml/hr/ft^2		
10 psi	5	
Mullen Burst Strength	190	lb in^{-2}
Thickness	13 - 14	mils
Density	405	gm^{-2}
Capacity	1.05	meq g^{-1}
	0.038	meq cm^{-2}
Dimensional Stability	Good	

Description:

The Ionac membrane is somewhat cheaper and less chemically stable
than the Du Pont one, but proved quite suitable for short-term
laboratory studies.

Surface Profilometric Measurement

The principle of a 'Talysurf' measurement technique is shown in the
first figure.   The stylus slowly traverses the workpiece and
accurately follows the surface irregularities.   The stylus is
equipped with an optical transducer;   the vertical movements are
converted into an electrical signal.   This signal may be processed
for display in either of the following ways:

a) a graph representing the profile, with considerable magnification
   of the vertical height (1K to 50K x), and a smaller magnification
   (20 to 100 x) of the horizontal spacing.

b) a (simultaneous) meter indication of the Roughness Average, Ra

Ra is defined as the arithmetical average of the departures of the
profile above and below the reference line (centre of mean line)
throughout the set sampling length.   (See the second and third
figures).

PRINCIPLE OF THE TALYSURF

a) Schematic of the Measurement Principle

    A Amplifier Circuitry

    T Traverse Unit

    P Pick-up

    S Stylus

    W Workpiece

    M Meter

    R Recorder (electrographic)

b) Definition of Centre Line

Over a length L, the centre line is drawn such that the sum of

the areas bounded by the surface profile above the line is equal

to the sum of those below the line

Area A + C + E + G = Area B + D + F + H

c) Definition of Roughness Average, Ra

$$Ra = \frac{h_1 + h_2 + h_3 \ldots}{L} / l$$

$$= \frac{1}{L} \int_o^L h.dl$$

where L is the sampling length
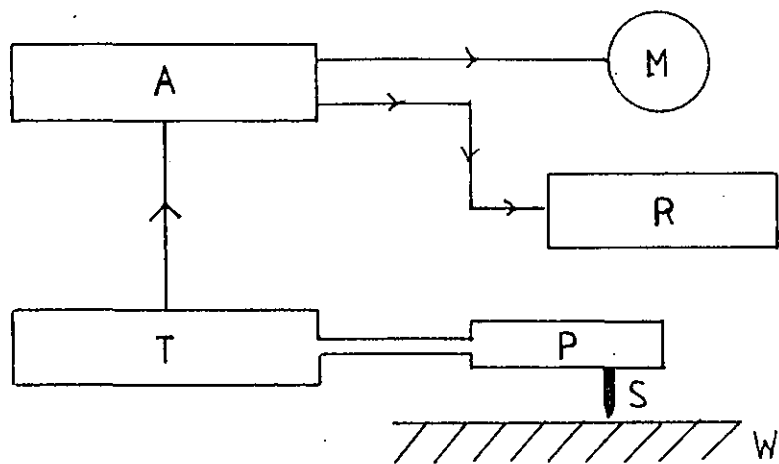
a)
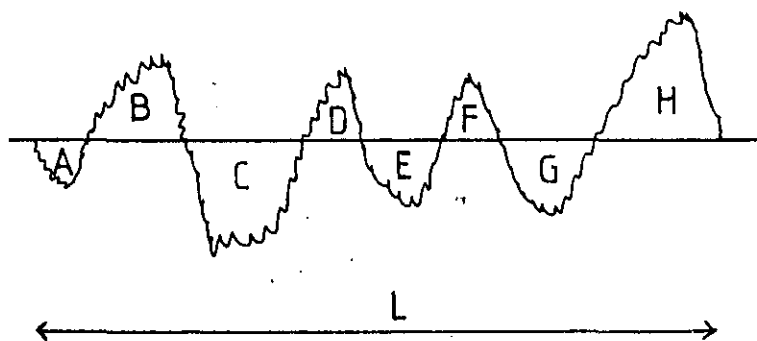
b)
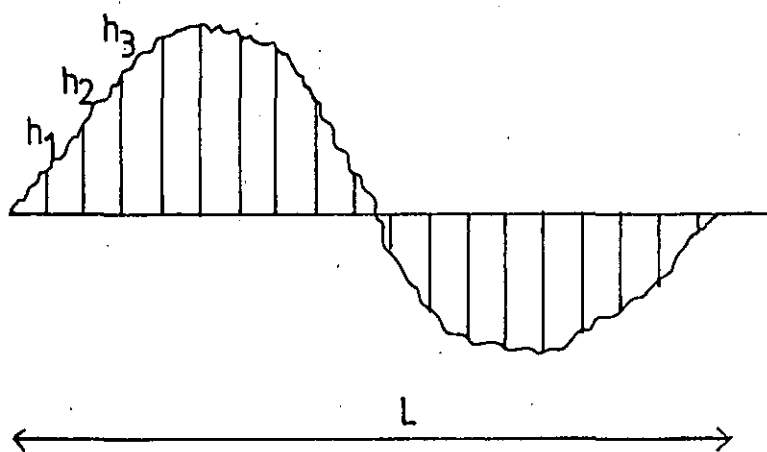
c)

REFERENCES

1. "Mining Annual Review"

   Mining J., London, (1975)

2. Nurnberg H.W.

   Electrochimica Acta $\underline{22}$ (1977) 935

3. Reynolds O.

   Phil. Trans. Roy. Soc., London, (1883)

4. Prandtl L.

   "The Mechanics of Viscous Fluids"

   Durand G.W.F. (Ed.), Julius Springer, Berlin (1935)38

5. ref. 4 p. 136

6. Nikuradse J.

   Beilage zu Forschung auf dem Gebiete des Ingenieurwesens, Ausg. B.

   Bd. $\underline{4}$, July-Aug. (1933)

7. Moody G.

   Trans. Amer. Soc. Mech. Engrs. $\underline{66}$ (1944) 671

8. von Karman T.

   Collected Works. Vol. II

   Butterworths, London (1956) 70

9. Theodorsen T. & Regier A.

   N.A.C.A. report no. 793 (1944)

10. Newman J.

    "Electrochemical Systems"

    Prentice Hall, New Jersey (1973)

11. Taylor G.I.

    Phil. Trans. Roy. Soc.   A223 (1923) 289

12. Taylor G.I.

    Proc. Roy. Soc.   A102 (1923) 541

13. Taylor G.I.

          ibid.   A157 (1936) 546

14. Schlicting H.

    "Boundary Layer Theory"

    McGraw-Hill, New York, 6th Ed. (1968)

15. Lin C.C.

    "The Theory of Hydrodynamic Stability"

    Cambridge University Press, Cambridge (1955)

16. Flower J.R., Macleod N. & Shahbendrian A.P.

    Chem. Eng. Sci. 24 (1969) 637

                 24 (1969) 651

17. Donnelly R.J. et al.

    Proc. Roy. Soc.   A246 (1958) 312

18. idem.

               A258 (1960) 101

19. idem.

               A281 (1964) 130

20. idem.

               A283 (1965) 509, 520, 531

21. Chandrasekhar S.

   Proc. Roy. Soc.   A246 (1958) 301

22. Pai S.I.

   N.A.C.A. report no. 892 (1943)

23. Wattendorf F.L.

   Proc. Roy. Soc.   A148 (1935) 565

24. Taylor G.I.

   ibid.   A151 (1935) 494

25. Gabe D.R.

   J. Applied Electrochem.   4 (1974) 91

26. Fage A.

   Proc. Roy. Soc. (London) A165 (1933) 501

27. Comish R.J.

   ibid.   A140 (1933) 227

28. Goldstein S.

   Cambridge Philosophical Soc. 33 (1937) 41

29. Martin B.W. & Payne A.

   Proc. Roy. Soc. (London) A328 (1972) 123

30. Di Prima R.C.

   J. Fluid Mech.   9 (1960) 621

31. Chandrasekhar S.

    Proc. Natn. Acad. Sci., U.S.A.   46 (1960)   137

32. Chandrasekhar S.

    Proc. Roy. Soc. (London)   A265   (1962)   188

33. Krueger E.R. and Di Prima R.C.

    J. Fluid Mech.   19   (1964)   528

34. Kaye J. and Elgar E.C.

    Trans. Amer. Soc. Mech. Engrs.   80   (1958)   753

35. Yamada Y.

    Bull. Jap. Soc. Mech. Engrs.   5   (1962)   302

36. Snyder H.A.

    Proc. Roy. Soc. (London)   A265   (1962)   198

37. Astill K.N.

    Trans. Amer. Soc. Mech. Engrs. J. Heat Transfer

    86   (1964)   388

38. Astill K.N., Gonley J.T. and Martin B.W.

    Proc. Roy. Soc.   (London)   A307   (1968)   55

39. Macleod N. & Ruess T.

    Chem. Eng. Sci.   30   (1975)   235

40. Kosterin S.I., Koshmarov Y.A. & Finatev Y.P.

    Int. Chem. Eng.   2   (1962)   460

41. Bircumshaw L.L. & Riddiford A.C.

   Quart. Revs. (London)　6　(1952)　157

42. Ibl N.

   Chem. Ing. Tech.　35　(1963)　353

43. Ibl N.

   Proc. "Surface 66",　(1966)　48

44. Vielstich W.

   Z. Electrochem.　57　(1953)　646

45. Tobias C.W., Eisenberg M.& Wilke C.R.

   J. Electrochem.　Soc.　99　(1952)　359C

46. Ibl N.

   Chem. Ing. Tech.　33　(1961)　69

47. Ibl N.

   Galvanotechnik und Oberfla_chenschutz　7　(1966).　256

48. Vetter K.J.

   "Electrochemical Kinetics – Theoretical Aspects"

   Academic Press, London,　(1967)

49. Bird, R.B., Stewart W.E. and Lightfoot E.N.

   "Transport Phenomena"

   John Wiley & Sons Inc., New York　(1960)

50. Newman J.

   Adv. Electrochem.　Electrochem. Engng.　5　(1967)　87

51. Newman J.

Ind. Eng. Chem. 60 (1968) 12

52. Planck M.

Ann. Physik u Chem. 39 (1890) 161

53. Nernst W.

Z. Physik. Chem. 47 (1904) 52

54. Ibl N. (Chairman)

"Proposed Nomenclature For Transport Phenomena in Electrolytic Systems",

I.U.P.A.C., (1978)

55. Simmers D.A. and Coney J.E.R.

h J. Mech. Engng. Sci. 21 (1979) 59

56. Sorour M.M. and Coney J.E.R.

J. Mech. Engng. Sci. 21 (1979) 65

57. Eisenberg M., Tobias C.W. and Wilke C.R.

Chem. Engng. Progr. Symp. Ser. 51 (1955) 1

58. Eisenberg M., Tobias C.W. and Wilke C.R.

J. Electrochem. Soc. 101 (1954) 306

59. Levich V.G.

"Physicochemical Hydrodynamics"

Prentice Hall, N. Jersey, (1962)

60. Ibl N.

Electrochim. Acta 1 (1959) 117

61. Colburn A.P.

   Trans. A.I. Ch. E.   29 (1933) 174

62. Hubbard D.W. & Lightfoot E.N.

   Ind. Eng. Chem. Fundamentals   5 (1966) 370

63. Deissler R.G.

   N.A.C.A. report no. 1210 (1955)

64. Lin C.C., Moulton R.W. & Putnam G.L.

   Ind. Eng. Chem.   45 (1953) 636

65. Vieth W.R., Porter J.H. & Sherwood T.K.

   Ind. Eng. Chem. Fundamentals 2 (1963) 1

66. Simmers D.A. and Coney J.E.R.

   Int. J. Heat and Fluid Flow   1 (1979) 77

67. ibid.

   Int. J. Heat and Fluid Flow   2 (1979) 85

68. Robinson D.J.

   Ph.D. Thesis, Sheffield Univ.   (1970)

69. Matuschok J.

   Chem. Ztg.   25 (1901) 601

70. Iimori S.

   Z. anorg. u. allgem. Chem.   167 (1927) 145

71. Kolthoff I.M. & Pearson E.A.

Ind. Eng. Chem. Anal. Edn. <u>3</u> (1931) 381

72. Chin D.T., Viswanathan K. & Gutowski R.

J. Electrochem. Soc. <u>124</u> (1977) 713

73. Sedahmed G.H., Abd-el-naby B.A. & Abdel-khalik A.

J. Appld. Electrochem. <u>7</u> (1977) 355

74. Krishna M.S. & Jagannadharaju G.J.V.

Indian J. Technol. <u>3</u> (1965) 263

75. Bazan J.C. & Arvia A.J.

Electrochim. Acta <u>10</u> (1965) 1025

76. Leitz F.B. & Marincic L.

J. Appld. Electrochem. <u>7</u> (1977) 473

77. Arvia A.J., Carrozza J.S.W. & Marchiano S.L.

Electrochim. Acta <u>9</u> (1964) 1483

78. Lin C.C.

Ind. Eng. Chem. <u>43</u> (1951) 2136

79. Rotte J.W.

Chem. Eng. Sci. <u>24</u> (1969) 1009

80. Sioda R.E.

Electrochim. Acta <u>13</u> (1968) 375

81. Despic A.R., Konjovic M.N. & Mitrovic M.

    J. Appld. Electrochem.   7 (1977) 545

82. Arvia A.J. & Carrozza J.S.W.,

    Electrochim. Acta!   7 (1962) 65

83. Robinson D.J. & Gabe D.R.

    Trans. Inst. Met. Finish.   48 (1970) 35

84. Gabe D.R. & Robinson D.J.

    Trans. Inst. Met. Finish.   49 (1971) 17

85. Carbin D.C. & Gabe D.R.

    Electrochim. Acta.   19 (1974) 645

    J. Applied Electrochem.   5 (1975) 129, 137

86. Carbin D.C.

    Ph.D. Thesis, University of Sheffield (1972)

87. Kreysa G., Pionteck S. & Heitz E.

    J. Appld. Electrochem.   5 (1975) 305

88. Cornet I., Lewis W.N. and Kappesser R.

    Trans. Inst. Chem. Engrs.   47 (1969) T222

89. Cornet I. and Kappesser R.

    ibid.   47 (1969) T194

90. Sedahmed G.H., Abd-el-naby B.A. & Abdel-Khali A.

    Corr. Sci.   17 (1977) 865

91. Eisenberg M., Tobias C.W. & Wilke C.R.

    J. Electrochem. Soc.   100 (1953) 513

92. Tvarusko A.

    ibid.   119 (1972) 43

93. Pickett D.J. & Stanmore B.R.

    J. Applied Electrochem.   5 (1975) 95

94. Postlethwaite J., Ong K.L. & Pickett D.J.

    Symp. Electrochem. Eng., Newcastle Univ. Vol 1, (1971)

95. Shemitt L.W. & Sedahmed G.H.

    J. Applied Electrochem.   6 (1976) 474

96. Mohanta S. & Fahidy T.Z.

    ibid.   7 (1977) 237

97. Podesta J.J., Paus G.F. & Arvia A.J.

    Electrochim. Acta   19 (1974) 583

98. Smith A.F.J. & Wragg A.A.

    J. Applied Electrochem.   4 (1974) 219

99. Pickett D.J. & Ong K.L.

    Electrochim. Acta   19 (1974) 875

100. Ross T.K. & Wragg A.A.

    Electrochim. Acta   10 (1965) 1093

101. Fenech E.J. & Tobias C.W.

　　　Electrochim. Acta 　　　　　　　2　(1960)　311

102. Wragg A.A. & Nasiruddin A.K.

　　　ibid. 　　　　　　　　　　　　18　(1973)　619

103. Devanthan M.A. & Guruswarmy V.

　　　Elektrokhimiya 　　　　　　　　7　(1971)　1818

104. Tobias C.W. & Hickman R.G.

　　　Z. Phys. Chem. 　　　　　　　229　(1965)　145

105. Pickett D.J. & Stanmore B.R.

　　　J. Appld. Electrochem. 　　　　2　(1972)　151

106. Arvia A.J., Bazan J.C. & Carrozza J.S.W.

　　　Electrochim. Acta 　　　　　　11　(1966)　881

107. Wragg A.A. & Ross T.K.

　　　ibid. 　　　　　　　　　　　　13　(1968)　2192

108. Gordon A.R. & Cole A.

　　　J. Phys. Chem. 　　　　　　　40　(1936)　733

109. Eisenberg M., Tobias C.W. & Wilke C.R.

　　　J. Electrochem. Soc. 　　　　103　(1956)　413

110. Bazan J.C. & Arvia A.J.

　　　Electrochim. Acta 　　　　　　10　(1965)　1025

111. Arvia A.J., Marchiano S.L. & Podesta J.J.

　　　Electrochim. Acta　　　　　　12　(1967)　259

112. Wilke C.R., Eisenberg M. & Tobias C.W.

　　　J. Electrochem. Soc.　　　　100　(1953)　517

113. Robinson D.J. & Gabe D.R.

　　　Electrochim. Acta　　　　　　17　(1972)　1129

114. Ramaraju C.V., Parvatalingeswara Rao V., Krishna M.S. &

　　　Jagannadha Raju C.J.V.

　　　Indian J. Technol.　　　　　7　(1969)　38

115. Heitz E. & Kreysa G.

　　　"Grundlagen der Technischen Elektrochemie"

　　　Verlag Chemie, Weinheim　(1977)

116. Newson J.D. & Riddiford A.C.

　　　J. Electrochem. Soc.　　　　108　(1961)　695

117. Bierlein J.A. & Becsey J.G.

　　　Techniques of Electrochemistry Vol. 2　　117

　　　Yeager E. & Salkind A.J.　(Eds.)

　　　Wiley - Interscience　(1966)

118. Adams R.A.

　　　Electrochemistry at Solid Electrodes

　　　Marcel Dekker Inc., N.Y.　(1969)

119. Marchiano S.L. & Arvia A.J.

　　　Electrochim. Acta　　　　　　　15　(1970)　325

120. Pickett D.J.

　　　"Electrochemical Reactor Design"

　　　Elsevier, London　(1977)

121. Fouad M.G. & Ahmed A.M.

    Electrochim. Acta   14 (1969) 651

122. Bohm U.

    ibid.   15 (1970) 1841

123. Baizer M.

    Paper Presented at the Symposium on Electrochemical Reaction
                        Engineering, Southampton, 1979

124. Sorour M.M. and Coney J.E.R.

    J. Mech. Engng. Sci.   21 (1979) 403

125. Eisenberg M.

    Adv. in Electrochem. Electrochem. Eng. Vol 2

    Delahey P. & Tobias C.W. (Eds.)

    Interscience, New York (1962)

126. Robertson P.M. & Ibl N.

    J. Appld. Electrochem.   7 (1977) 323

127. Robertson P.M., Schwager F. & Ibl N.

    J. Electroanal. Chem.   65 (1975) 883

128. Patents pending

    German DOS 2,415,784, 2 Oct (1975)

         DOS 2,503,819, 5 Aug (1976)

129. Volk W.

    Chem. Engng.   86 (1979) April 23, 128

                                 June   4, 133

                                 Sept. 10, 131

                                 Nov. 19, 149

                                 Dec. 11, 93

130. U.S. Patent 3,859,195, 7 Jan. (1975)

    Du Pont

131. Keating K.B. & Williams J.M.

  80th Annual A.I. Ch. E. Meeting,

  Boston, Mass., 1975

132 Stuart J.T.

  J. Fluid Mech.   4 (1958) 1

133. Newman J.S. & Tiedemann W.

  Advances Electrochem. & Electrochem. Eng. Vol. II

  Gerischer H. and Tobias C.W. (Eds.), Wiley, N.Y. (1978) 353

134. Liebenow C.

  Z. Electrochem.   4 (1897) 58

135. Heise G.W.

  Trans. Electrochem. Soc. 75 (1939) 147

136. Bennion D.N. & Newman J.S.

  J. Appld. Electrochem.   2 (1972) 113

137. Sioda R.E.

  Electrochim. Acta   13 (1960) 1559

138. Sioda R.E.

  Electrochim. Acta   15 (1970) 783

139. Sioda R.E.

  Electrochim. Acta   16 (1971) 1569

140. Sioda R.E.

  J. Electroanal. Chem. Interfacial Electrochem. 34 (1972) 399

141. Sioda R.E.

   J. Electroanal. Chem. Interfacial Electrochem. 34 (1972) 411

142. Sioda R.E.

   Electrochim. Acta   17 (1972) 1939

143. Sioda R.E.

   J. Appl. Electrochem.   5 (1975) 221

144. Wroblowa H.S. & Razummey G.

   J. Electrochem. Soc.   121 (1974) 124C

145. Wilson E.J. & Geankoplis C.J.

   Ind. Eng. Chem. Fund.   5 (1966) 9

146. Colquhoun - Lee I & Stepanek J.

   Chem. Eng. (Lond.)   No. 282 (1974)   108

147. Tentorio A. & Casolo - Ginelli U.

   J. Appld. Electrochemistry   8 (1978) 195

148. Backhurst J.R.

   Ph.D. Thesis,

   University of Newcastle (1967)

149. Backhurst J.R., Coulson J.M., Goodridge F., Plimley R.E. and

   Fleischmann M.

   J. Electrochem. Soc.   116 (1969) 1600

150. Fleischmann M. and Oldfield J.W.

   J. Electroanal. Chem.   29 (1971) 211

151. Fleischmann M. and Oldfield J.W.

   J. Electroanal. Chem.   29 (1971) 231

152. Fleischmann M., Oldfield J.W. & Porter D.F.

   J. Electroanal. Chem.   29 (1971) 241

153. Fleischmann M., Oldfield J.W. and Tennakoon L.

   J. Applied Electrochem.   1 (1971) 103

154. Goodridge F., Holden D.I. Murray H.D. and Plimley R.E.

   Trans. Instn. Chem. Engrs.   49 (1971) 128

155. Goodridge F., Holden D.I., Murray H.D. and Plimley R.E.

   Trans. Instn. Chem. Engrs.   49 (1971) 137

156. Backhurst J.R., Fleischmann M., Goodridge F., and Plimley R.E.

   Brit. Pat. 1,194,181   10 June (1970)

   (Assigned to N.R.D.C.)

157. Walker A.T.S.

   Ph.D. Thesis, University of Exeter, Dec. 1977

158. Wragg A.A. & Walker A.T.S.

   Paper Presented at "Chempor '78", University of Minho, Braga, Portugal
   Sept. 1978

159. Goodridge F.

   Electrochim. Acta   22 (1977) 929

160. Coeret F., Le Goff P. & Vergnes F.

   Rottenburg P.A. (Ed.)

   Proc. Int. Symp. Fluid., NL University Press (1967)

161. Jottrand P.R. & Grunchard F.

Paper Presented at the Symposium on Interaction Between Fluids &

Particles, London, I.Chem.E. (1962)

162. Jagannadharaju G.J.V. & Venkata Rao C.

Ind. J. Tech.   3 (1965) 201

163. Smith J.W. & King D.H.

Can. J. Chem. Eng.   53 (1975) 41

164. Flett D.S.

Chem. Ind.   7 (1971) 300

165. Wilkinson J.A.E. & Haines K.P.

Trans. Inst. Min. Met. 81 (1972) 157

                                    82 (1973) C119

166. Lopez - Cacicedo C.L.

Trans. Inst. Met. Fin. 53 (1975) 74

167. Van Der Heiden G., Raats C.M.S. and Boon H.F.

Chem. Ind. July (1978) 465

168. Kuhn A.

Chem. Ind. July (1978) 447

169. Kuhn A.T. & Houghton R.W.

Topics in Pure and Applied Electrochem., S.A.E.S.T., Karaikudi,

India (1979) 133

170. Ibl N., Adam E., Venczel J and Schalch E.

Chem. Ing. Tech.   34 (1971) 202

171. Venczel J.

   Electrochim. Acta   15 (1970) 1909

172. Janssen L.J.J. and Hoogland J.G.

   Electrochim. Acta   15 (1970) 1013

                              18 (1973)   543

173. Fouad M.G. & Sedahmed G.H.

   Electrochim. Acta.   17 (1972)   665

174. Ibl N. and Venczel J.

   Metalloberflasche   24 (1970)   365

175. Roald B. and Beck W.

   Trans. Electrochem. Soc.   98 (1951)   277

176. Kreuter T., Krueger F. & Thiele W.

   G.D.R. Patent 92,907

177. Mohanta S. and Fahidy T.Z.

   J. Appl. Electrochem.   7 (1977)   235

178. Ettel V.A. & Gendron A.S.

   J. Appl. Electrochem.   8 (1978)   277

179. Mohanta S. and Fahidy T.Z.

   U.S. Patent 3,821,057 (1974)

180. Ettel V.A., Tilak B.V. & Gendron A.S.

   J. Electrochem. Soc.   121 (1974)   867

181. Gendron A.S. & Ettel V.A.

Can. J. Chem. Eng.   <u>53</u> (1975) 36

182. Ettel V.A., Gendron A.S. & Tilak B.V.

Metall. Trans. B   <u>6B</u> (1975) 31

183. Ettel V.A. and Gendron A.S.

Chem. Ind.   <u>3</u> (1975) 376

184. Janssen L.J.J.

Electrochim. Acta   <u>23</u> (1978) 81

185. Janssen L.J.J.

Electrochim. Acta   <u>24</u> (1979) 693

186. Gendron A.S., Matthews R.R. & Wilson W.S.

C.I.M. Bull.   (1977) 95

187. Schreiber M.L.

J. Soc. Motion Picture Engrs. <u>74</u> (1965) 505

188. Fouad M.G., Sedahmed G.H. and El-Abd H.A.

Electrochim. Acta   <u>18</u> (1973) 279

189. Vogt H.

Ir. Thesis,

Stuttgart University (1977)

190. Kappesser R., Comet I & Greif R.

J. Electrochem. Soc.   <u>118</u> (1971) 1957

191. Makrides A.C. and Hackerman N.

   J. Electrochem. Soc.   105 (1958) 156

192. Fouad M.G. & Zatout A.A.

   Electrochim. Acta   14 (1969) 909

193. Ibl N.

   Adv. Electrochem. Electrochem. Eng. 2 (1966) 49

   (Ed. - Tobas C.W.), Wiley.

194. Ibl N. & Schadegg K.

   J. Electrochem. Soc.   114 (1967) 54

195. Carbin D.C. and Gabe D.R.

   Electrochim. Acta   19 (1974) 653

196. Denbigh K.G.

   "Chemical Reactor Theory"

   Cambridge University Press, Cambridge (1966)

197. Dart M.C., Gentles J.D. and Renton G.D.

   British Patent 1,025,282 (1966)

198. Pickett D.J.

   Electrochim. Acta   20 (1975) 803

199. Walker A.T.S. & Wragg A.A.

   Electrochim. Acta   22 (1977) 1129

200. Sudall S.J.

   M.Sc. Thesis., U.M.I.S.T. (1970)

201. Sudall S.J.

Ph.D. Thesis, U.M.I.S.T. (1975)

202. Satyanarayana A., Krishna M.S., Raju G.J.N., Jagannadha R. &
Venkcata C.

Ind. J. Technol. $\underline{6}$ (1968) 42

203. Wagner C.

Adv. Electrochem. & Electrochem. Eng. $\underline{2}$ (1966) 1

Tobias C.W. (Ed.) Interscience, New York.

204. Chilton T.H., Drew T.B. & Jerbens R.H.

Ind. Eng. Chem. $\underline{36}$ (1944) 510

205. Mizushina T.

Adv. Heat Transfer $\underline{7}$ (1971) 87

Irvine T.F. & Hartnett J.P. (Eds.)

Academic Press, London.

206. Mizushina T., Ito R., Hiraoka A., Ibusuki A. & Sakaguchi I.

J. Chem. Eng. Japan $\underline{2}$ (1969) 89

207. Sioda R.E.

Electrochim. Acta $\underline{19}$ (1974) 57

208. Pickett D.J.

Electrochim. Acta $\underline{18}$ (1973) 835

209. Ibl N.

Proc. 24th Int. Cong. Pure & App. Chem. (1974) 31

210. Bassett J., Denney R.C., Jeffrey G.H. & Mendham J.

"Vogel's Textbook of Quantitative Inorganic Analysis" 4th Ed.,
Longman, London, (1978)

211. Lingane J.J.

"Electroanalytical Chemistry"

2nd Ed., Interscience, New York (1958)

212. Goodridge F.

Proc. 24th Int. Cong. Pure & Applied Chemistry

5 (1974) 19

213. Goodridge F.

Paper Presented at a Meeting on "Electrochemistry – Material

Recovery & The Environment", Shell Thornton Research Centre,

Jan. (1979)

214. Beck F. & Guthke H.

Chem. Ing. Techn.   41 (1969) 943

215. Fleischmann M, Jansson R.E.W., Ashworth G.A. & Ayre P.J.

Brit. Prov. Pat. 18,305, Apr. (1974)

216. Ashworth G.A.

Ph.D. Thesis

University of Southampton (1977)

217. Jansson R.E.W. and Marshall R.J.

Chem. Eng.   315 (1976) 769

218. Jansson R.E.W. and Marshall R.J.

J. Appld. Electrochem.   8 (1978) 287

219. Jansson R.E.W., Marshall R.J. & Rizzo J.E.

J. Appld. Electrochem.   8 (1978) 281

220. Jansson R.E.W. & Tomov N.R.

Chem. Eng.   (1977) 867

221. Ghoroghchian J., Jansson R.E.W. & Jones D.

J. Appld. Electrochem.

222. Ghoroghchian J.

Ph. D. Thesis,

Southampton Univ. (1977)

223. Jansson R.E.W. & Ashworth G.A.

J. Appld. Electrochem.   7 (1977) 309

224. Anon.

Anti Corrosion June (1977) 19

225. von Fraunhofer J.A. & Banks C.H.

"Potentiostat and its Applications"

Butterworths, London (1975)

226. Rechnitz G.A.

"Controlled Potential Analysis"

Pergamon, London (1963)

227. Charlot G., Badoz-Lambling J. and Tremillon B.

"Electrochemical Reactions"

Elsevier, Amsterdam (1962)

228. Robertson P.M., Scholder B., Theis G. & Ibl N.

Chem. Ind.   July (1978) 459

229. Williams J.M. & Olson M.C.

Paper Presented at 82nd A.I.Ch.E. Meeting,

Atlantic City, N.J., Sept. (1976)

230. Kennedy I.F.T. & Das Gupta S.

Finisher's Management   July (1978) 7

231. Fleet B. & Das Gupta S.

Ger. Offen. 2,534,357, 26 Feb. (1976)

232. Das Gupta S. & Fleet B.

Nature 263 (1976) 122

233. Salt Gram Winter '78 No. 18

Akzo Zout Chemie.

"The Realisation of Fluidised Bed Electrolysis"

234. Lopez Cacicedo C.L. & Tyson A.G.

Submitted to J. Appl. Electrochem. (1980)

235. Wheeler E.M.

Prod. Finish. June (1979) 20 & 22

236. Grassmann P., Ibl N. & Trub J.

Chem. Ing. Tech. 33 (1961) 529

237. Ferreira O.F. & Jansson R.E.W.

Paper Presented at the Symposium on Electrochemical Reaction
                                    Engineering, Southampton, (1979)
238. Tvarusko A & Watkins.

J. Electrochem. Soc. 113 (1971) 580

Electrochim.Acta. 14 (1969) 1109

239. Brenner A.

Proc. Amer. Electroplater's Soc. 95 (1940) 4

240. Shenoi B.A., Indira K.S. & Subramanian R.

Metal Finishing July (1970) 40 ;

Aug. (1970) 57 ;

Sept.(1970) 56

241. Walker R. and Clements J.F.

Metal Finishing. Apr. (1970) 100

242. Kochergin S.G. & Vyaseleva G.Y.

Consultants Bureau, N.Y. 1966

243. Eggett G., Hopkins W.R., Garlick T.W. & Ashley M.J.

I.Chem.E. Symp. Ser. No. 42, p. 27

244. Ismail M.I., Al-TaWeel A.M. & El. Abd. M.Z.

J. Appl. Electrochem. 4 (1974) 347

245. Somasundara Rao K., Jagannadha Raju G.J.V. & Venkata Rao C.

Ind. Chem. Eng. 5 (1963) 100

246. Mohanta S. & Fahidy T.Z.

Can. J. Chem. Eng. 50 (1972) 248

50 (1972) 434

247. Eisner S.

Plating Oct. (1971) 993, Nov. 1099, Dec. 1183

248. Eisner S.

Brit. Pat. 1,257,541

22 Dec. 1971

249. Matsuda H.

J. Electroanal. Chem. 38 (1972) 159

250. Filinovski V.Y. and Pleskov Y.V.

"The Rotating Disc Electrode"

Consultants Bureau, London (1976)

251. Opekar F. and Beran P.

J. Electronanal. Chem.   69 (1976) 1

252. Riddiford A.C.

Adv. Electrochem. Electrochem. Eng. 4 (1966) 47

253. Jahn D. and Vielstich W.

J. Electrochem. Soc. 109 (1962) 849

254. Albery W.J. and Hitchman M.L.

"The Ring Disc Electrode"

Oxford University Press, Oxford (1971)

255. Narasimham K.C. and Udupa H.V.K.

Metal Finishing   18 (1972) 11

256. Deslouis C. and Epelboin I.

Electrochim. Acta   22 (1977) 921

257. Kolthoff I.M. and Laitinen H.A.

J. Phys. Chem.   45 (1941) 1079

258. Nisancioglu K. and Newman J.

J. Electrochem. Soc. 121 (1974) 241

259. Jordan J., Javick R.A. and Ranz W.E.

J. Amer. Chem. Soc. 80 (1958) 3846

260. Vielstich W. and Barz F.

Chem. Ing. Tech.   49 (1977) 299

261. Nicolson R.S.

Anal. Chem. 42 (1970) 130R

262. Jordan J. and Javick R.A.

Electrochim. Acta 6 (1962) 23

263. Bucur R.V. and Bartes A.

Electrochim. Acta 22 (1977) 499

24 (1979) 173

264. Ross T.K. and Badhwar R.K.

Corr. Sci. 5 (1965) 29

265. Brunner E.

Z. Phys. Chem. 47 (1904) 56

266. Nernst W. and Merriam E.S.

Z. Phys. Chem. 53 (1905) 235

267. Sackus O.

Z. Phys. Chem. 54 (1906) 641

268. Jablczynski K.

Z. Phys. Chem. 64 (1908) 748

269. Wilderman M.

Z. Phys. Chem. 66 (1909) 445

270. King C.V.

Trans. Electrochem. Soc. 102 (1955) 193

271. King C.V.

J. Amer. Chem. Soc.   57 (1935) 828

272. King C.V. and Schack M.

J. Amer. Chem. Soc.   57 (1935) 1212

273. King C.V. and Cathkart W.H.

J. Amer. Chem. Soc.   59 (1937) 63

274. King C.V. and Howard P.L.

Ind. Eng. Chem.   29 (1937) 75

275. Salzberg H. and King C.V.

J. Electrochem.Soc.   97 (1950) 290

276. King C.V. and Lang F.S.

J. Electrochem. Soc.   99 (1952) 295

277. King C.V. and Mayer N.

J. Electrochem. Soc.   100 (1953) 473

278. Kataoka K., Doi H. and Komai T.

Int. J. Heat Mass Transfer   20 (1977) 57

279. Kataoka K., Doi H. and Hongo T.

J. Chem. Engng. Japan   8 (1975) 472

280. Mitzushina T., Ito R., Kataoka S., Yokoyamu S., Nakashima Y. and Fukuda A.

Chem. Engng. Japan   32 (1968) 795

281. Kataoka K.

J. Chem. Engng. Japan   8 (1975) 271

282. Matic D., Lovrecek B. and Skansi D.

J. Appl. Electrochem.   8 (1978) 391

283. Ellison B.T. and Schmeal W.R.

J. Electrochem. Soc.   125 (1978) 524

284. Edwards J. and Wall A.J.

Inst. Min. & Metall.   (1966) 307

285. Kar G., Healy T.W. & Fuerstenau D.W.

Corr. Sci.   13 (1973) 375

286. Johansson G.

Talanta   12 (1965) 163

287. Heitz E.

Werks. u. Korr.   15 (1964) 63

288. Wendt F.

Ingen.-Arch.   4 (1933) 577

289. Nadebaum P.R. and Fahidy T.Z.

J. Electrochem. Soc.   122 (1975) 1035

290. Nadebaum P.R. and Fahidy T.Z.

Can. J. Chem. Engng.   53 (1975) 259

291. Nadebaum P.R. and Fahidy T.Z.

   J. Appld. Electrochem.   5 (1975) 249

292. Nadebaum P.R. and Fahidy T.Z.

   Nature Phys. Sci.   241 (1973) 45

293. Strafelda F. and Kozak D.

   Collection Czech Chem. Commun. 26 (1961) 3168

294. Strafelda F. and Singer E.

   Collection Czech Chem. Commun. 31 (1965) 3042

295. Farooque M. and Fahidy T.Z.

   Electrochim. Acta.   24 (1979) 547

296. Spencer M.S., Carnell P.J.H. and Skinner W.J.

   Ind. Eng. Chem. Proc. Des. & Dev. 8 (1969) 191

297. Carnell P.J.H., Skinner W.J. and Spencer M.S.

   Brit. Patent   1,071,923

   14 June (1967)

298. Nadebaum P.R. and Fahidy T.Z.

   J. Appld. Electrochem.   10 (1980) 13

299. Prunet J. and Guillen A.

   French Patent   1,264,597

   12 May (1960)

300. Societe Industrielle Des Coussinets

   Brit. Pat. 871,698 ,

   June 28 (1961) ;

   French Patent 1,189,952 ,

301. Cleave A.H.W.

U.S. Patent 1,535,577

Apr. 28 (1925)

302. Nordblom G.F. and Bodamer G.W.

U.S. Patent 3,414,486

Dec. 3 (1968);

Nordblom G.F.

U.S. Patent 3,419,901

Dec. 31 (1968)

303. Gordy J.

U.S. Patent 3,778,360

Dec. 11 (1973)

304. Johnson G.W.

Brit. Pat. 506,590

May 30 (1939)

305. Arrigo Pini S.P.A.

Brit. Pat. 1,044,776

Oct. 5 (1966),

306. Holland F.S.

Brit. Pat. 1,444,367

July 28 (1976)

307. Holland F.S.

U.S. Pat. 4,028,199 (1977)

Brit. Pat. 1,505,736 (1978)

308. Holland F.S.

Chem. Ind. (1978) 453

309. Holland F.S. and Rolskov H.

Effluent Water Treatment Conv.

Birmingham (1978)

310. Swalheim D.A.

Trans. Electrochem. Soc. 86 (1944) 395

311. Kar G., Co^{rn}et I. and Fuerstenau D.W.

J. Electrochem. Soc. 119 (1972) 33

312. Beard L.R., Gabe D.R. and Melbourne S.H.

Trans. Inst. Met. Fin. 44 (1966) 1

313. Sherwood T.K. and Ryan J.M.

Chem. Eng. Sci. 11 (1958) 81

314. von Hahn E.A. and Ingraham T.R.

Trans. Amer. Inst. Mech. Engrs. 236 (1966) 1098

239 (1967) 1895

315. Newman J.

Electrochim. Acta 22 (1977) 903

316. Pini G.C. and DeAnna P.L.

Electrochim. Acta 22 (1977) 1423

317. Sedahmed G.H., Abdel-Khalik A., Abdallah A.M. and Farahat M.M.

J. Appld. Electrochem. 9 (1979) 563

318. Hixson A.W. and Wilkens G.A.

Ind. Eng. Chem. 25 (1933) 1196

319. Walsh F.C. and Houghton R.W.

Unpublished work.

320. Heitz E., Kreysa G. and Loss C.

J. Appld. Electrochem. 9 (1979) 243

321. Walsh F.C.

Unpublished work.

322. Brenner A.

"Electrodeposition of Alloys" Vols. 1 and 2

Academic Press, London, (1963)

323. Walsh F.C. and Gabe D.R.

Paper Presented at a Conference on the Fundamentals of Electroplating

and Metal Finishing,

Loughborough Univ. of Technology, Sept. (1980)

324. Watson S.A.

Plating 62 (1975) 851

325. Gabe D.R.

Metallurgist 5 (1973) 72

326. Loss C. and Heitz E.

Werks. u. Korr. 24 (1973) 38

327. Foroulis Z.A. and Uhlig H.H.

J. Electrochem. Soc. 111 (1964) 13

328. Butler G. and Stroud E.G.

Brit. Corr. J. 1 (1965) 110

329. Giuliani L., Tamba A. and Modena C.

Inst. Corr. Sci. 11 (1971) 485

330. Makrides A.C.

Corrosion 18 (1962) 338 t

331. Makrides A.C.

J. Electrochem. Soc. <u>107</u> (1960) 869

332. Syrett B.C.

Corrosion <u>32</u> (1976) 243

333. Udupa K.S., Subramanian G.S. and Udupa H.V.K.

Ind. Chemist. May (1963) 238

334. Benner P.E.

U.S. Patent 3,448,026

June 3 (1969)

335. Lacroix F.

U.S. Patent 1,019,969

Mar. 12 (1912)

336. Cowper-Coles S.O.

U.S. Patent 1,127,966

Feb. 9 (1915)

337. Schaefer R.A.

U.S. Patent 2,391,039

Dec. 18 (1945)

338. Rennie J., Pratt J.M. and Milner D.J.

Brit. Pat. 1,349,672

10 April (1974)

339. Fulweiler S.B.

U.S. Patent 3,583,897, June 8 (1971)

340. CPAC INC.

Leicester, New York.

Sales information regarding the SilvPAC cells.

341. Fischer O.

British Patent   1,259,374

5 Jan (1972)

U.S. Patent   3,560,366

342. Goold R., Wojcik C.W. and Cooper G.D.

Australian Patent   59,229

13 Mar.   (1975)

343. Julien M.A.

British Patent   224,916

Feb. 12   (1925)

344. Cooley A.C.

U.S. Patent   3,551,317

Dec. 29 (1970)

345. Ibl N.

Chem. Ing. Tech. No. 36   6 (1964) 601

346. Raub E.

Plating and Surface Finishing   Feb. (1976) 29

347. Rossman J.

Metal Ind.   30 (1932)   321, 396, 436, 468

348. Rossman J.

Trans. Electrochem.   Soc. 85 (1944) 169

349. Mantell C.L.

J. Electrochem. Soc.   106 (1959) 70

350. Wranglen G.

J. Electrochem. Soc.   97 (1950) 353

351. Walker R. and Sandford A.R.B.

  Chem. Ind. Oct. (1979) 642

352. Kroll W.J.

  Trans. Electrochem. Soc. __87__ (1945) 551

353. Shafer W.M. and Harr C.R.

  J. Electrochem. Soc. __105__ (1958) 413

354. Mehl E.

  Powder Metallurgy (1958) 33

355. Kumar D. and Gaur A.K.

  J. Electrochem. Soc. India __22__ (1973) 211

356. Mital C.K.

  J. Electrochem. Soc. India __22__ (1973) 251

357. Calusaru A.

  "Electrodeposition of Metal Powders"

  Elsevier, Oxford, (1979)

358. Harper S. and Marks A.A.

  Copper Development Association (1972) 22

  Conf. Paper 059/2

359. Gurevich L.I. and Pomosov A.V.

  Poroshk. Metall.   no. 1 (1969) 13

               no.11 (1969) 6

               no. 12 (1972) 1

               no. 2 (1973) 1

360. Haynes R.

  "Production and Characterisation of Metal Powders"

  Course on Powder Metallurgy, Loughborough University of Technology,

  22 Sept. (1975)

361. British Metal Sinterings Association

"Testing Procedure for Iron Powders" (1968)

362. Loshkarev M. et al.

Chem. Abs.   41 (1947) 4386 c

43 (1949) 5674 g

363. Calusaru A. and Kutu J.

Nature (London)   211 (1966) 1080

364. Calusaru A. and Kutu J.

J. Electroahal. Chem. 20 (1969) 283

365. Calusaru A.

Electrochim. Acta   12 (1967) 1507

366. Calusaru A. and Moldovan A.

Electrochim. Acta   17 (1972) 1299

19 (1974) 341

367. Enchev I.D. and Kharizanov K.

Metallurgiya no. 9 (1974) 94

368. Bondarenko A.V.

Sov. Powder Metl & Met. Cer. No. 6 (1971) 431

369. Milner A. and Morris T.M.

Proc. 3rd Euro. Powder Met. Symp.

(1971) Part 2.

370. Tyrrell H.J.V.

J. Inst. Metals   76 (1949) 17

371. Sedzimir J., Bogacz Z. and Szymanska H.

Archiv. Hutnic.   20 (1975) 193

372. Popov K.I., Keca D.N. and Maksimovic M.D.

J. Appld. Electrochem.   7 (1977) 77

373. Popov K.I., Maksimovic M.D. and Ostojic G.R.

J. Appld. Electrochem.   7 (1977) 331

374. Popov K.I., Pavlovic M.G., Maksimovic M.D. and Krstajic S.S.

J. Appld. Electrochem.   8 (1978) 503

375. Popov K.I., Djukic L.M., Pavlovic M.G. and Maksimovic M.D.

J. Appld. Electrochem.   9 (1979) 527

376. Despic A.R. and Purenovic M.M.

J. Electrochem. Soc.   121 (1974) 329

377. Diggle J.W., Despic A.R. and Bockvis J.O'M.

J. Electrochem. Soc.   116 (1969) 1503

378. Loshkarev M., Ozerov A. and Kudriavtzev N.

Zh. Prikl. Khim. (U.S.S.R.) 22 (1949) 294

379. Ibl N.

Helv. Chim. Acta   37 (1954) 1149

380. Ibl. N., Javet P. and Stahel F.

Electrochim. Acta   .   17 (1972) 733

381. Gorbachev S.V.

Zhur. Fiz.Khim. (U.S.S.R.)   24 (1950) 888

382. Popov K.I., Keca D.N., Vidojkovic S.I., Lazarevic B.J. and Milojkovic V.B.

J. Appld. Electrochem.   6 (1976) 365

383. Prithviraj V., Achiaryulu S.L.N. and Tamhankar R.V.

Trans. Ind. Inst. Metals   23 (1970) 51

384. Yurev B.P., Golubkov L.A. and Grankina L.S.

Tr. Leningrad. Politech. Inst. 304(1970) 102

385. Bondarenko A.V., Kalmykov Y.V., Kutnyakhovn V.M. and Kletsko G.P.

Sb. Mosk. Inst. Stali Spalov   60 (1970) 212

386. Naganathan K., Annamalai P.C. and Srinivisan R.

Trans. S.A.E.S.T.   5 (1970) 31

387. Fedyushkina Y.A. and Pomosov A.V.

Sov. Powder Met. and Met. Cer. No. 8 (1971) 434

388. Natanson E.M., Shvets T.M., Melnichenko Z.M. and Sperkach V.S.

Sov. Powder Met. and Met. Cer. No. 5 (1971) 347

389. Pomosov A.V., Murashova I.B. and Artamonov V.P.

Sov. Powder Met. and Met. Cer. No. 5 (1969) 341

390. Yurev B.P. and Sukhanova L.P.

Sov. Powder Met. and Met. Cer. No. 6 (1969) 438

391. Yurev B.P. and Aladzhalov L.A.

Sov. Powder Met. and Met. Cer. No. 5 (1969) 345

392. Yurev B.P. and Golubkov L.A.

Sov. Powder Met. and Met. Cer. No. 7 (1967) 525.

393. Dube R.K. and Prasad P.M.

J. Electrochem. Soc. 122 (1975) 1473

394. Duisenberg C.E. and Bedford R.H.

U.S. Patent 2,791,555 (1957)

395. Adams W.M.

U.S. Patent 3,342,718 (1967)

396. Walsh F.C. and Gabe D.R.

J. Appl. Electrochem. , in press.

397. Gorbunova K.M. and Polukarov Y.M.

Adv. Electrochem. Electrochem. Engng. 5 (1967) 249

391. Yurev B.P. and Aladzhalov L.A.

  Sov. Powder Met. and Met. Cer. No. 5 (1969) 345

392. Yurev B.P. and Golubkov L.A.

  Sov. Powder Met. and Met. Cer. No. 7 (1967) 525

393. Dube R.K. and Prasad P.M.

  J. Electrochem. Soc.   122 (1975) 1473

394. Duisenberg C.E. and Bedford R.H.

  U.S. Patent 2,791,555 (1957)

395. Adams W.M.

  U.S. Patent 3,342,718 (1967)

396. Walsh F.C. and Gabe D.R.

  J. Appl. Electrochem. , in press.

397. Gorbunova K.M. and Polukarov Y.M.

  Adv. Electrochem. Electrochem. Engng. 5 (1967) 249

398. Coeuret F. and Legrand J.

  J. Appl. Electrochem. 10 (1980) 785

399. Legrand J., Dumargue P. and Coeuret F.

  Electrochim. Acta 25 (1980) 669

400. Singh P.C. and Mishra P.

  Chem. Engng. Sci. 35 (1980) 1657

401. Billings J. and Ritchie I.M.

Electrochim. Acta   25 (1980) 733

402. Strickland P.H. and Lawson F.

Proc. Aust. Inst. Min. Met.   NO. 236 Dec. (1970) 25

NO. 237 Mar. (1971) 71

403. Scott K.

J. Appl. Electrochem.   II (1981) 339

404. Raub E. and Muller K.

Fundamentals of Metal Deposition

Elsevier, London (1967) p.97

405. Gedansky L.M. and Hepler L.G.

'Thermochemistry of silver and its compounds'

Englehard Technical Bulletin, July 1969

406. Newman J.S. and Trainham J.A.

Inorganic Materials Research Division, UCLA, April (1974)

Annual Report for 1973

407. ibid.,   June (1976)

408. Kuhn A.T. and Houghton R.W.

J. Appld. Electrochem.   4 (1974) 69

409. Vaaler L.E.

J. Electrochem. Soc. 125 (1978) 204

410. Marangozis J. and Johnson A.I.

Can.J. Chem. Engng.   Dec. (1962) 231

4II. Javet P.., Ibl N. and Hintermann H.E.

Electrochim. Acta   12 (1967) 78I

4I2. 'Technology of the Eco-cell Process'

Ecological Engineering Ltd., Internal Publication

4I3. Bertorelle E., Bellobono I.R. and Bordonali C.

Trans. Inst. Metal Finish.   35 (1957) 23I

4I4. Walsh F.C., Gardner N.A. and Gabe D.R.

Paper presented at the 'Electrochemical Reaction Engineering

Symposium', Southampton, April (1979)